UNIVERSITY OF NAPLES "FEDERICO II"

POLYTECHNIC SCHOOL AND OF BASIC SCIENCES

EDUCATIONAL AREA: MATHEMATICS, PHYSICS, NATURAL SCIENCES

PhD IN CHEMICAL SCIENCES
XXVI CYCLE
2011-2014

COURSE OF SYNTHESIS,STRUCTURE AND REACTIVITY OF ORGANIC MOLECULES

Synthesis, properties and applications of bioinspired nitrogen and/or group 16 aromatic heterocycles

DR. LOREDANA LEONE

Supervisor

Prof. Alessandra Napolitano

Assessor

Prof.Maria Rosaria Iesce

PhD Coordinator

Prof. Luigi Paduano

UNIVERSITA' DEGLI STUDO DI NAPOLI "FEDERICO II"

SCUOLA POLITECNICA E DELLE SCIENZE DI BASE

AREA EDUCAZIONALE:MATEMATICA, FISICA, SCIENZE NATURALI

DOTTORATO DI RICERCA IN SCIENZE CHIMICHE
XXVI CICLO
2011-2014

CORSO DI SINTESI, STRUTTURA E REATTIVITA' DELLE MOLECOLE ORGANICHE

Sintesi, proprieta' e applicazioni di composti aromatici eterociclici bioinspirati contenenti azoto e elementi del gruppo 16

DR. LOREDANA LEONE

Tutore
Prof. Alessandra Napolitano

Relatore
Prof.Maria Rosaria Iesce

Coordinatore
Prof. Luigi Paduano

Index

Abstract **6**

1. Introduction **9**

1.1. Overview of heterocyclic compounds containing nitrogen and sulphur as biologically relevant compounds **9**

1.2. Pheomelanin pigments: biogenesis and origin of the 1,4-benzothiazine structural units. **26**

2. Methods **35**

2.1 EPR spectroscopy **35**

2.2 Computational analysis **41**

2.3 Time resolved fluorescence **42**

3. Results and discussion **47**

3.1. Photochromism and acidichromism of $\Delta^{2,2}$-Bi-(2H-1,4-benzothiazine). **47**

3.2. Synthesis of 1,4-benzothiazines and investigation of their oxidation reactivity **57**

3.3. Oxidative coupling of 3-phenyl-(2H-1,4-benzothiazine) promoted by peroxides or biometals. **66**

3.4. Benzothiazine based cyanine dyes: a) synthesis and characterization of dimeric cyanines. **78**

3.5. Benzothiazine-based cyanine dyes: b)Cyanines by condensation of benzothiazines with aldehydes **88**

3.6. Role of benzothiazine structural units in pheomelanin properties: UV-independent prooxidant effects of natural and model pigments. **110**

3.7. Photochemistry of pheomelanins: spectroscopic investigation of benzothiazole building blocks **128**

3.8. Photochemistry of pheomelanins: Spectroscopic investigation of natural and synthetic pigments and related 1,4-benzothiazines **145**

4. Conclusions **157**

5. Experimental section **161**

5.1. General methods **161**

5.2 Photochromism and acidichromism of $\Delta^{2,2}$-Bi-(2H-1,4-benzothiazine). **165**

5.3. Synthesis of 1,4-benzothiazines and investigation of their oxidation reactivity **167**

5.4. Oxidative coupling of 3-phenyl-(2H-1,4-benzothiazine) promoted by peroxides or biometals. **169**

5.5. Benzothiazine-based cyanine dyes: a) synthesis and characterization of dimeric cyanines. **171**

5.6. Benzothiazine-based cyanine dyes: b)Cyanines by condensation of benzothiazines with aldehydes **174**

5.7. Role of benzothiazine structural units in pheomelanin properties: UV-independent prooxidant effects of natural and model pigments. **180**

5.8. Photochemistry of pheomelanins: spectroscopic investigation of benzothiazole building blocks **184**

5.9 Photochemistry of pheomelanins: Spectroscopic investigation of natural and synthetic pigments and related 1,4-benzothiazines **187**

6. References **189**

Publication list **197**

Abstract

A prominent position among naturally occurring N,S heterocyclic systems is occupied by 1,4-benzothiazines that form the key structural unit of pheomelanin pigments responsible for the red hair phenotype, typically found in red hair individuals with pale skin and enhanced susceptibility to skin cancer and melanoma. The chromophore exhibited by these pigments has been associated to the presence of the $\Delta^{2,2'}$-bi-(2*H*-1,4-benzothiazine) system. This is an indigo type chromophore which has not so far been fully exploited in the field of functional dyes. This $\Delta^{2,2'}$-bi-(2*H*-1,4-benzothiazine) exhibits a significant pH dependence, with a bathochromic shift from red to blue in acids and a marked photochromism under sunlight with reversible conversion in organic solvents of a yellow-orange species with abs max at 450 nm to a red one with abs max at 480 nm. Another related chromophore based on a push pull system occurs in the natural pigments cyanines, having organic nitrogen centers, one of the imine and the other of the enamine type. Some of these cyanines are currently used as biological reporters and in other technological applications .

In this PhD project the research activity has been focused on 1,4-benzothiazine systems. Inspired by the peculiar properties of the chromophore exhibited by pheomelanin and natural cyanines the access to new classes of dyes with potential technological applications has been explored. The role of the benzothiazine structural units in the biological function of pheomelanin pigment was also addressed.

Structural re-examination of the stable yellow isomer of $\Delta^{2,2'}$-bibenzothiazine by an integrated 2D NMR and theoretical approach revealed that the stable yellow species is in fact the *cis* isomer. A novel picture of $\Delta^{2,2'}$-bibenzothiazine as a four-state system with photochromic and pH-dependent behavior was proposed.

Stable 3-substituted 1,4-benzothiazines, namely the 3-phenyl- and the 3-methyl-2*H*-1,4-benzothiazine were obtained by improvement of previously reported procedures in 50-60%

average yields.

When exposed to peroxides or biologically relevant metals at micromolar concentration and in the presence of strong acids, 3-phenyl-*2H*-1,4-benzothiazine is efficiently converted to a green-blue $\Delta^{2,2'}$-bi(2*H*-1,4-benzothiazine) via colorless intermediates identified as single-bonded dimers. A resonance-stabilized benzothiazinyl radical intermediate was evidenced and characterized by EPR spectroscopy. Interestingly, 3-phenyl-*2H*-1,4-benzothiazine proved useful for the visual detection of peroxides in aged ethereal solvents and an efficient inhibitor against corrosion of the rusty iron objects induced by concentrated HCl.

Two different approaches were pursued for the synthetic access to benzothiazine cyanines, one involving reaction with *dialdehydes* that may allow for the build-up of a *conjugated bridge* between the two benzothiazine units and the other based on the *condensation* of the benzothiazine *with aromatic* para *N*-alkyl substituted *aldehydes.* All these products showed a marked pH dependence of the chromophores, associated in some cases to high molar extinction coefficients (up to 18,000), and emission of fluorescence tunable with the pH conditions.

The chemistry of benzothiazine units accounting for the biological function of pheomelanin pigments was also addressed. Though commonly regarded as photosensitizer agents capable of amplifying generation of reactive oxygen species following UV radiation, recently, pheomelanin has also been implicated in UV-independent pathways of oxidative stress. To get an insight into these processes the reactivity of natural and synthetic pheomelanins toward critical cellular antioxidants was investigated.

A marked ability of pheomelanin from red human hair, but not of eumelanin from black human hair to reduce the levels of GSH and NADH was evidenced. In the absence of oxygen GSH and NADH depletion was not observed while the presence of enzymes as superoxide dismutase and catalase did not modify the effect of pheomelanin suggesting a ROS independent mechanism. The mechanism of GSH oxidation by red hair pheomelanin was investigated by EPR spectroscopy.

During a visit at the Department of Chemical Physics of Lund University (Sweden) in the research unit headed by professor Sundstrom, the photochemistry of putative structural subunits of pheomelanin including benzothiazoles, benzothiazine dimers and dihydroisoquinolines as well as of the natural pigments and synthetic models was investigated. Steady state absorption and emission spectra at different pHs showed marked differences that can be accounted for in terms of the ionization state of the functional groups. Time resolved measurements under different pH conditions allowed for identification of short lived species and characterization of fast processes like intramolecular and solvent proton transfer that are primary processes of excited state deactivation. Analysis of the results indicated the major role of the benzothiazine units compared to benzothiazole and 3-substituted units in determining the behaviour of natural pheomelanins.

1.Introduction

1.1 Overview of heterocyclic compounds containing nitrogen and sulphur as biologically relevant compounds

Heterocyclic compounds containing nitrogen and elements of the 16 group mainly oxygen and sulphur are widespread in nature and represent the core structural units of biologically active compounds as well as of dyes and other functional systems that have raised interest in a variety of fields.

Restricting to the most common five and six membered ring systems oxazoles, thiazoles, oxazine and thiazine the most outstanding example of naturally occurring benzothiazole derivatives is provided by the luciferins that fireflies use to generate light (bioluminescence) in a multistep process mediated by luciferases (**Figure 1**).[1]

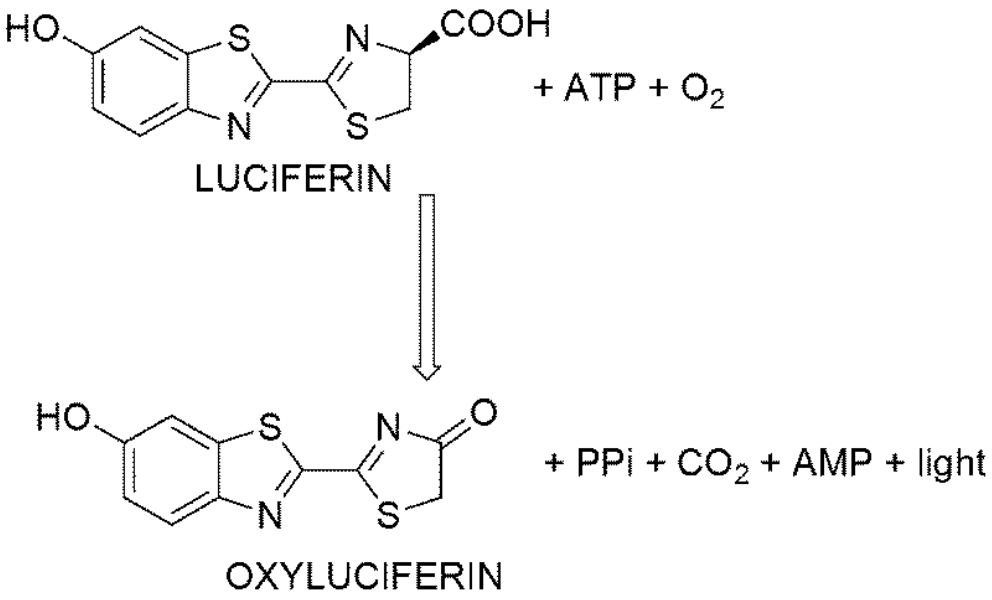

Figure 1. *The luciferin-luciferase reaction*

Several drugs include thiazole units like epothilones[2] produced by the myxobacterium Sorangium cellulosum So ce90 (**Figure 2**) , a new class of antimicrotubuline agents that display improved potency against Taxol-resistant tumor cell lines.

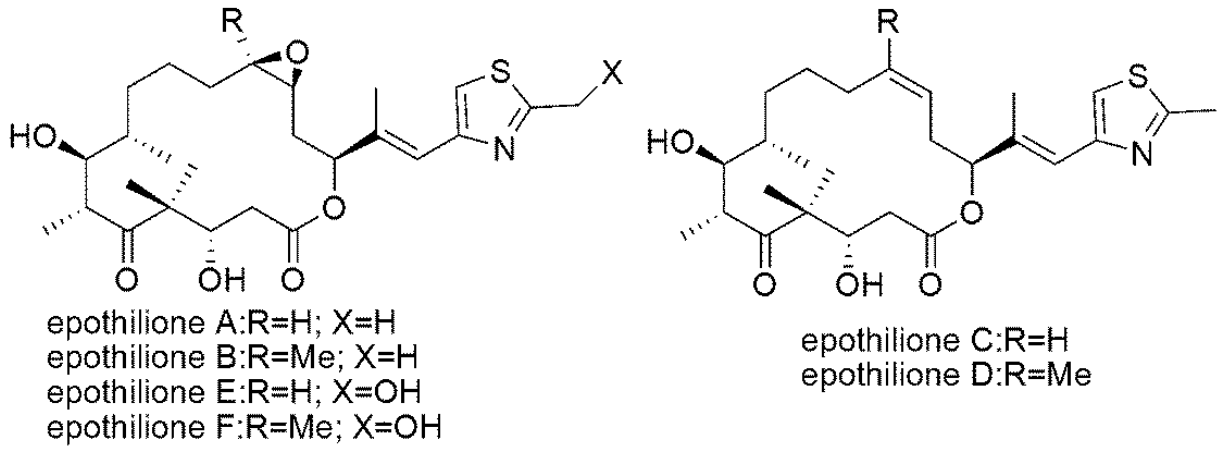

Figure 2. *Structure of Epothilones A-F*

Additionally, thiazoles are frequently cropping up in peptide research. For example, the pseudopeptide dolastatin 10 (**Figure 3**) is an exceptionally potent antineoplastic agent,[3] and other thiazole-containing marine cyclic peptides have demonstrated significant cytotoxicity.[4]

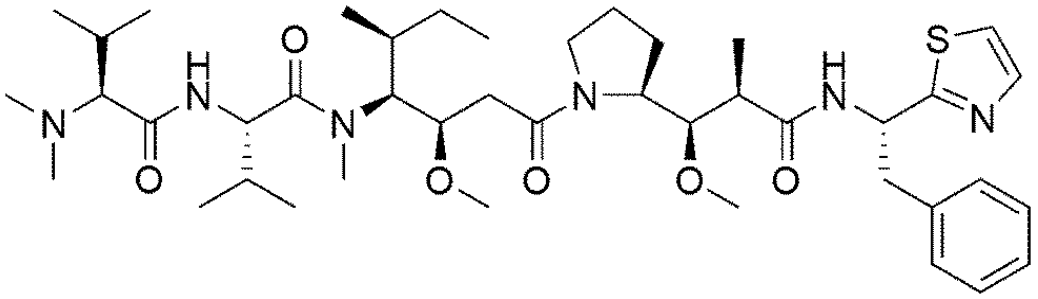

Figure 3. *Structure of Dolastatin 10*

Bengazole A (**5**) and related homologues isolated from marine sponges of the genus *Jaspis* are remarkable examples of bisoxazole containing natural products [5] Bengazole A (**Figure 4**) exhibits potent in vitro antifungal activity against *Candida albicans* [6] .

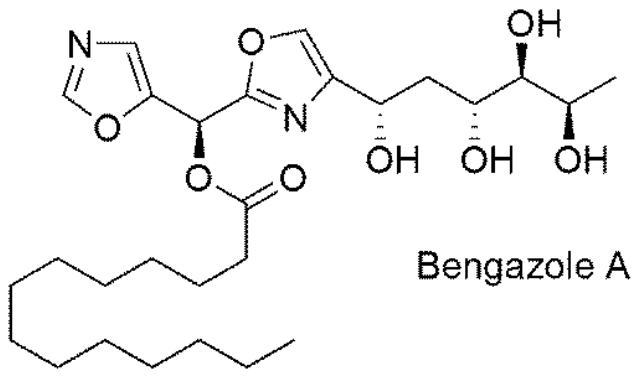

Figure.4 *Structure of Bengazole A*

The phenothiazine structure (**Figure 5)** occurs in various neuroleptic drugs, e.g. chloropromazine[7], and antihistaminic drugs, e.g. promethazine[8].

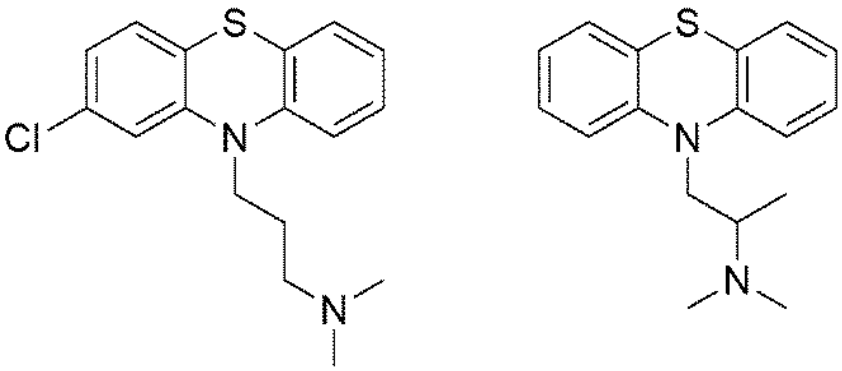

Figure 5. *Phenothiazine drugs*

The phenothiazine ring system appears prominently in dyes widely used for biological staining, like thionine (**Figure 6**), a strongly staining metachromatic dye[9] and structurally related compounds.

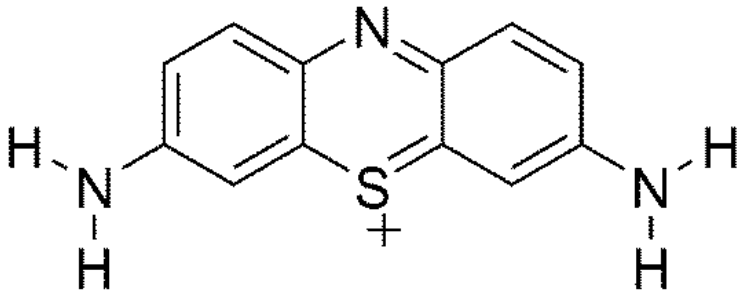

Figure 6. *Structure of thionine*

Moreover, oxazine and thiazine dyes have found application as antimalarian drugs[10]. (**Figure 7**)

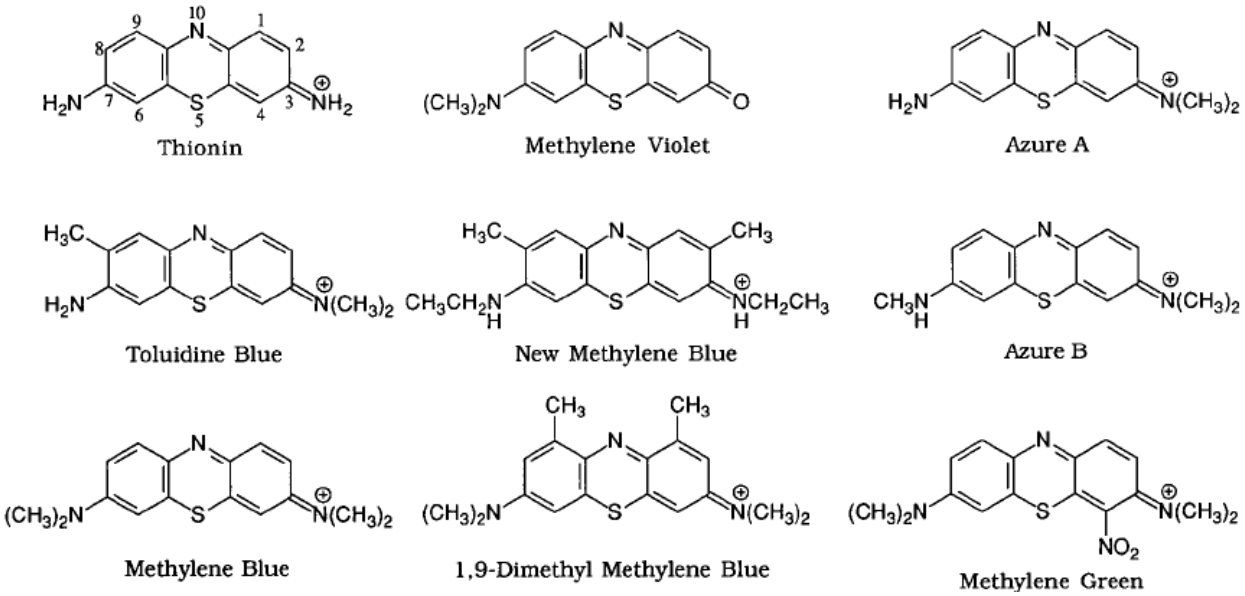

Figure 7. Structure of some thiazine-based antimalarian drugs

Based on this overview it is clear that the N/S heterocycles offer a variety of opportunities for research given their properties and biological activities. In this PhD project attention has been focused on 1,4-benzothiazines that form a class of compounds occurring in nature whose peculiar properties as illustrated in the following open the access to new classes of dyes with potential technological applications.

1.1.2 The 1,4-benzothiazines

A prominent position among naturally occurring N,S heterocyclic systems is occupied by 1,4-benzothiazines that form the key structural unit of pheomelanins the pigments responsible for the red hair phenotype, typically found in individuals of Celtic origin, with red hair pale skin, blue-green eyes and freckles. The chromophore exhibited by these pigments has been associated to the presence of the $\Delta^{2,2'}$-bi-(2*H*-1,4-benzothiazine), occurring in a group of low molecular weight pheomelanins termed trichrochromes[11] (**Figure 8**), but other benzothiazine containing structures within the pigment contribute to the intense absorption in the visible region.

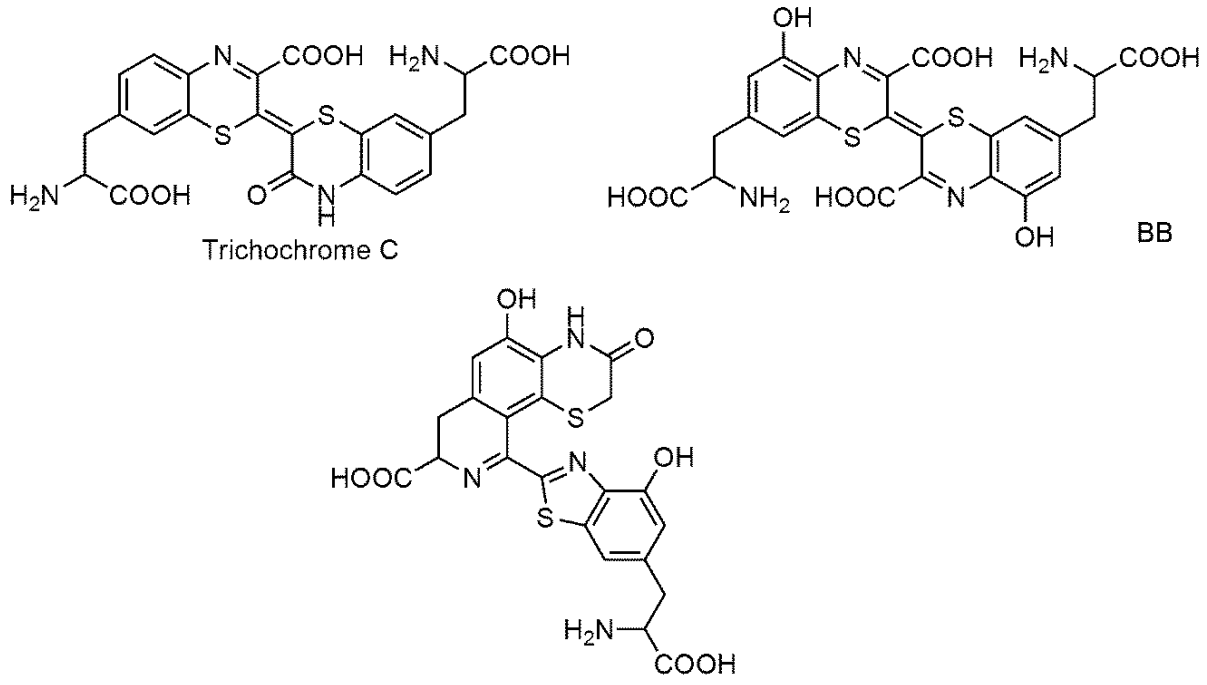

Figure 8. *Structure of some benzothiazine compounds responsible for the visible absorption in pheomelanin*

The absorption properties of the benzothiazine occurring in pheomelanins have been extensively investigated to define the commonly recognized role of these pigments to act as photosensitizer determining ultimately the enhanced susceptibility of red hair individuals to actinic damage[12,13].

In this PhD project the research activity has been focused on 1,4-benzothiazine systems starting from the $\Delta^{2,2'}$-bi-(2*H*-1,4-benzothiazine) chromophore exhibited by the natural pheomelanin pigments with the aim of exploring the access to new classes of dyes with potential technological applications. The role of the benzothiazine structural units in the biological function of pheomelanin pigment was also addressed. . Hence the results of the research work will be presented following these two main lines of research that is 1) new dyes based on the 1,4-benzothiazine system and 2) role of the 1,4-benzothiazine system in the properties of pheomelanin pigments.

1.1.2 Functional dyes

The quest of organic chromophores exhibiting tailored electronic features has been extremely active during the last decades. The term functional dyes first introduced in 1981 by a Japanese group has been increasingly used to refer to a variety of molecules that have been newly synthesized or re-appreciated because of their potential exploitation in high-technology (hi-tech) applications different from the well-known traditional applications.[14] Among such applications particular interest has been focused on optoelectronics, such as dye sensitized solar cells, photochromic materials, liquid crystal displays, and the newer emissive displays such as organic light emitting devices; electronic materials, such as organic semiconductors; imaging technologies, such as electrophotography (photocopying and laser printing), thermal printing, and especially ink-jet printing; “invisible” imaging by using infrared absorbers in optical data storage, computer-to-plate and security printing; biotechnology as dye-affinity chromatography for the purification of proteins and enzymes; biomedical applications, such as fluorescent sensors and anticancer treatments such as photodynamic therapy.

Typically, a number of different classes of molecules have been explored as sensitizers in dye sensitized solar cells to replace the Rutenium complexes that are highly expensive.[15] Such dyes feature one or more electron donating structure linked through a conjugated bridge to electron acceptors units as in the example shown in **Figure 9**:

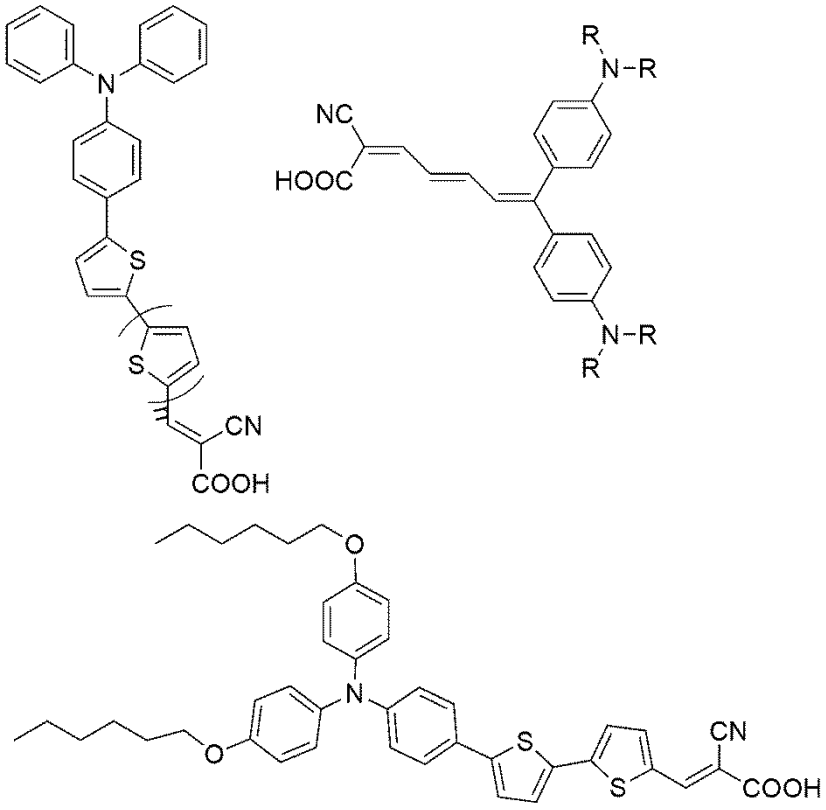

Figure 9. *Examples of structural classes designed for application as dye sensitized solar cells.*

Other fields in which the potential of functional dyes has been explored include hybrid materials from TiO_2 or SiO_2 nanoparticles and dyes exhibiting photochromic effects upon UV visible irradiation for applications in photocatalysis.[16] Organic/inorganic hybrids combining the chemical and thermal resistance properties of microporous mineral substrates and the color of the organic molecule have been explored to obtain stable and durable organic dyes; [17] inclusion in zeolites of solvatochromic dyes may provide highly sensitive vapour and chemical sensing tools. [18]

In all these fields biological chromophores representing the functional units of light harvesting systems or plant pigments have often been considered as a valuable inspiration or a starting basis in the design of the novel compounds. In addition to chemical stability and intense absorption in the visible region, the design of functional dyes is focused on single molecule or polymer systems exhibiting photochromic, solvatochromic properties or any change of the chromophoric properties associated to modification of external parameters or aggregation state.

The most widely investigated classes of organic photochromes are based on the ring opening/ring closure reactions in photoinduced electrocyclic reactions like in the case of dithienylethenes, spiropyran, spiroxazines, naphthopyrans. In these, the UV irradiation of the colorless forms results in the electrocyclic ring opening with generation of isomeric open forms merocyanines that are intensely colored because of their extended conjugation [19] ***(Figure10)***

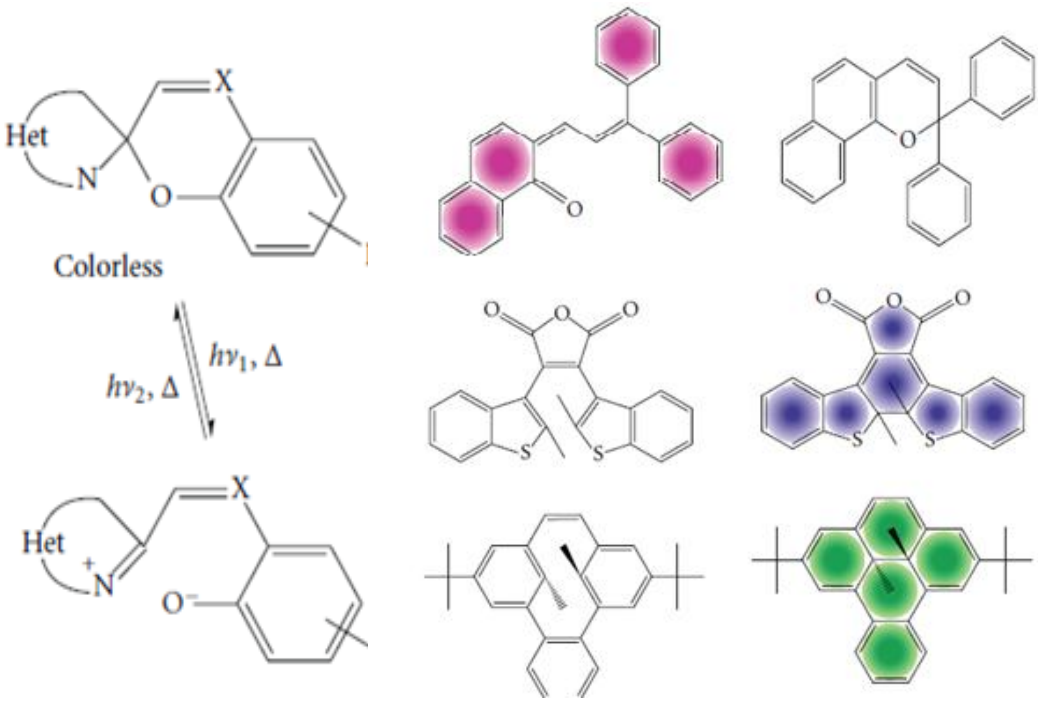

Figure 10. *Mechanism of photoinduced ring opening to merocyanine dyes and some representative examples of photochromic switch families.*

This property has several applications including implementation of optical data storage materials as shown in **Figure 11** for naphthopyran included into a rigid polymeric matrix [20].

Another example of photochromic compounds is provided by synthetic flavylium salts, benzopyrilium derivatives structurally close to anthocyanins. Their photochromism is based on the photoinduced trans cis isomerization reaction that produces the cis form that undergoes ring closure to form the flavylium form. The picture of **Figure 12** shows photochromic gels in the visible region prepared by the incorporation of flavylium salts in a gelator polymer . The chromophore switches from its yellow chalcone form to the red flavylium cation upon irradiation[21] .

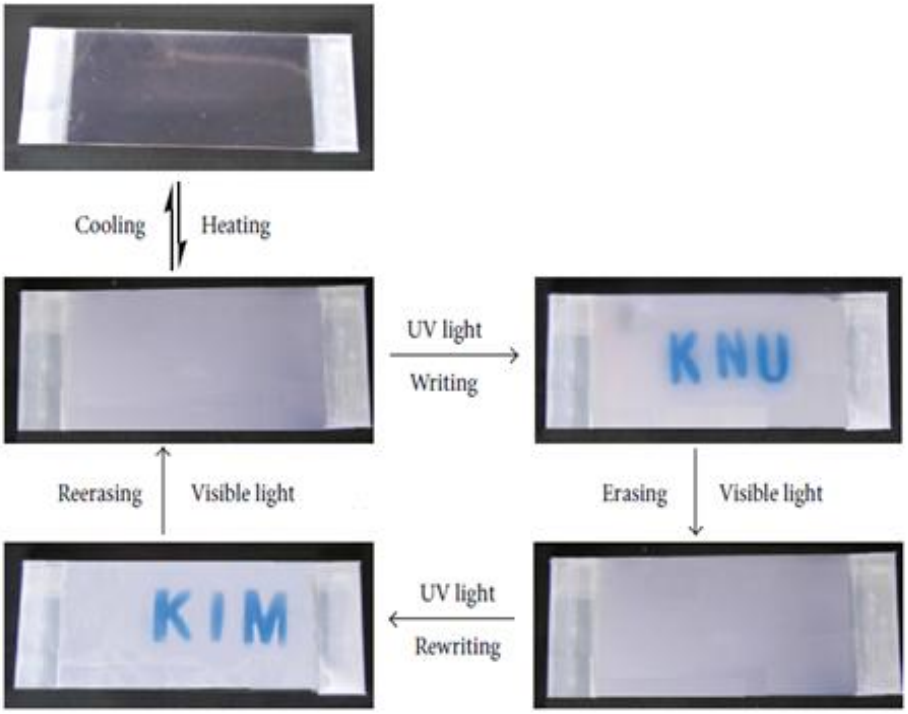

Figure 11. *Writing and erasing based on the reversible photochromism of a spiroxazine linked to a polymer matrix.*

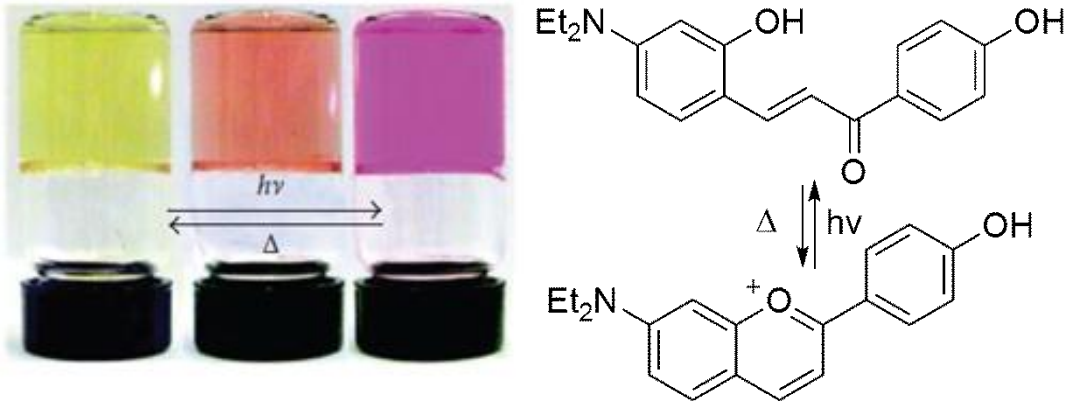

Figure 12 *Photochromic gels in the visible region obtained by incorporation of synthetic flavylium compounds into a polymeric gelator.*

1,10-fused ring phenothiazine dyes of the type shown in **Figure 13** have been proposed as new kind of solvent sensitive fluorescent dyes with unique sensitivity of strongly fluorescence in protic solvents than in aprotic solvents [22].

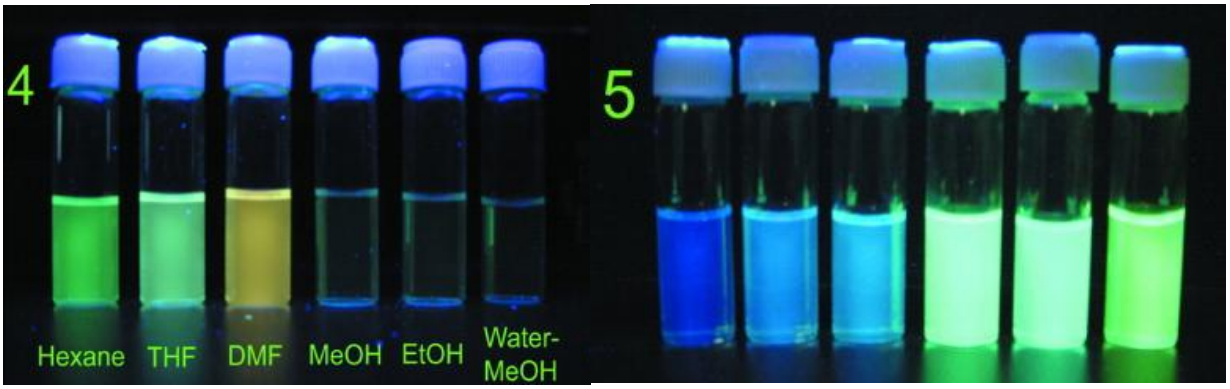

Figure 13.*Solvent sensitive fluorescent dyes from 1,10-fused ring phenothiazine dyes*

1.1.3 The indigo chromophore

A class of chromophoric systems of potential practical interest but so far little explored in materials science is represented by indigoid nitrogenous heterocycles. The indigo chromophore contains two donor X (S, or NH) and two acceptor groups (=O) arranged as shown to form a doubly cross-conjugated push pull system (**Figure 14**).

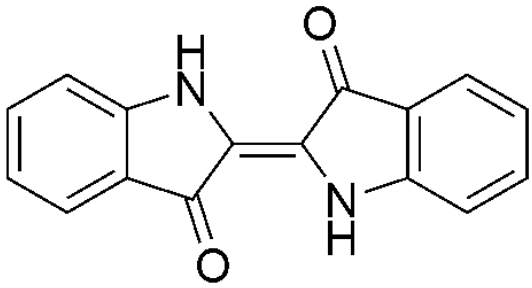

Figure 14. *The Indigo chromophore*

This class of cromophores includes indigo occurring in the Indigofera tinctoria in the form of the O-glucoside and the 6,6'dibromoindigo that is the tyrian purple, a secretion produced by certain species of predatory sea snails in the family of Muricidae, a type of rock snail by the name Murex The synthetic variant thioindigo is widely used for dying polyester fabrics.

1.1.4 The $\Delta^{2,2'}$-bibenzothiazine chromophore

The $\Delta^{2,2'}$-bi-(2*H*-1,4-benzothiazine) chromophore featured by trichochromes is closely related to indigo (**Figure 15**).

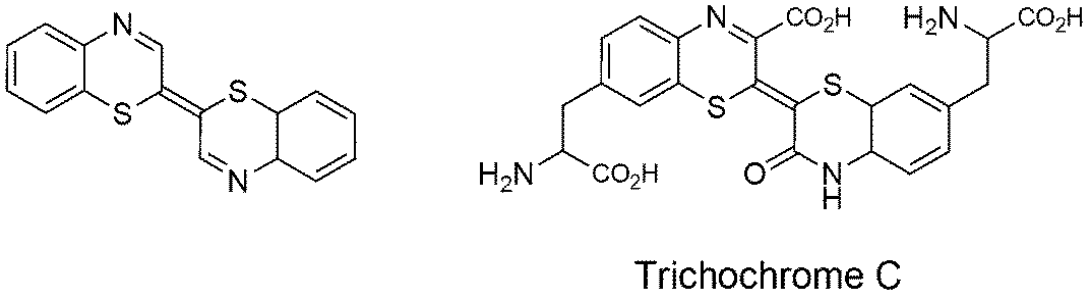

***Figure* 15.** *$\Delta^{2,2'}$-bi-(2H-1,4-benzothiazine) and trichochromes structures.*

In addition to 2*H*-1,4-benzothiazine, the trichochromes include also the 3-oxobenzothiazine ring system, which lowers the electron acceptor character of the imine group.

A significant pH dependence is observed for these chromophores, with a bathochromic shift from red to blue in acids. Such a marked shift would be a consequence of the peculiar disposition of the cross-conjugated push-pull systems which would be highly sensitive to protonation at the imine-type nitrogen(s) with consequent enhancement of the "pull" component (**Figure 16**).

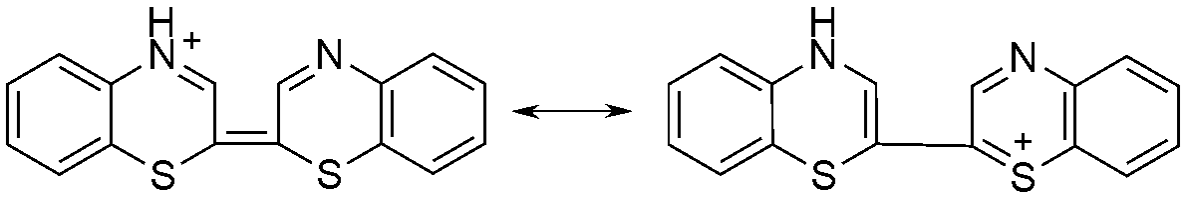

Figure 16. *Structure of the cation formed from $\Delta^{2,2'}$-bi-(2H-1 ,4-benzothiazine) system in acid.*

Such chromophores are highly tunable with marked chromophoric changes associated to the position and electron donor/acceptor character of the substituent on the benzene moiety.[23] (**Figure 17**)

In addition to the pH-dependence, the parent ring system exhibits marked photochromism under sunlight with reversible conversion in organic solvents of a yellow-orange species with abs max at 450 nm to a red one with abs max at 480 nm. Unambiguous structural characterization of the stable yellow species of unsubstituted $\Delta^{2,2'}$-bibenzothiazine by X-ray analysis was precluded by the failure to grow suitable crystals. However, although the X-ray diffraction spectrum of the 3-phenyl derivative indicated a cis configuration about the central double bond, it was assumed that the most stable form of bibenzothiazine was the trans isomer based on classic chemical arguments.[24] This conclusion has recently been supported by computational analysis of the chromophores.[25] The analogous dimer from 1,4-benzoxazine also exhibit photochromism associated to cis/trans isomerization but the shift of the wavelength absorbance is less marked (<20 nm) and has been so far reported only for the 3-substituted systems.[26]

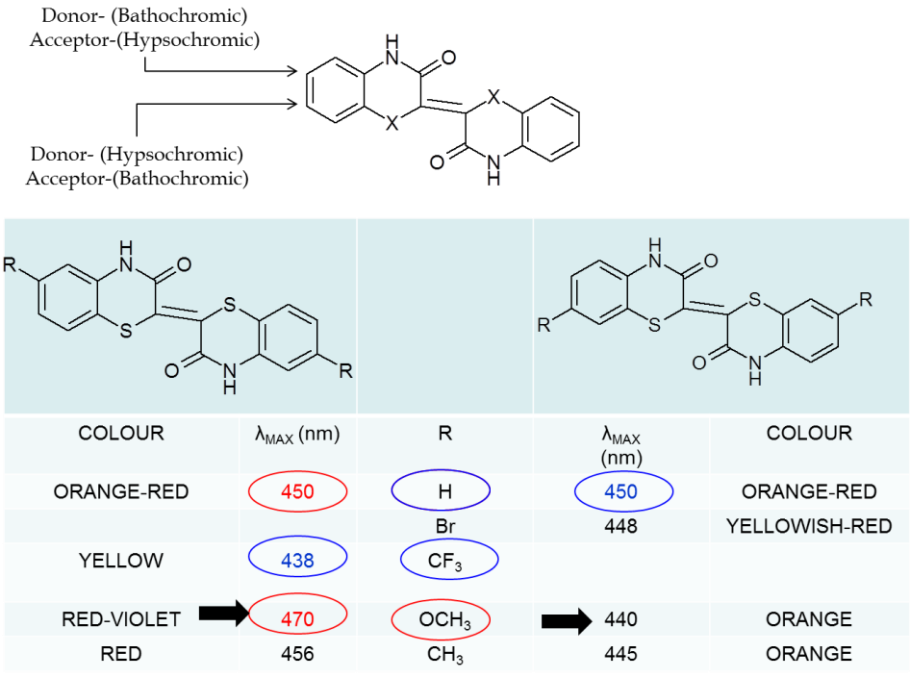

Figure 17. *Effect of substituents on the chromophore system of* $\Delta^{2,\ 2'}$*-bi-(3-oxo-2H-1,4-benzothiazine).*

1.1.5 The cyanine chromophore.

Another relevant chromophore based on a push pull system occurs in the cyanines comprising a group of red pigments of fruits and vegetables, the betacyanines, like betain occurring in red beet (*Beta vulgaris L.*) (**Figure 18**).

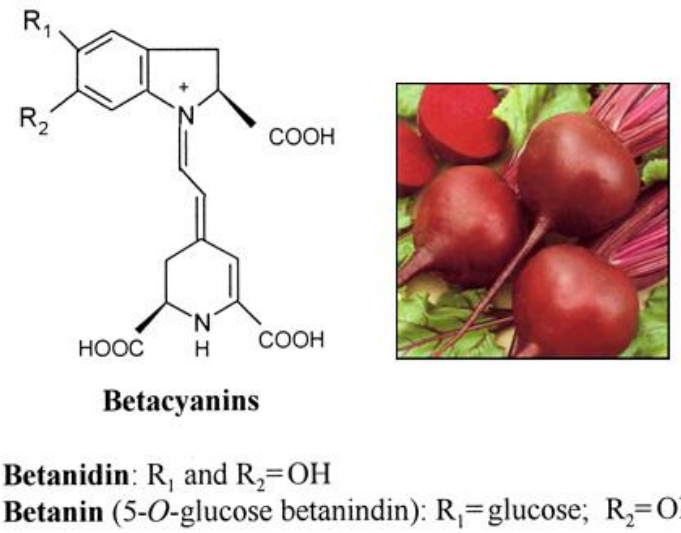

Figure 18 *Structure of betacyanins and their main natural source.*

The term cyanine is now used to refer to a broad class of dyes having organic nitrogen centers, one of the imine and the other of the enamine type, which may be included into an heterocyclic system, linked through a variable number of double bonds, also called the methyne chain, generally in the trans configuration (**Figure 19**). The most common heterocyclic systems that can be found in cyanine dyes, are quinoline, benzoquinoloine, benzimidazole, pyridine, benzothiazole, benzoxazole, indole, benzindole , etc.

Cyanine dyes are also called monomethine, trimethine, pentamethine and heptamethine, based on the for n= 0,1 ,2 and 3 respectively.

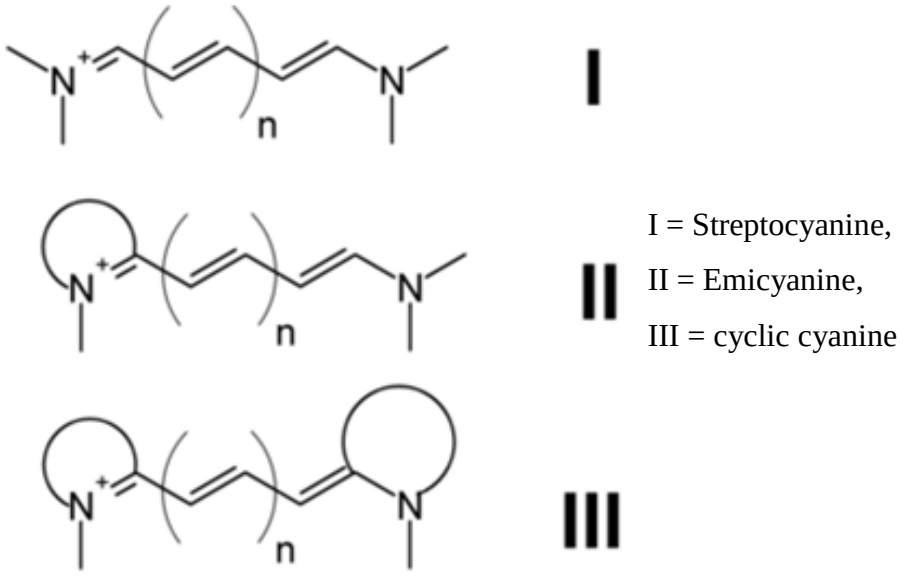

Figure 19. *Some groups of cyanines.*

Cyanine dyes have a relatively good stability, high molar absorption coefficients (~10^5 M^{-1} cm^{-1}) and medium fluorescence intensity.

For heterocyclic containing cyanine dyes, they can be also classified in symmetrical and unsymmetrical , if the nature of the aromatic groups connecting the ring structures joined by the

methine chain are not the same. A number of cyanine systems featuring symmetric or asymmetric scaffolds have been synthesized (**Figure 20**).

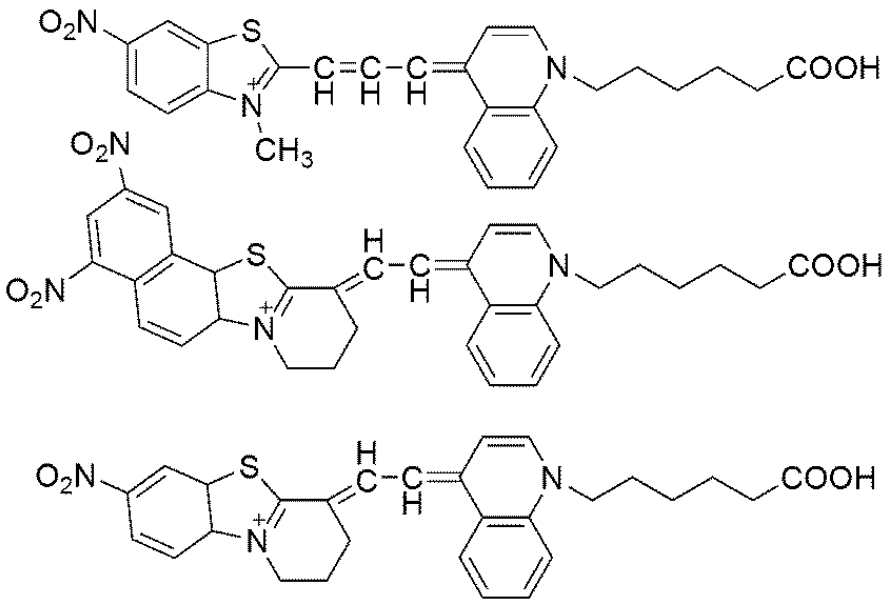

Figure 20. *Examples of asymmetric cyanines.*

Some of these cyanines, like the indoline cyanines are commercially available, and exhibit very high molar extinction coefficients (ranging from 150,000 to 250,000 $M^{-1}cm^{-1}$) and an intense fluorescence emission (**Figure 21**).

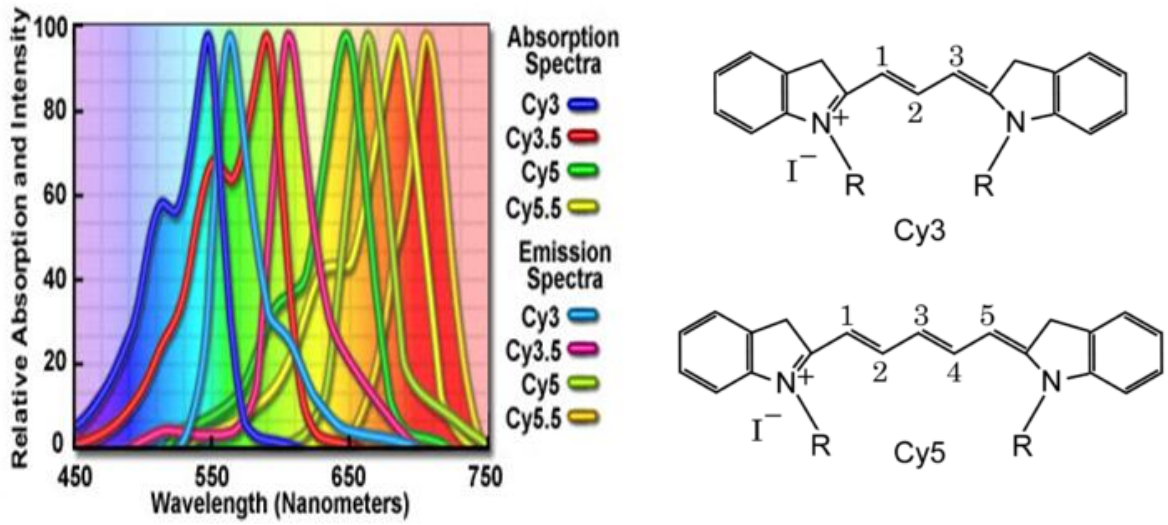

Figure 21. *Structure and absorption emission spectra of indoline cyanines.*

Because of these properties cyanine dyes are used in several fields including biology in the form of biomolecule conjugates (proteins, nucleic acids) to act as fluorescence reporters, laser technologies, as well as analytical applications. As an example, the acidichromism of a peculiar class of cyanines, the merocyanines has been exploited for the sensing of anions in organic solvents or water/organic solvents mixtures [27] (**Figure 22**)

Cyanine dyes can also be employed as sensitizers in DSSC , dye-sensitized solar cells[28] (**Figure 23**) , as an alternative to expensive heavy-metal-based polypyridil complexes, because of their large absorption coefficientes, easy preparation, low cost, with no need to use precious metal resources easy handling and the absorption spectrum can be finely tuned by tailoring their stuctures.

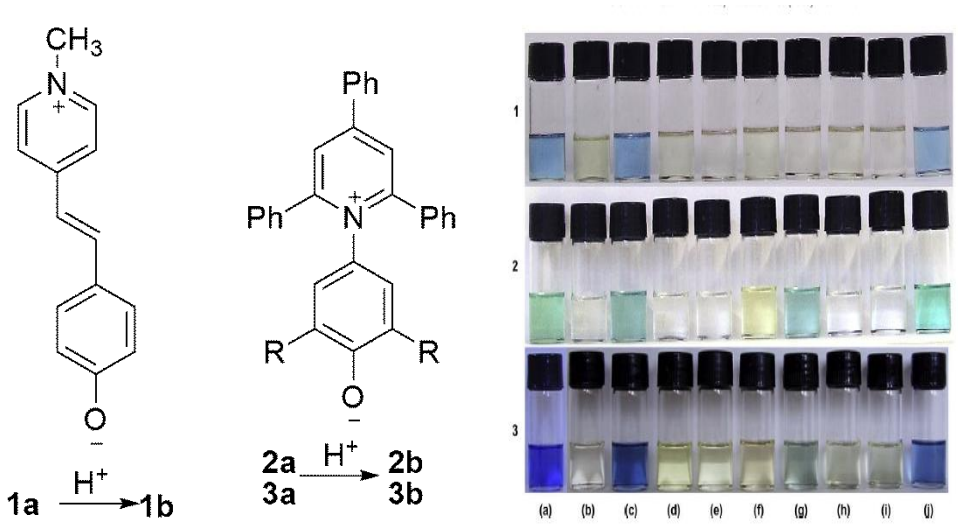

Figure 22. *Some merocyanine dyes and their color changes in the presence of different anions . Solutions in trichloromethane of (a) dyes 1a–3a, (b) 1b–3b, the protonated forms , and protonated dyes in the presence of (c) CN^- , (d) Cl^-, (e) Br^-, (f) I^-, (g) $H_2PO_4^-$, (h) HSO_4^-, (i) NO_3^-, and (j) F^-,as tetra-n-butylammonium salts.*

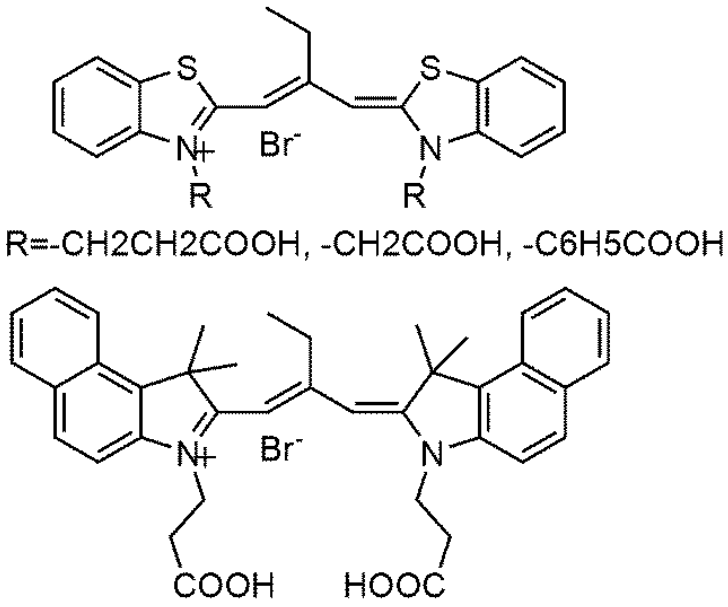

Figure 23. *Example of a cyanine dyes in DSSC*

1.2 Pheomelanin pigments: biogenesis and origin of the 1,4-benzothiazine structural units.

The pigments responsible for the red hair phenotype, pheomelanin, typically found in individuals of Celtic origin, with red hair pale skin, blue-green eyes and freckles, have always stimulated the curiosity of researchers. In recent years, interest in these pigments has been renewed by clinical data suggesting association of a fair complexion and red hair in Caucasians with an abnormal susceptibility to actinic damage and skin cancer [12,13]. The biogenetic relationship with the other more widely diffused group of epidermal melanin pigments, eumelanin ,determining black pigmentation was first recognized in the 1960s by Prota and Nicolaus[29], who proposed that red hair pigments might be formed in vivo by some deviation of the normal course of melanogenesis involving cysteine, which would have explained the common origin of dark and red melanins in melanocytes.

Yet, the factors controlling prevalence of either pathway have remained unclear for a long time. A fundamental breakthrough came in 1995 with the discovery that people with red hair display mutations in the human melanocortin 1 receptor (MC1R), similarly to what was seen in the case of mouse coat models.[30] The *mc1r* gene encodes a 317–amino acid G-coupled receptor, MC1R. Human *mc1r* sequence variants are associated with red hair and fair skin in the Caucasian population.[31-33] These variant alleles are extremely common and in northern European populations <50% of the *mc1r* genes encode the 'wild-type' or consensus protein. Three alleles in particular, Arg151Cys, Arg160Trp and Asp294His together make up 22% of the *mc1r* genes and account for 60% of all cases of red hair.[33] Thus, a single locus, can contribute significantly to human pigmentary variation.

In wild-type eumelanic subjects, MC1R activation induces eumelanin synthesis via tyrosinase activation (**Figure 24**). Among red haired individuals, homozygous for alleles of the *mc1r* gene

can be found, that show varying degrees of diminished function. The main consequence is a decrease in the amount of eumelanin pigments with prevalence of the pheomelanin variant. At the biochemical level, this change is the result of the drop in tyrosinase activity favoring the concomitant intervention of cysteine in the pathway.[34] Non-enzymatic addition of the SH group to the oxidation product of tyrosine, dopaquinone, leads to the formation of isomeric cysteinyldopas.[35-37] As a result, the intramolecular cyclization pathway of 5,6-dihydroxyindole formation leading to eumelanin polymers is inhibited, and an alternate 1,4-benzothiazine route to pheomelanins and trichochromes becomes dominant.

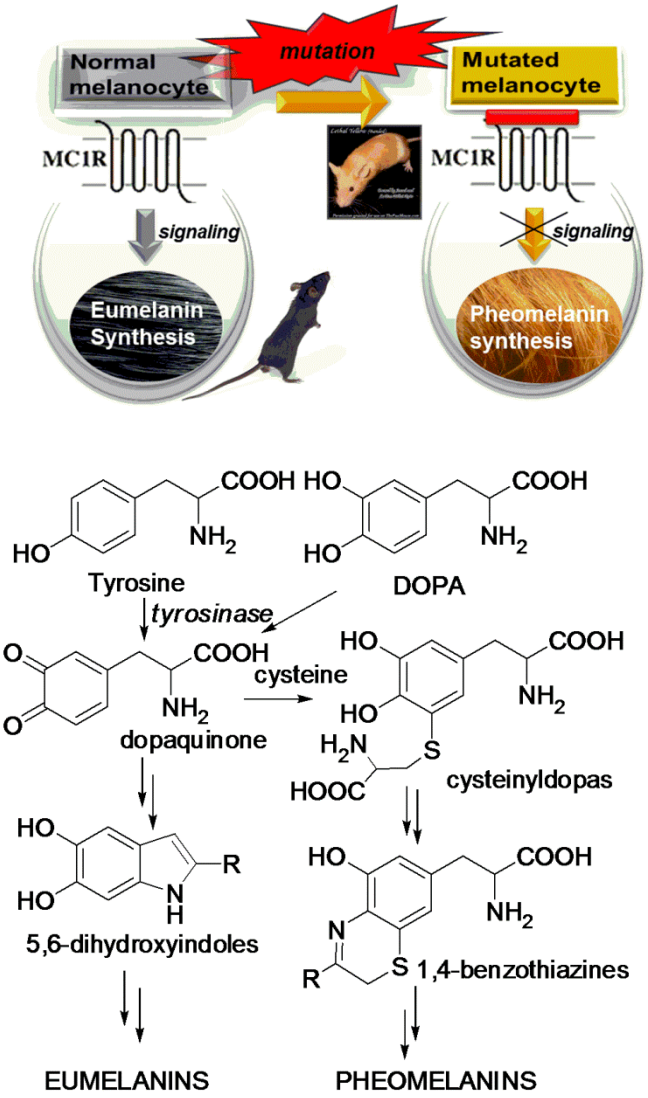

Figure 24. *The melanocortin 1 receptor (MC1R), the tyrosine/tyrosinase pathway and their role in human and mammalian pigmentation.*

In the later stages of pheomelanogenesis oxidation of 5SCD followed by intramolecular cyclization would then lead to the generation of a transient *o*-quinoneimine which can either undergo redox exchange with the parent cysteinyldopa to give a dihydrobenzothiazine or isomerize with or without concomitant decarboxylation to give 2*H*-1,4-benzothiazine derivatives (**Scheme 1**). Notably, when the reaction is carried out in the presence of zinc ions, decarboxylation of the quinoneimine is substantially inhibited, and the 3-carboxy derivative is the main product which persists in the reaction medium for relatively long periods of time due to the stabilizing effect of the metal.

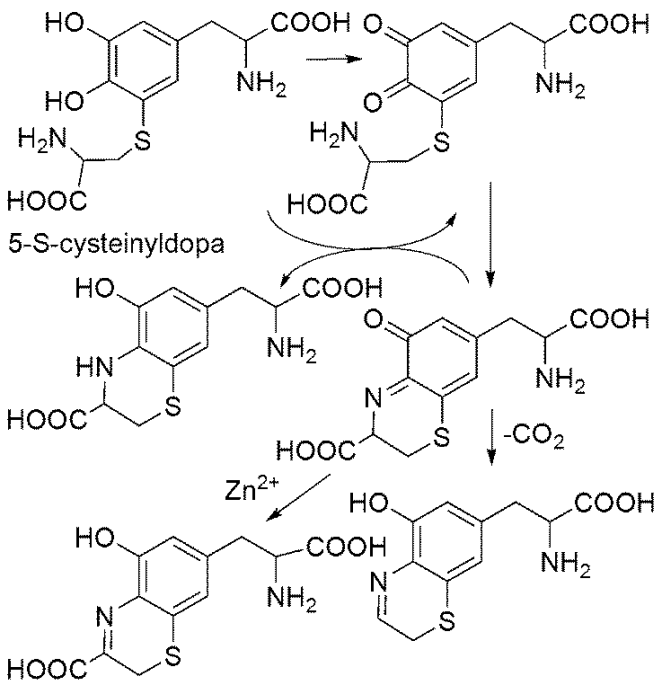

Scheme 1. *Origin of the benzothiazine system via intramolecular cyclization of cysteinyldopa.*

Just formed, the 2*H*-1,4-benzothiazine derivatives may follow diverse routes reflecting the presence or the absence of the carboxyl group on the 3-position, and the specific reaction conditions.

Scheme 2 illustrates the variety of structural scaffolds that have been identified by oxidative conversion of cysteinyldopa and/or of related 1,4-benzothiazines under different biomimetic conditions. Alkaline or hydrogen peroxide treatment of 1,4-benzothiazines leads to a stable 3-oxo derivative as in path *a*.[38-40] Complex oligomers like those indicated in path *b* are produced by peroxidase/H_2O_2 oxidation of cysteinyldopa after reductive treatment, suggesting formation of benzothiazine intermediates that would then couple through C-C and C-O bonds at the benzene moieties.[41]

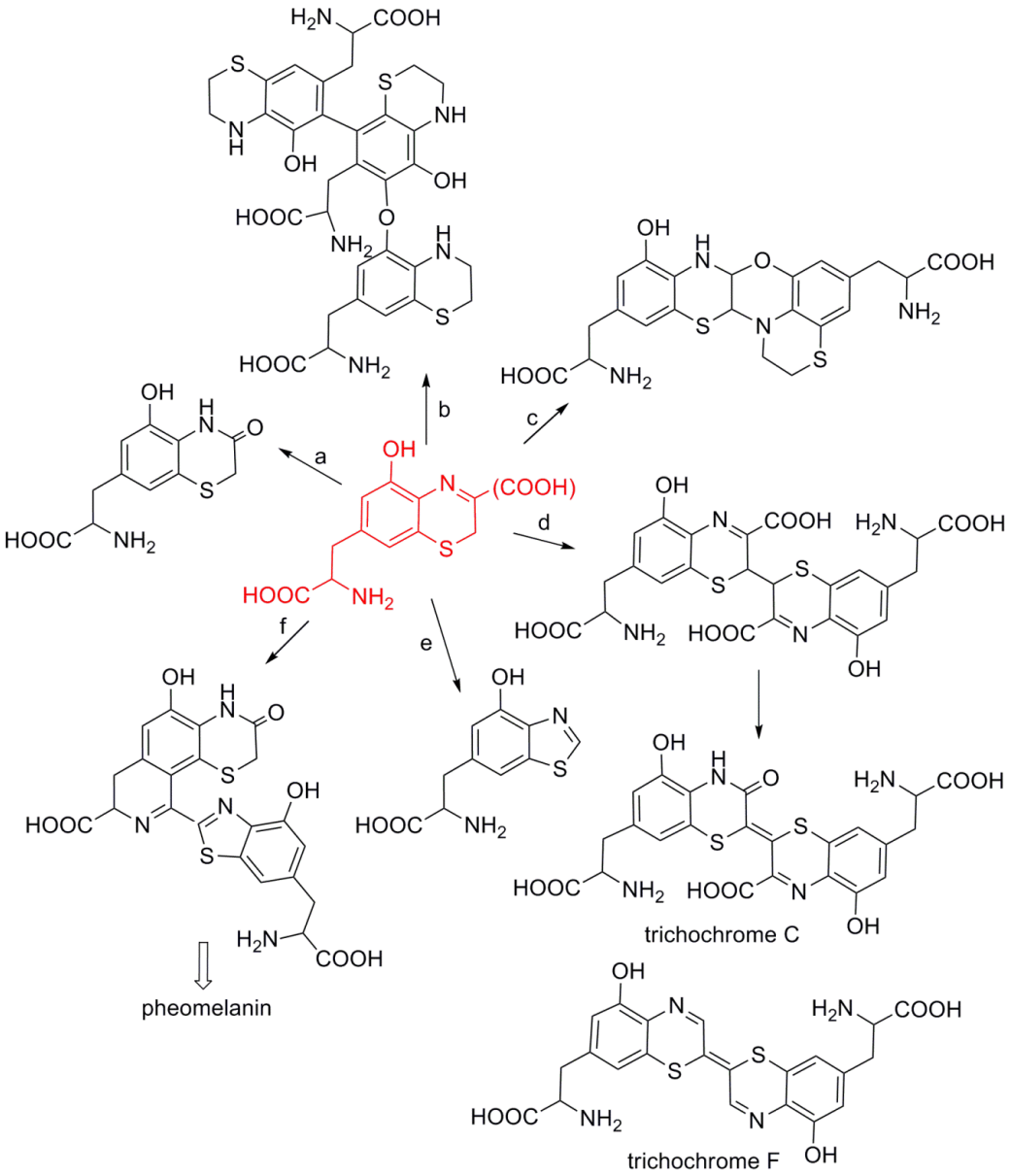

Scheme 2. *Overall view of the molecular scaffolds that may originate from biomimetic chemistry of 1,4-benzothiazine compounds*

Tyrosinase-catalyzed oxidation of cysteinyldopa follows an alternate pathway, as in *c*, in which an unusual cycloaddition process apparently takes place involving both benzothiazine and quinoneimine intermediates.[42] It should be noticed that routes *b* and *c* have so far been observed only in biomimetic chemical studies, so their interest would be mainly in relation to the reaction behavior of cysteinyldopa-derived benzothiazine systems rather than to a possible relevance to natural pheomelanin buildup. An intriguing oxidative dimerization process (path *d*) can be observed by spontaneous oxidation under mild condition.[43]

Further oxidative steps lead to unusual bibenzothiazine derivatives commonly referred to as the trichochromes. These latter comprise four main variants, two of which consist of symmetric bibenzothiazine derivative (trichochromes E and F) while the other two are mixed systems (trichochromes B and C).[11] The trichochromes were originally discovered in red human hair and are known to arise from cysteinyldopas, mainly the 5-*S*-isomer, but their mode of formation, the direct precursors and actual biological relevance remain little defined. Trichochrome formation by oxidation of 5-*S*-cysteinyldopa has been reported to be a minor process which is dramatically enhanced under strongly acidic, non-natural conditions, suggesting a possible artifactual generation under the harsh acidic conditions used for pheomelanin extraction from red hair. Model studies[43] showed that trichochrome generation from 5-*S*-cysteinyldopa is favored in the presence of zinc ions, which are typically found in skin and hair, suggesting a possible role of this metal *in vivo*.

By far, one of the most typical, chemically and biologically relevant characteristic of the 2*H*-1,4-benzothiazines is their tendency to undergo ring contraction either spontaneously or following UV irradiation to give benzothiazole products as in path *e*.

Facile conversion to benzothiazoles is an important feature of benzothiazine chemistry. Pending mechanistic issues should incite investigation of this transformation which is triggered or mediated by a variety of factors including UV light, oxidizing agents, metal cations.

1.2.1 Photochemical properties of pheomelanin

Although extensive epidemiological and biological studies over more than half a century have shown that mutation at several pigmentation genes is involved in predisposition to skin cancer and melanoma,[44] red hair and a fair complexion associated with high levels of pheomelanins have traditionally been regarded as a most important risk factor.[45] This familiar observation has prompted intense studies aimed to understand the (photo)chemical behavior of pheomelanins and to assess the possible causal role of these pigment in UV susceptibility and skin cancer development. A commonly held view is that pheomelanins may act as potent UV photosensitizers leading to intense production of reactive oxygen species (ROS) which contribute directly to the increased susceptibility of red haired individuals to actinic damage and skin cancer. This concept was pioneered by Chedekel et al.[46] and has spurred unabated interest in the photochemical and photobiological properties of pheomelanins.[47-50]

Experiments on congenic mice of black, yellow, and albino coat colors after exposure to predominantly UVB (280–320 nm) or UVA (320–400 nm) radiation have shown that pheomelanin had 3-fold greater specific activity in photosensitizing adjacent cells to caspase-3 independent apoptosis, and this occurs at a frequency greater than the apoptosis induced by UV absorption on DNA.[50]

Simon and coworkers demonstrated that different molecular components may be involved in the transient absorption, emission and oxygen photoconsumption responses of pheomelanin.[51-53] Moreover, pheomelanin-containing melanosomes from human hair were shown to display low photo-ionization threshold values relative to eumelanins[54] supporting a possible role of pheomelanins in the onset of UV-induced skin cancer in redheads.

The characteristic absorption and photochemical properties of pheomelanins are generally attributed to ‘‘benzothiazine’’ structural units derived biogenetically from 5-S-cysteinyldopa.

This notion, however, conveys little or no information about the structural chromophores responsible for the photoreactivity of pheomelanins.

At pH 7.4, natural and synthetic pheomelanins show a defined maximum around 305 nm, which is not affected by reductive treatment with sodium borohydride, and a monotonic decrease in the absorption in the range 350–550 nm. These features are not compatible with a significant proportion of structural units related to 2H-1,4-benzothiazine and 2H-1,4-benzothiazine-3-carboxylic acid, the early borohydride reducible pheomelanin precursors featuring absorption maxima above 340 nm. Rather, these features would better accommodate a contribution by the nonreducible 3-oxo-3,4-dihydrobenzothiazine (λ_{max} 299 nm) and benzothiazole (λ_{max} 303 nm) structural motifs, which are generated in the later stages of pheomelanogenesis in vitro.

Recently, the first ultrafast absorption spectroscopy measurements for synthetic pheomelanin have been reported, and have highlighted the fast generation of a transient species with an absorption maximum centered at 780 nm[55]. This species has been attributed to a photoexcitation product whose action spectrum peaks in the range between 350 and 360 nm, thus resembling the reported absorption spectrum of benzothiazines. It was argued that the reactive chromophore of pheomelanins is of low molecular weight but is present and exhibits similar photophysics in the aggregated state, and may be adequately described in terms of ‘‘benzothiazine’’ structural motifs which are biogenetically derived from the key pigment precursor, 5-S-cysteinyldopa[56].

It must be noted, however, that the occurrence of benzothiazine units in the pheomelanin backbone is largely a matter of surmise, and has so far lacked direct and unambiguous experimental support. Moreover, the term ‘‘benzothiazine’’ is commonly associated with a broad range of structural motifs which exhibit however different chromophoric features. Nonetheless, this notion has become a central axiom in pheomelanin research and has in part been built upon the identification of trichochromes, featuring the peculiar $\Delta^{2,2}$-bi(2H-1,4-benzothiazine) skeleton[11] . The configuration of the double bond in these pigments and the associated chromophoric features have recently been reexamined by computational analysis[25] . Similar to

pheomelanins, trichochromes exhibit a marked photoreactivity and the possibility to access to multiple electronic states upon UV and visible photoexcitation [57].

Though commonly cited among the primary determinants of the red colorations of hair in the true ‘‘pheomelanic’’ phenotype, the trichochromes themselves have been a subject of controversy and even their actual occurrence in human hair tissues has been questioned. In fact, trichochrome formation by oxidation of 5-S-cysteinyldopa has been reported to be a minor process which is dramatically enhanced under strongly acidic, non natural conditions, suggesting a possible artifactual generation under the harsh acidic conditions used for pheomelanin extraction from red hair[58].

1.2.2.Pheomelanin in the dark

A further issue of great relevance to the mechanisms of toxicity associated to pheomelanic pigmentation has recently been disclosed by a series of papers that claimed identification of UV - independent pathway for the induction of melanoma.[59-62] Actually, compelling evidence for a direct relationship between sun exposure and melanoma is still missing, and issues have been raised of why, at variance with other forms of skin cancer, melanoma is not restricted to sun-exposed areas of the body, and ultraviolet radiation signature mutations are infrequently oncogenic drivers. Experiments have been described showing that induction of an activating mutation in the melanoma oncoprotein kinase BRAF into red mice carrying an inactivating mutation in the *Mc1r* gene resulted in a high incidence of invasive melanomas in the absence of UV stimulation[44]. Moreover, the same study demonstrated that the skin of pheomelanic mouse contained higher levels of oxidative DNA and lipid damage than albino-*Mc1re/e* mouse skin. These data clearly showed a strong association between pheomelanin and oxidative stress; however the actual mechanisms implicated in pheomelanin-induced UV-independent oxidative stress, DNA damage and melanomagenesis have remained unclear. In a related paper[62] two

possible not mutually exclusive pathways by which the pheomelanin pathway could mediate oxidative stress and melanomagenesis were postulated:

1) although pheomelanin is not located in the nucleus, it might cause damage by promoting the formation of ROS which could overwhelm cellular antioxidant reserves and cause oxidative damage to biomolecules including free nucleobases in the cytosol;

2) the pheomelanin biosynthetic pathway depletes cysteine-based cellular antioxidants making the cell more vulnerable to elevated ROS levels. A hint to the peculiar properties of pheomelanins in the dark was provided by a recent work showing that synthetic pheomelanins can behave as pro-oxidant promoting formation of melanin pigments from catecholamines and dopa, a process requiring the presence of oxygen.[63]

2.Methods

The research work developed during this PhD project was carried out also through several collaborations with other research groups. The different experimental and computational methodologies that were used and led to the results presented in this thesis are briefly summarized in the following

2.1 EPR spectroscopy

Electron paramagnetic resonance spectroscopy (EPR) is a powerful tool for investigating paramagnetic species, including organic radicals, inorganic radicals, and triplet states. The basic principles behind EPR are very similar to the more ubiquitous nuclear magnetic resonance spectroscopy (NMR), except that EPR focuses on the interaction of an external magnetic field with the unpaired electron(s) in a molecule, rather than the nuclei of individual atoms.

From an applicative point of view almost all pure substances contain magnetic nuclei and are thus accessible to NMR spectroscopy, while only few pure substances contain unpaired electrons and are thus accessible to EPR spectroscopy. This is because chemical binding is based on electron pair formation with spin cancellation. Most stable compounds are thus diamagnetic, while the compounds that can be seen by EPR have to be paramagnetic.

As known, a molecule or atom has discrete states, each with a corresponding energy. The energy differences between the atomic or molecular states is what is being measured in a spectroscopic experiment. It is possible to measure these energy differences, ΔE, according to Planck's law, which states that electromagnetic radiation will be absorbed if:

$$\Delta E = hn$$

where h is Planck's constant and n is the frequency of the radiation. The absorption of energy causes a transition from the lower energy state to the higher energy state.

The energy differences studied in EPR spectroscopy are predominately due to the interaction of unpaired electrons in the sample with a magnetic field produced by a magnet . This effect is called the Zeeman effect. Because the electron has a magnetic moment, it acts like a bar magnet when you place it in a magnetic field, B_0. It will have a state of lowest energy when the moment of the electron, μ, is aligned with the magnetic field and a state of highest energy when μ is aligned against the magnetic field. The two states are labeled by the projection of the electron spin, M_s, on the direction of the magnetic field. Because the electron is a spin ½ particle, the parallel state is designated as $M_s = - ½$ and the antiparallel state is $M_s = + ½$. From quantum mechanics, the most basic equations of ESR is obtained:

$$E = g\mu_B B_0 M_S = \pm ½ g\mu_B B_0$$

and

$$\Delta E = hn = g\mu_B B_0$$

g is the g-factor, which is a proportionality constant and equal to 2.0023 for most samples, but which varies depending on the electronic configuration of the radical or ion. μ_B is the Bohr magneton, which is the natural unit of electronic magnetic moment.

Because the energy differences between the two spin states can be changed by varying the magnetic field strength, there are alternative means to obtain spectra. It is possible to apply a constant magnetic field (**Figure 25)** and scan the frequency of the electromagnetic radiation as in conventional spectroscopy. Alternatively, it is possible to keep the electromagnetic radiation

frequency constant and scan the magnetic field. A peak in the absorption will occur when the magnetic field tunes the two spin states so that their energy difference matches the energy of the radiation. This field is called the field for resonance.

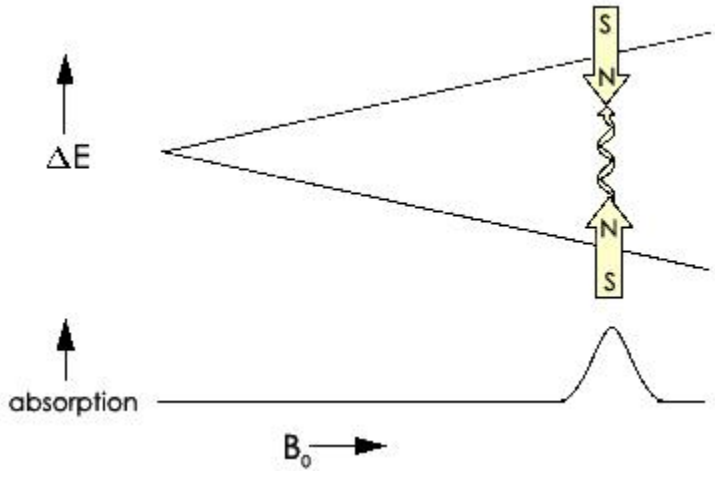

Figure 25. *Variation of the spin state energies as a function of the applied magnetic field .*

The field for resonance is not a unique fingerprint for identification of a compound because spectra can be acquired at several different frequencies. Being independent of the microwave frequency, the g-factor $g = h\nu/(\mu_B B_0)$ is much better for that purpose.

Measurement of g-factors can give us some useful information; although it does not tell us much about the molecular structure of our sample. However, the unpaired electron, which gives the ESR spectrum, is very sensitive to its local surroundings. The nuclei of the atoms in a molecule or complex often have a magnetic moment, which produces a local magnetic field at the electron. The interaction between the electron and the nuclei is called the hyperfine interaction. It gives us a wealth of information about our sample such as the identity and number of atoms which make up a molecule or complex as well as their distances from the unpaired electron.

Figure 26 depicts the origin of the hyperfine interaction. The magnetic moment of the nucleus acts like a bar magnet and produces a magnetic field at the electron, B_1. This magnetic field opposes or adds to the magnetic field from the laboratory magnet, depending on the alignment of the moment of the nucleus.

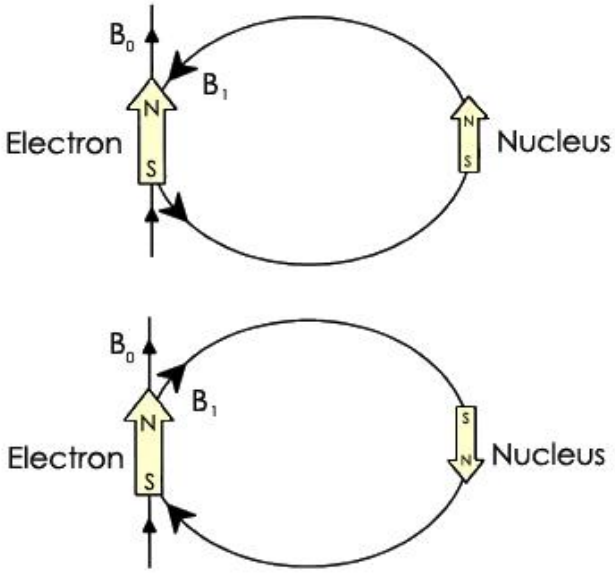

***Figure 26**. Local magnetic field at the electron, B_1, due to a nearby nucleus .*

When B_1 adds to the magnetic field, we need less magnetic field from our laboratory magnet and therefore the field for resonance is lowered by B_1. The opposite is true when B_1 opposes the laboratory field. For a spin ½ nucleus such as a hydrogen nucleus, it is possible to observe that the single EPR absorption signal splits into two signals which are each B_1 away from the original signal, as shown in **Figure 27**.

If there is a second nucleus, each of the signals is further split into a pair, resulting in four signals. For N spin 1/2 nuclei, 2^N ESR signals will be generally observed. As the number of nuclei gets larger, the number of signals increases exponentially. Sometimes there are so many signals that they overlap and we only observe the one broad signal.

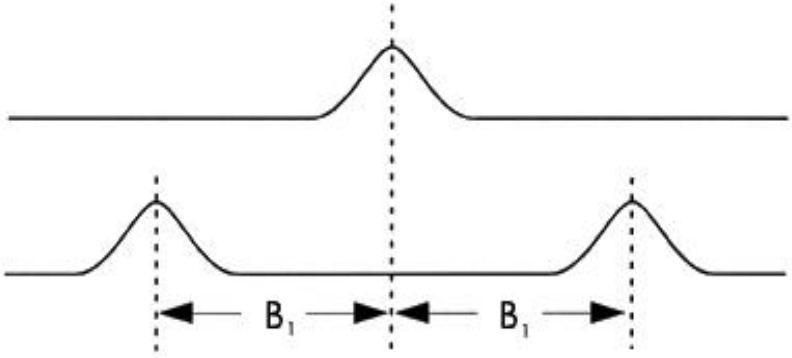

Figure 27. *Splitting in an ESR signal due to the local magnetic field of a nearby nucleus .*

An EPR spectrometer is composed by four fundamental elements: i. a monochromatic microwave source; ii. a waveguide for guiding the microwave power to the sample; iii. a cavity designed to ensure a proper coupling between the sample and the incoming wave; iv. a detector for microwave power to detect the response of the sample to microwave irradiation. A schematic drawing of an ESR spectrometer is represented in **Figure 28.**

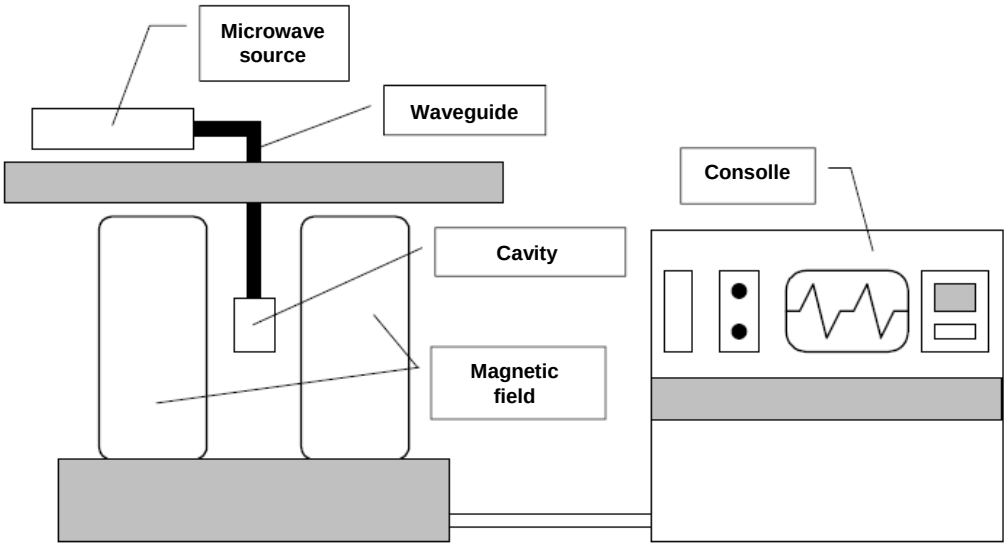

Figure 28. *Schematic representation of an ESR spectrometer.*

The magnetic field is generated by an electromagnet, usually water-cooled, which is able to provide a stable and uniform field in the area where the sample is placed. The microwave source can be a gunn diode or a klystron; in both cases, a microwaves beam is generated at a

fixed frequency between 9 and 10 GHz (X-band). This generated microwave beam goes to the sample and is then sent through the waveguide. The cavity, in which the sample is placed, is at the center of the two magnetic field poles and receives the microwaves through the waveguide. The cavity is designed in order to get inside a regular distribution of the magnetic field lines generated by the electromagnetic radiation coming from the source and perpendicular to the static magnetic field generated by a solenoid. Finally, the "consoles" is the interface between the spectrometer and the user from which it is possible to make all the settings and set the parameters for the spectra recording.

In this PhD project , some EPR measurement were needed in order to identificate radical intermediates or to characterize radical species. These experiments were carried out in collaboration with both Dr. Gerardino D'Errico of the Dept. of Chemical Sciences of University of Naples "Federico II" and Dr. Luca Valgimigli of the Department of Chemistry "Ciamician", University of Bologna.

In detail the EPR experiments carried out in Bologna were as follows:

X-band EPR spectra were collected at 298 K in a CW spetrometer equipped with a variable temperature unit, after mixing a solution of the sample in open (presence of atmospheric oxygen) suprasil quartz bulbe with 1 mm i.d. To increase S/N ratio up to 8 spectra were accumulated and digitally averaged.

Whereas the measurement performed in Neaples were recorded using a Bruker spectrometer. The instrumental settings were as follows: sweep width, 160.0 G; resolution, 1024 points; modulation frequency, 100.00 kHz; modulation amplitude, 5.0 G. The amplitude of the field modulation was preventively checked to be low enough to avoid detectable signal overmodulation. EPR spectrum was measured with a microwave power of 6.394 mW to avoid microwave saturation of resonance absorption curve. Several scans, typically 128, w ere accumulated to improve the signal-to-noise ratio.

2.3 Computational analysis

The computational analysis needed in this PhD project were performed by Professor Orlando Crescenzi of the Dept. of Chemical Sciences of University of Naples "Federico II". All calculations were performed with the Gaussian package of programs.[64] Geometry optimizations were carried out at the DFT level, with a hybrid functional (PBE0)[65] and a reasonably large basis set [6-31+G(d,p)]. For each species, different tautomers/conformers were explored. Computations were performed either in vacuo, or by adoption of a polarizable continuum medium (PCM) [66] to account for the influence of the solution environment. In view of the faster convergence, a scaled van der Waals cavity based on universal force field (UFF) radii[67] was used, and polarization charges were modeled by spherical Gaussian functions[68]. Vibrational-rotational contributions to the free energy were also computed. Additional energy computations were performed for the neutral form in vacuo at the MP2 level with different basis sets, and at the CBS-QB3 level. UV/Vis spectra of the main species were computed in vacuo or in solution using the time-dependent density functional theory (TD-DFT) approach[69], with the PBE0 functional and the 6-311++G(2d,2p) basis set. To produce graphs, transitions below 5.6 eV were selected, and an arbitrary Gaussian line width of 0.15 eV was imposed; the spectra were finally converted to a wavelength scale. NMR shielding tensors were computed within the Gauge-Including Atomic Orbitals (GIAO) ansatz[70] at the PBE0/6-311+G(d,p) level. Computed isotropic shieldings were converted into chemical shifts using as reference the values obtained at the same level for benzene.

2.3 Time-resolved fluorescence

During my three month visit at the Department of Chemical Physics at Lund University in Sweden , I carried out different experiments on a number of samples, in order to investigate their excited state behavior. This work, in collaboration with Professor Villy Sundstrom and Amal El-Nahhas, allowed me to learn the basic principles underlying time-resolved fluorescence measurement and to familiarize with the advanced laser instruments of the LLC (Lund Laser Center) .

Here are some details about the streak camera,the detector used for the time-resolved experiments

The streak camera is an ultra high-speed detector which captures light emission phenomena occuring in extremely shorttime periods. It measure ultra-fast light emitting phenomena and delivers intensity vs time vs positions (or wavelength) information. No other instruments which directly detect ultra-fast light phenomena have better temporal resolution than the streak camera.

Since the streak camera is a two dimensional device, it can be used to detect several tens of different light channels simultaneously. For example, used in ombination with a spectroscope, time variation of the incident light intensity with respect to wavelength can be measured (time resolved spectroscopy). Used in combination with proper optics, it is possible to measure time variations of the incient light with respect to position (time and space-resolved measurement)

The operating principle of the streak camera is described in **Figure 29**. The light being measured passes through a slit and is formed by the optics into a slit image on the pjhotocatode of the streak tube.At this point , four optical pulses which vary slightly in terms of both time and space, and which have different optical intensities, are input through thes slit and arrive at the photocatode

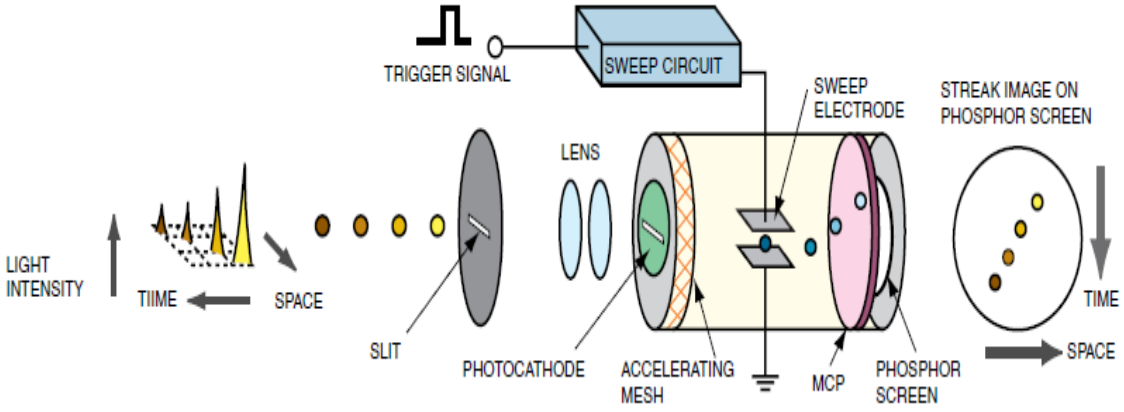

Figure 29. *The operating principle of the streak camera*

The incident light on the photocatode is converted into a number of electrons proportional to the intensity of the light, so that these four optical pulses are converted into a number of electrons proportional to the intensity of the light, so that these foir optical pulses are converted sequentially into electron, where they are accelerated and bombarded against a phosphor screen. As the electrons produced from the four optical pulses pass between a pair of sweepo electrodes, high voltage is applied to the sweep electrodes at a timing synchronized to the incident light **Figure 30** . This initiates a high-speed sweep (the electrons are swept from top to bottom). During the high speed-sweep, the electrons, which arrive at slightly different times, are deflected in slightly different angles in the vertical direction, and enter the MCP (micro-channel plate).

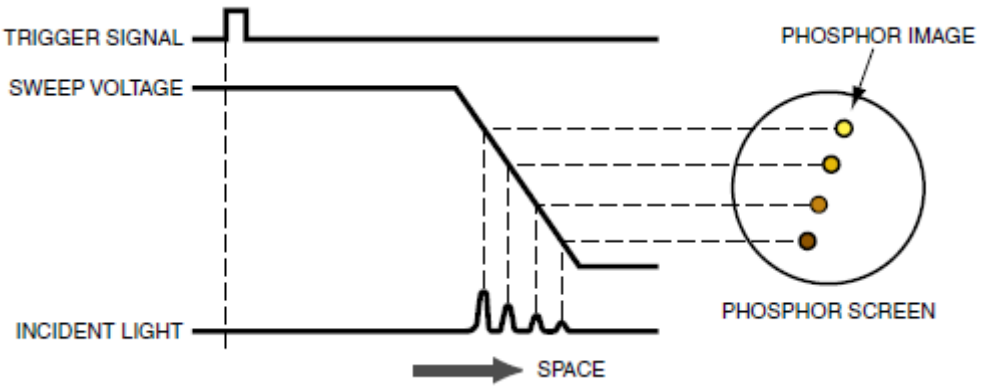

Figure 30. *Operation timing at the time of sweep*

As the electrons pass the MCP, they are multiplied several thousand of times, after which they

impact against the phosphor screen, where they are converted again into light.

On the phosphor screen, the phosphor image corresponding to the optical pulse which was the earliest to arrive is placed in the uppermost position, with the other images being arranged in sequential order from top to bottom, in other words, the vertical direction on the phosphor screen serves as the time axis. Also, the brightness of the various phosphor images is proportional to the intensity of the respective incident optical pulses. The position in the horizonthal direction of the phosphor image corresponds to the horizontal location of the incident light.

In this way, the streak camera can be used to convert changes in the temporal and spatial light intensity of the light being measured into an image showing the brightness distribution on the phosphor screen. Thus, the optical intensity from the phosphor image can be found, and the time and the incident light position from the location of the phosphor image.

The main features of a streak camera are :

1)Simultaneous measurement of light intensity on both the temporal and wavelength axis. By positioning a multichannel spectroscope in front of the slit (for incident light) of the streak camera, the spatial axis is reckoned for the wavelength axis . This enables changes in the light intensity on the various wavelengths to be measured (timeresolved spectroscopy)

2) High temporal resolution of less of 0.2 ps. Thisvalue corresponds to the time it takes for light to advance 0.06 mm
3) A wide range of phenomena can be measured simply by replacing the modular sweep unit
4) A streak tube detector can be selected to match any wavelength range from X-rays to near infrared rays
5) It has ultra high sensitivity. Th streak tube converts light into electrons , and then multiply it electrically. By this , it can measure faint light phenomena not to be seen by the human eye. This enables monitoring of extremely faint light , even single photoelectron can be detected

6)A dedicated readout system is available which allows images recorded by the streak camera,

that is streak images, to be displayed on video monitor and analyzed in real time.

The basic system configuration of the streak camera is rapresented in **Figure 31.** To be able to detect fast phenomena, the streak camera needs a trigger section and a readout section.

The trigger section controls the timing of the streak sweep and has to be adjusted so that the sweep is initiated when the light being masured arrives at the streak camera. For this purpose, a dalay unit is used which controls how long the trigger signal which initiates the streak sweep is delayed.Also a frequency divider is used, that divides the frequency of the external trigger signal if the repetition frequency of the trigger signal is too high. Also, in cases where the trigger signal cannot be produced from the devices such as a laser, it has to be produced from the light being meseaured itself, and this requires a PIN photodiode.

The readout section reads and analyzes streak images produced onn the phosphor screen , which is on the output side of the streak camera. Because the streak image is faint and disappears in an instant, a high sensitivity camera is used.

In addition to the units which make up this basic configuration, there are spectroscopes, optics and other peripheral equipments which can be used depending on each applications.

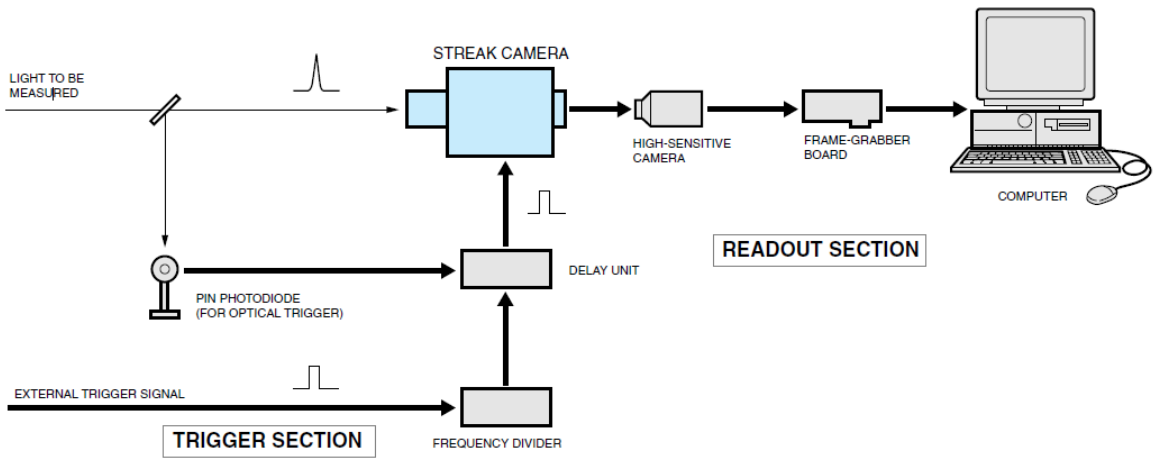

Figure 31. *Basic system configuration of the streak camera*

The experiments that were carried out at LLC in Lund university were as follws:

Time resolved fluorescence data were collected using a Hamamatsu streak camera C6860 device coupled to a Chromex spectrograph. The temporal resolution varied between ~10 to 60 ps depending on the investigated time range. The 266 nm laser beam used to excite the sample was generated by frequency tripling 150 fs, 800 nm, Ti:Sa pulses at a repetition rate of 82 MHz (Spectra-Physics, Tsunami). The laser beam was focused on the sample in a 2 mm rotating quartz cuvette. Fluorescence was collected at magic angle using two 1-inch diameter 50 mm focal length quartz lenses and focused on the spectrograph. All time-resolved fluorescence measurements were performed at room temperature (20 ± 1°C), under aerated conditions.

3.Results and Discussion

3.1 Photochromism and acidichromism of $\Delta^{2,2}$-Bi-(2H-1,4-benzothiazine)

3.1.1 Background

As a first approach to develop new benzothiazine-based dyes that could be exploited in various applications, the $\Delta^{2,2'}$-bi-(2*H*-1,4-benzothiazine)[11] system (BBTZ) the core structural unit of low molecular weight pheomelanin pigments trichochromes[71], characterized by an intriguing photochromic and pH-dependent chromophore[24] was revisited.

According to the original report (**Scheme 3)** appeared in the seventies, BBTZ exists under ordinary conditions in a stable yellow form which was assigned the *trans* or *E*-configuration (*E*-BBTZ), without however detailed spectral characterization or other experimental piece of evidence. Upon irradiation, the yellow isomer (λ_{max} = 453 nm) was reported to give an unstable red species with a maximum at 470 nm and a detectable shoulder around 530 nm, which was consistently assigned the structure of the *cis* or *Z*-isomer (*Z*-BBTZ). In acidic media, a deep violet chromophore was described as a result of a 100-nm bathochromic shift in the parent absorption maximum. Such a marked shift would be a consequence of the peculiar disposition of the cross-conjugated push–pull systems, which would be highly sensitive to protonation at the imine-type nitrogen atom(s) with consequent enhancement of the "pull" component.

Parallel to that study, an X-ray investigation of 3,3-diphenyl derivatives of BBTZ (3,3-DPBBTZ) revealed that the most stable forms in those cases possess a *cis* configuration[72]. This unexpected observation was attributed to the stacking interactions between the phenyl rings stabilizing the *cis* configuration relative to the *trans* isomer. Since then, however the structural and spectral

characterization of the various forms of the parent BBTZ was never addressed in detail, due also to the failure to obtain useful crystals for X-ray analysis. This issue of conflicting configurations of the BBTZ system was only marginally addressed in subsequent papers dealing with trichochromes[73], remaining therefore unsettled.

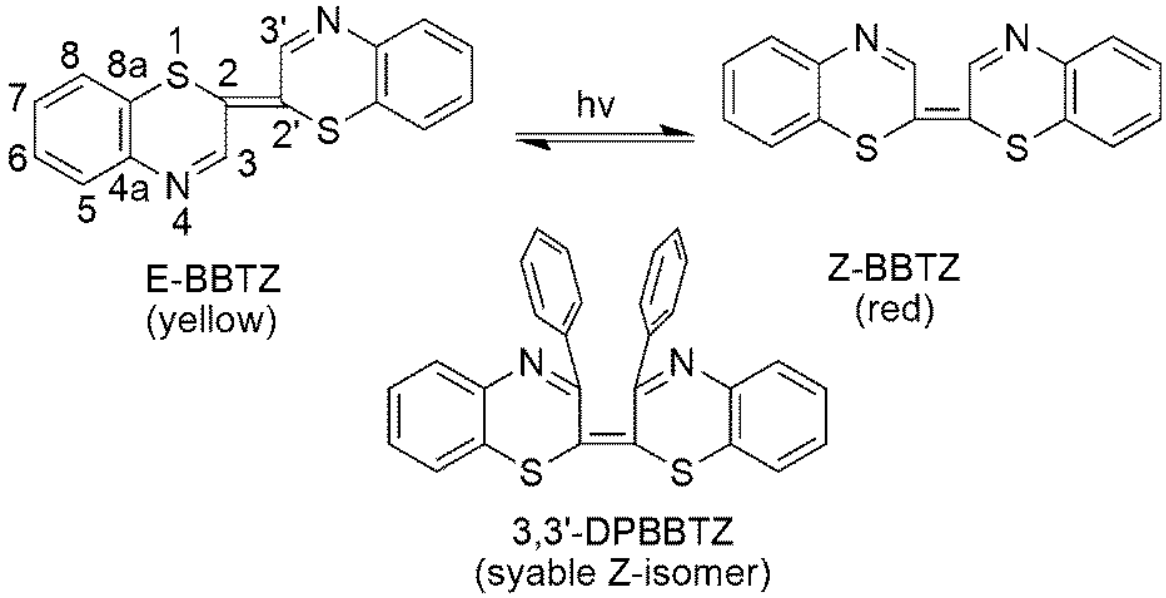

Scheme 3. *Early notions about BBTZ structure and chromophore.*

In order to exploit the potential of BBTZ, the synthesis, structural characterization and chromophoric properties were revisited by an integrated experimental and computational approach

3.1.2 Synthesis and characterization of BBTZ

BBTZ was prepared following the reported synthesis[24] with some modifications in order to improve the overall procedure. An o-aminothiophenol, as an in situ generated sodium salt to improve its nucleofilicity, reacts with bromo-acetaldehyde diethyl acetal in anhydrous DMSO at 100 °C to give 1-(2-aminophenylthio)-2,3-diethoxyethane that was isolated after a

chromatographic purification. (**Figure 32**)

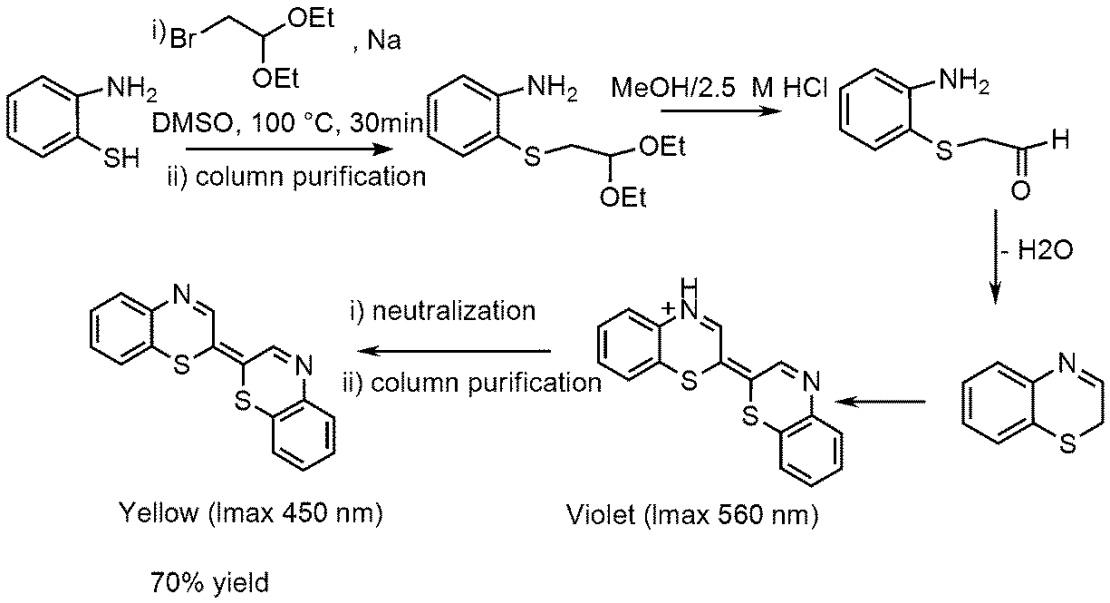

Figure 32. *Synthesis of BBTZ*

According to the previous reported protocol, the reaction mixture had to be left for over 12 h to reach a satisfactory yield; however, it was noted that the reaction time can be considerably lowered to 1-2 hours and it can be carried out even at room temperature if the amount of sodium used to form the o-aminothiophenol salt is increased.

The isolated 1-(2-aminophenylthio-)2,3-diethoxyethane is then treated with acidic methanol in order to remove the aldehyde protective groups and immediately after the cyclization occurs a deep violet solution is obtained. This may be interpreted considering that the intermediate monomeric 2H-1,4-benzothiazine generated is extremely unstable and dimerizes almost instantly. The reaction mixture is then treated with 1 M Na_2CO_3 and the yellow precipitate obtained is collected by centrifugation and purified by column chromatography (diethyl ether/hexane, 9:1). This is a really critical purification procedure because of BBTZ photoreactivity and it must be carried out rigorously in the dark.. In order to characterize also the other BBTZ isomer, solutions of the yellow BBTZ in benzene or dichloromethane were exposed to sunlight in quartz vials and the conversion of the yellow to red form was followed by TLC

analysis. At maximum degree of conversion the solution was taken to dryness and rapidly purified by column chromatography and then subjected to spectral characterization as quickly as possible due to its tendency to return to its most stable isomer, especially when left in the dark. Assignment of the proton and carbon resonances followed from analysis of 2D NMR spectra for the yellow species and from proton and carbon spectra of the red species, are shown in **Figure 33**

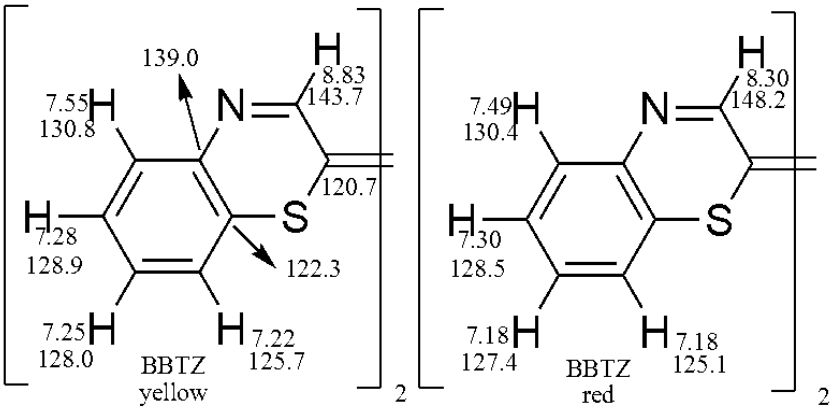

Figure 33. *Experimental proton and carbon resonances of yellow BBTZ(right) and red BBTZ (left).For red BBTZ the quaternary carbons resonances could not be obtained*

3.1.3 Computational analysis

DFT calculations employing the PBE0 functional[65] [TD-PBE0/6-311++G-(2d,2p)//PBE0/6-31+G(d,p)] were performed to characterize the BBTZ chromophore and associated electronic transitions. Quite surprisingly, the predicted absorption maximum of the *cis* forms virtually overlapped that of the stable yellow species, whereas that of the *trans* isomer matched the absorption spectrum of the unstable red species generated by exposure to sunlight. This unexpected result hinted at an incorrect assignment of the configurations of the two species. Unfortunately, it was not possible to grow suitable crystals of the yellow stable form of BBTZ to clarify its configuration unambiguously. However, strong suggestive evidence in support of the structural reassignment came from complete ^{1}H NMR and ^{13}C NMR characterization of the yellow and red species, which gave results that matched fairly well with the spectra of the *cis*

and *trans* isomers, respectively, simulated within the Gauge–Including Atomic Orbitals (GIAO) ansatz[70] at the PBE0/6-311+G(d,p).

Simple energetic consideration also lent support to this assignment, inasmuch as most computational levels explored, including notably the PBE0/6-31+G(d,p) level adopted for geometry optimizations, MP2 calculations with sufficiently large basis sets, as well as the high accuracy CBS-QB3 model chemistry[74], predicted a higher stability for the *cis* form. More compelling evidence supporting structural revision of the stable yellow species to the *cis* isomer came from a gradient-selected X-half filtered NOESY-HSQC experiment[75] (**Figure 34)**, which allows NOE cross-peaks to be detected between chemically equivalent protons, exploiting the statistical mixture of different $^{12}C–^{1}H$ and $^{13}C–^{1}H$ isotopomers in natural abundance to break the equivalence of the protons. To minimize the influence of any imperfect suppression of the diagonal signals, the experiment is acquired without heteronuclear decoupling during acquisition; therefore, the NOEs are observed in correspondence of the ^{13}C satellite peaks of the proton signal. The spectrum thus obtained displayed prominent $H^3–H^3$ NOE, which strongly supported the *cis* configuration of the inter-ring double bond (the interproton distance measured in the DFT model is 1.90 Å) and effectively ruled out the *trans* configuration (4.67 Å).

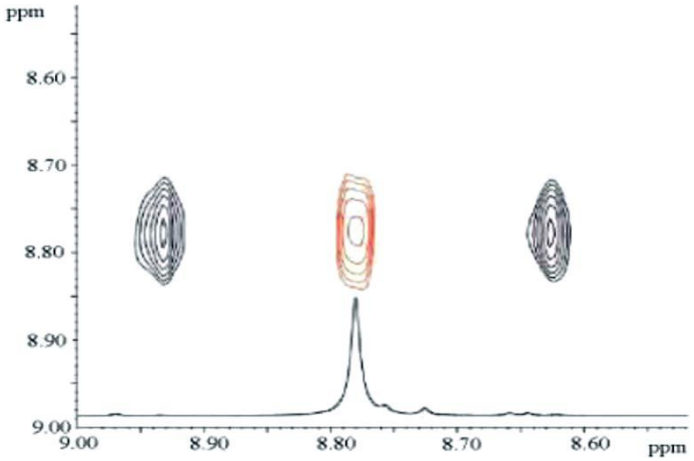

Figure 34..*X-half filtered NOESY-HSQC spectrum (CDCl3) of the yellow form of BBTZ (selected region).*

The counterintuitive prevalence of the *cis* form can be rationalized based on the tendency of the push–pull RS– CH=CH=NR system to adopt a *trans* arrangement (i.e., corresponding to the situation in Z-BBTZ). For the *cis* benzothiazine isomer, the expected planar skeleton (C_{2v} symmetry) is found; by contrast, the *trans* isomer displays a C_i equilibrium structure, in which deviations from planarity are localized in the thiazine rings, and only marginally affect the planarity of the S–C2(C3)=C2'(C3')–S' system (**Figure 35)**. The planar (C_{2h}) *trans* structure represents in fact a first-order saddle point, some 1.6 kcalmol^{-1} in energy above the C_i conformer. Unfavorable non-bonded interactions between the H3 protons and the sulfur centers on the opposite ring are relieved to some extent by distortion of the C_{2h} structure (S–H3 distance = 2.50 Å) to the C_i conformer (2.61 Å).

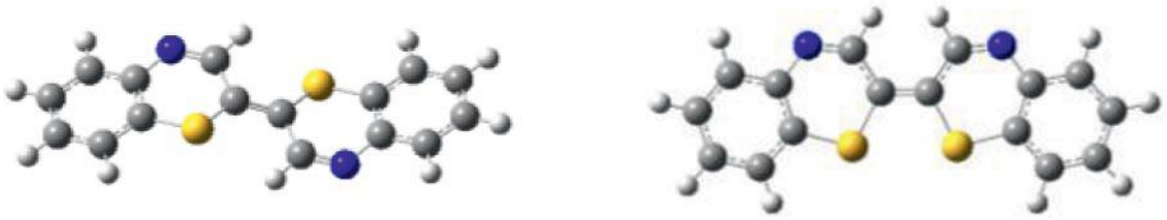

Figure 35. *Geometry optimized structures of E-BBTZ (left) and ZBBTZ (right) at the PBE0/6-31+G(d,p) level of theory.*

3.1.4 Characterization of the chromophoric properties

Efficient control and regulation of chromophores is an essential requisite for practical applications. Because a strong acid-induced shift was originally described as the most spectacular property of BBTZ, the acidichromic behavior of this chromophore was re-examined. **Figure 36** shows the absorption profile of *Z*-BBTZ at neutral pH and after acidification to pH < 4. As previously reported, a violet species with an intense maximum at 556 nm developed (**Figure 37)**, which reversibly shifted to the original maximum upon neutralization. The reaction

proved to be completely reversible over at least five cycles. Under more forcing acidic conditions, for example, in 2 M HCl, a new species became detectable that had apparently escaped the attention of previous workers. This latter species, supposedly a diprotonated derivative, exhibited an absorption maximum at 590 nm, and its formation was accompanied by a distinct color change of the solution from violet to deep blue. Plots of absorbance at 556 and 453 nm vs. pH indicated a p*K*a value of ca. 2.5 for the protonated species, whereas it was not possible to obtain reliable information on the acidity constant of the diprotonated species.

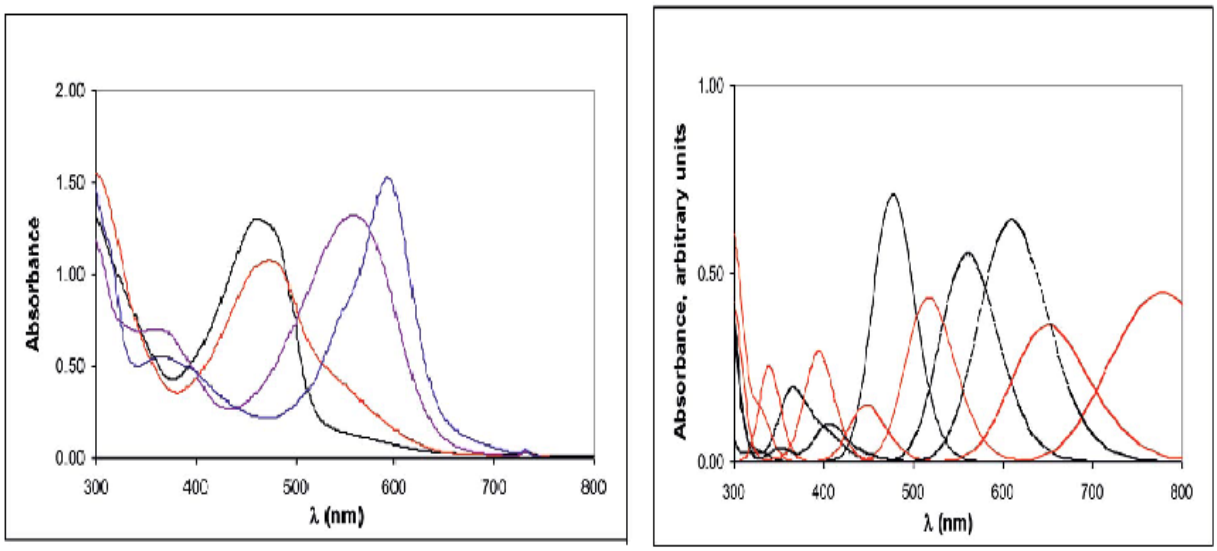

Figure 36. *(left) Acid-dependent behavior of BBTZ chromophore: neutral, yellow species (black), photoirradiated species (red); pH 4 (violet), 2 M HCl (blue); (right) computed spectra for the neutral, monocation and dication species of BBTZ. Full line, neutral forms: cis, C_{2v} minimum (black), trans C_i minimum (red) (relative energy 1.6 kcalmol^{-1}). Dashed line, N-monoprotonated forms: cis C_s minimum (black), trans C1 minimum (red) (relative energy 3.3 kcal mol^{-1}). Dashed-dotted, N,N-diprotonated forms: cis C2 minimum (black), trans C2 minimum (red) (relative energy, 4.8 kcalmol^{-1}).*

Both the absorption maximum and NMR spectroscopic data of the first formed violet species in acids were in fairly good agreement with DFT predictions for an *N*-protonated derivative with a *cis* configuration. Attempts to characterize the blue diprotonated product by ^{1}H NMR

spectroscopy were unsuccessful, because the compound could be generated only in a strongly acidic aqueous medium where the solubility was poor.

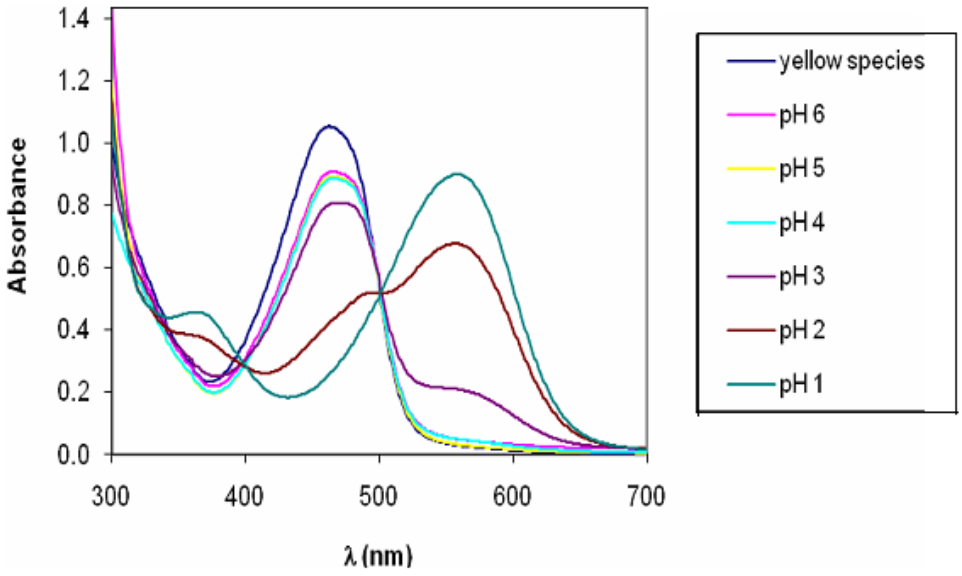

Figure 37. *Changes in the UV-Vis absorption intensity of Z-BBTZ as a function of pH*

Apparently, addition of acids to DMSO or other organic solvents was insufficient to generate the diprotonated species. Nonetheless, both chemical arguments and DFT calculations concurred to support the structure of an *N*,*N*- diprotonated species in a *cis* configuration for the blue chromophore (**Figure 38**).

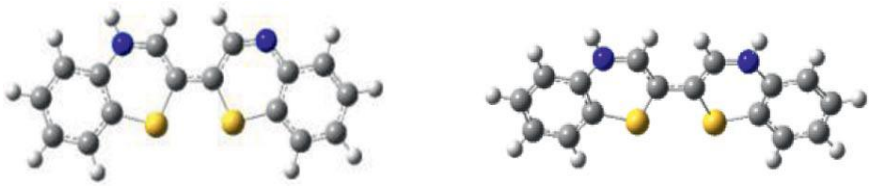

Figure 38.. *Geometry optimized structures of mono- (left) and diprotonated (right) derivatives of BBTZ at the PBE0/6-31+G(d,p) level of theory.*

Interestingly, DFT energy data for both the mono- and di-*N*-protonated species predicted a

greater stabilization of the *cis* against the *trans* isomers compared to the neutral forms . On the basis of these data, a novel picture of BBTZ as a four-state system with photochromic and pH-dependent behavior (**Figure 39**) is proposed (**Scheme 4**).

Figure 39. *BBTZ as a four-state chromic system. From left to right: Z form; E form, protonated form, diprotonated form.*

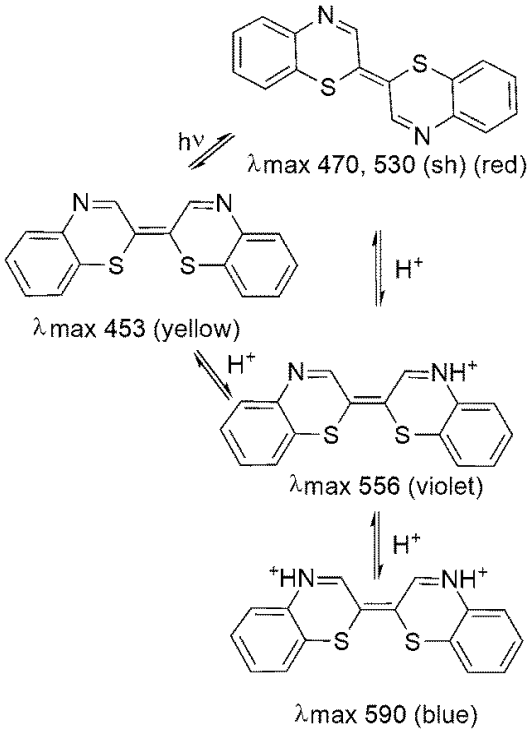

Scheme 4. *Schematic illustration of the revised four-state BBTZ system. Regulatory effects of light and protons are highlighted.*

3.1.5 The acidichromic behaviour of BBTZ chromophore: exploring applications

The potential of BBTZ for photo- and pH-controlled reversible writing processes was briefly assessed in a preliminary set of experiments. A silica gel plate was dipped into a dichloromethane solution of BBTZ and then dried. The yellow-orange plate thus obtained was exposed to HCl vapors through a handmade mask containing the letter L to generate a well-defined image (**Figure 40** , right panel).

This image was instantaneously erased by exposure to vapors of ammonia. Conversely, exposure of the yellow plate to HCl vapors generated a blue background on which a yellow letter L was clearly inscribed by the above mask-aided operation using ammonia vapors (Figure , left panel). The same write–erase–rewrite operations could be repeated several times without apparent modification. The color on plate was fairly resistant in the absence of acidic or alkaline vapors and in the dark or under low light intensity condition

Figure 40. *Writing initials with BBTZ. Left panel: neutral background, HCl vapors through the mask. Right panel: HCl-exposed background, NH3 vapors through the mask*

3.2 Synthesis of 1,4-benzothiazines and investigation of their oxidation reactivity

Based on consideration of the variety of chromophores provided by the $\Delta^{2,2'}$-bibenzothiazine systems depending on light exposure and pH conditions, the reversibility of the color changes and the stability of the compounds, availability of a series of 1,4-benzothiazines on a large scale is a highly desirable goal and a preliminary step to access to the different groups of benzothiazine-based dyes as will be presented in the following chapters.

3.2.1 Synthetic approach to 1,4-benzothiazines

The main synthetic route to the 1,4-benzothiazines compounds involves treatment of an *o*-aminothiophenol with a haloacetoaldehyde (in the acetal form) / ketone followed by removal of the protection and cyclization. Use of the aldehyde in the protected acetal form would allow to get the 3-unsubstituted 1,4-benzothiazine. This latter however is highly unstable under the acidic reaction conditions needed to remove the aldehyde protection and favour cyclization so that only the dimeric $\Delta^{2,2'}$- bibenzothiazine in the protonated form is invariably obtained as a result of the oxidative coupling of the transiently generated 1,4-benzothiazine (**Figure 41**)

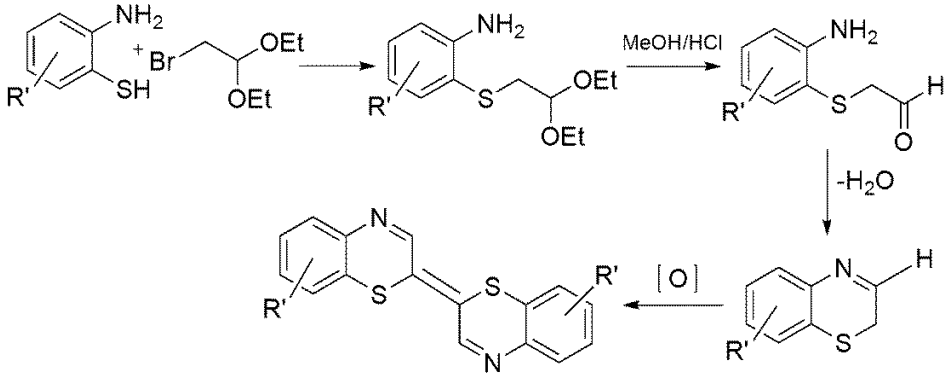

Figure 41. *Synthesis and reactivity of the 3-unsubstituted 1,4-benzothiazine*

To obtain more stable 1,4-benzothiazines monomers attention was redirected to the preparation of 3-substituted 1,4-benzothiazines.

Using an alpha-halogenated ketone, instead of a haloacetoaldehyde, a 1,4-benzothiazine carrying an R group of the starting ketone at 3-position can be obtained (**Figure 42**).

Following this latter strategy, two 3-substituted-1,4-benzothiazine monomers could be obtained, namely 3-phenyl-2H-1,4-benzothiazine and 3-methyl-2H-1,4-benzothiazine.

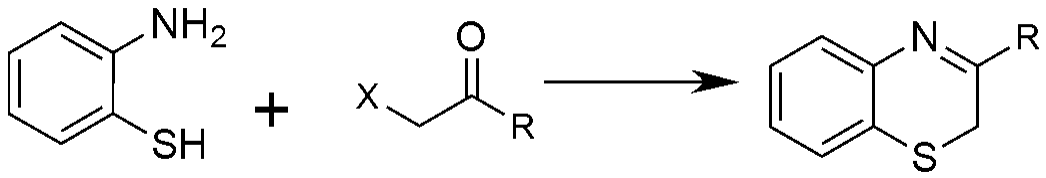

Figure 42. *Synthesis of 1,4-benzothiazine carrying at 3-position the R group.*

3.2.2. Synthesis of 3-phenyl-2H-1,4-benzothiazine

3-phenyl-2*H*-1,4-benzothiazine was obtained following an improved version of a previously reported procedure[76] in which the *o*-aminothiophenol is reacted with phenacyl bromide in anhydrous diethyl ether (**Figure 43)**. In our hands the reaction proceeded rapidly leading in 2 h to an almost complete conversion of the starting materials. The yellow solid that separated was washed with diethyl ether affording the compound in pure form in 82% yield.

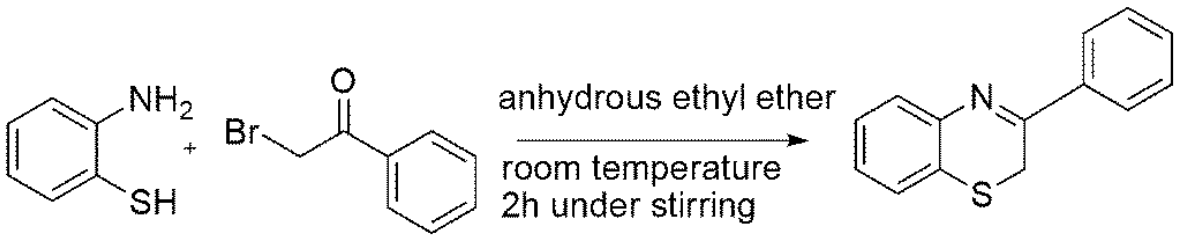

Figure 43. *Synthesis of 3-phenyl-2H-1,4-benzothiazine.*

This compound was subjected to a complete spectral analysis. Proton and carbon resonances

assignment of 3-phenyl-2H-1,4-benzothiazine is shown in **Figure 44**.

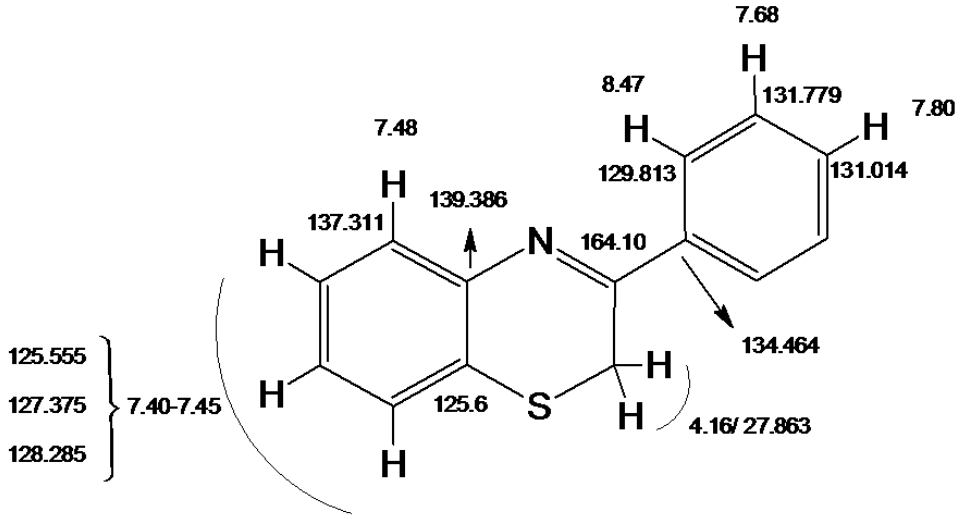

Figure 44. *^{1}H and ^{13}C NMR resonances of 3-phenyl-2H-1,4-benzothiazine.*

3.2.3 Preliminary investigation of 3-phenyl-1,4-benzothiazine reactivity

3-phenyl-1,4-benzothiazine proved a highly stable product, because it can be obtained as a intense yellow solid and stored at room temperature. It is easily dissolved in methanol, chloroform and dichloromethane.

In organic solvents (e.g., methanol) or in a neutral aqueous medium, 3-phenyl-1,4-benzothiazine is fairly stable to a broad range of chemical and enzymatic oxidants, remaining virtually unchanged over prolonged periods of time up to several days.

However, in acidic media , the oxidative coupling of the monomeric 1,4-benzothiazine can take place. In the case of the parent 1,4-benzothiazine the marked reactivity and the ease to further oxidation of the 2,2'-coupling product hampers not only isolation but even detection of this species. By contrast, it is known from literature that starting from 7-(2-amino-2-carboxyethyl)-3-carboxy-5-hydroxy-2*H*-1,4-benzothiazine, an intermediate of pheomelanin biosynthesis, or the model compound 3-methoxycarbonyl-5-methoxy-7-methyl-2*H*-1,4-benzothiazine, the 2,2'-

dimers can be obtained by oxidation under acidic conditions with ammonium persulphate[43] (**Figure 45**).

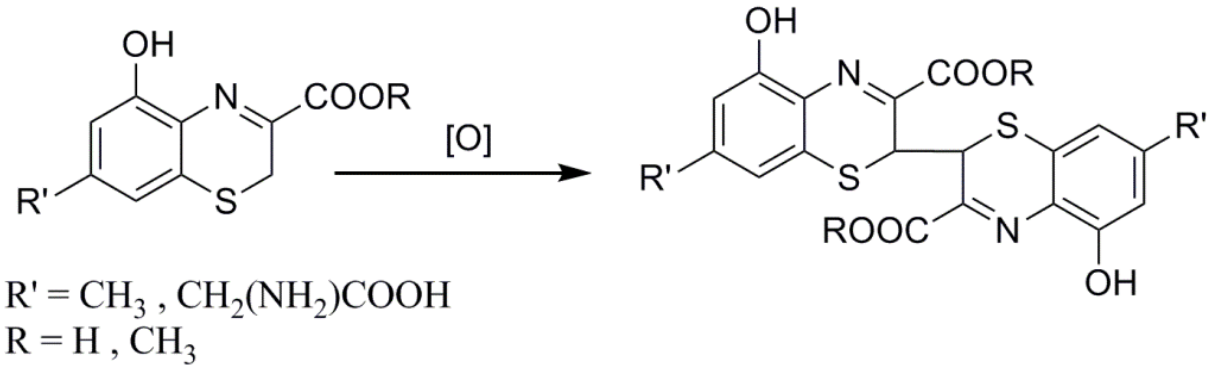

Figure 45. *Formation of 2,2'-bibenzothiazine by oxidation of 3-carboxysubstituted 1,4-benzothiazines*

Other oxidation conditions that have been reported for dimerization of 3-aryl substituted benzothiazines include picric acid in ethanol under reflux, nitrobenzene, ethanol/HCl or ethanol /sodium hydroxide at room temperature in the presence of oxygen.[77] with the highest yields (about 60%) obtained with picric acid. Moreover, in the presence of peroxides or biometals at micromolar concentrations, and under strong acidic conditions, 3-phenyl-2H-1,4-benzothiazine is efficiently converted into its double bond dimer (this will be illustrated in more details in chapter 3.3).

3.2.4 Synthesis of 3-methyl-2H-1,4-benzothiazine.

The synthetic procedure followed for 3-phenyl-2H-1,4-benzothiazine synthesis, was extended to another commercially available alpha halogen ketone, chloroacetone (**Figure 46**). The reaction was carried out under similar conditions by reacting at room temperature chloroacetone with *o*-aminothiophenol in anhydrous diethyl ether under vigorous stirring. The reaction was carried out over 24 h at which time a solid was formed and separated from the reaction mixture. The solid

was washed repeatedly with chloroform and the remaining solid and the supernatants were examined by TLC and then by NMR. Only the supernatant was found to contain a single component that was identified as the desired benzothiazine while the solid proved to be a mixture of several species. The isolation yield of the benzothiazine in the optimized procedure was 48%.

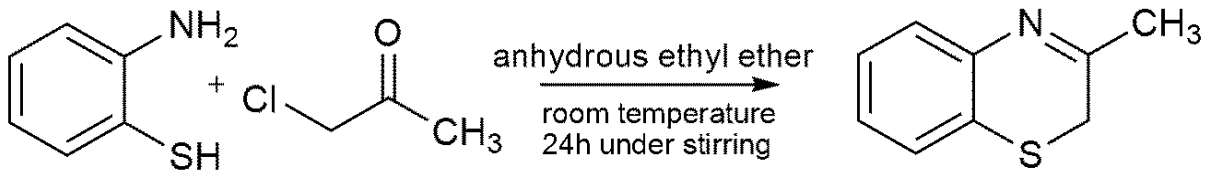

Figure 46. *Synthesis of 3-methyl -2H-1,4-benzothiazine.*

Proton and carbon resonances assignment of 3-methyl-1,4-benzothiazine is shown in **Figure 47**.

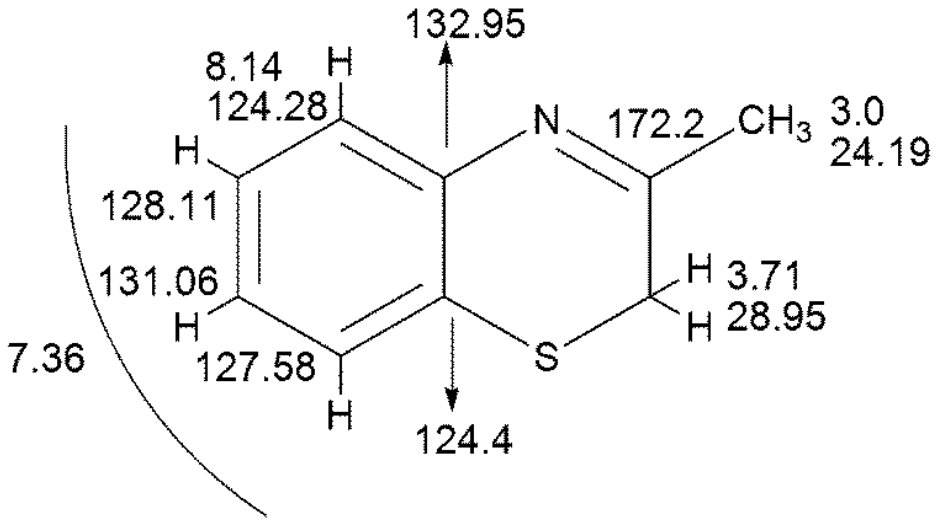

Figure 47. *^{1}H and ^{13}C NMR resonances of 3-methyl-2H-1,4-benzothiazine.*

3.2.5 Preliminary investigation of 3-methyl-1,4-benzothiazine reactivity

The reaction conditions developed in the case of the 3-phenyl-1,4-benzothiazine were extended to 3-methyl-1,4-benzothiazine. When exposed to methanol in the presence of 3M HCl the compound reacted smoothly within 24 h. After extraction of the mixture with chloroform

/bicarbonate solution a rather simple reaction pattern was apparent consisting of a major yellow product at Rf 0.5 (eluant hexane-ethyl acetate 8:2 v/v) and another minor component orange in color at Rf 0.35 in the same eluent. After chromatographic purification, the two components could be obtained in pure form and subjected to spectral analysis.

Mass spectrometric analysis of the orange component in the electrospray ionization mode gave a pseudomolecular ion peak at *m*/*z* 323 as expected for $\Delta^{2,2'}$-bi-(3-methyl-2H-1,4-benzothiazine). However, the aromatic region of the ^{1}H NMR spectrum clearly provided evidence for the presence of resonances due to two different 1,4-benzothiazine units; moreover the aliphatic region showed two doublets (1H each) at 2.9 ppm with J= 16 Hz, suggesting diastereotopic methylene protons and a singlet (3H) at 1.42 ppm, significantly shielded with respect to the methyl group of the starting benzothiazine. These latter resonances showed one bond correlation with carbons at 48.45 and 26.72 ppm, respectively, and with a C carbons at 56.11 ppm and 164.61 ppm in the HMBC spectrum. These and other elements from comparative analysis of the 2D spectra led us to assign the compound the structure shown in **Figure 48.**

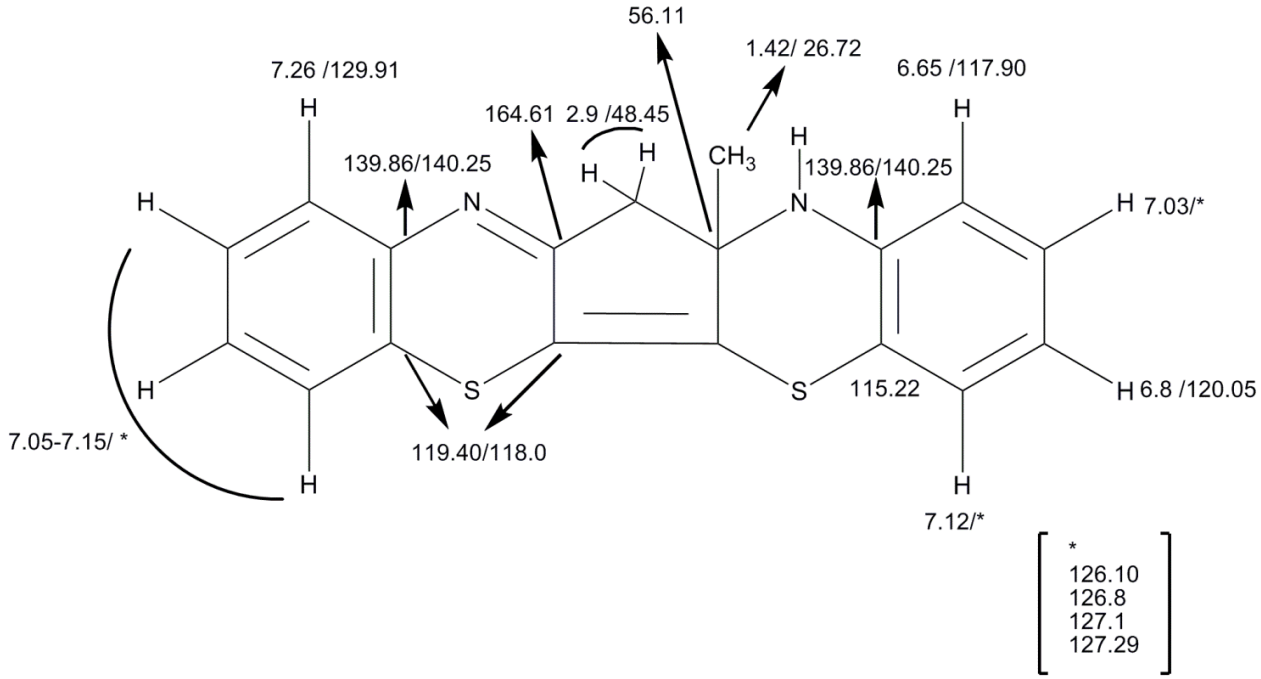

Figure 48. *^{1}H and ^{13}C NMR resonances of the condensated compound.*

Consistent with this structural formulation was also the UV spectrum (**Figure 49)** showing an absorption maximum at 414 nm ipsochromically shifted when compared to that of $\Delta^{2,2'}$-bi-(2*H*-1,4-benzothiazine) system (453 nm) because of the lack of one half of the doubly conjugated cross coupled system. The absorption maximum was shifted batochromically to 501 nm on treatment with acids as expected considering the persistence of one of the push- pull system of the bibenzothiazine unit.

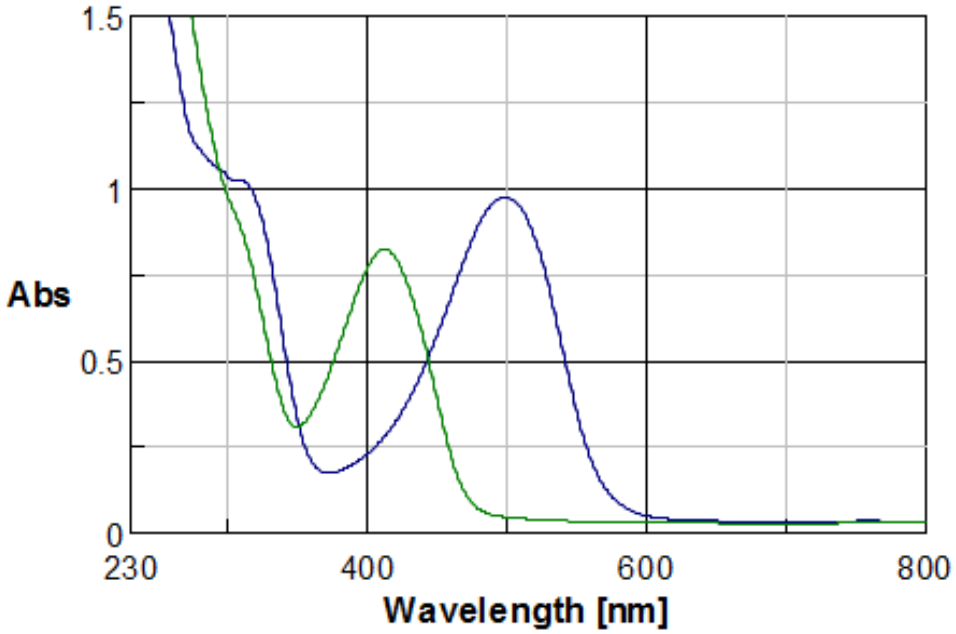

Figure 49 *Uv/VIS spectra under neutral and acid conditions of the condensated compound .*

As to the possible mechanism of formation of this compound, this may be envisaged as involving in addition to the oxidative coupling leading to the formation of the double bond at 2 position an imine enamine attack as depicted in **Figure 50**, though the sequence of the events could not defined based on the available evidence.

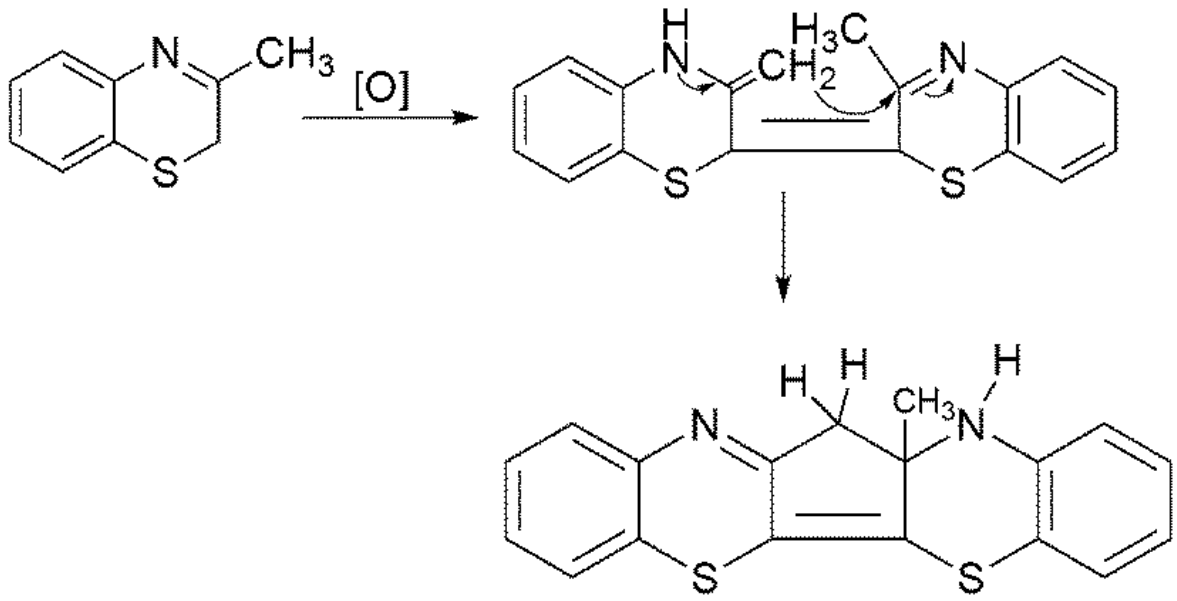

Figure 50. *Proposed mechanism of formation of the condensated product*

As to the other component of the reaction mixture, this was isolated by column fractionation and subjected to spectral analysis. It was noticed that the compound had a marked tendency to undergo partial decomposition when taken in solution even in the cold and in the absence of light giving rise to a pattern of species most of which exhibiting only UV absorption. Spectral analysis was initially attempted in methanol. The proton spectrum showed in the aliphatic region resonances closely similar to those of the condensated compound that is two doublets at 3.11 ppm and the singlet at 1.40 ppm while analysis of the sp^2 region indicated the presence of two different benzothiazine units although the pattern of resonances that is 6.84-7.39 ppm covered a range different with respect to that observed for the previous compound. Unfortunately, no satisfactory carbon spectrum could be obtained in spite of several efforts and further structural investigation was hampered by a marked instability of this compound on standing in solution even in the cold. Further studies will be directed at exploring conditions under which this interesting compound would be sufficiently stable to warrant running a complete NMR characterization.

Separate experiments showed that the Rf 0.35 compound was not generated from the

condensated benzothianine dimer under the reaction conditions, nor was compound that was fully characterized formed from the other suggesting that, in spite of the similarity of the proton spectrum, the formation routes of the two components of the reaction mixture were distinct and parallel. In addition, neither of the two components of the reaction mixture was formed when the reaction was carried out with exclusion of air .

3.3 Oxidative coupling of 3-phenyl-(2H-1,4-benzothiazine) promoted by peroxides or biometals

3.3.1 Background

The oxidation behaviour of 1,4-benzothiazines, was extensively investigated in the 70's. Fujii et al[78] reported that oxidation of 3-phenyl-1,4-benzothiazine with picric acid in ethanol leads to a symmetrical dimer identified as the 2,2'-bi-(3-phenyl-2H-1,4-benzothiazine). The structure of this product was later questioned by Bottex[79] that assigned to the dimer an asymmetric structure involving the Nitrogen of one unit and the 2 position of the other. Further studies showed that oxidation of 1,4-thiazines under the same conditions (picric acid in ethanol) gave only products arising from a symmetrical dimerization[80]. Moreover, in the case of 3-phenyl-2H-1,4-benzothiazine the dimers were formed even under milder conditions, that is acidic ethanol in the presence of oxygen, although with lower yields. It should be noted that the dimerization of 3-phenyl-1,4-benzothiazine should lead to the formation of a mixture of the meso/DL pair of diastereoisomers, however, only one stereoisomer was obtained from these reactions and X-ray analyses showed that this stereoisomer was the meso one.

We have now re-examined this reaction with a view of obtaining the $\Delta^{2,2'}$-bi-(2H-1,4-benzothiazine) system starting from a stable benzothiazine that is the 3-phenyl-1,4-benzothiazine that differently from the 3-unsubstituted compound can be prepared and stored. The oxidation reaction was carried out with the aim of isolating either the 2,2' dimer and investigating the optimal conditions to get the corresponding $\Delta^{2,2'}$-bi-(2H-1,4-benzothiazine).

3.3.2 The green blue chromophore of $\Delta^{2,2'}$-bi-(3-phenyl-2H-1,4- benzothiazine) system

In organic solvents (e.g. methanol) or in a neutral aqueous medium, the 3-phenyl-1,4-benzothiazine was fairly stable to a broad range of chemical and enzymatic oxidants, including potassium ferricyanide, hydrogen peroxide, or, notably, peroxidase/ H_2O_2, remaining virtually unchanged over prolonged periods of time up to several days. However, exposure of 3-phenyl-1,4-benzothiazine to H_2O_2 in a strongly acidic medium (i.e. methanol/conc aq HCl 3:1 at room temperature) resulted in a fast and efficient reaction leading to a stable blue-green chromophore (λ_{max} 598 nm) in a few minutes. In the absence of H_2O_2 no detectable chromophore formation was observed over the time scale of 1 h. HPLC analysis of the reaction mixture revealed the very rapid accumulation in the initial stages of the reaction of colorless intermediates that were eventually converted to the green chromophore, with no other detectable intermediate/reaction product.(**Figure 51**). This was also confirmed by proton NMR monitoring of the reaction course.

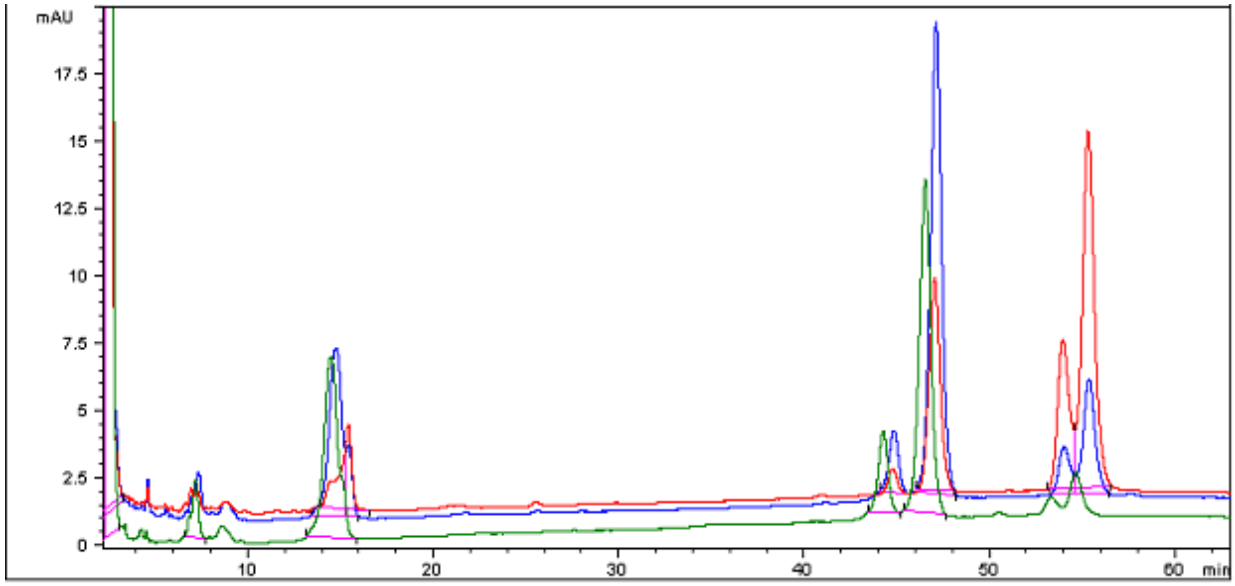

Figure 51. *LC-ESI(+)MS analysis of the oxidation of 3-phenyl-1,4-benzothiazine (50 μM) by H_2O_2 (100 μM) at 1 min (green plot), 5min (blue plot) and 15 min (red plot). The RT 15.2 min species was identified as the 3-phenyl-1,4-benzothiazine, the RT 45.4 and 47.7 min were identified as the single bond dimers and the RT 54.4 and 55.7 min were identified as the double bond 2,2'-bibenzothiazines*

3.3.3 Isolation and spectral characterization

Work up of the mixtures allowed isolation and spectral characterization of the colorless intermediates as the meso/DL pair of diastereoisomers of the single-bonded dimers which were amply investigated by computational analysis, whereas the chromophoric species proved to be a mixture of $\Delta^{2,2'}$-bi-(3-phenyl-2H-1,4- benzothiazine) Z/E isomers (**Scheme 5**) in an approximate ratio of 3:1.

Assignment of the Z-configuration to the major component of the mixture was made possible by comparison of the experimental and computed ^{1}H NMR spectra . For the mixture of isomeric **3**, an overall ε_{598} = 5700 ± 45M^{1} cm ^{1} in methanol/36% HCl 3:1 v/vwas determined, which suggested a potential application for colorimetric determination of H_2O_2.

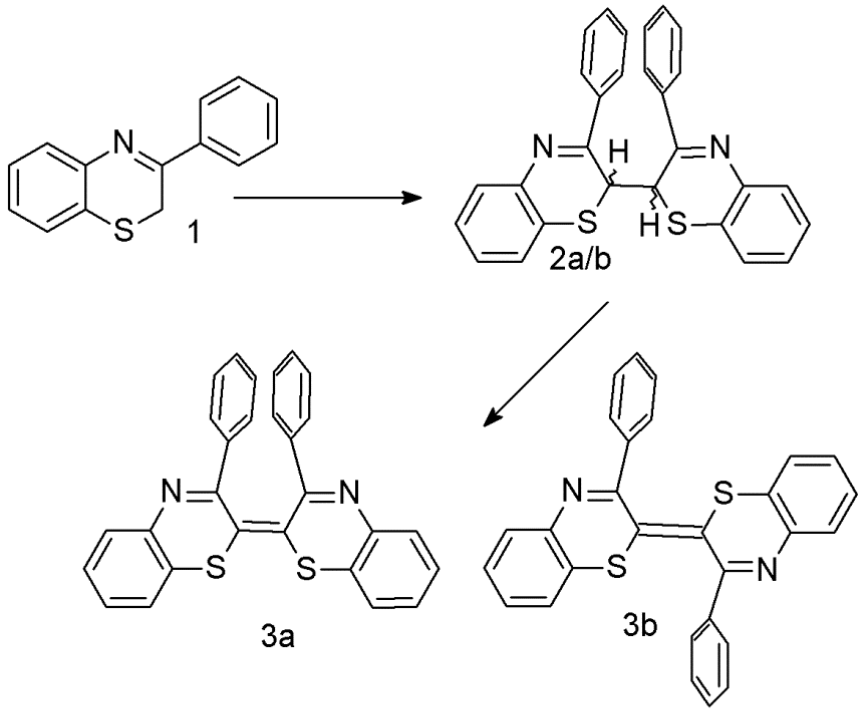

Scheme 5*. Structures of Dimeric Oxidation Products of 3-phenyl-1,4-benzothiazine*

3.3.4 Mechanicistic studies

The mechanism by which H_2O_2 mediates conversion of the monomeric 3-phenyl benzothiazine to its double bond dimer under acid conditions was then investigated. **Figure 52** shows the spectrophotometric course of the oxidation of the monomer with acidic H_2O_2 (left panel) leading to formation of the green chromophore. Data showed the relatively fast conversion of 3-phenyl-1,4.-benzothiazine to the final product following the addition of acid. The chromophore of the single bond dimers was closely similar to that of the monomer. The conversion of single bond dimers to the double bond ones was therefore separately followed (right panel). The pseudo-first-order rate constant of 0.089 ± 0.005 min^{-1} was determined with a concentration of the monomer at 50 μM and H_2O_2 at 500 μM, based on the formation of the double bond system at 598 nm and decay of the single bond dimer at 320 nm (**Figure 53**).

Oxygen proved to be critical for chromophore formation from both monomer and single bond dimers since no significant reaction occurred under an argon atmosphere.

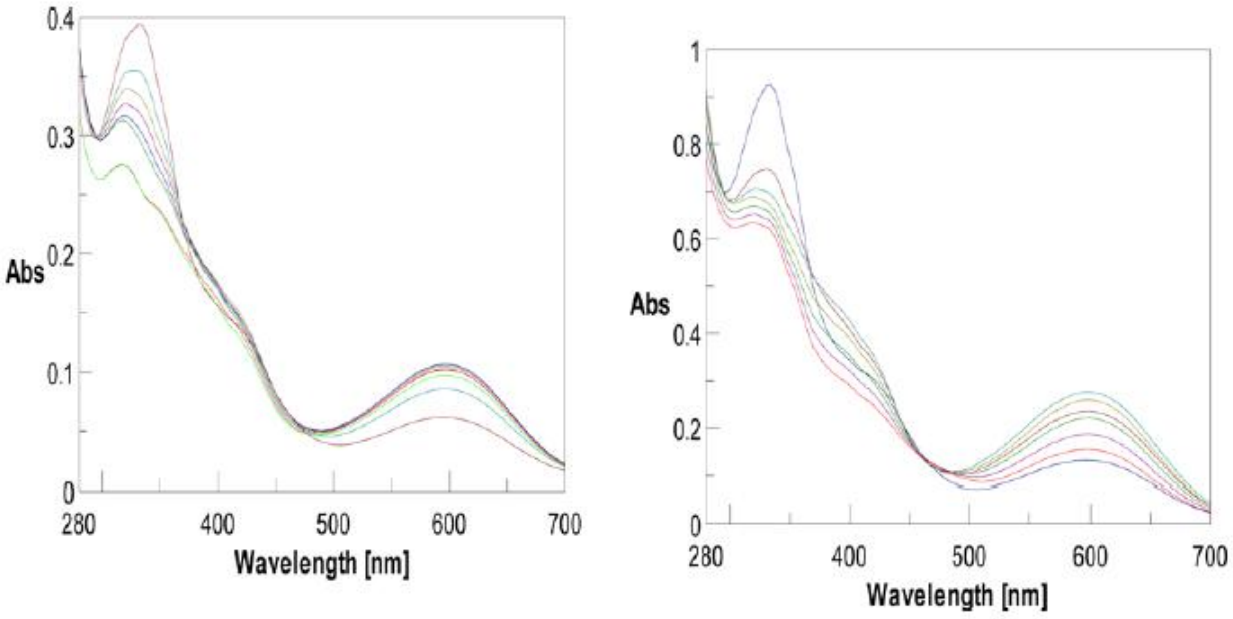

Figure 52. *Monitoring of chromophore formation by oxidation of 1 (left) and dimers 2 (right) at 50 μM in air-equilibrated methanol/ 36% HCl 3:1 v/v solutions by 500 μM H_2O_2 at 5 min intervals over 30 min*

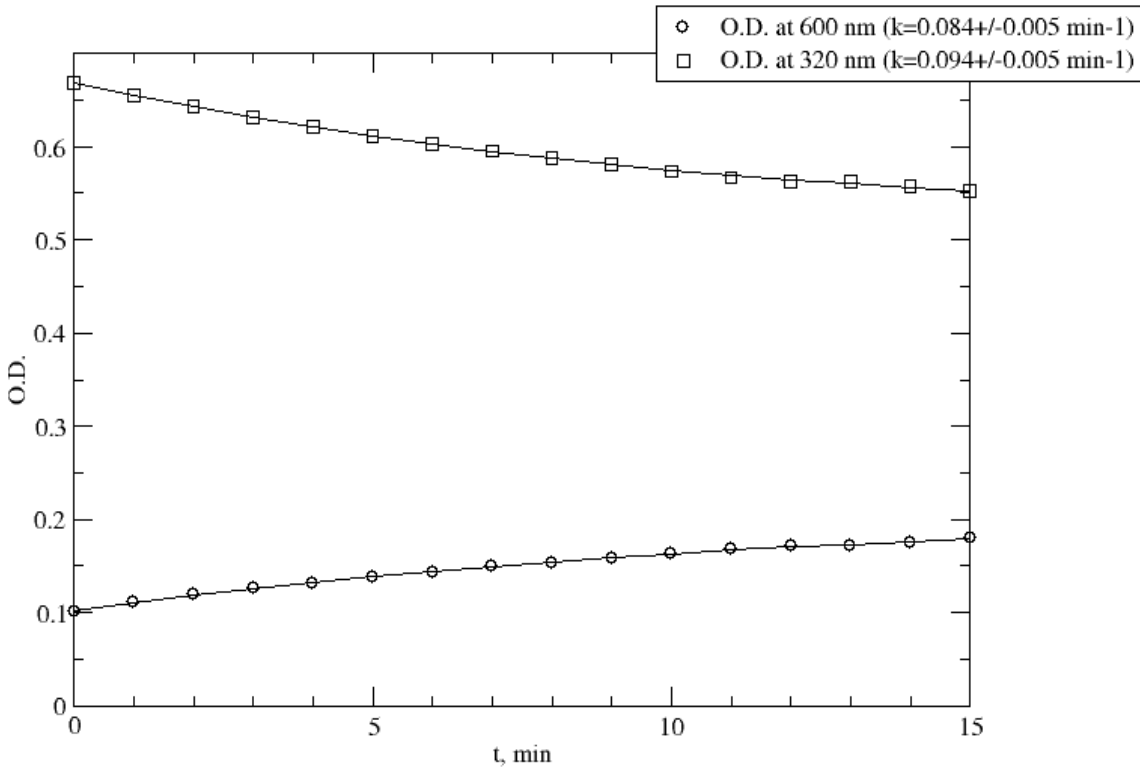

Figure 53. *Pseudo first-order fitting of the oxidation kinetics of 50 μM 3,3'-diphenyl-2H,2'H-2,2'-bi-1,4- benzothiazine with 500 μM hydrogen peroxide, as monitored spectrophotometrically at two different wavelengths*

3.3.5 Formation of the $\Delta^{2,2'}$-bi-(3-phenyl-2H-1,4- benzothiazine) by other oxidants and redox active biometals.

In another series of experiments, the ability of a series of acid-compatible oxidants to bring about conversion of 3-phenyl-1,4-benzothiazine to its final dimers was investigated. Besides H_2O_2 , other peroxides such as t-BuOOH, m-chloroperbenzoic acid (MCPBA), and benzoyl peroxide also induced acid-dependent chromophore formation, whereas persulfate at the same concentration proved ineffective.

In a screening aimed at identifying other oxidants capable of promoting the oxidative coupling reaction, it was found that some redox-active transition metal ions (e.g., Fe(III), V(V), and

Cu(II)) were also able to generate the chromophore (**Figure 54**), whereas Fe(II) was inactive even in the presence of peroxides (i.e., under Fenton-type conditions, both at neutral and acidic pH)

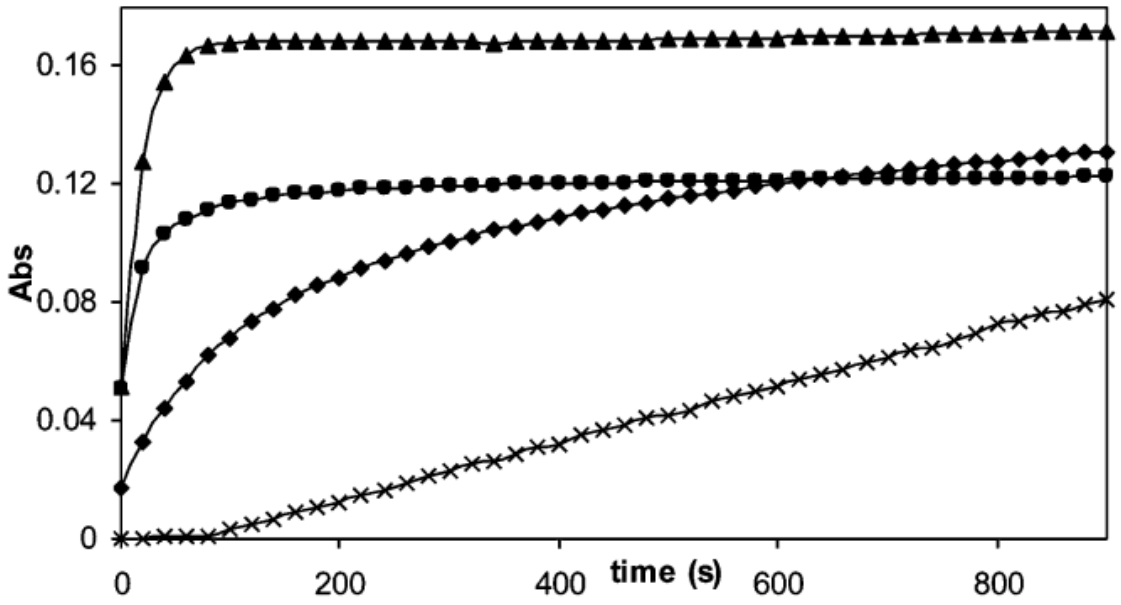

Figure 54 *. (a) Kinetic analysis of chromophore formation at 598 nm by reaction of 50 μM 1 with 100 μM* V^{5+} *(triangles)* Fe^{3+} *(squares),* Cu^{2+} *(circles), and* H_2O_2 *(crosses) in methanol/ 36% HCl 3:1 v/v solutions at 25 C.*

A possible mechanism accounting for the reported observations is given in **Scheme 6**. In this scheme, peroxides or metal ions induce conversion of protonated monomer to the resonance-stabilized benzothiazinyl radical **1**$^{\cdot}$. This conversion may be the result of two alternative, not mutually exclusive, routes, that is, direct H-atom abstraction and electron transfer with concomitant/sequential proton transfer. The former path is likely to be mediated mainly by oxygenated species on the protonated benzothiazine, while the latter would occur only on the enamine tautomer of the monomer and would be prevalent in the presence of metal ions alone.

The equilibrium of the imine and enamine forms of 3-phenyl-1,4-benzothiazine in an acidic medium should be considered in this regard . Further work is necessary to clarify this issue.

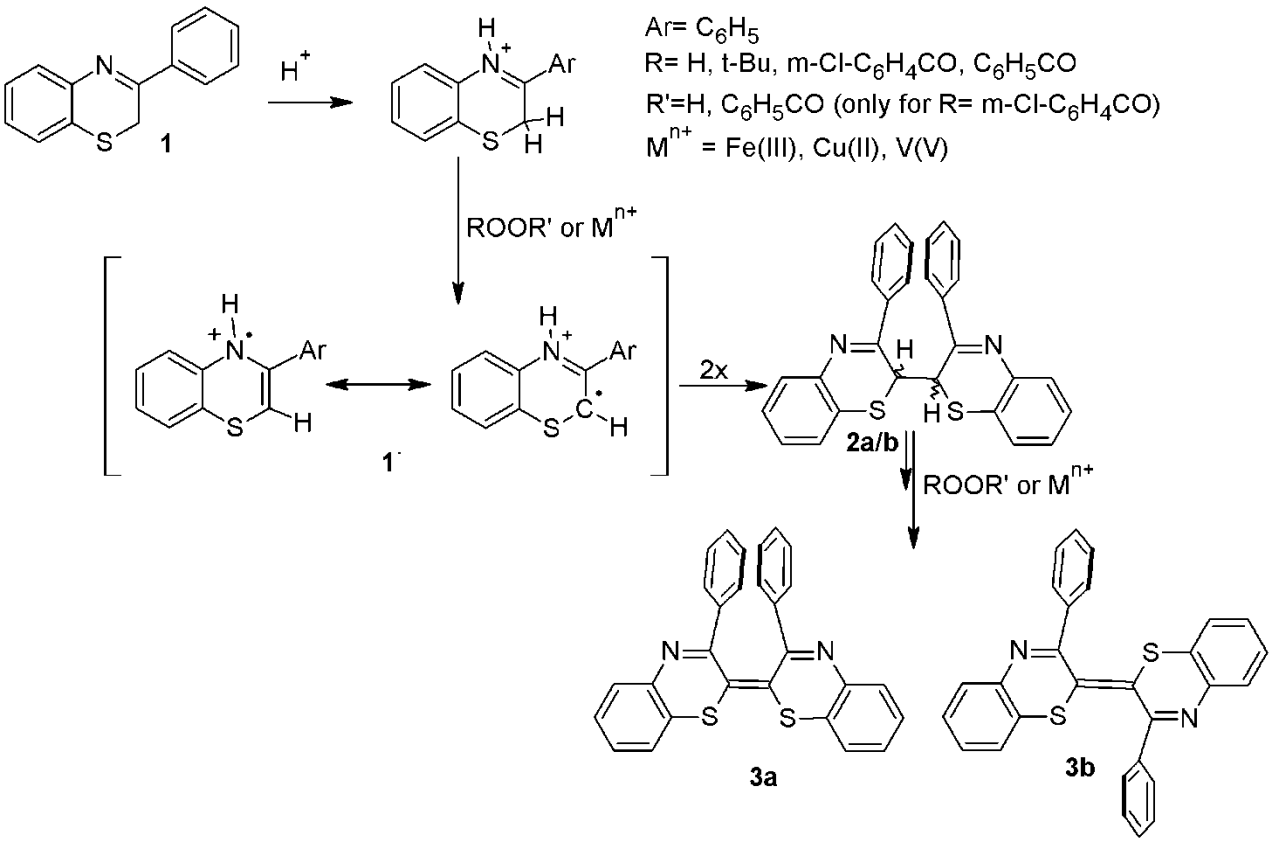

Scheme 6 . *Proposed Mechanism of Formation of Blue-Green Dimers by Oxidation of 3-phenyl-1,4-benzothiazine in Acidic Medium (All Formula Numbers Refer to Protonated Products)*

Self coupling of the monomer would then give the single bond dimer , which would eventually be converted to the double bond dimer by acid-assisted dehydrogenation. Spectrophotometric and HPLC analyses concurred to indicate that conversion between the two dimers represents the rate determining step of the process.

3.3.6 EPR experiments and computational analysis of the radical intermediates

In support of the proposed scheme, the acid-promoted (3 M HCl) oxidation of the monomer in the presence of H_2O_2 and atmospheric oxygen in MeOH was monitored by electron paramagnetic resonance (EPR) spectroscopy, which revealed the generation of a signal (**Figure 55**) attributed to a C/N-centered radical (g=2.0051) with hyperfine features fully consistent with the structure of protonated radical 1•[81] Assignment was unambiguously confirmed by comparison of the experimental data with simulated EPR spectra for the neutral and protonated radical form, using calculated (B3LYP[82]/EPR-II[83]//B3LYP/N07D[84]) hyperfine constants further optimized with the Monte Carlo method[85].

EPR spectra consistently gave good agreement with those calculated for protonated **1•** but not for the neutral species, for which large coupling (10 G) with (C2)H is predicted as a consequence of the larger spin density in position 2 .

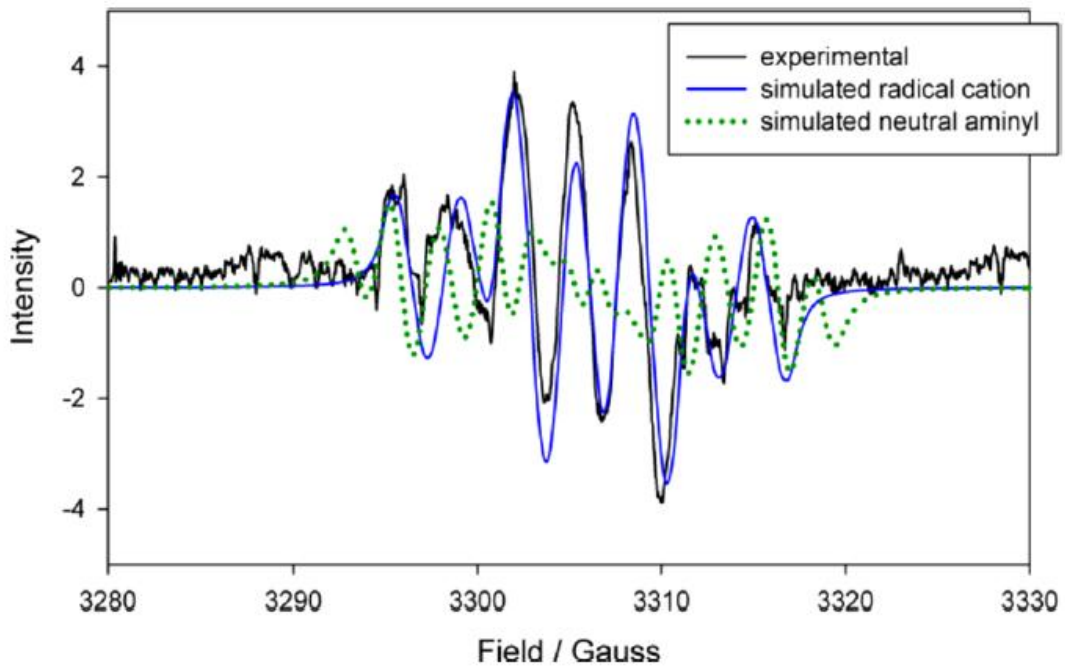

Figure 55*. EPR spectrum of a solution of 1 in acidic MeOH and simulated spectra of the neutral and protonated free-radical* ***1•****.*

The role of acids in triggering the H-atom abstraction from the 3-phenyl-1,4-benzothiazine was then investigated at the PBE0[86]/6-31þG(d,p) level. The unrestricted formulation was used to describe radicals, and for each species, different conformers were explored. Computations were performed either in vacuo or adoption of a polarizable continuum medium[87]. Predicted variations in free-energy changes associated with H-atom abstraction from the monomer and, for comparison, from the parent 2H-1,4-benzothiazine are reported in **Table 1**

Product/conditions	$\Delta\Delta_{rxn}$ G°
benzothiazine, neutral form, in vacuo	0.0
benzothiazine, neutral form, MeOH	0.5
benzothiazine, monoprotonated form, MeOH	-7.2
1, neutral form, in vacuo	2.5
1, neutral form, MeOH	3.1
1, neutral form, MeOH	-2.8

***Table 1**. Computed Free Energy (kcal mol $^{-1}$) of Radical Formation from **1**.*

Consistent with the experimental observations, calculations predicted that protonation results in a marked decrease in free-energy changes for H-atom abstraction from both the monomer and the parent benzothiazine. This effect would reflect a potentiation of the push-pull stabilization of the carbon-centered free radical at C2 induced by protonation at the imine group.

The role of oxygen in the proposed free-radical coupling/dehydrogenation scheme deserves further investigation. Since product analysis did not reveal formation of other products besides the dimers, and the mass balance was completely accounted for by these species, it follows that any oxygenated intermediate, such as a peroxyl radical, must eventually be converted to the final products with loss of oxygen.

3.3.7 Oxidative coupling of the 3-phenyl-1,4-benzothiazine: potential applications

Based on these results, the scope of the new chromogenic system was briefly assessed. Interestingly, the 3-phenyl-1,4-benzothiazine proved to be useful for the visual detection of peroxides in aged ethereal solvents such as THF, ethyl ether, dioxane (**Figure 56)**. Typically, the solvent to be tested was mixed with a monomer solution of 200 μM in 3:1 methanol/36% HCl (3:1 v/v), and the absorbance at 598 nm was measured spectrophotometrically. The method can be conveniently used for routine peroxide quantitation also on a visual basis.

As a curious aside to these experiments, it was noticed that addition of rusty iron objects to the typical mixture promoted oxidation of as high as 6 mM in a very fast and efficient manner. Under these conditions, the monomer was found to serve as an efficient inhibitor against corrosion of the rusty iron objects induced by concentrated HCl (**Figure 57**).

Figure 56. *Development of the chromophore of 3 on addition of 200 μM 3-phenyl-1,4-benzothiazine in 3:1methanol/36% HCl to an ethyl ether sample kept 1 month in air on the laboratory bench at a 3:1 v/v ratio before (A) and after (B) passage through a basic alumina column.*

Figure 57. *Rusty iron nails before (bottom) and after (middle) immersion in 36% HCl overnight and in the presence of 6 mM 1 (top)*

On average, the 3-phenyl-1,4-benzothiazine could decrease weight loss from rusty iron nails or staples immersed in concentrated HCl by ~50% over 24 h. Though the mechanism by which the monomer inhibits corrosion is at present unclear, it is conceivable that the effect is related in some way to the reduction of Fe(III) to Fe(II), slowing down rust generation or passivating the metal surface with Fe(II) oxides[88].

An experimental protocol was also developed for detection of peroxide or metal-containing samples involving addition of the solutions to be tested to 200 μM 1 in methanol followed by the immediate addition of concentrated HCl. After careful mixing, spectrophotometric reading at 598 nm after 10min at room temperature against the blank solution in the absence of added oxidant revealed the presence of peroxides or metal salts. Minimal detection limits with this protocol, as set by a ΔA598 of 0.05, were 50 μM for H_2O_2, 100μM for t-BuOOH, 100 μM for MCPBA, 20 μM for benzoylperoxide, and 30-50 μM for metal ions.

From the above data, a two-input logic gate "OR" system can be represented with the extra value of the proton switch (**Figure 58**). Biologically and technologically relevant inputs such as peroxides and redox-active biometals lead to a colorimetric output at 598 nm, completing the H^+-

switched OR logic gate. We plot the "truth table" for the response of these inputs in which output "1" is a ΔA598 of at least 0.05 and "0" is no change in A598 .

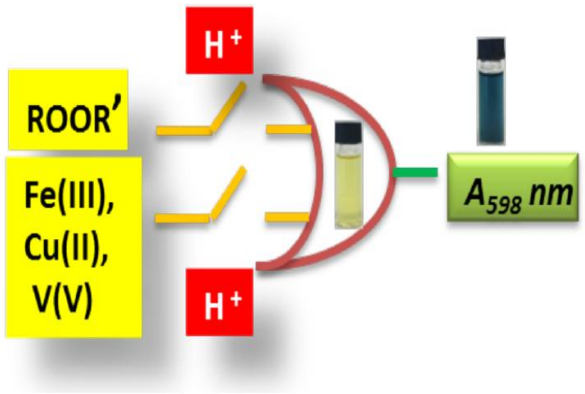

Input			Output[b]
H^+	ROOR	Metal ions[a]	
0	1	0	0
1	1	0	1
0	0	1	0
1	0	1	1
1	1	1	1
0	1	1	0

[a] Fe(III), Cu(II) or V(V)

[b] Output "1" is $\Delta A_{598} \geq 0.05$, "0" is no change in A_{598}

Figure 58. *Proton switched "OR" logic gating with peroxide and biometal inputs and colometric output based on the oxidation of 1. and truth table for the proton switched two inputs OR logic gating based on the oxidation of* ***1***

3.4 Benzothiazine based cyanine dyes: a) synthesis and characterization of dimeric cyanines

In the search for new benzothiazine based functional dyes, further to investigation of the $\Delta^{2,2'}$-bi-(2*H*-1,4-benzothiazine) system, another route was explored that may allow the access to benzothiazine-based cyanines. Two different classes of these dyes were developed that will be illustrated in this chapter and in the following.

3.4.1 Dimeric bnenzothiazine based cyanines

The first group of benzothiazine cyanine dyes that was investigated shows an extension of the conjugated system as =N-C=CH-CH=C-S- compared to those exhibited by $\Delta^{2,2'}$-bi-(2*H*-1,4-benzothiazine) system, a characteristic that should expectedly result in a larger batochromic shift in acid.

The only report in the literature on the access to dimeric benzothiazine cyanine dyes from 2H-1,4-benzothiazine dates back to 1975 and describes a 48 h TFA treatment[89] of 1-(*o*-aminophenylthio)-2,2-diethoxyethane, the same synthetic precursor of the $\Delta^{2,2'}$-bi-(2*H*-1,4-benzothiazine) system to obtain the 2,2'-(1,2-etandiilidene)-bis-(2H-1,4-benzothiazine) (**Figure 59**) as the main product . However, this reaction presents some unsettled issues regarding its mechanisms, such as the actual origin of the C_2H_2 bridge connecting the two benzothiazine units.

We have initially re-examined this intriguing reaction also in order to get some insight into the mechanistic aspects.

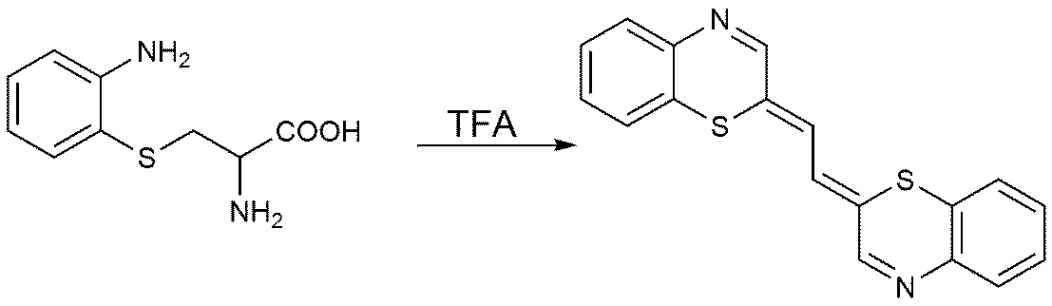

Figure 59. *Synthesis of 2,2'-(1,2-etandiilidene)bis(2H-1,4-benzothiazine.*

Prolonged TFA treatment of 1-(*o*-aminophenylthio)-2,2-diethoxyethane gave quite a simple pattern of products, mainly two red components with Rf=0.6 and Rf=0.4, (dichlorometnane/methanol) 99:1) together with a more retained yellow product. All of these compounds were isolated through a chromatographic purification on silica gel (dichlorometane/methanol) 98:2) and characterized.

Based on 1D and 2D NMR data (**Figure 60**), the most abundant product (Rf=0.4) was identified as the benzothiazine cyanine dimer, 2,2'-(1,2-etandiilidene)bis(2H-1,4-benzothiazine).

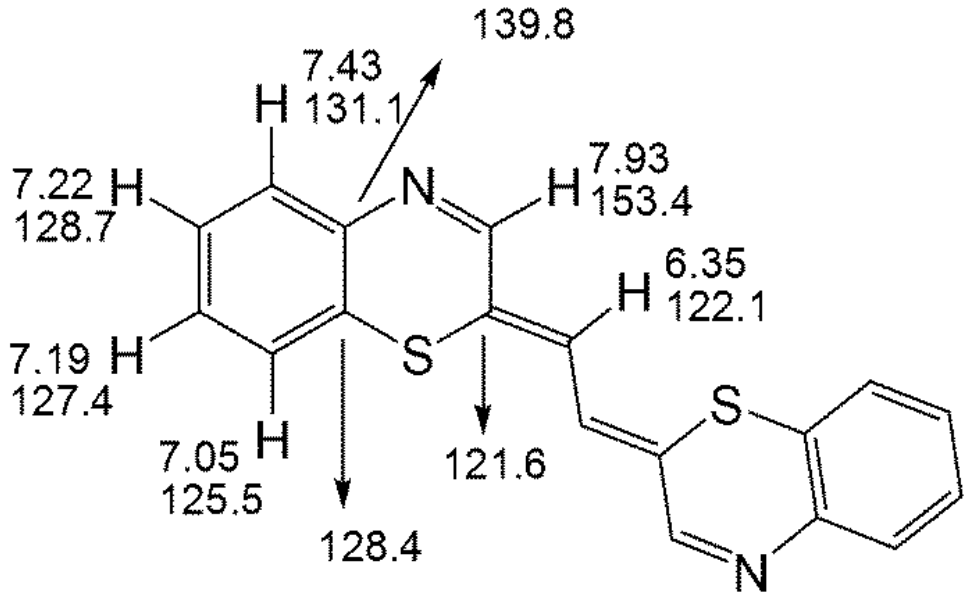

Figure 60. *^{1}H and ^{13}C resonances of 2,2'-(1,2-etandiilidene)bis(2H-1,4-benzothiazine).*

The other red product (Rf=0.6) showed a more complex pattern of signal and it was not further characterized. However some proton signals would suggest an asymmetric isomer of the dimeric cyanine. The most retained yellow compound was found the be the $\Delta^{2,2'}$-bi-(2*H*-1,4-benzothiazine).

Subsequent experiments were performed in order to understand the mechanism of formation of this product. At first, the reaction was repeated under controlled atmosphere, in order to assess whether oxygen had any role in the reaction. At the same reaction time (48 h) a minimal 1-(*o*-aminophenylthio)-2,2-diethoxyethane consumption was observed and the final products were barely formed.

In another experiment, the reaction was carried out using an excess of formaldehyde that could act as a carbon source and favor the building up of the methylene bridge. However, even in this case, it was not possible to see any enhancement in product formation.

These results suggest that construction of the symmetric C_2H_2 bridge may take place at the expenses of an intermediate that could act as the carbon source for cyanine formation and this could also account for the low isolation yields of 2,2'-(1,2-etandiilidene)bis(2H-1,4-benzothiazine). (15%) .

3.4.2 Chromophoric properties of 2,2'-(1,2-etandiilidene)bis(2H-1,4-benzothiazine).

The chromophore of the cyanine presents the expected acidochromic behaviour, as shown in **Figure 61.**

The neutral form shows an absorption maximum at 520 nm that undergoes a batochromic shift to 600 nm at pH 1, likely due to the monoprotonated form. On further acidification, another shift occurs at 650 nm , that corresponds to the diprotonated form . It should be noted that this shift is some 50 nm higher than that observed for the simple $\Delta^{2,2'}$-bi-(2*H*-1,4-benzothiazine).

These shifts are totally reversible under basic conditions. **(Figure 62).**

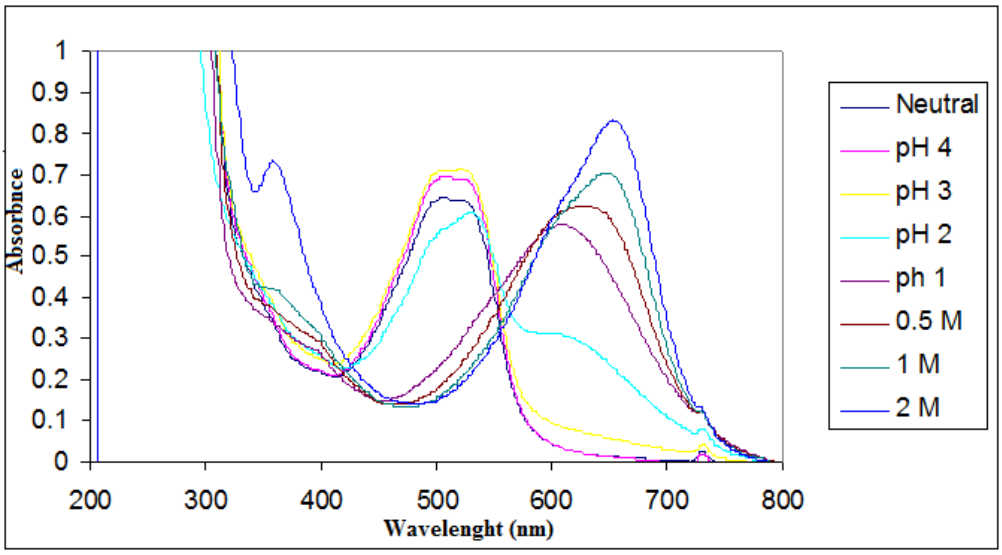

Figure 61.*Absorption spectra of 2,2'-(1,2-etandiilidene)bis(2H-1,4-benzothiazine) in acidic conditions*

Figure 62. *Chromophoric behavior of of 2,2'-(1,2-etandiilidene)bis(2H-1,4-benzothiazine)*

3.4.3 Synthesis of the symmetric benzothiazine cyanine from 3-phenyl-1,4-2H-benzothiazine

Based on these results, the reaction with TFA was extended also to the 3-phenyl-1,4-benzothiazine. The reaction proceeds very smoothly and again, the consumption of the starting material was almost complete after 48 hours. After extraction with CH_2Cl_2, and chromatographic purification, the red compound was obtained in pure form and subjected to a complete spectroscopic characterization. The ^{1}H NMR spectrum provided evidence for a highly

symmetric structure with a clear pattern of resonances for a single 1,4-benzothiazine moiety and the phenyl substituent and an additional singlet (1H) at 6.85 ppm. Complete 2D NMR characterization (COSY/ROESY/HMBC) led to assign the compound the 2,2'-(1,2-etandiilidene)bis(3-phenyl-2H-1,4-benzothiazine) structure with assignment of the proton and carbon resonances as shown in **Figure 63**. Assignment of the double bond configuration by spectroscopic techniques like ROESY contact was not conclusive. The relative stability of the possible isomers that is the *Z,Z* or the *E,E* in the *s*-cis or s-trans conformation was evaluated by computational analysis at the DFT level. The lowest energy is associated to the Z,Z isomer in the s-trans conformation.

Low isolation yields (25%) were observed also for this product. To investigate the mechanism of formation of the benzothiazine cyanine the reaction was repeated in an oxygen-free atmosphere. The mixture was worked up as usual and TLC analysis showed that the starting benzothiazine has remained almost unaltered even after a reaction time of 48 h.

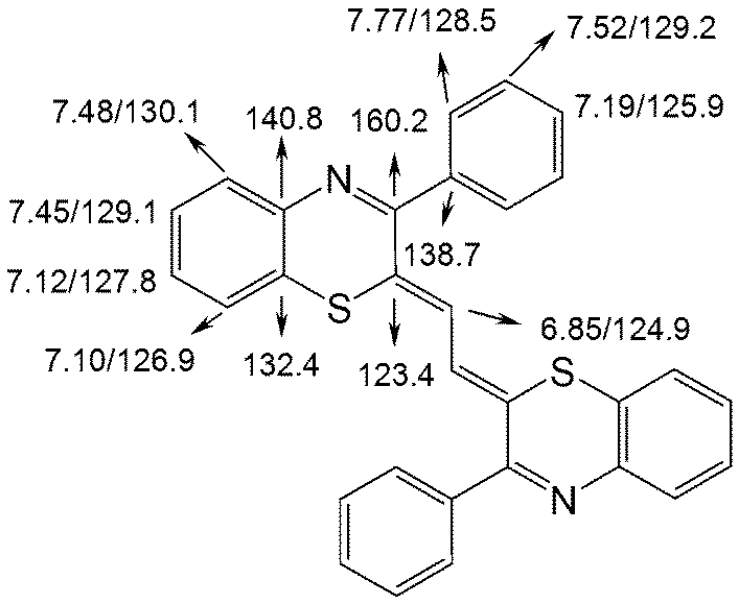

Figure 63 *^{1}H and ^{13}C NMR resonances of compound 2,2'-(1,2-etandiilidene)bis(3-phenyl-2H-1,4-benzothiazine).*

At this point , a different synthetic approach was necessary in order to improve this reaction. The most intuitive strategy would involve the addition of an external carbon source, and to achieve this purpose, the reaction was carried out in the presence of aldehyde compounds that may allow for the build-up of a conjugated bridge between the two benzothiazine units.

When a trifluoroacetic acid solution of 3-phenyl-1,4-benzothiazine was treated with excess formaldehyde at rt, the solution became rapidly green, but a satisfactory consumption of the starting compound was observed only after 48h. After removal of TFA the mixture was extracted with $CHCl_3$ (**Figure 64**).

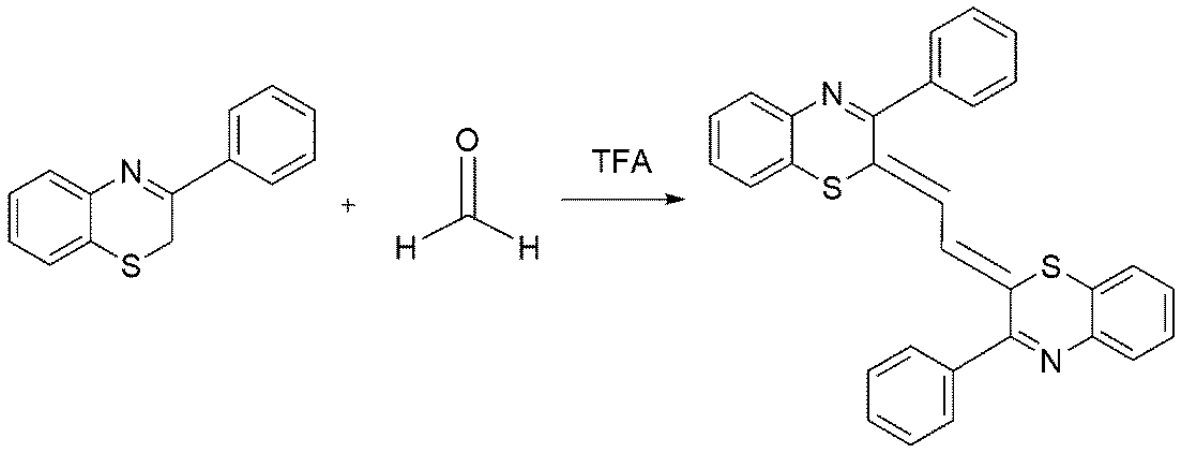

Figure 64. *Synthesis of 2Z,2'Z-(1,2-etandiilidene)bis(3-phenyl-2H-1,4-benzothiazine).*

TLC analysis showed the presence of a main product (R_f 0.4, CH_2Cl_2) red in color together with a yellow product (R_f 0.7) identified again as the $\Delta^{2,2'}$-bi-(2*H*-1,4-benzothiazine) by comparison with the available standard. The effect of the stoichiometric ratio of the reagents was then investigated in the range benzothiazine/formaldehyde 1:0.5, 1:1 ; 1:2.5 and 1:10. Comparative analysis of the reaction mixtures at 48 h showed that the 1:10 ratio resulted in a complete consumption of the starting benzothiazine and was the condition of choice to optimize the yields which were up to 25%.

The possible effects of water and temperature on the reaction course were also explored for the reaction mixtures at 1:1 and 1:10 stoichiometric ratios but neither of these parameters proved

to affect significantly the reaction course in terms of rate and product distribution with respect to the conditions initially adopted. The reaction was then repeated in MeOH/3M HCl (**Figure 65)** the conditions previously used for benzothiazine oxidative dimerization using the benzothiazine/formaldehyde at 1:10 ratio . After 4 h chloroform extraction and TLC analysis showed a complete consumption of the starting benzothiazine and the presence of the red component corresponding to the benzothiazine cyanine. Column chromatography purification of the reaction mixture gave the product in 41 % yield

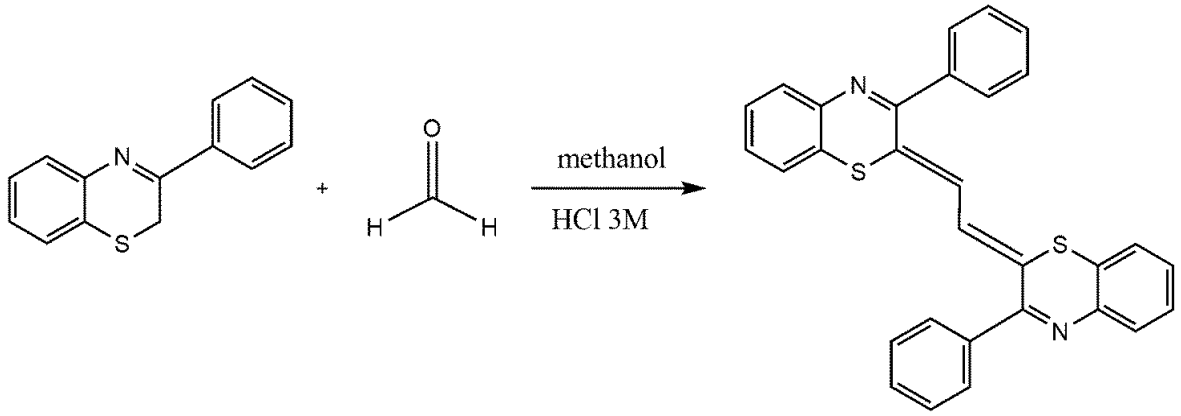

Figure 65. *Synthesis of 2Z,2'Z-(1,2-etandiilidene)bis(3-phenyl-2H-1,4-benzothiazine) in acid methanol with formaldehyde.*

The effect of the variation of the reaction parameters on the reaction course did not allow to draw conclusions on the mechanism of formation of the benzothiazine cyanine although the lack of product formation in the absence of oxygen would indicate that the reaction requires an oxidative step. Moreover the presence of a C-2 bridge between the benzothiazine units rather than a C-1 bridge that could be expected as the result of the nucleophilic reactivity of the benzothiazine in the enamine form onto the electrophilic formaldehyde would point to the symmetric coupling of an intermediate formed in the reaction medium rather than a multi-step process.

In other experiments, consideration of the structure of the benzothiazine cyanine led us to investigate whether the same product could be obtained by reaction of 3-phenyl-1,4-

benzothiazine with a bifunctional aldehyde that may provide the two carbons conjugated bridge between the benzothiazine units (**Figure 66)**. To this aim the reaction was carried out using glyoxal at 1/10 molar ratio with respect to the benzothiazine. After 1.5 h that is a significantly shorter time with respect to the other conditions explored the starting products were consumed and the cyanine dye was well apparent and could be obtained in 49% yield after column purification.

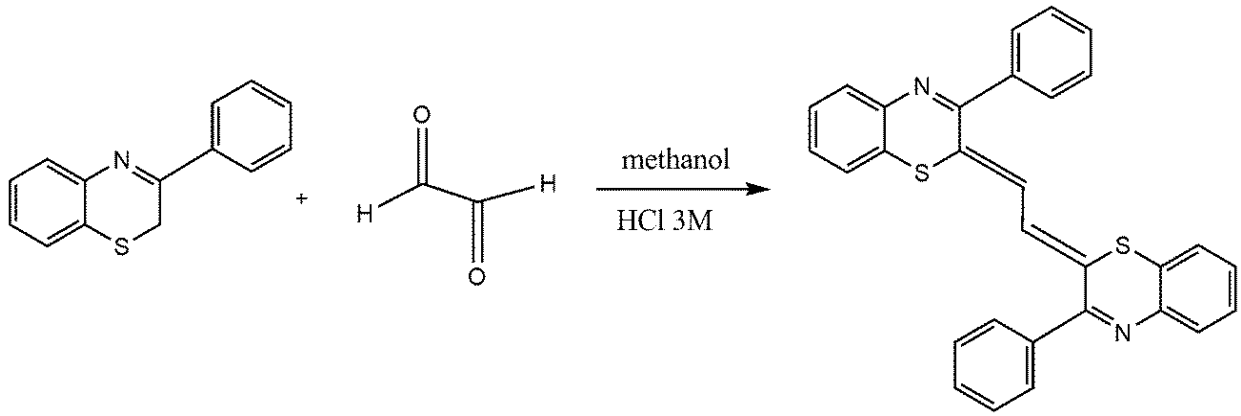

Figure 66. *Synthesis of 2Z,2'Z-(1,2-etandiilidene)bis(3-phenyl-2H-1,4-benzothiazine) by reaction of 3-phenyl-1,4-benzothiazine with glyoxal.*

Based on these results, it was taken into account the possibility that the reaction could be improved with increasing temperature. At first , the reaction was carried out in dioxan at 80°C, however, both the removal of the solvent and the workup were really difficult to achieve. Moreover it seemed , according to TLC analysis, that only the starting material was present in the reaction mixture. As a second approach , the reaction was carried out in acetonitrile at 70°C (**Figure 67)**. In this case, the consumption of the starting benzothiazine was observed after 5 hours and the reaction mixture, after extractive workup with chloroform, was found to be the desired product in pure form and this was confirmed also by NMR analysis.

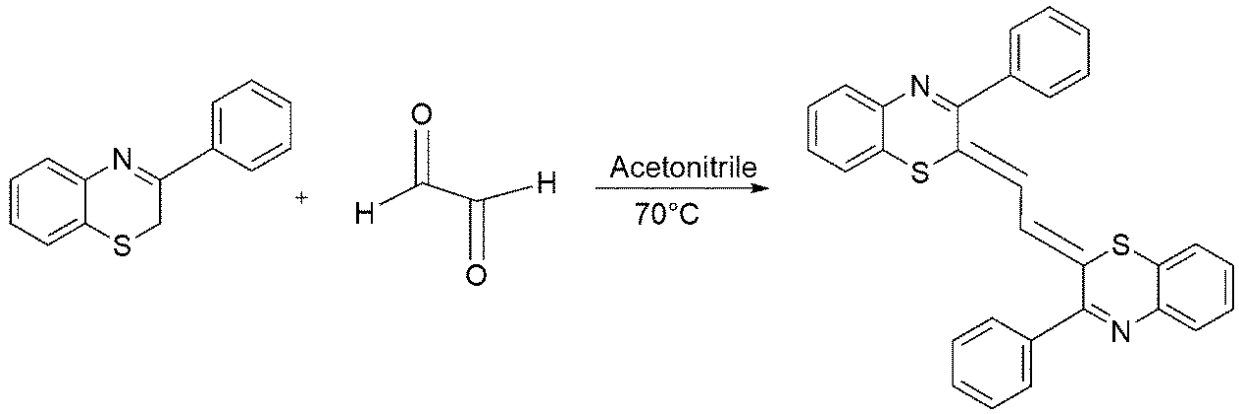

Figure 67. *Synthesis of 2Z,2'Z-(1,2-etandiilidene)bis(3-phenyl-2H-1,4-benzothiazine) with glyoxal and higher temperatures*

In conclusion, the reaction in acetonitrile at 70°C , proved to be the best synthetic approach for this compound, as it can be obtained in high yields (>60%) and without chromatographic purification

When the reaction was carried out using malondialdehyde in place of glyoxal in methanol solution in the presence of HCl, a dark mixture was immediately obtained with a significant consumption of the starting materials only after 24 h. After extraction with $CHCl_3$, TLC analysis of the mixture showed a complex pattern of products with no predominant components and this reaction was therefore no further investigated.

The reaction of formaldehyde in TFA was then extended to 3-methyl-2*H*-1,4-benzothiazine using a 1:10 molar ratio. TLC analysis showed a very smooth reaction and only after one week the presence of a complex pattern of products could be observed . A major component red in color (rf 0.5 in eluanthexane-ethyl acetate 8:2) could not be identified as any of the products obtained from the benzothiazine under the other conditions explored. In methanol/HCl the reaction proceeded more rapidly giving a pattern of products similar to that observed from the benzothiazine in the absence of formadehyde, but definitely more complex. The same product pattern was also obtained when glyoxal was used in place of formaldehyde.

3.4.4 Chromophoric properties of 2Z,2'Z-(1,2-etandiilidene)bis(3-phenyl-2H-1,4-benzothiazine)

The UV-vis and absorption properties of 2Z,2'Z-(1,2-etandiilidene)bis(3-phenyl-2H-1,4-benzothiazine) was analysed under neutral and acidic conditions (**Figure 68**). This compound showed an absorption maximum at 486 nm in methanol; a bathochromic shift to 617 nm was observed in the presence of HCl at 0.1 M final concentration. A further shift to 655 nm was obtained in 2M HCl. The molar extinction coefficients were measured for the abs at 486, 617, 655 nm as log ε 3.75, 3.61, 3.78, in the order. These absorption changes may be interpreted in terms of different states of protonation of the two benzothiazine nitrogen corresponding to the neutral, monocation and dication forms. This is in good agreement with results obtained with the $\Delta^{2,2'}$-bibenzothiazine for which absorption at 453, 556 and 590 nm were obtained for the neutral, monocation and dication although in the case of the cyanine under investigation the bathochromic shift observed on acidification was greater (131 nm vs 103 nm), on account of the more extended conjugation of the monocation of the cyanine compared to that of the parent $\Delta^{2,2'}$-bibenzothiazine.

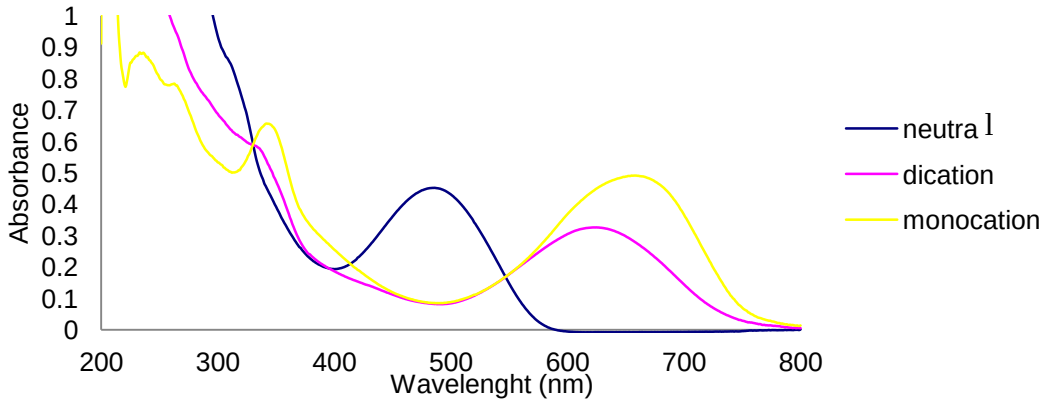

Figure 68.*Uv/Vis spectra of the 2Z,2'Z-(1,2-etandiilidene)bis(3-phenyl-2H-1,4-benzothiazine) in methanol (blue trace), methanol/0.1 M HCl (magenta trace) methanol/2 M HCl (yellow trace)*

3.5 Benzothiazine-based cyanine dyes: b)Cyanines by condensation of benzothiazines with aldehydes

Cyanine dyes are typically characterized by organic nitrogen centers, one of the imine and the other of the enamine type, which may be included into an heterocyclic system, linked through a variable number of double bonds generally in the trans configuration. In the case of the dimeric benzothiazine cyanines seen in the previous chapter , the chromophoric system presents a nitrogen and a sulfur center =N-C=CH-CH=C-S-.

However, it should be noted that this is not the only way to obtain a benzothiazine cyanine system. If the 1,4-benzothiazine reacts with an aromatic para *N*-alkyl substituted aldehyde, the classical cyanine chromophore could be built.

Herein, an alternative approach to the benzothiazine cyanine dyes was developed (**Figure 69**), involving reaction of the available 3-substituted benzothiazine with aldehydes. Specifically, commercially available aldehydes having in the para position an electrondonating group were chosen in order to construct in the expected condensation product the push pull system peculiar of cyanine dyes in which the “pull” side should be the imine function of the benzothiazine ring. Aldehydes bearing in the para position a hydroxyl group were also selected, as this group may act as the donor (push side) and is also expected to give rise to an additional chromophoric shift on deprotonation under basic conditions.

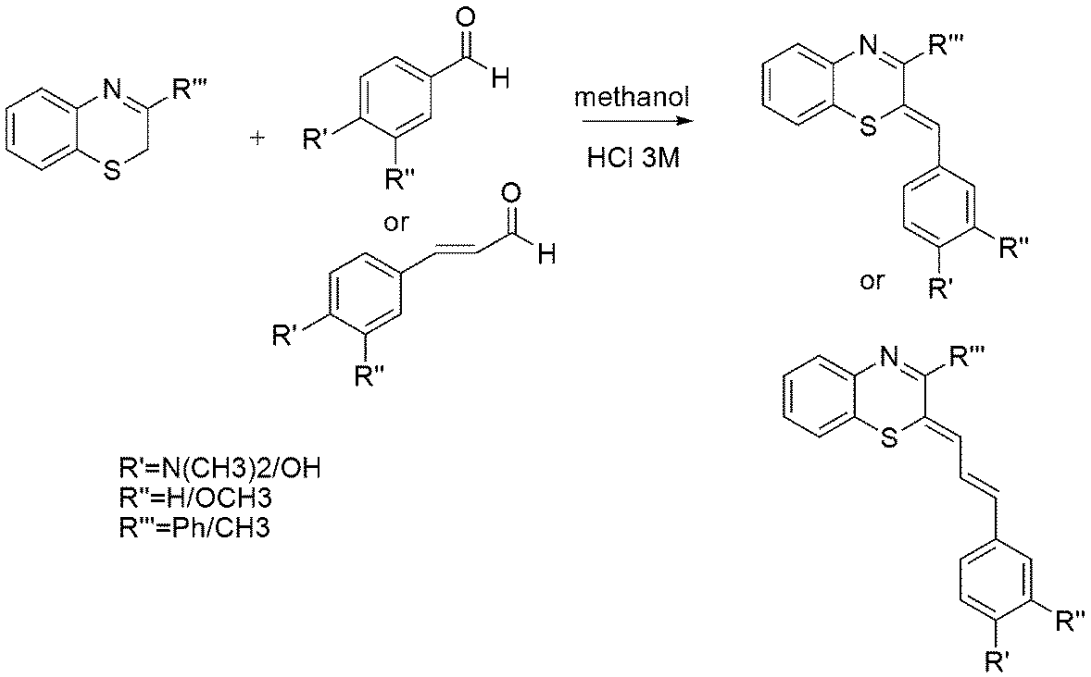

Figure 69. *General reaction scheme for the synthesis of cyanine dyes by reaction of 3-substituted-1,4-benzothiazine with aldehydes* .

At first, the typical reaction conditions for benzothiazine dyes synthesis were used, that is acidic methanol, in the presence of a variable excess of the desired aldehyde (1:0.5, 1:1 ; 1:2.5 and 1:10.) in order to find the optimal reaction conditions, that favour reaction of the benzothiazine with the functionalized aldehyde over self-coupling.

Further to this screening, the optimal conditions in terms of product yields involved treatment of the methanolic solution of the benzothiazine with a 10 fold molar excess of the aldehyde, followed by addition of HCl to a 3M final concentration. Yet, the aldehyde that remains in the reaction mixture is really difficult to remove, also because it is not easily separated from the condensation product by column chromatography under a variety of elution conditions. Therefore the synthesis were preferably carried out using a 1:1 molar ratio.

Under these conditions, it was possible to synthesize a number of benzothiazine/aldehyde condensation products (**Figure 70,72,74,76**) that were subjected to full spectral characterization

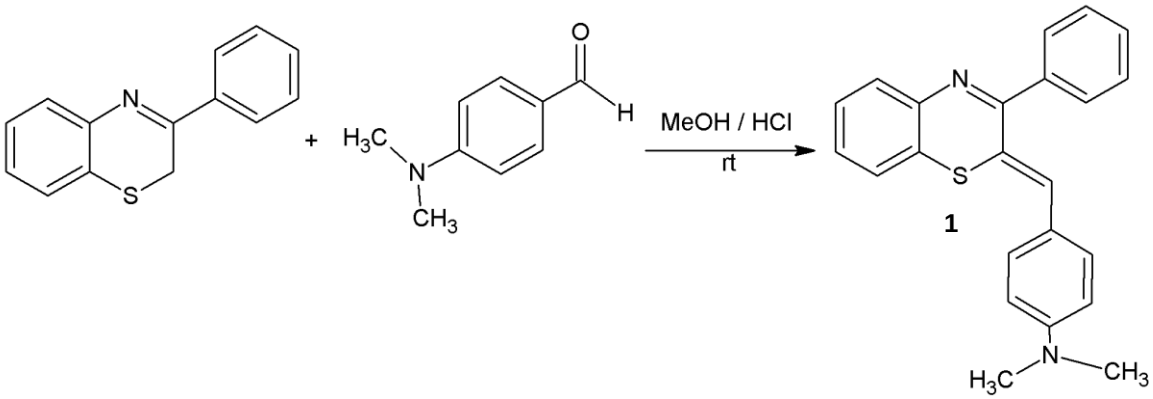

Figure 70. *Condensation between 3-phenyl-1,4-benzothiazine and p-dimethylaminobenzaldehyde*

The main component of the reaction was purified by column chromatography (44% yield) and subjected to complete structural characterization by NMR and MS analysis and formulated as the cyanine **1.** A complete assignment of the proton and carbon resonances is shown in the **Figure 71**.

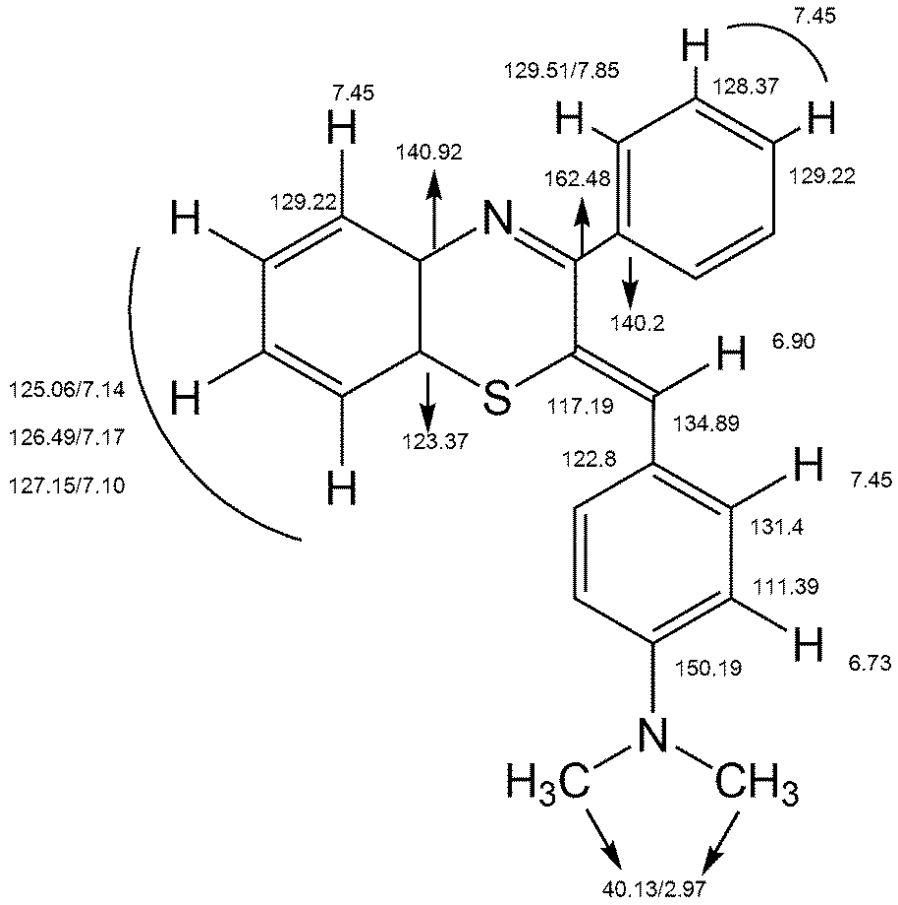

Figure 71. *^{1}H and ^{13}C NMR resonances of compound **1**.*

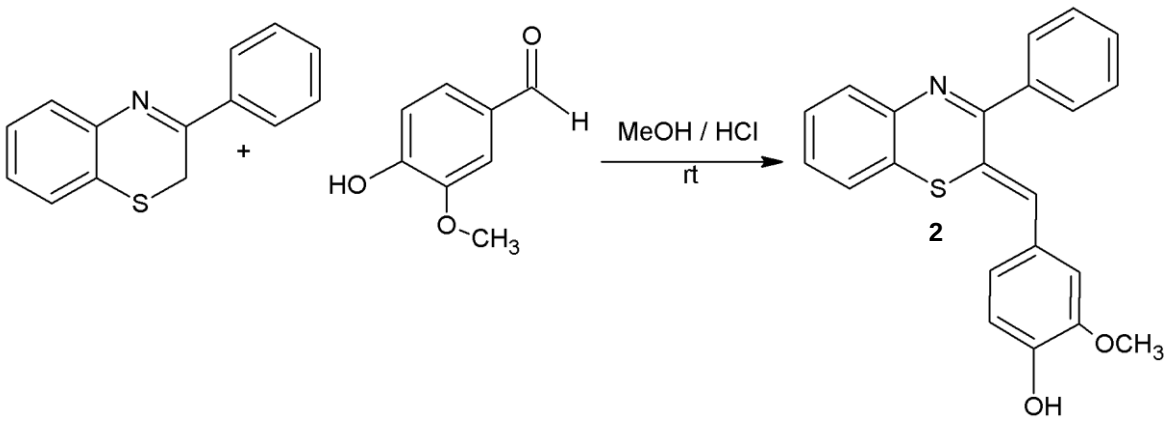

Figure 72. *Condensation between 3-phenyl-1,4-benzothiazine and 4-hydroxy-3-methoxy-benzaldehyde (vanillin)*

The main product of the reaction was isolated in pure form (40% yield) by column chromatography fractionation and subjected to complete spectral characterization leading to formulation of structure **2**. Assignment of proton and carbon resonances of the cyanine **2** is reported in the **Figure 73.**

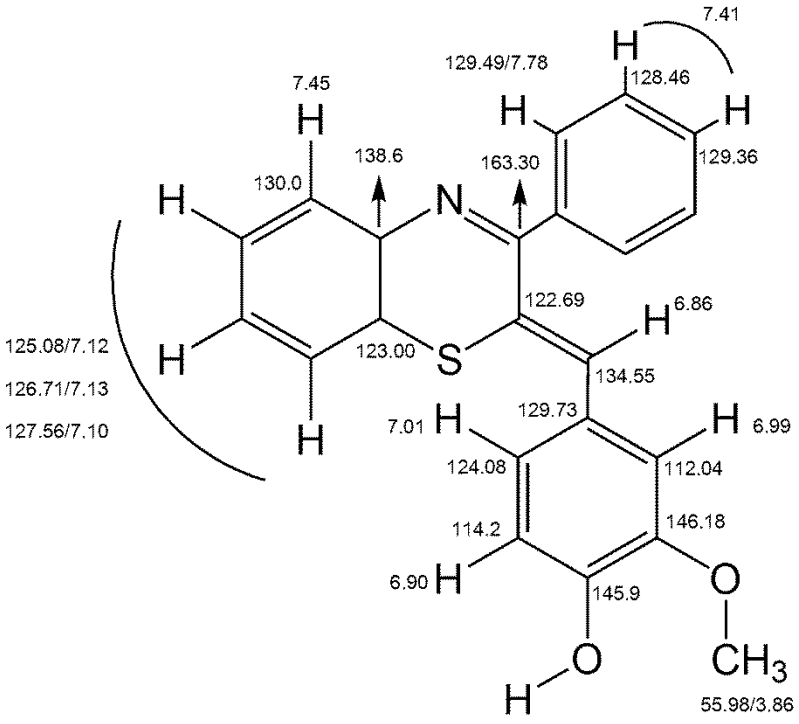

Figure 73 *^{1}H and ^{13}C NMR resonances of compound **2**.*

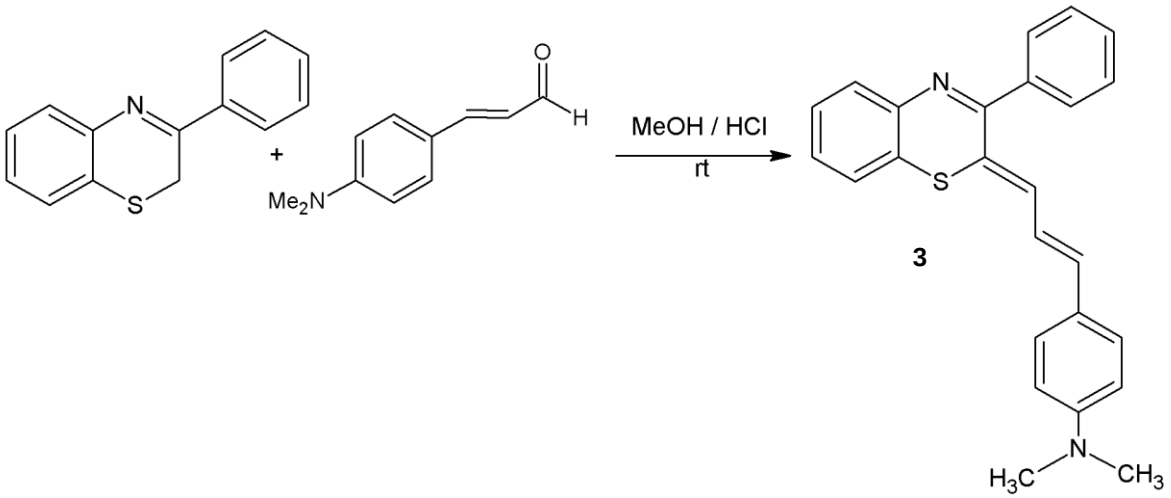

Figure 74. *Condensation between 3-phenyl-1,4-benzothiazine and p- dimethylaminoynnamaldehyde*

The mixture was extracted with $CHCl_3$ and the main reaction product isolated by column purification in 33% yield. A complete NMR characterization of the cyanine compound **3** is reported in **Figure 75**.

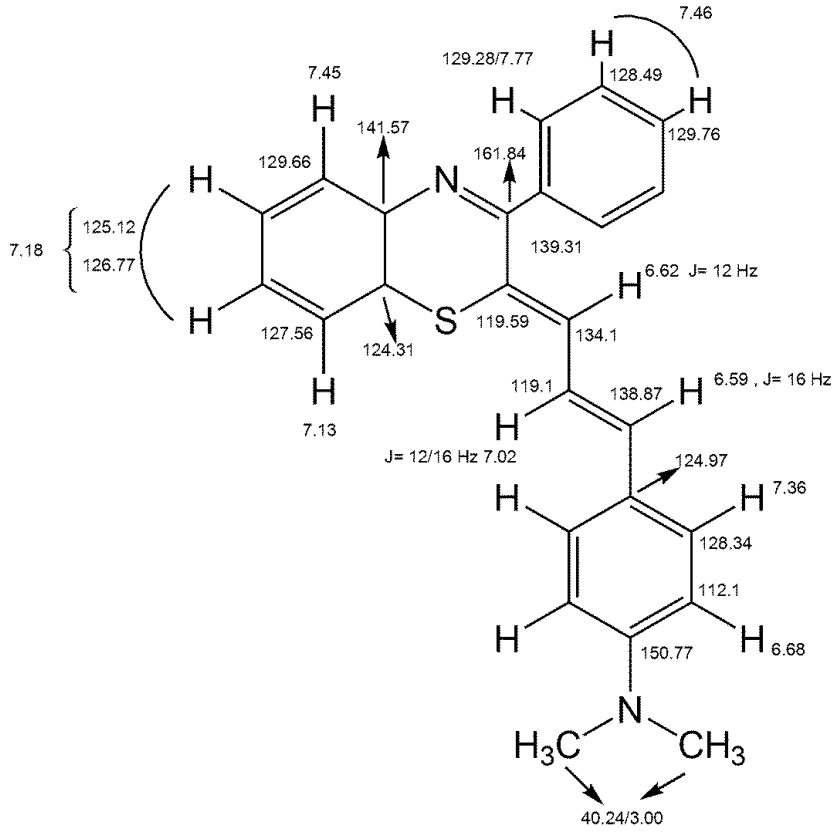

Figure 75 *^{1}H and ^{13}C NMR resonances of compound **3.***

The disubstituted double bond was assigned the *E* configuration based on the coupling constant of the 6.59 and 7.02 ppm protons, whereas the configuration of the other double bond could not be definitely assessed as no diagnostic ROESY contact could be observed. Computational analysis of the relative energy of the possible isomers in the accessible conformations, and comparison of the computed and experimental Uv/Vis spectra suggested that the isolated product is the Z,E isomer as shown in **Figure75** .

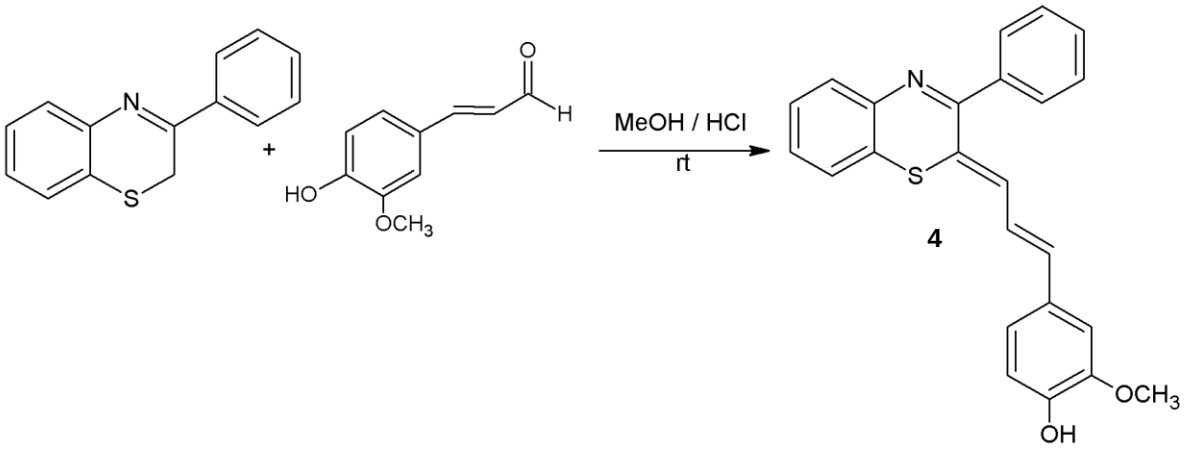

Figure 76. *Condensation between 3-phenyl-1,4-benzothiazine and 4-hydroxy-3-methoxycinnamaldehyde (ferulaldehyde)*

The main product of the reaction was isolated in pure form (60% yield) by column chromatography fractionation and subjected to complete spectral characterization leading to formulation of structure **4**. Assignment of proton and carbon resonances of the cyanine **4** is reported in the **Figure 77.**

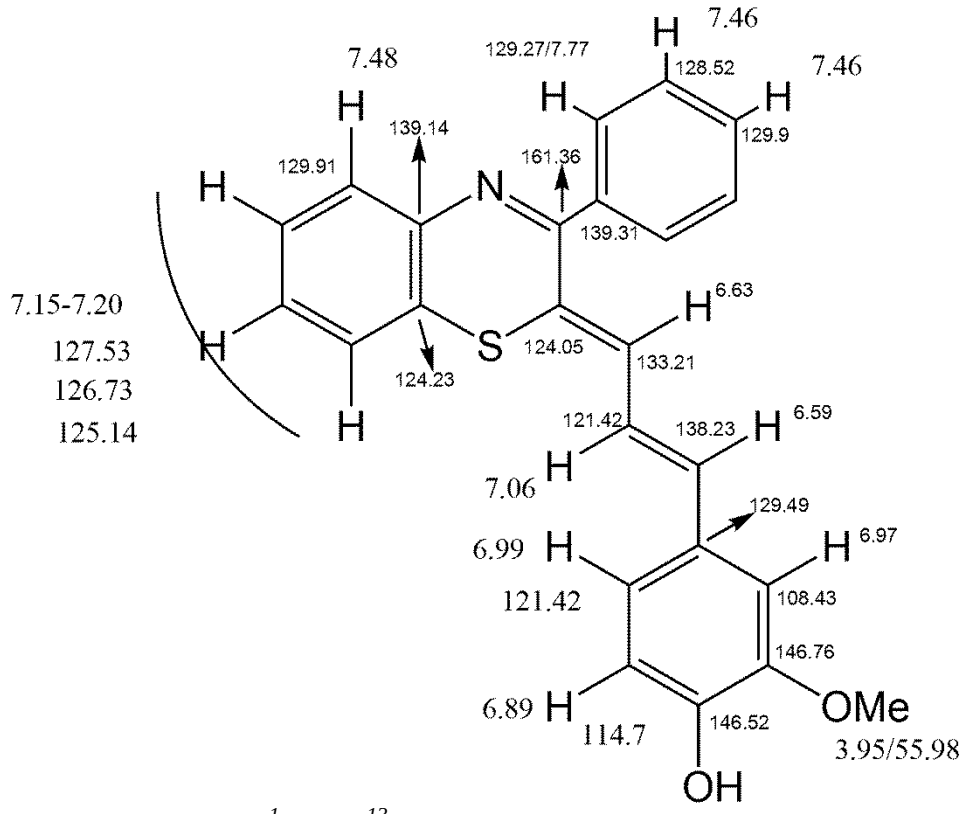

Figure 77. *^{1}H and ^{13}C NMR resonances of compound **4**.*

A similar series of reactions was carried out using 3-methyl-1,4-benzothiazine and p-dimethylaminobenzaldehyde, vanillin, and p-dimethylaminocinnamaldehyde as the aldehyde reagents. The reaction mixtures were extracted in $CHCl_3$ and sodium carbonate and the main product isolated through column purification in 60%, 44%, 32% and 35% yields for p-dimethylaminobenzaldehyde, vanillin, p-dimethylaminocinammaldehyde and ferulaldehyde, in that order. All these compounds were subjected to spectroscopic analysis and formulated as the condensation products **5-8** shown below with assignment of the proton and carbon resonances (**Figure 78-81**). The configuration shown for condensation product of p-dimethylaminocinnamaldehyde was supported by computational analysis as in the case of the analogous product obtained with 3-phenyl-1,4-benzothiazine (see exp).

.

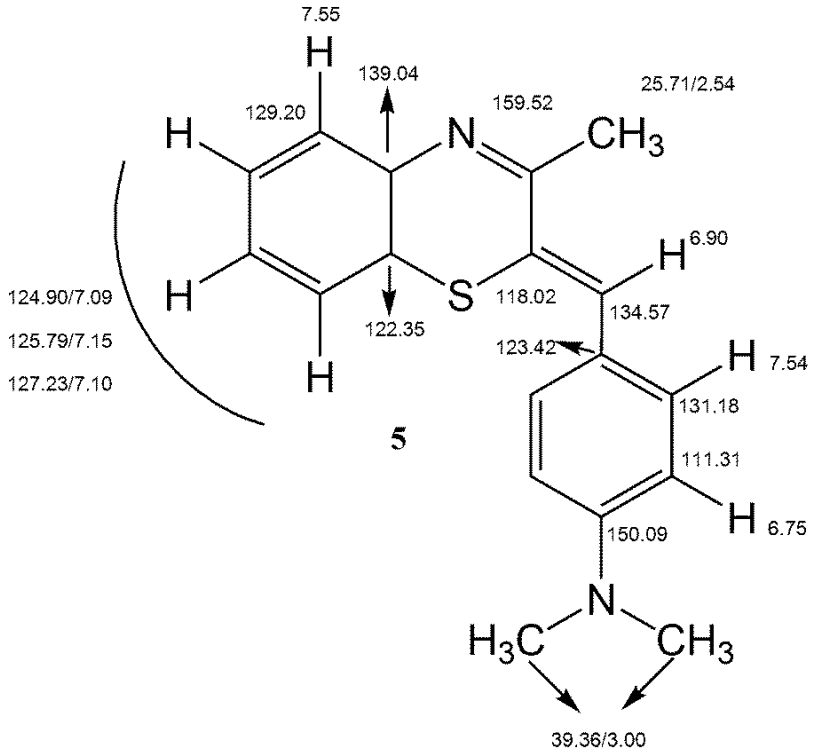

Figure 78 *^{1}H and ^{13}C NMR resonances of compound **5**, product obtained from 3-methyl-1,4-benzothiazine and p-dimethylaminobenzaldehyde*

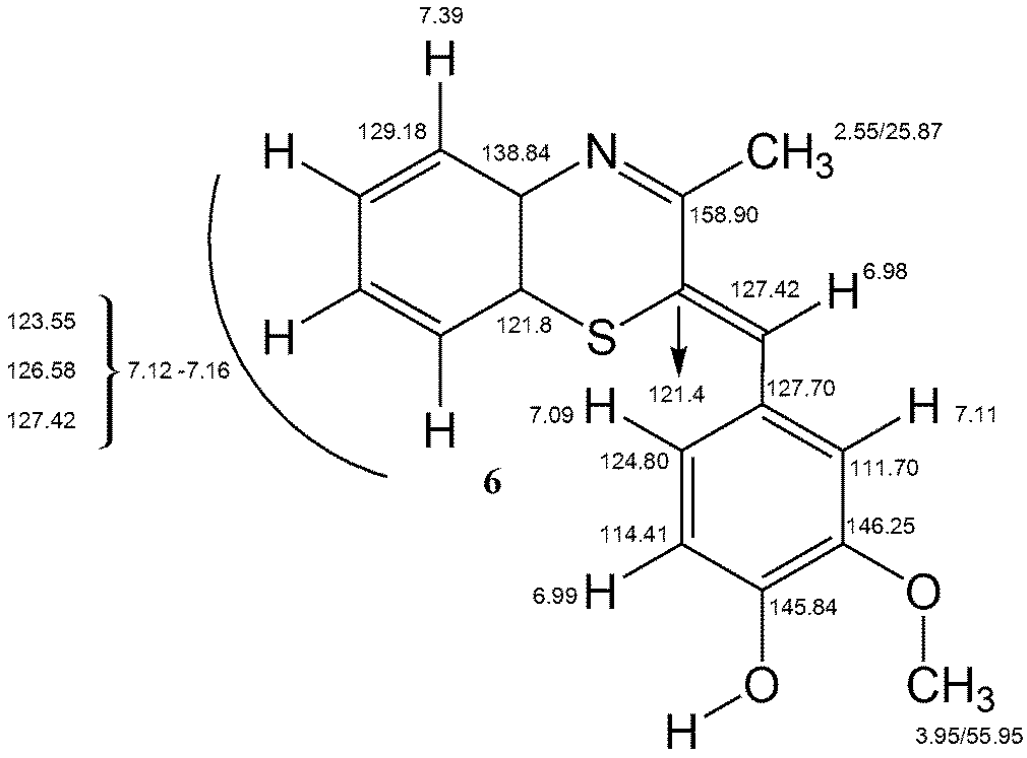

Figure 79 *^{1}H and ^{13}C NMR resonances of compound **6**, product obtained from 3-methyl-1,4-benzothiazine and 4-hydroxy-3-methoxy-benzaldehyde (vanillin)*

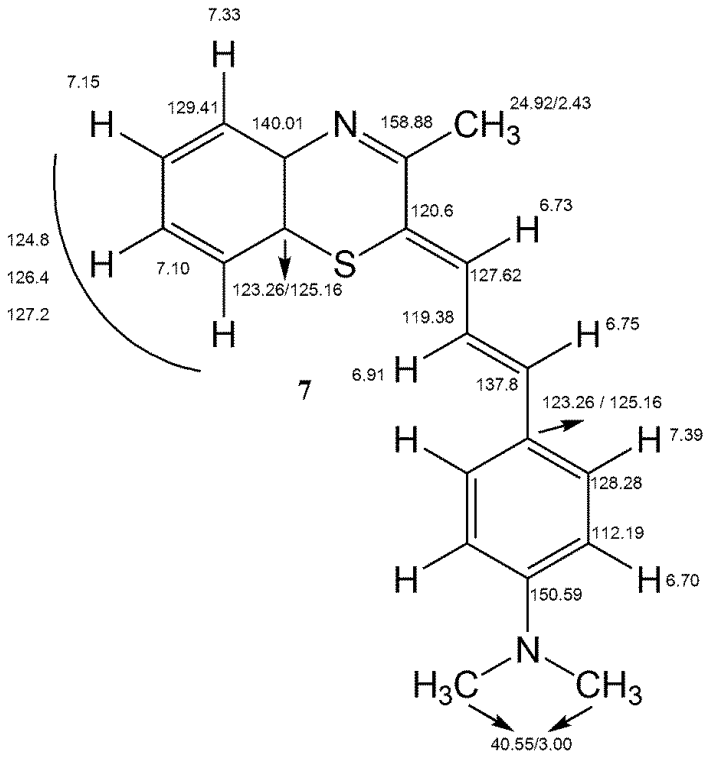

Figure 80 *^{1}H and ^{13}C NMR resonances of compound **7**, product obtained from 3-methyl-1,4-benzothiazine and p- dimethylaminoynnamaldehyde*

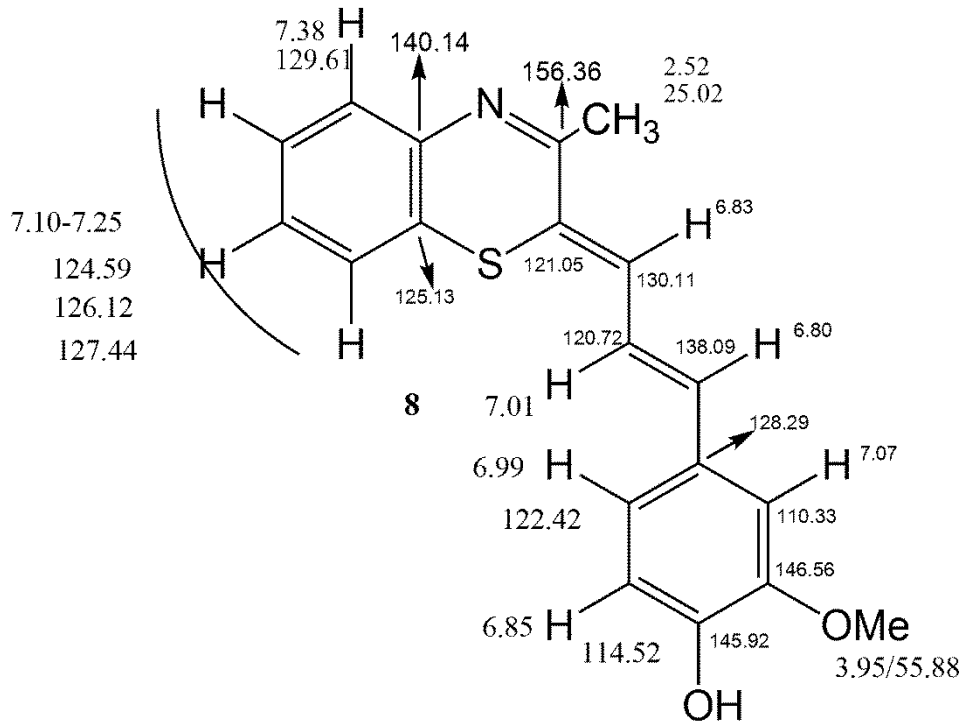

Figure 81 *^{1}H and ^{13}C NMR resonances of compound **8**, product obtained from 3-methyl-1,4-benzothiazine and 4-hydroxy-3-methoxycinnamaldehyde (ferulaldehyde)*

3.5.2 Characterization of the Uv-Vis absorption and fluorescence emission properties of the cyanines

As a further step of the research work the UV-vis and absorption properties of the benzothiazine cyanine compounds isolated and characterized were analysed under neutral and acidic conditions.

The UV/Vis spectra of the cyanines obtained by reaction of 3-substituted 1,4-benzothiazine with para *N*-alkyl substituted aldehydes are reported in **Table 2**, while the spectra of the compounds obtained by condensation with the vanilline ferulaldehyde having the 3-methoxy-4-hydroxy functionalities are reported in **Table 3**

Compound	λ_{max} *(nm)* ε *($M^{-1}cm^{-1}$)*		
	Methanol	*Methanol /first shift*	*Methanol / second shift*
1	440 (9200)	605 (9300)	481 (5100)
3	464 (18200)	686 (19100)	520 (10700)
5	429 **(**7200)	581 (11700)	481 (3200)
7	458 (4500)	644 (5600)	505 (2300)

Table 2. *Absorption maxima and molar extinction coefficients of the cyanines from 3-substituted-1,4-benzothiazine with the N-dimethylamino aldehydes.*

Compound	λ_{max} *(nm)* ε *($M^{-1}cm^{-1}$)*	
	Methanol / HCl	*Methanol NaOH*
2	530 (12200)	467 (12500)
4	580 (13500)	492 (12600)
6	505 (5500)	450 (7500)
8	553 (6600)	390 (9400)

Table 3. *Absorption maxima and molar extinction coefficients of the cyanines from 3-substituted-1,4-benzothiazine with the vanilloid aldehydes.*

It can be observed that all the cyanines show a batochromic shift on acidification. However, only those obtained from the p-dimethylamino substituted aldehydes show an ipsochromic shift on further acidification. As expected, the cyanines obtained from the aldehydes bearing a OH group at the para position, show a chromophoric shift in alkali.

In all cases the molar extinction coefficients of the acid forms is higher than that of the species prevailing under neutral conditions. This is also true for the alkali shifts with the compounds obtained from vanillin and ferulaldehyde. The molar extinction coefficients of the cyanines obtained from 3-phenyl-1,4-benzothiazine are invariably higher than those obtained from 3-methyl-1,4-benzothiazine.

All of the absorption changes observed may well be interpreted in terms of the cyanine type structures proposed for the compounds investigated. Thus the batochromic shift on acidification observed for all the chromophores can be ascribed to the enhanced “pull” characteristic of the imine C=N system in the protonated $C=NH^{+}$ form. Larger batochromic shift are expected for the cyanines obtained from p-dimethylaminocinnamaldehyde compared to those obtained from the p–dimethylaminobenzaldehyde on account of the more extended conjugated double bonds

system connecting the "donor" "acceptor" groups. On the other hand, compounds obtained from vanillin in which the push tendency of the OH group is clearly lower with respect to the $N(CH_3)_2$ group exhibit a lower batochromic shift (around 100 nm) in the acid form. Yet, the absorption wavelength of the acid forms of the vanillin condensation products (530 nm for the 3-phenyl and 505 for the 3-methyl) are higher than that of the cyanine from aldehydes substituted with the dimethylamino group in concentrated acids (481 nm) as protonation results in a severe abatement of the electrondonating characteristic of this group.

For all these compounds, great changes of absorbance in different acidic or basic conditions were observed. On this basis, a detailed analysis of the absorbance spectra at different HCl concentrations was run for every cyanine synthesized and the results are shown in **Figure 82-89**

.

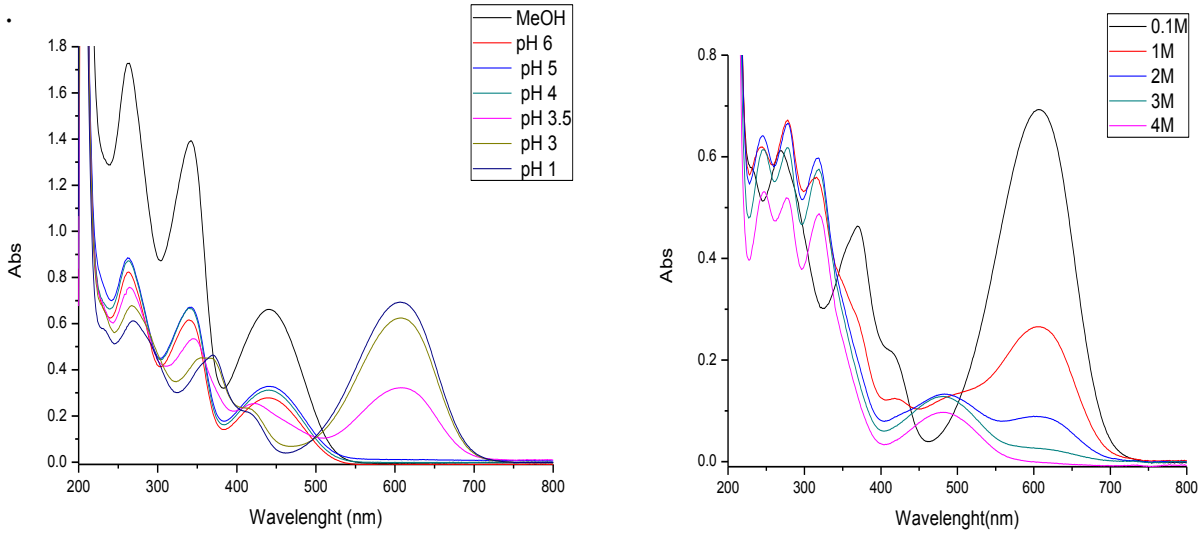

Figure 82. *UV-vis absorption spectra in different pH condition of compound* ***1***

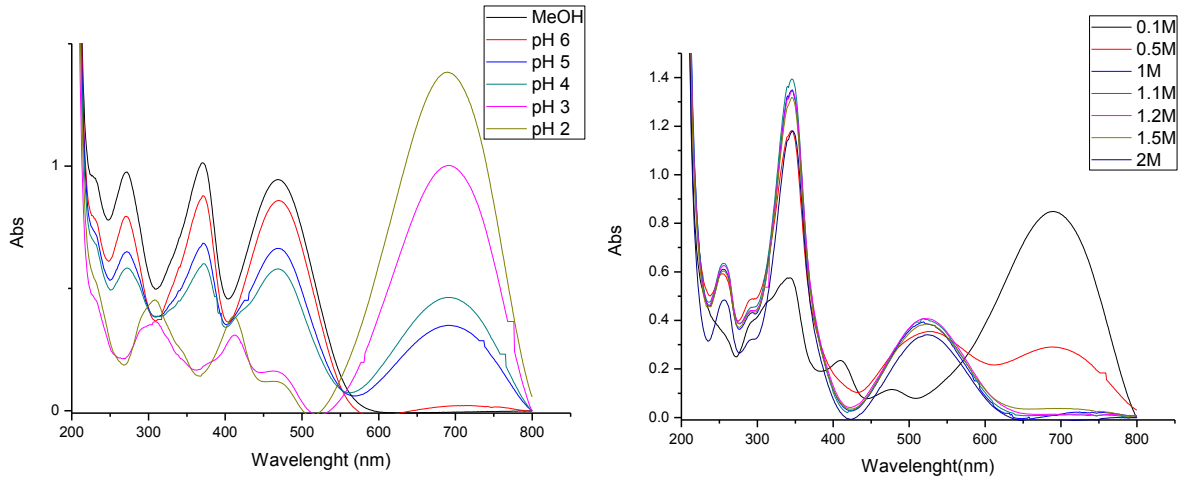

Figure 83. *UV-vis absorption spectra in different pH condition of compound* ***2***

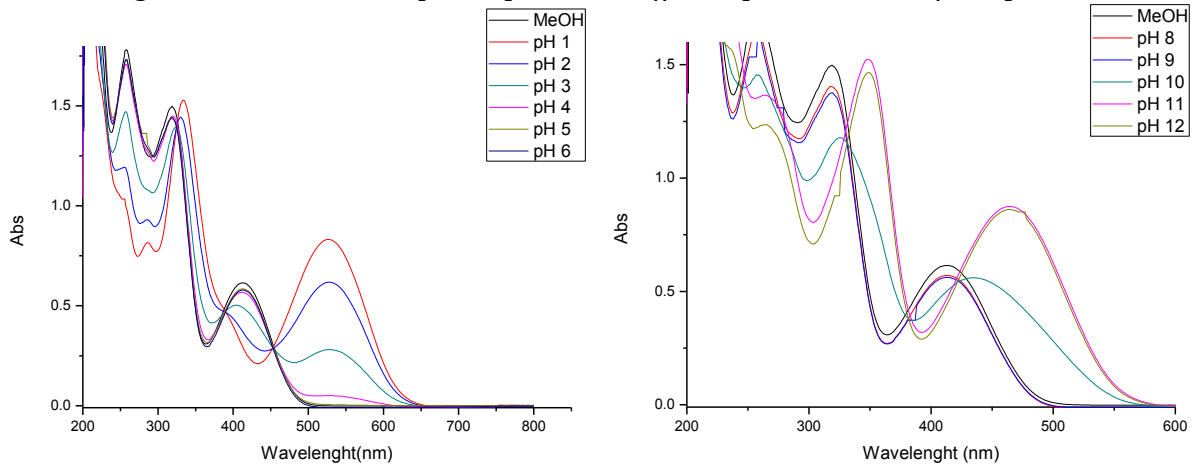

Figure 84. *UV-vis absorption spectra in different pH condition of compound* ***3***

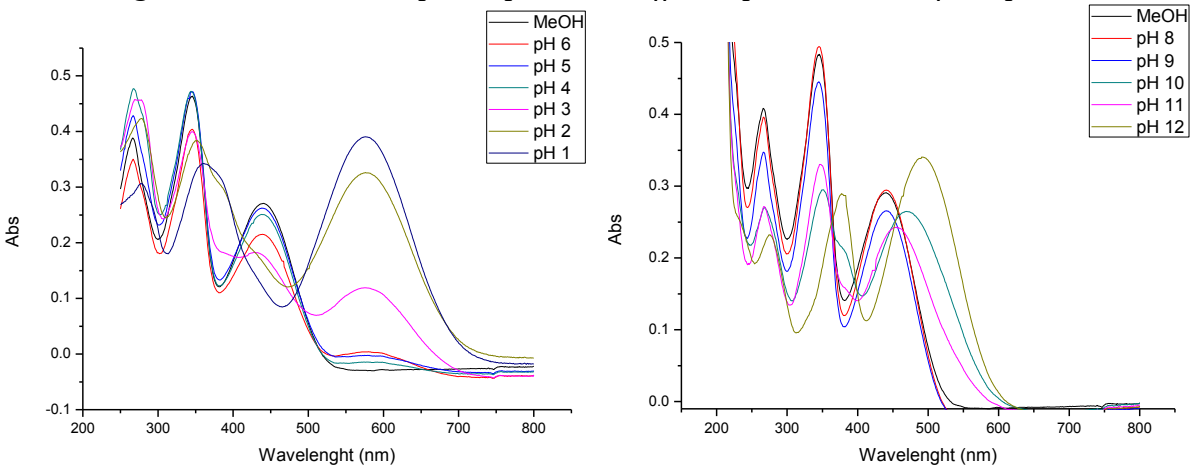

Figure 85. *UV-vis absorption spectra in different pH condition of compound* ***4***

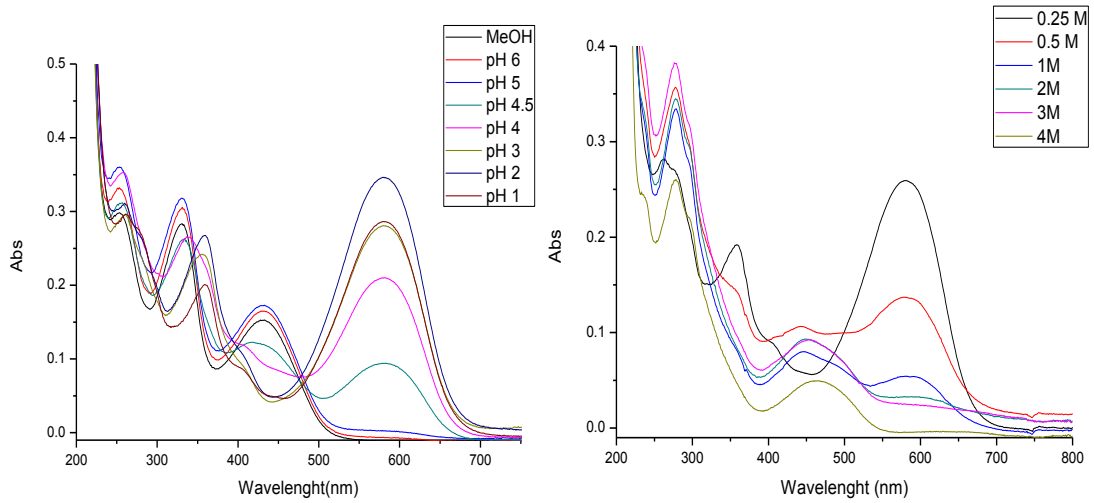

Figure 86. *UV-vis absorption spectra in different pH condition of compound* ***5***

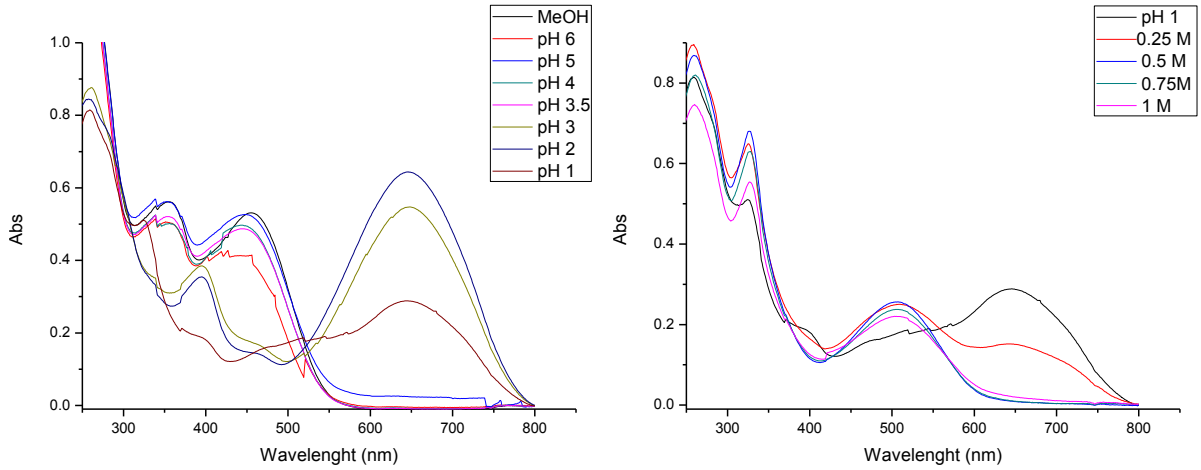

Figure 87. *UV-vis absorption spectra in different pH condition of compound* ***6***

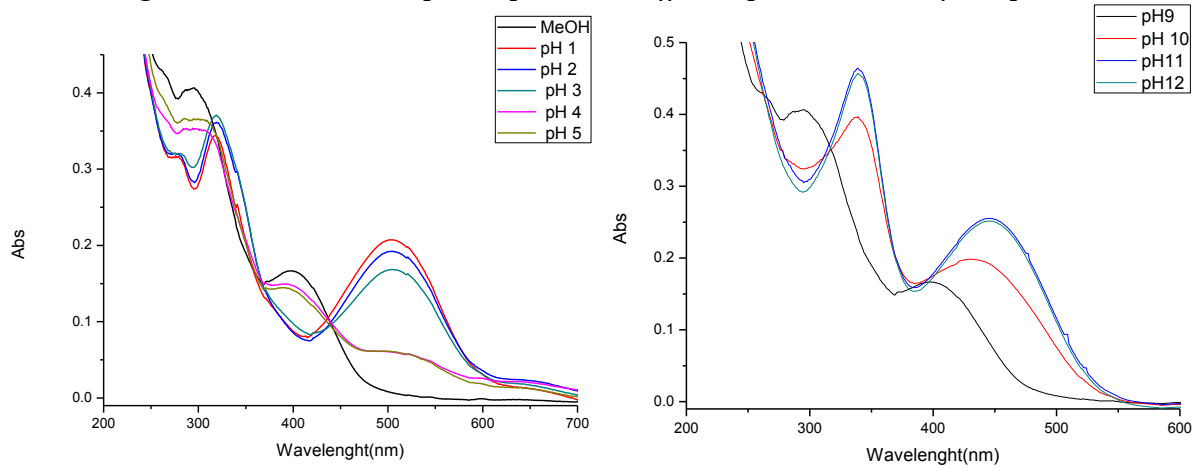

Figure 88 *UV-vis absorption spectra in different pH condition of compound* ***7***

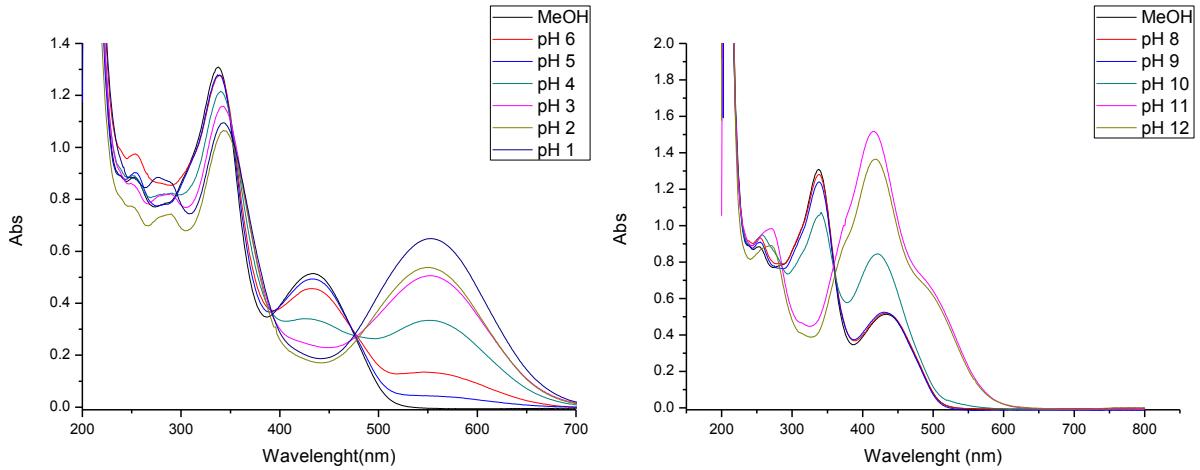

Figure 89. *UV-vis absorption spectra in different pH condition of compound* ***8***

From this Uv-Vis spectra, it can be observed that the batochromic shift on acidification occurs between pH 3-4 for all the compounds examined. Therefore these compounds are more easily converted to their protonated forms compared to both the dimeric cyanines benzothiazines and the the parent $\Delta^{2,2'}$-bibenzothiazine dimer (around pH 2). Under strong acid conditions (4M HCl) the cyanines derived from para-N-dimethylaminobenzaldehyde undergo a further ipsochromic shift on account of the protonation of the dimethylamino group with loss of its donor capacity. On the other hand the cyanines derived from p-N-dimethylaminocynnamaldehyde undergo the batochromic shift under milder acidic conditions (HCl 0.5M) Under basic conditions, the batochromic shift for the vanillin-type cyanines occurs around pH 10. **Table 4** reports all the pK_a calculated from these spectra.

Compound	pK_{a1}	pK_{a2}
1	3.5	
2	2.8	10.1
3	3.8	
4	3.5	9.8
5	4.2	
6	4.8	9.7
7	3.4	
8	3.7	10.3

Table 4. *Calculated pK_a for cyanines* ***1-8***

Finally, the fluorescence emission properties of these compounds (**Figure 90-97**) were analysed in methanol, under different acid and basic concentration conditions and in dichloromethane.

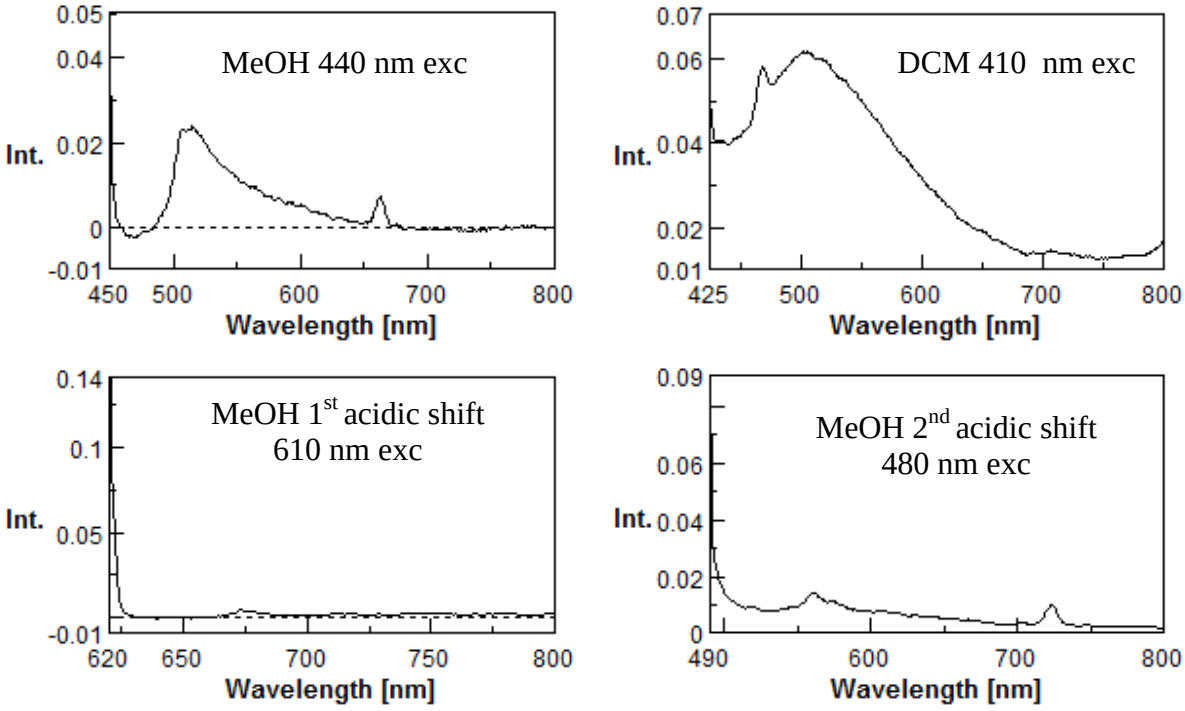

Figure 90**. Fluorescence spectra of compound **1

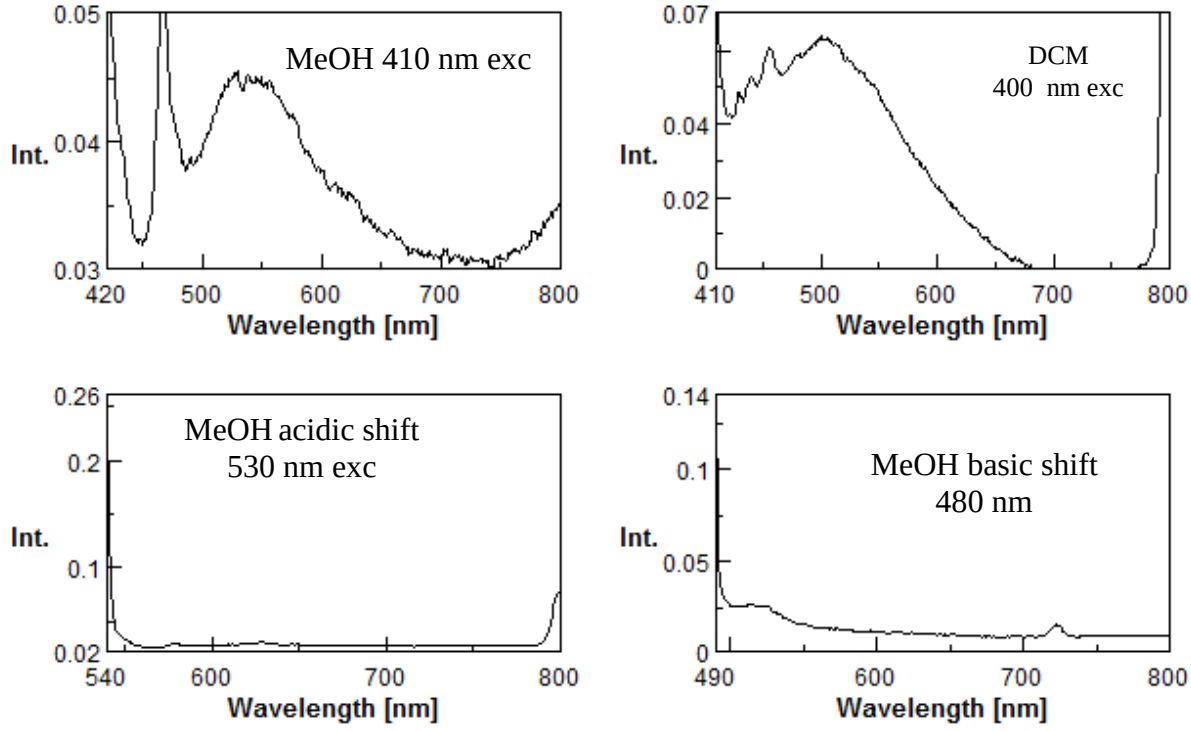

Figure 91**. Fluorescence spectra of compound **2

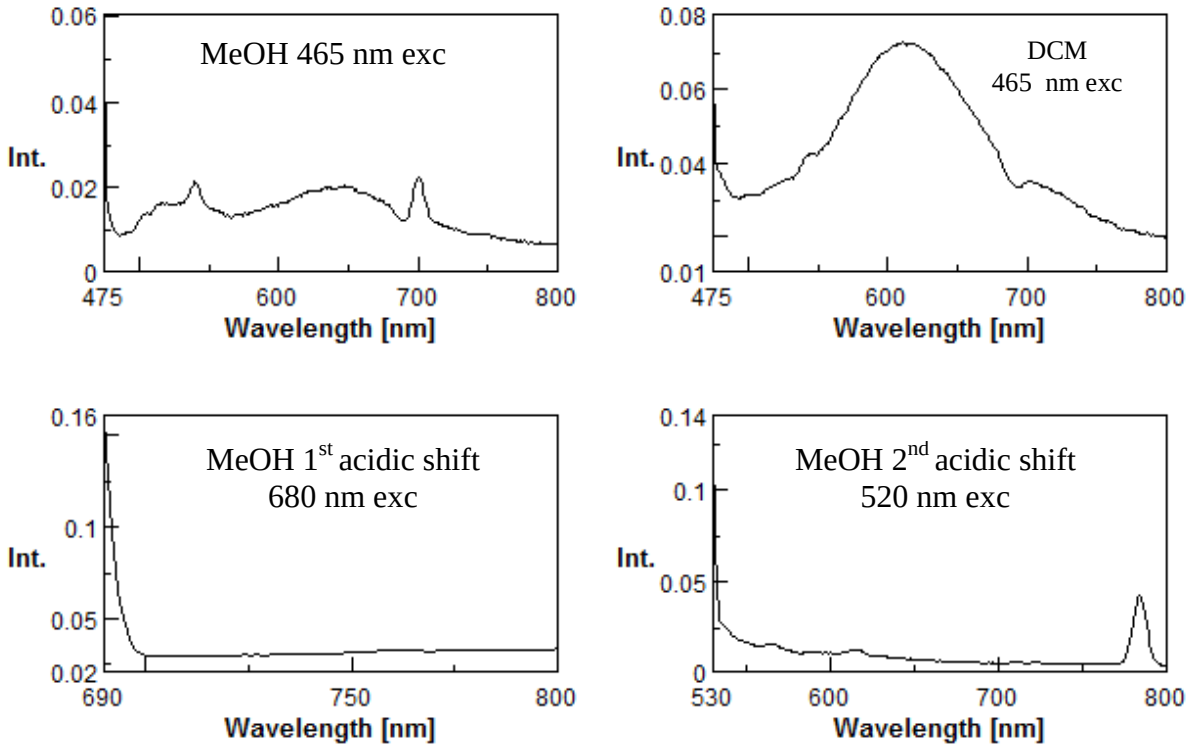

Figure 92**. Fluorescence spectra of compound **3

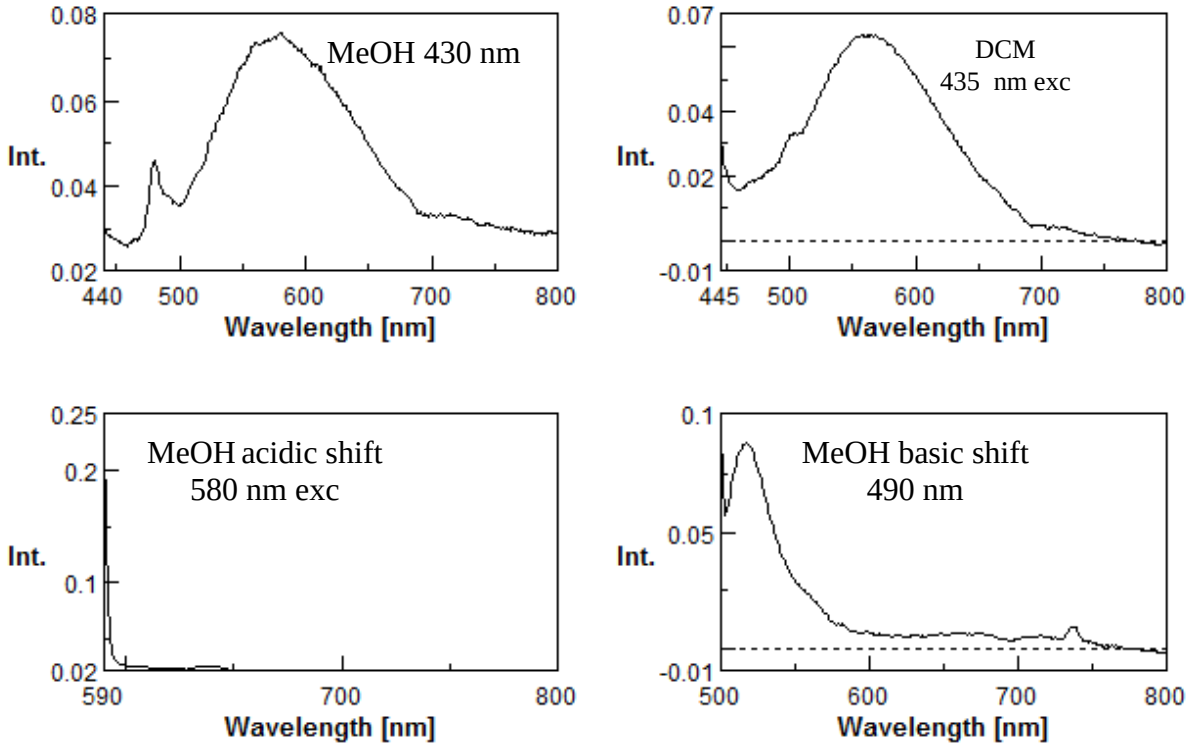

Figure 93**. Fluorescence spectra of compound **4

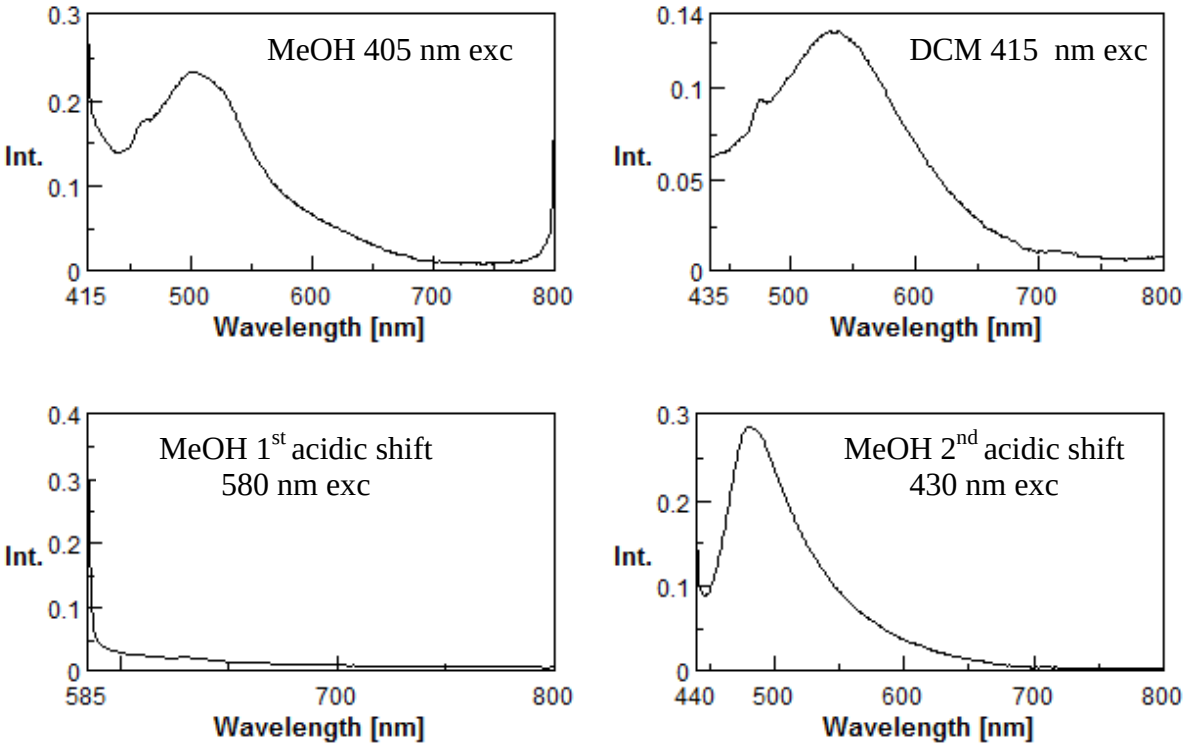

***Figure 94**. Fluorescence spectra of compound* **5**

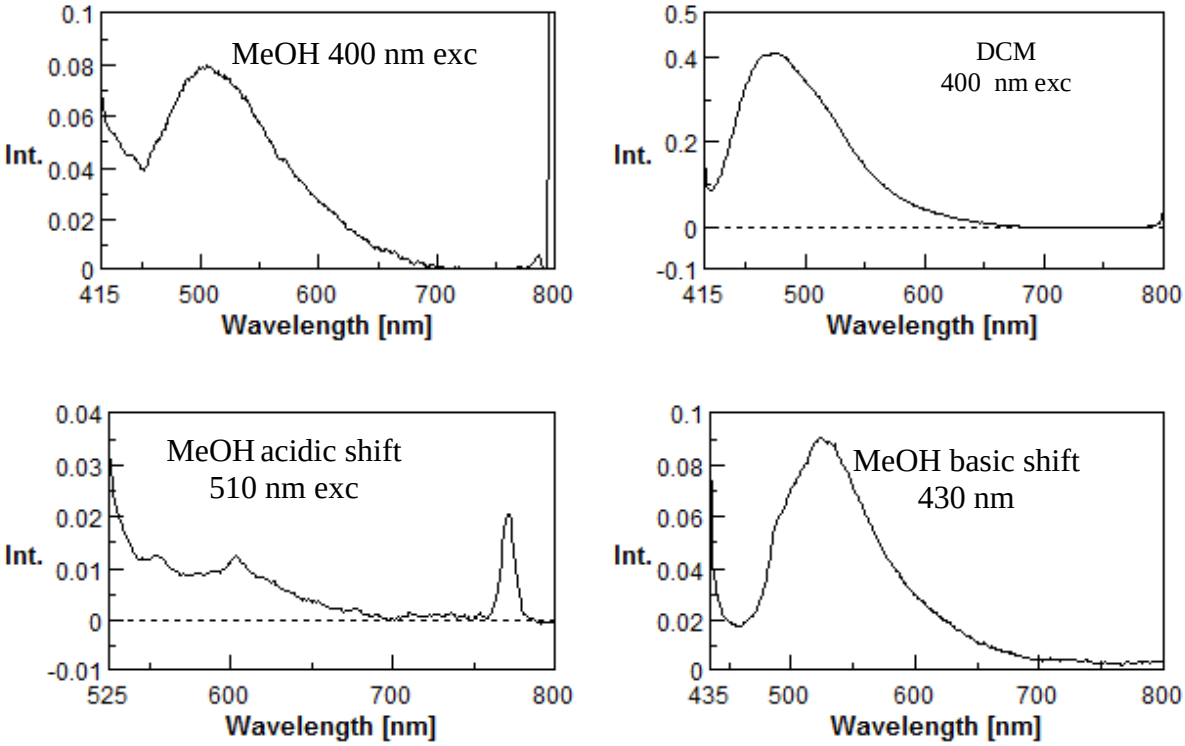

Figure 95**. Fluorescence spectra of compound* ***6

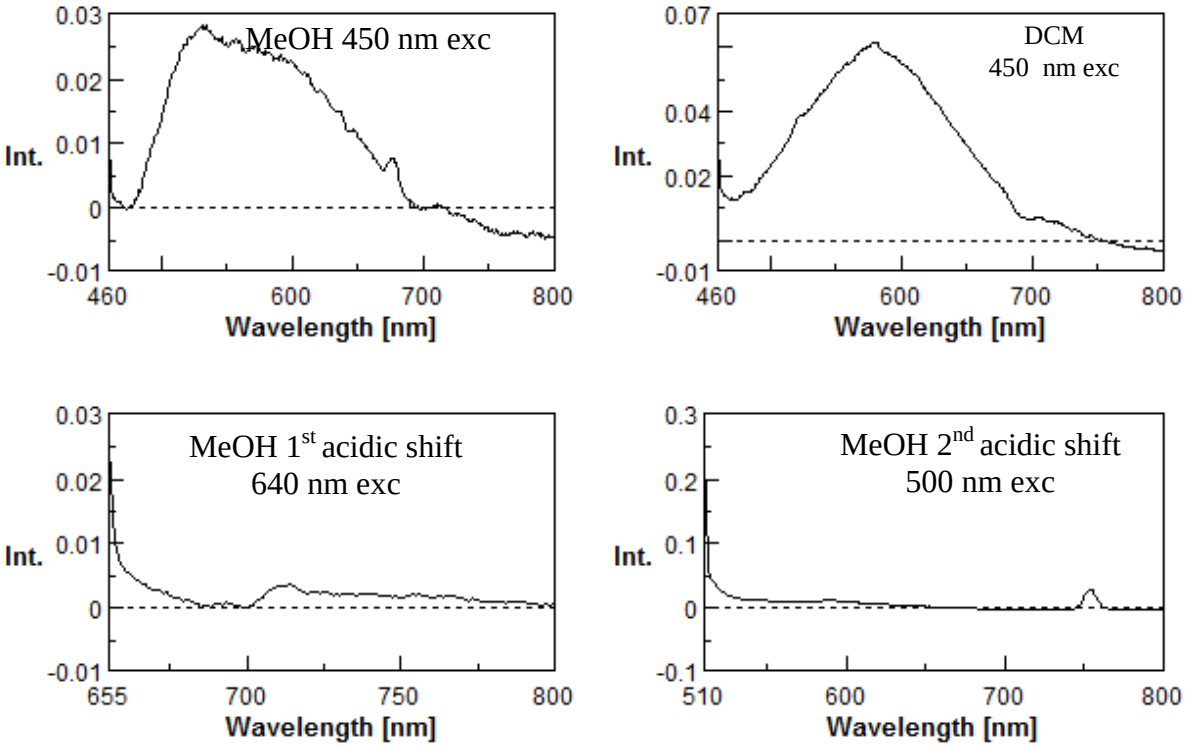

Figure 96**. Fluorescence spectra of compound **7

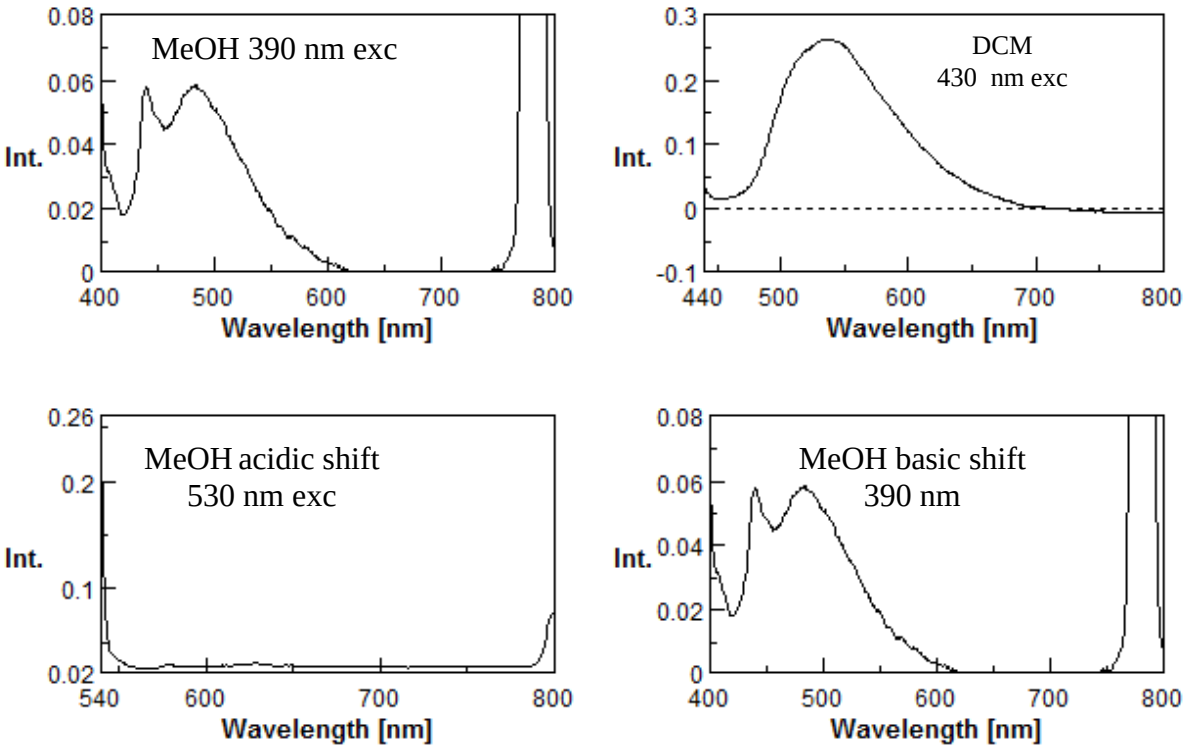

Figure 97**. Fluorescence spectra of compound **8

From these spectra it can be observed that the highest fluorescence emission was exhibited by the condensation product of 3-methyl-1,4-benzothiazine with vanillin. Also the compounds obtained from ferulaldehyde and condensation product between 3-methyl-1,4-benzothiazine and para-N-dimethylamino-benzaldehyde show a modest emission of fluorescence .As a general trend, the fluorescence is almost completely switched off in acidic conditions. This behavior is common for almost all the compounds investigated, with the only exception represented by the product obtained from 3-methyl-1,4-benzothiazine and para-N-dimethylamino-benzaldehyde. In this case the fluorescence is switched off where the first protonation occurs, but switches on again under more acidic conditions when the second protonation takes place.

To evaluate the potential of these compounds as fluorescence reporter the fluorescence quantum yield was determined (**Table 5**) in comparison with the standard compound rhodamine b, according to the equation shown below[90]:

$$\emptyset_x = \emptyset_{st} \times \frac{F_x}{A_x}\frac{A_{st}}{F_{st}} \times \frac{\eta_x^2}{\eta_{st}^2}$$

Where ∅ is the quantum yield, F is the area of the fluorescence spectrum , A is the absorbance intensity and η the is the refractive index.

Table 5: *Emission wavelengths and quantum yields of cyanines 1-8 compared to the standard rhodamine b*				
Compound	λ_{max} *excitation (nm)*	λ_{max} *emission (nm)*	*Quantum yield DCM*	*Quantum yield MeOH*
1	440	547	0.001	0.00022
2	413	527	0.00049	0.00012
3	464	631	0.00089	0.00023
4	430	560	0.00033	0.00034
5	429	545	0.0021	0.0038
6	401	502	**0.011**	**0.0018**
7	458	611	0.0013	0.0023
8	400	525	0.004	0.00099

These quantum yields confirm the general trend already discussed before, that is the highest fluorescence is associated to the 3-methyl-benzothiazine condensation products. Moreover, the fluorescence observed in dichloromethane are higher compared to methanol, with the only exception rapresented by the cyanine obtained from 3-methyl-1,4-benzothiazine and para-N-dimethylaminobenzaldehyde.

Table 6, instead , shows the quantum yield for the basic shifts that occur in the cyanines containing 4-hydroxy-3-methoxy moiety on the aromatic portion of the cyanine. Again, the highest quantum yield is observed for the condensation product involving 3-methyl-benzothiazine and vanillin.

Table 6: ***Emission wavelengths and quantum yields of cyanines obtained from 4-hydroxy-3-methoxy aldehydes in basic conditions compared to the standard rhodamine b***			
Compound	λ_{max} ***excitation (nm)***	λ_{max} ***emission (nm)***	***Quantum yield MeOH/ NaOH***
2	480	-	-
4	490	520	0.00093
6	430	530	**0.0011**
8	390	500	0.0007

Finally , the quantum yield of the diprotonated form of 3-methyl-1,4-benzothiazine and para-N-dimethylamino-benzaldehyde cyanine was determined and it turned out to be the same quantum yield calculated for its neutral form (0.0038)

3.6 Role of benzothiazine structural units in pheomelanin properties: UV-independent prooxidant effects of natural and model pigments.

3.6.1 Background

As already mentioned in the introduction, the positive correlation between red hair and melanoma has been attributed to both the poor antioxidant and photoprotective properties of pheomelanins compared with the dark eumelanins, and the capacity of pheomelanin to act as photosensitizer inducing generation of reactive oxygen species (ROS) upon irradiation with UV light[46,91] However, the question as to how eumelanin and pheomelanin may have a direct role in melanoma or skin cancer has remained open. Recent works have provided evidence for UV-independent pathways of carcinogenesis in red hair phenotypes , in which pheomelanin toxicity has been accounted for in terms of an enhanced formation of ROS which could overwhelm cellular antioxidant reserves and cause oxidative damage to biomolecules including free nucleobases in the cytosol[62]

Based on this background, with the aim of providing an interpretation at molecular level for ROS production in red hair individuals, a series of experiments were carried out to probe the reactivity of natural and synthetic pheomelanins toward cellular antioxidants that are critical for maintaining the redox balance.

3.6.2 Pigments extraction and isolation

Preliminarily, red hair pheomelanin was obtained by purification from hair by enzymatic digestion, not altering the structure of the pigment (RHP) and, for comparison, purified human black hair eumelanin (BHE) and synthetic melanin from 5SCD (CD-mel) were prepared according to standardized protocols[92]

Isolation of natural melanin pigments represents quite a difficult task because of the close association of proteins and other biological components with melanin. The impact of isolation procedure on the structural and physical properties of natural melanins has now been fully appreciated[93].

Harsh hydrolytic treatments with boiling mineral acids or alkali largely used in the past have been abandoned following realization that, in spite of the lack of visual changes, pigment skeleton and functionalities are profoundly affected. Heating of melanins with or without hydrochloric acid at reflux has been shown to lead to extensive decarboxylation[94,95] and care must be taken to avoid extremes in pH and temperature. In general, no attempt should be made to separate melanin from these internal proteins, because such a separation would destroy the granules. Current strategies revolve on the attack of the keratin matrix by breaking disulfide bonds and exposure to proteolytic digestion.[96]

Homogenization of the finely minced hair sample is required prior to exposure to proteolytic agents to favour their action. This can be achieved by use of a glass/glass potter such as Tenbroeck homogenizer while other mechanical devices (grinder, ultrasonic disrupters) currently employed for tissue homogenization prove often inappropriate. It is preferable to use freshly collected hair samples, as photoaging induces structural modifications not only in pheomelanins[97] but also in eumelanins.[98] By sequential use of proteinase K, papain and protease type XIV, and pre-treatment of the tissue with dithiothreitol, protein removal can be efficient. The enzymatic extraction preserves the integrity of the melanosome, removes most of the external proteins, and therefore should be the preferred choice for isolation of melanin from hair samples [93,95]

On chemical analysis, purified RHP showed a 11-fold enrichment in melanin with respect to the starting hair. The content of pigment in RHP was estimated as 57% based on EPR analysis (from the ratio of the double integration of the RHP and CD-mel spectra).

3.6.3 RHP promotes GSH and NADH autoxidation

In an initial experiment the effect of RHP on the autoxidation of GSH, the most important cellular antioxidant, and NADH, a central component of the respiratory chain and a critical index of the metabolic state of the mitochondria in terms of energy production and intracellular oxygen levels[99], was investigated. RHP proved soluble in the neutral phosphate buffer solution at the concentrations used as was CD-mel.

Figure 98 shows the effects of RHP on the levels of GSH and NADH at physiologically relevant concentrations after incubation in the dark in air-equilibrated metal-free buffer.

Data showed a remarkable increase in the oxidation rate of both compounds in the presence of RHP compared to the controls, whereas less marked variations were noticed with BHE. HPLC analysis with UV and electrochemical detection consistently indicated a rise in GSH disulfide (GSSG) levels with GSH decrease, confirming a redox reaction.

Formation of NAD^+ was similarly observed in the reaction mixture of NADH with RHP.

In other experiments using NADPH, with RHP at 1:1 w/w ratio, a complete consumption was obtained at 24 h with concomitant formation of $NADP^+$ (not shown). Similar effects were observed using a model CD-mel, confirming that the pigment was the active component of the RHP sample. Separate experiments on the effect of RHP on the autoxidation of GSH at 2 mM concentration, using the colorimetric Ellman's thiol assay[100] ,showed a similar trend with a 90% consumption of GSH after 3-h incubation with RHP 1:2 w/w versus a negligible consumption with BHE (see **Figure 99**).

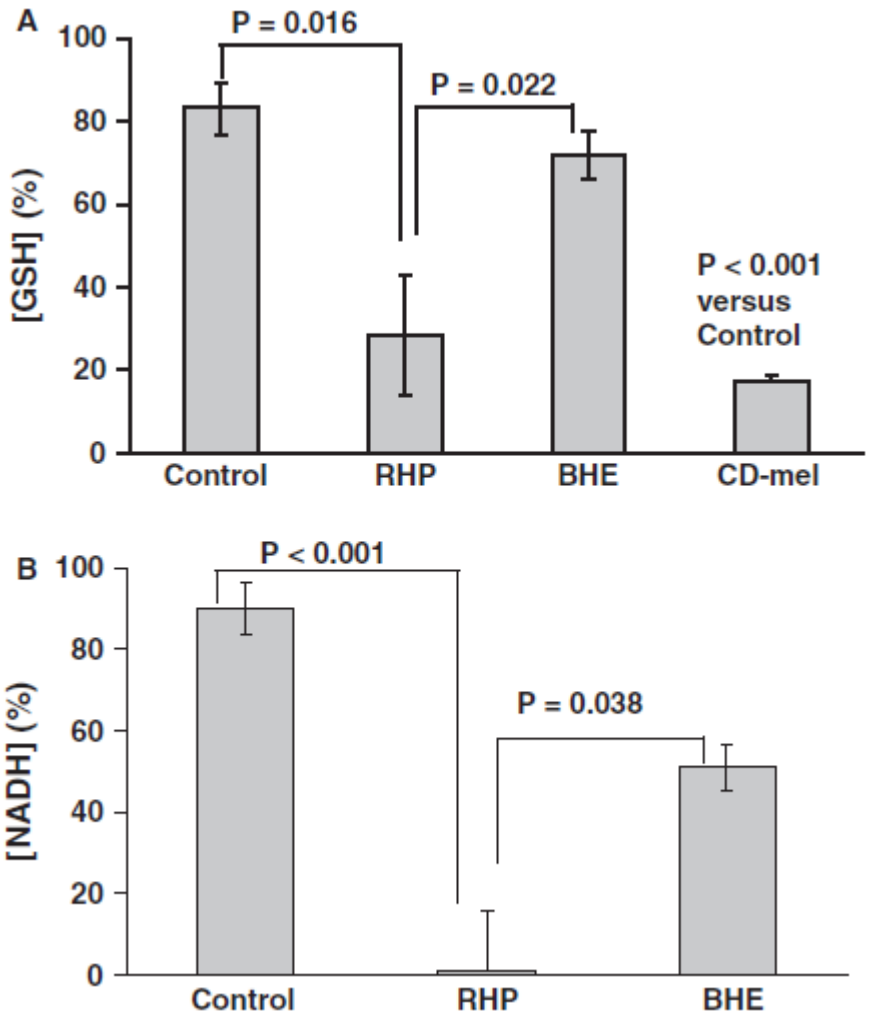

Figure 98. *Residual (%) GSH (A) and NADH (B) after 1 h (GSH) or 24 h (NADH) in 0.1 M phosphate buffer (pH 7.4) in the absence (control, n =7) or in the presence of RHP (n =5), BHE (n =5) or CD-mel (n =5) (initial substrate concentration: 150μM; substrate/ melanin=1:1 w/w). All values are expressed as the mean SD. Significant differences were determined by independent samples two-tailed t test. P < 0.05 is considered significant; exact P-values are shown in each plot.*

Good linear correlations between RHP concentration (w/v) and GSH consumption at various intervals of time were observed (**Figure 100**)

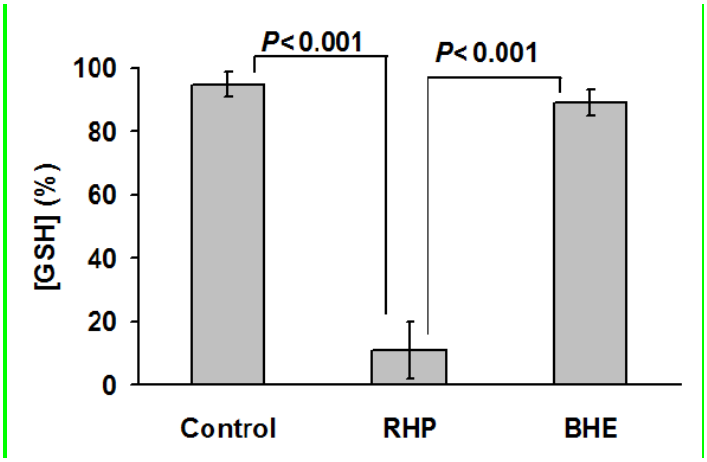

Figure 99. *Residual (%) GSH after 3 h in 0.1 M phosphate buffer (pH 7.4) in the absence (control, n=5) or in the presence of RHP (n=5) or BHE (n=5). (Initial substrate concentration: 2 mM; substrate/melanin=1:2 w/w). All values are expressed as the mean ± s.d. Significant differences were determined by independent samples two-tailed t-test. P < 0.05 is considered significant; exact P-values are shown in each plot.*

No GSH or NADH depletion was observed in experiments carried out with exclusion of oxygen (**Figure 101**). ROS production from RHP and CD-mel in the presence of GSH in phosphate buffer (pH 7.4) was investigated by different methods including EPR spectroscopy method using 5,5-dimethyl-1-pyrroline-N-oxide (DMPO) as spin trap[9] and the nitroblue tetrazolium assay[8]. Yet, under a variety of conditions, no significant differences with respect to control experiments in the absence of melanin or GSH were observed. It is possible that ROS slowly generated under these conditions are entrapped by RHP itself as previously reported[19]

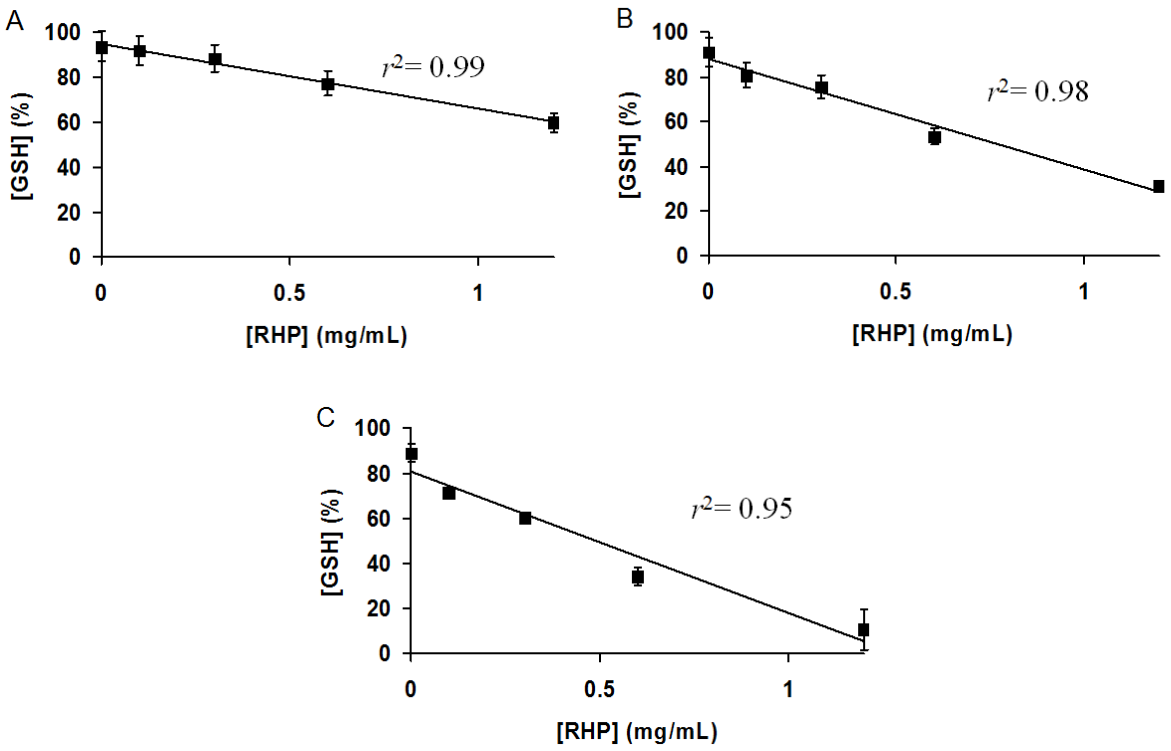

Figure 100. *Residual (%) GSH after 1 h (A), 2 h (B) or 3 h (C) in 0.1 M phosphate buffer (pH 7.4) in the presence of variable amounts of RHP (n=5 for each concentration) (initial concentration of GSH: 2 mM). All values are expressed as the mean ± s.d. Trend lines and correlation coefficients are indicated*

Notably, neither superoxide dismutase (SOD) nor catalase nor a combination of the two affected oxygen dependent GSH consumption in the presence of RHP (**Figure 101**).

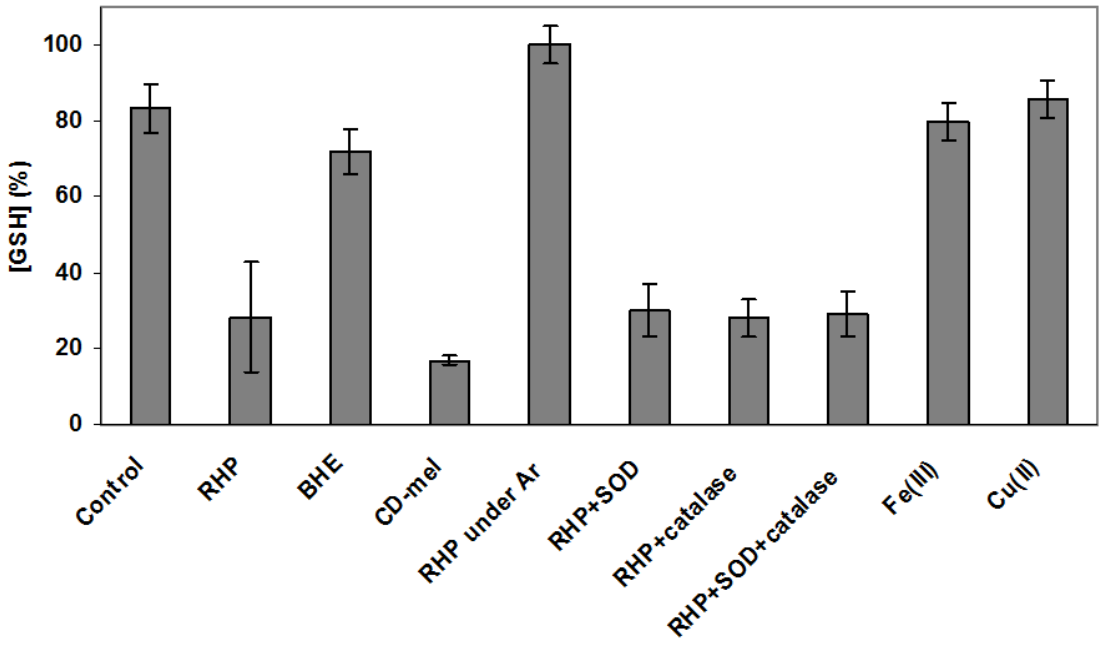

Figure 101. *Residual (%) GSH after 1 h in 0.1 M phosphate buffer (pH 7.4) under different reaction conditions as indicated in the Methods section. All values are expressed as the mean ± s.d (control, n= 7; other conditions, n= 5).*

Based on the above data, it was concluded that RHP does not produce significant levels of ROS but can induce depletion of GSH and NADH by a UV- and ROS-independent mechanism. Whether redox- active metal ions commonly present in natural melanins[101] played any role in the observed effects is difficult to assess. Indeed, EPR analysis revealed variable Fe^{3+} and Cu^{2+} content in the melanin samples under investigation (**Figure 102**) that, however, did not correlate with the extent of the observed effects. In separate experiments aimed at assessing the effect on GSH autoxidation of Fe^{3+} or Cu^{2+} at 30 or 6 □M concentration, respectively, that is at levels comparable to those reported for purified red hair melanonosomes[101] , no appreciable enhancement of the substrate decay with respect to the control was observed, suggesting that the effects of RHP on antioxidant depletion are not primarily due to the presence of metal ions.

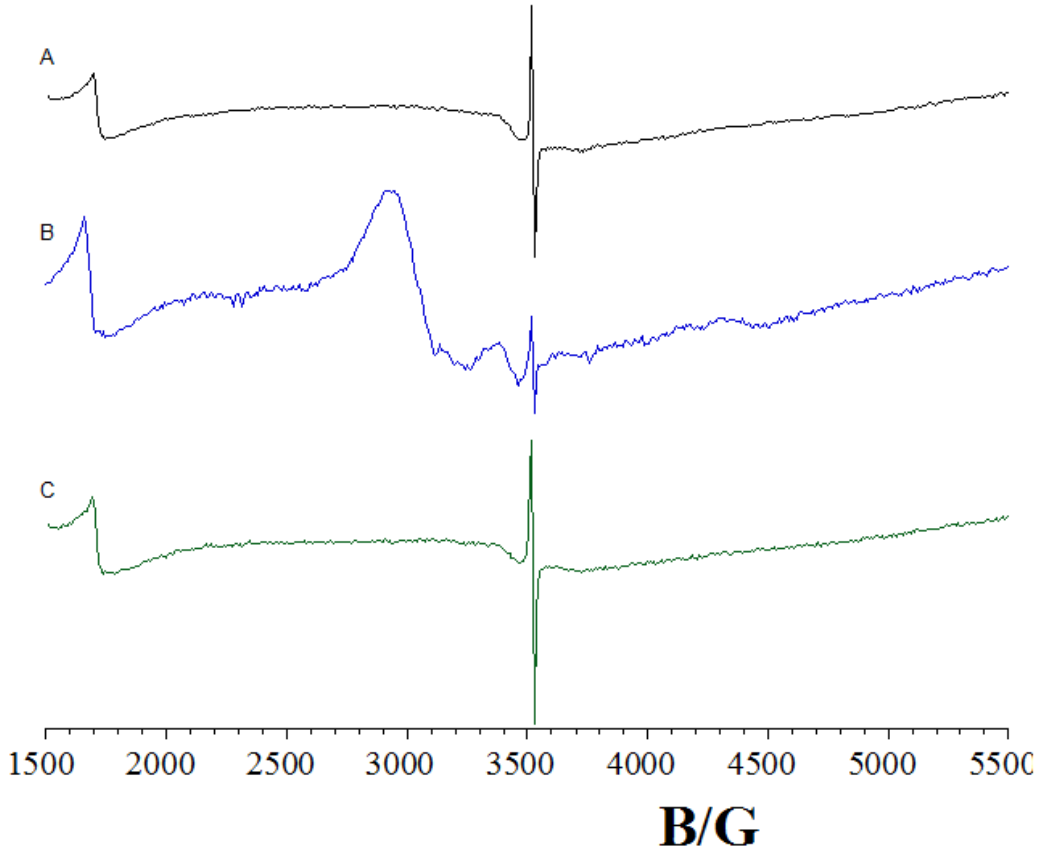

Figure 102. *EPR spectra of CD-mel (A), RHP (B) and BHE (C). The signal at low magnetic field is due to iron ions. The intermediate signals indicate the presence of copper(II) ions. The singlet signal is from the melanin stable radical (g=2.005). The presence of iron ions in the CD-mel sample is likely due to contaminants from the phosphate buffer used for melanin preparation.*

3.6.4 GSH affects pheomelanin EPR signal in RHP

In subsequent experiments, the mechanism of GSH oxidation by RHP was investigated by EPR spectroscopy. Both eumelanin and pheomelanin give characteristic EPR signals that reflect the different p-electron properties of the two pigments. Whereas at the X-band eumelanins give a single slightly asymmetric line 0.4–0.6 mT wide with a pH-dependent g-factor close to 2.004, pheomelanins exhibit broader signals with the total width approximately 3 mT and g =

2.005[81,92]

Furthermore, in pheomelanin spectra, a clear hyperfine coupling of unpaired electrons with nitrogen nuclei is detectable from the presence of a peak (or a shoulder) on both sides of the central line.

The EPR spectrum of RHP revealed the presence of the signals for both the eumelanin and the pheomelanin components (**Figure 103**). The ratio between the two components can be estimated according the well assessed approach reported in the literature[102,103]

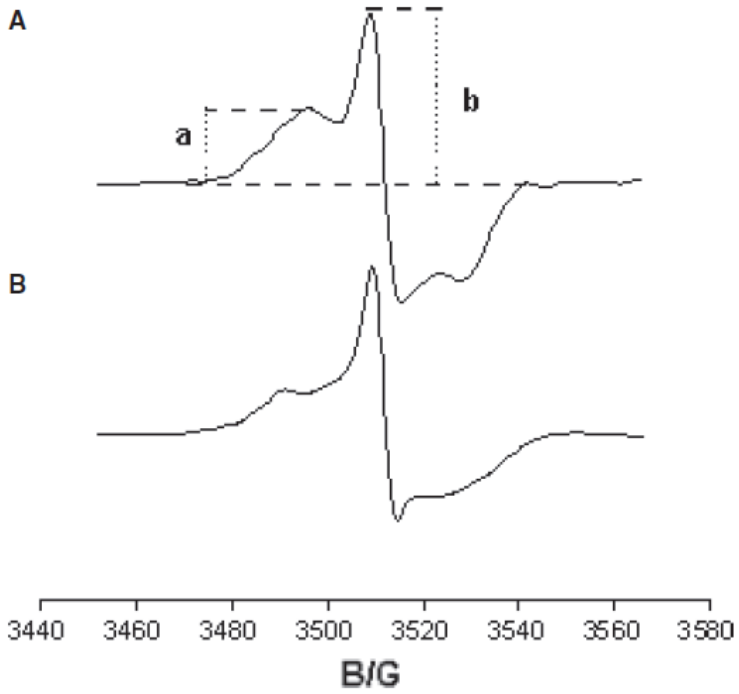

Figure 103*. EPR spectrum of RHP alone [0.5 mg/ml in 0.1 M phosphate buffer (pH 7.4)] (A) and after 24 h incubation with GSH (1: 5 w/w) (B). The height of the major peak, b, and that of the additional peak due to nitrogen hyperfine coupling, a, are indicated.*

In our sample, an initial pheomelanin/eumelanin ratio of 2.5 was estimated. Following incubation with GSH, a detectable decrease in the pheomelanin component relative to the eumelanin component was apparent (i.e., the pheomelanin/eumelanin ratio falls to 1.2) (**Figure 103B**), with a concomitant increase in signal linewidth. The origin of the signal broadening in

the presence of GSH was not assessed and may deserve further attention. The effect apparently reflects an increase in the coupling constant due to a decreased spin delocalization and a confinement of the unpaired electron closer to the nitrogen, but other effects relating, for example, to intermolecular interactions governed by H-atom transfer from GSH could be involved as well.

No significant changes of the EPR signal of RHP were observed in the absence of GSH over 24 h (**Figure 104**). A significant broadening of the EPR signal was observed also for CD-mel after 24-h incubation with GSH at 1: 5 w/w ratio (**Figure 105**).

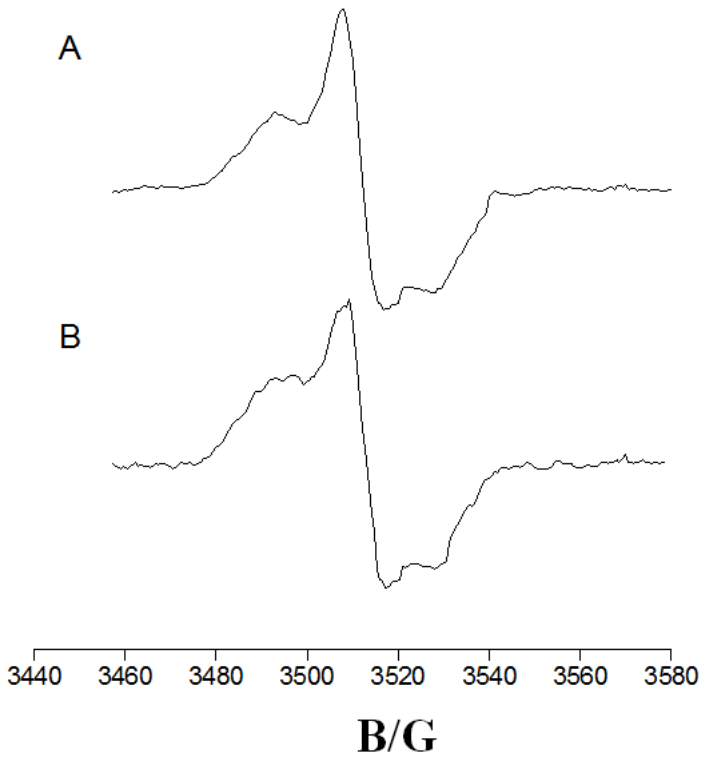

Figure 105*. EPR spectrum of RHP (0.5 mg/mL 0.1 M phosphate buffer (pH 7.4)) before (A) and after (B) 24 h incubation in the absence of GSH.*

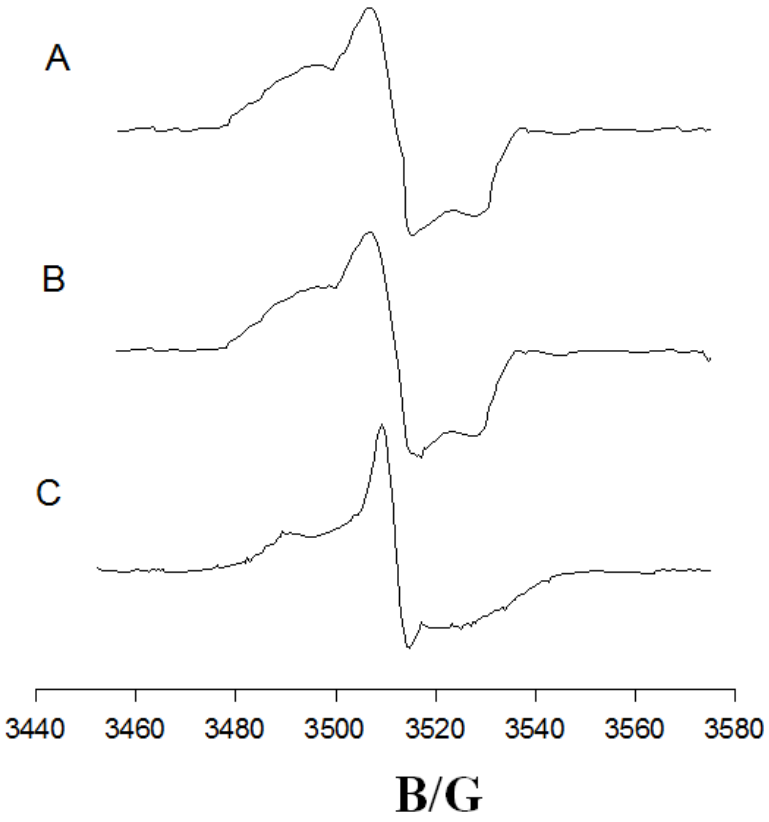

Figure 106. *EPR spectrum of CD-mel (0.5 mg/mL 0.1 M phosphate buffer (pH 7.4)) before (A) and after 24 h incubation in the absence (B) or in the presence (C) of GSH (1: 5 w/w).*

3.6.5. RHP promotes melanin formation in the absence of enzymes

The potent pro-oxidant properties of RHP toward GSH and NADH, and previous observations of the pro-oxidant properties of synthetic CD-mel toward catechol compounds[97] prompted further experiments aimed at assessing whether the natural pigment is able to promote the oxidation of melanin precursors, for example DOPA and 5SCD.

Figure 107 reports the effect of RHP on the rate of oxidation of DOPA and 5SCD at 1 mM concentration in air equilibrated phosphate buffer at pH 7.4, in the dark.

As in the previous study[97] , the results revealed the unexpected ability of RHP to promote the oxidative conversion of 5SCD and DOPA to pigment polymers under conditions of complete exclusion of light.

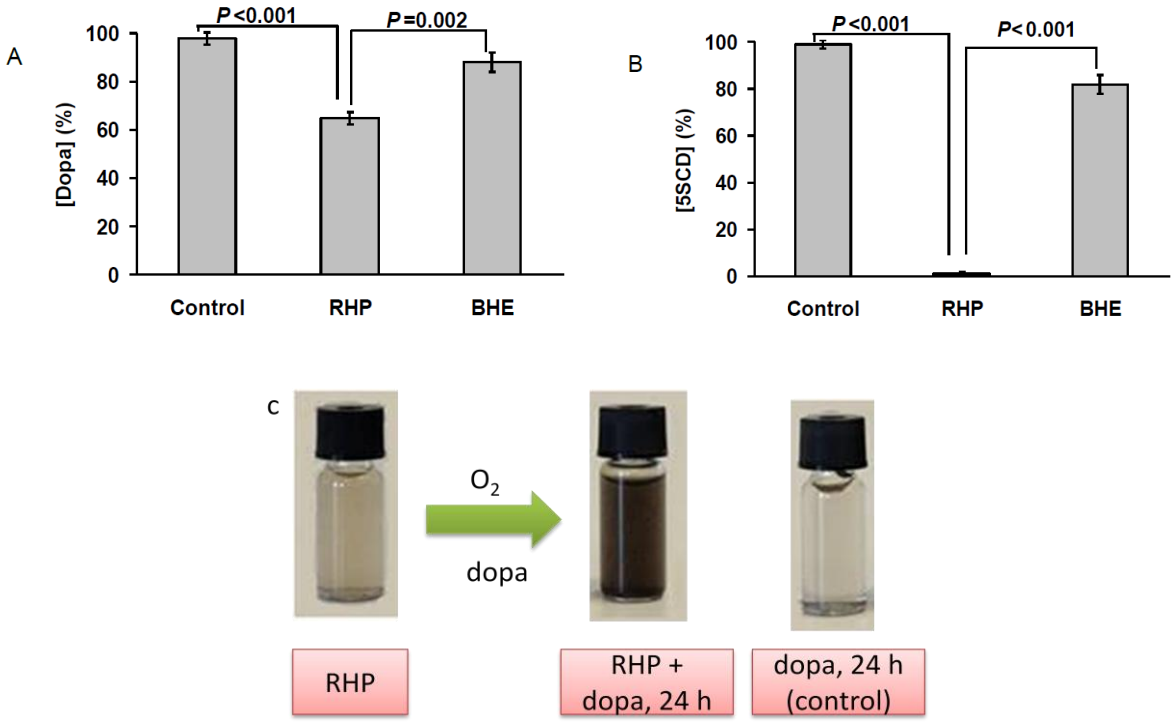

Figure 107*. Residual (%) DOPA (A) and 5SCD (B) after 24 h (DOPA) or 3 h (5SCD) in 0.1 M phosphate buffer (pH 7.4) in the absence (control, n =5) or in the presence of RHP (n =5) or BHE (n =5) (initial concentration of substrate: 1 mM; substrate/melanin=1/2 w/w). All values are expressed as the mean SD. Significant differences were determined by independent samples two-tailed t test. P < 0.05 is considered significant; exact P-values are shown in each plot. (C) Visual course of the oxidative conversion of DOPA to eumelanin promoted by RHP.*

The differences in the conversion rate reflect the higher intrinsic oxidizability of 5SCD relative to DOPA. The effect of RHP on DOPA oxidation leading to accumulation of a eumelanin-like polymer is shown in **Figure 107**(C). Unlike RHP-melanin, BHE had a negligible effect on 5SCD and DOPA oxidation. Control experiments indicated moreover that oxidation of melanin precursors is completely inhibited under an argon atmosphere, ruling out a role of adsorption and other physical phenomena.

Little or no effect on the oxidation rates was observed n the presence of SOD, catalase or both enzymes.

3.6.6 Red human hair pheomelanin is a potent pro-oxidant

The results of this study provide unambiguous evidence that RHP, but not BHE, behaves like a unique pseudobiocatalyst, accelerating autoxidation of two important cellular antioxidants and melanin precursors in the absence of UV stimulation. The reactions can be initiated by simple addition of the compounds to purified RHP in aqueous buffer in the presence of air at room temperature. This behavior is an unique characteristic of RHP, as other natural pigments or biopolymers don't seem to induce similar effects. The origin of this effect is probably due to a combination of factors that cause pheomelanin to play different biological roles with respect to eumelanin, namely a greater solubility, a peculiar chemical nature reflecting the lack of the extended, highly conjugated and tightly stacked molecular components that account for the black and compact character of eumelanin granules and, possibly, the different ability to chelate and retain metal ions[101]. A photoelectron emission microscopy determination of the oxidation potential of human eumelanosomes and pheomelanosomes revealed ionization thresholds of 4.6 and 3.9 eV corresponding to oxidation potentials of -0.2± 0.2 and +0.5 V ± 0.2 vs normal hydrogen electrode, respectively[104]. Moreover, studies of the effect of added melanosomes on the reduction of Fe(III)-cytochrome showed pheomelanosomes are stronger reducing agents than eumelanosomes, consistent with the measured oxidation potentials[104]. Based on the observed potentials and those known for some important cellular ingredients, pheomelanosomes were predicted to induce greater oxidative stress (via reduction of O2) than eumelanosomes. Although the above conclusions suggested a different reactivity with respect to the results obtained so far , it is worth noting that both of them suggest a role of pheomelanins in promoting oxidative stress. Conversely, it remains to be assessed how these results can be reconciled with a recent report[105] showing that both eumelanin and pheomelanin lead to DNA breakage in the absence of light irradiation and that eumelanin is more harmful than pheomelanin. In that study, however, the effects of synthetic melanin samples were

attributed to Fenton-type reactions mediated by copper and iron ions and inhibited by catalase, a mechanism which does not apply to the present experiments.

Herein, data from EPR experiments suggested that RHP promotes GSH oxidation by a direct H-atom transfer from the thiol to free radical moieties of the pigment, causing selective decrease in the EPR response of the pheomelanin component. Notably a similar effect on the pheomelanin signal of red hair was reported following incubation with another reducing agent like ascorbic acid[106]. Subsequent interaction of reduced RHP with oxygen would regenerate the free radical population with concomitant formation of superoxide and other ROS, thus sustaining a redox cycle.

It has been shown that RHP consists mainly of benzothiazolylthiazinodihydroisoquinoline units[40] which arise by oxidative coupling of two benzothiazine units. It is therefore possible that the free radical signal of RHP reflects an o-aminophenol/o-quinoneimine= 2 semiquinoneimine equilibrium within the pigment (**Figure 108**) akin to the catechol/o-quinone= 2 semiquinone comproportionation equilibrium of eumelanins[81,107] and that GSH shifts the equilibrium toward the o-aminophenol component by H-atom transfer to the semiquinoneimine.

The decrease in the pheomelanin component in RHP in the presence of GSH evidenced by EPR analysis would suggest that a portion of the species resulting from the reducing action of GSH may undergo irreversible conversion into other species that cannot take part any more at the equilibrium shown. That this is due to the action of GSH and not to a spontaneous reaction of the pigment alone is shown by the negligible modification of the EPR spectrum of RHP after 24 h in the absence of GSH. Moreover, the similar effects observed in the case of CD-mel would indicate that changes of the EPR signal produced by GSH are specifically associated to the pheomelanin component of the purified RHP.

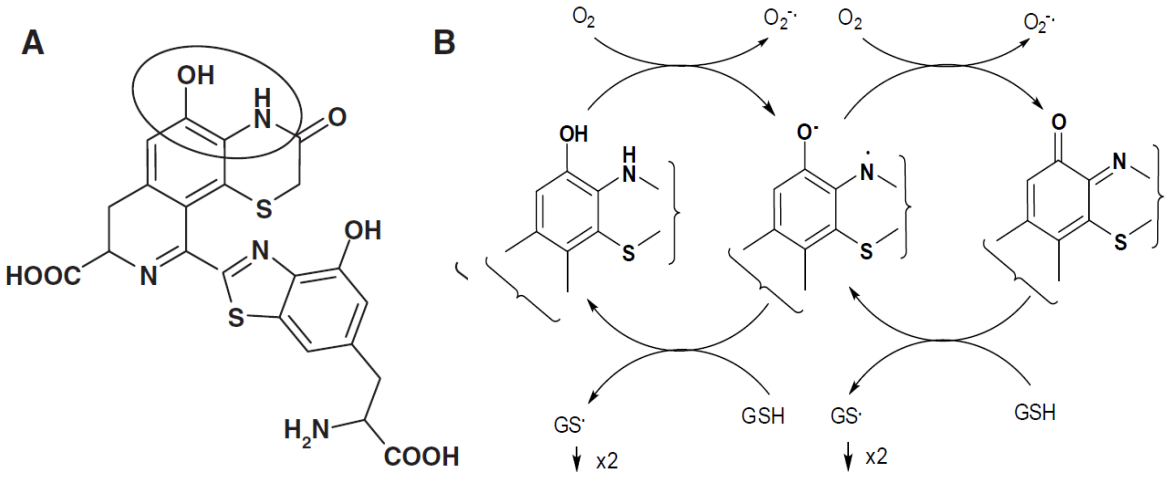

***Figure 108**. (A) Major structural component of RHP deduced from previous model studies and chemical analysis Highlighted is a possible redox-active moiety. (B) o-aminophenol-semiquinoneimine-o-quinoneimine conversion sequence supposedly implicated in the EPR detectable response of RHP to GSH. Reported structures are indicative and do not intend to be representative of the broad variety of isomers and tautomers contributing to RHP response to GSH.*

The scheme illustrated in **Figure 108** is clearly an oversimplification of the actual oxidation process that, depending on the relative concentration of the participating species, may involve additional mechanisms. Pheomelanin pigments are generated within the melanosomes, organelles that contain the biochemical machinery for production of pigments. Hair pheomelanosomes are less regularly shaped than eumelanosomes, may appear as ellipsoids and spheres showing microvescicular and proteinaceous matrices on which melanin deposition is spotty and granular, and do not maintain structural integrity upon extraction from the keratin matrix[101,108]

Once pheomelanosomes are mature, they are transferred to keratinocytes, where they are made available to come into contact with major cellular ingredients including GSH, NADH and other redox-active biomolecules. Thus, both in melanocytes and keratinocytes, the pigment

components of pheomelanosomes, which seems to be more accessible than those of the compact eumelanosomes, can induce a depletion of cellular antioxidants at micromolar concentrations.

DOPA or 5SCD oxidation by RHP is likely to occur by a redox exchange mechanism akin to that proposed in **Figure 108** for the oxidation of GSH and NADH. The implications of these results are manifold and highly relevant to the mechanisms of melanogenesis in a pheomelanin-forming environment. It can now be proposed that pheomelanin, once produced in small quantities in active melanizing cells, can grow partly in the absence of enzymatic assistance, with both eumelanin and pheomelanin precursors taking part in the nonenzymatic pigment growth process. This observation would point to a much broader and general relevance of the casing pheomelanin core/eumelanin shell model of melanogenesis than so far believed[51, 109] .

It is clear, however, that such processes are much slower than those mediated by melanogenetic enzymes, particularly in the case of DOPA, and may become relevant at high pigment to monomer ratios. Moreover, and most importantly, these data settle a long-lasting issue of what oxidizing system brings about pheomelanin synthesis, as it is known that the committed enzyme of melanogenesis, tyrosinase, is unable to oxidize 5SCD and benzothiazine intermediates thereof[110]. The common practice to produce synthetic pheomelanin from 5SCD in the presence of tyrosinase relies on the presence of catalytic amounts (5%) of DOPA that upon oxidation by the enzyme generates dopaquinone which is able to oxidizes 5SCD[53] .

Besides the relevance to melanogenesis, the observed abatement of the melanin precursor pool may also play a contributory role in determining the pro-oxidant background of red hair/pale skin for melanoma and skin carcinogenesis. 5SCD, such as DOPA, is a potential antioxidant and metal chelating agent[111] that is produced in response to a range of stimuli, including sun exposure, inflammation and a number of disease states regardless of constitutive pigmentation[112,113]. Circulating 5SCD levels are also abnormally high in melanoma patients[114]. Thus, 5SCD is part of the adaptive response of melanocytes to environmental cues independent

of their genetic background and, as such, is not a marker of pheomelanogenesis per se. Oxidative conversion of 5SCD to pheomelanin occurs only in the presence of an oxidizing environment where active eumelanogenesis is lacking. In this perspective, spontaneous pheomelanin growth may be seen as an oxidative stress-amplifying mechanism by which the antioxidant 5SCD is consumed in a toxic pigment-forming reaction, providing a permanent threat to a specific antioxidant defense of melanocytes. Such a chronic prooxidant condition would be exacerbated by, but is independent of, photostimulation. The burst in the ROS levels and particularly singlet oxygen associated to sun exposure in the absence of a defensive action by a photoprotective/scavenging pigment like eumelanin or cellular antioxidants at proper levels is expected to dramatically accelerate the processes that pheomelanin pigment is able to sustain per se, thus amplifying DNA damages and lipid peroxidation that are well-known hallmarks of photoaging and carcinogenesis[115,116]

The finding that purified RHP, but not BHE, is a potent pro-oxidant promoting the oxygen-dependent, Uv-independent depletion of crucial antioxidants for cell homeostasis and mitochondrial functions as well as of melanin precursors provides an unprecedented background to address some major questions concerning the role of pheomelanin synthesis in melanomagenesis[45,62]

First, it was hypothesized that pheomelanin generates ROS that cause DNA damage, and an issue was raised of what about the structure of pheomelanin causes ROS production. These results show that pheomelanin can bring about GSH and NADH autoxidation via direct H-atom exchange. The subsequent reoxidation of reduced pheomelanin by oxygen may generate ROS. Thus, pheomelanin-related DNA damage would be the result of a major antioxidant depletion via a direct interaction mechanism, with a concomitant partial contribution of ROS generation, and a reductive step would provide the necessary input to induce ROS generation by pheomelanins.

Second, it has been proposed that pheomelanin synthesis per se leads to GSH depletion. While

this is certainly true, these findings show that pheomelanin may specifically contribute to GSH depletion also by a direct UV-independent redox mechanism.

In addition, a third contributory mechanism could be suggested by which pheomelanin may cause oxidative stress, that is, the direct oxidative conversion of circulating precursors with antioxidant properties into new pheomelanin operating as pro-oxidant. This latter observation settles the issue of what actually brings about pheomelanin synthesis in the absence of enzymatic assistance.

These results may inspire new strategies to prevent and manage melanoma based on the inhibition of the prooxidant activity of pheomelanosomes to restore the firstline antioxidant armamentarium of melanocytes.

3.7. Photochemistry of pheomelanins: spectroscopic investigation of benzothiazole building blocks

3.7.1 Background

Following several studies on the reactivity of the putative pheomelanin biosynthetic intermediates[40,41] and chemical degradation analysis of pheomelanic tissues it seems now clear that pheomelanin structure includes in addition to benzothiazine-related units also benzothiazole moieties. Recently evidence has been obtained that a significant portion of benzothiazine units of pheomelanin in tissues undergoes ring contraction to benzothiazole on exposure to UVA.[97,98] It follows that characterization of the photoreactivity of benzothiazole moieties is central for dissecting the complex mechanisms underlying pheomelanin phototoxicity.

Despite the major role played in pheomelanin phototoxicity, the photoreactivity of these species has so far remained unexplored.

3.7.2 Aim of the study

By combining steady state and time resolved fluorescence methodologies an investigation of the main benzothiazole building blocks of pheomelanin, i.e. 6-(2-amino-2-carboxyethyl)-4-hydroxy-1,3-benzothiazole (BT) and 6-(2-amino-2-carboxyethyl)-4-hydroxy-1,3-benzothiazole-2-carboxylic acid (BTCA) was carried out in collaboration of the research unit headed by professor Villy Sundstrom of the Department of Chemical Physics of Lund University (Sweden). Consideration of the structure of these molecules featuring several ionisable functional groups (heterocyclic N, aromatic OH, COOH and aminoacid

functionalities) would suggest that excited state proton transfer to solvent (ESPT) and excited state intramolecular proton transfer (ESIPT) may play a crucial role. Such a behavior has been observed also in the case of structurally related molecules like the 2-(2-hydroxyphenyl)- 1,3-benzothiazole that has been the subject of detailed investigation.[117-119]

In order to help identification of the excited state processes we also investigated some model benzothiazoles like 2-methyl-1,3-benzothiazole (MB) and 4-hydroxy-6-methyl-1,3-benzothiazole (M-BT), having the chromophores of BT and BTCA but stripped of some of the functional groups like the hydroxyl group at the 4-position or the alanyl side chain at 6-position (**Scheme 7**).

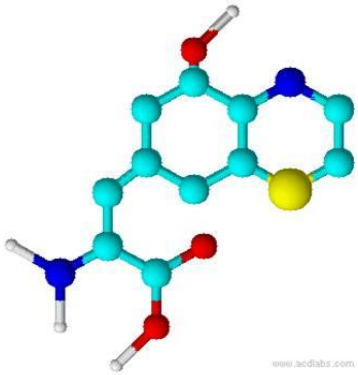

Benzothiazine

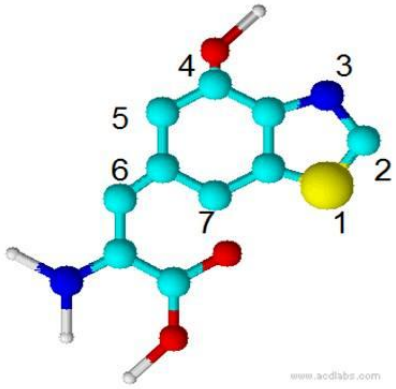

4-hydroxy-1,3-benzothiazole (BT)

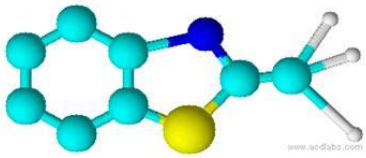

2-methyl-1,3-benzothiazole (MB)

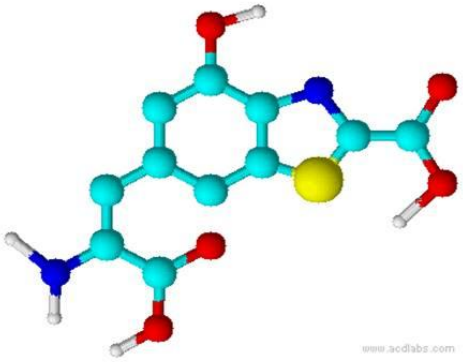

1,3-benzothiazole-2-carboxylic acid (BTCA)

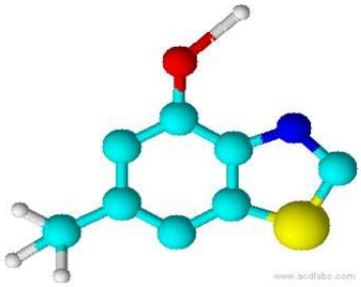

4-hydroxy-6-methyl-1,3-benzothiazole (M-BT)

Scheme 7. *Molecular structures of pheomelanin building blocks and model chromophores.*

While MB is commercially available, BT and BTCA were obtained by a one pot multistep procedure starting from 5-*S*-cysteinyldopa.[120] A similar synthetic route was developed to obtain M-BT. All benzothiazole compounds were investigated in aqueous buffer solutions at selected pHs in the range 1-12 (values specified below for each molecule), as well as in methanol (MeOH). At the lowest pH studied the heterocyclic nitrogen of benzothiazole as well as the aminoacidic amino group are mostly in the protonated form, and the aromatic and aminoacidic COOH groups are not dissociated according to the pK_a reported in Table 1.[121-124] At the highest pH all groups are deprotonated and BT is in its dianionic BT^{2-} form and BTCA in its trianionic form $BTCA^{3-}$ (the notation used for the different protonation states is summarized in **Table 7**).

Functional group (reference compound)	**Ground state pK_a** (ref)
NH^+ (4-hydroxy-1,3-benzothiazole)	1.84 (121)
COOH (1,3-benzothiazole -2-carboxylic acid)	3.3 (122)
COOH (tyrosine)	2.2 (123)
NH_3^+(tyrosine)	9.1 (123)
OH (4-hydroxy-1,3-benzothiazole)	8.8 (124)
==========	==========
[§]**BT Protonation state**	**Notation**
OH; NH^+; NH_3^+; COOH/ COO^-	BTH_2^{2+}
O^-; NH^+; NH_3^+; COOH/ COO^-	BT^{-+}
OH; N; NH_3^+; COOH/ COO^-	BT^+
O^-; N; NH_3^+; COO^-	BT^-
O^-; N; NH_2; COO^-	BT^{2-}

[§]Some species were combined in one disregarding their different COOH protonation states when it was not possible to distinguish between their individual contribution to the emission spectra.

Table 7. *Ground state pK_a values of functional groups occurring in the benzothiazoles under investigation, and notation used for the various protonation states of 4-hydroxy-1,3-benzothiazole.*

3.7.3 Steady state and time resolved fluorescence investigation of MB

Figure 109a/b displays the static absorption and fluorescence spectra of MB measured at pH 1 (in HCl solution), 2.5, 7, and 9.5 (phosphate buffer) and in MeOH. The absorption spectra of MB are very similar under all conditions examined whereas the fluorescence spectra differ significantly. In MeOH, the fluorescence spectrum is characterized by a small Stokes shift (λ_{max} ~ 330 nm) suggesting that fluorescence originates from a position close to the Franck-Condon geometry and that no significant photochemistry occurs. Similarly, at pH 9.5 the fluorescence spectrum peaks at λ_{max} ~ 340 nm (**Figure 109b**). At pH 1, the emission spectrum exhibits a red-shifted broad band centered at 410 nm (**Figure 109b**). Based on the pK_a= 1.84 of the heterocyclic nitrogen[121] (**Table 7**), at this pH the dominating ground state species is MBH^+ (88 %, NH^+).

Therefore we assign the 410-nm fluorescence to protonated MB, MBH^+. At pH 2.5, almost the same fluorescence spectrum is observed as at pH 1 (**Figure 109b**), although the ground state species present are MBH^+ (~18%) and MB (~82%) (as judged by the pK_a= 1.84 of the heterocyclic N,(**Table 7**). The fact that only MBH^+ fluorescence is observed at pH 2.5 (with 18 % ground state population) can be understood as a result of excited state proton transfer from the solvent to the photoexcited MB. The heterocyclic nitrogen is known to be a photobase,[124] i.e. a stronger base in the excited state. A Förster cycle calculation based on the fluorescence maxima of MB (λ_{max} ~ 340 nm at pH 9.5) and MBH^+ ((λ_{max} ~ 410 nm) results in a $\Delta pKa^* \approx 10$ pH units. Thus, it follows that proton transfer from the solvent to the thiazole nitrogen of the excited MB molecule is thermodynamically strongly favored. Consequently we conclude that the 410 nm fluorescence band at pH 2.5 originates from both the (18 %) ground state population of MBH^+ and the MBH^+ formed through ESPT from the solvent.

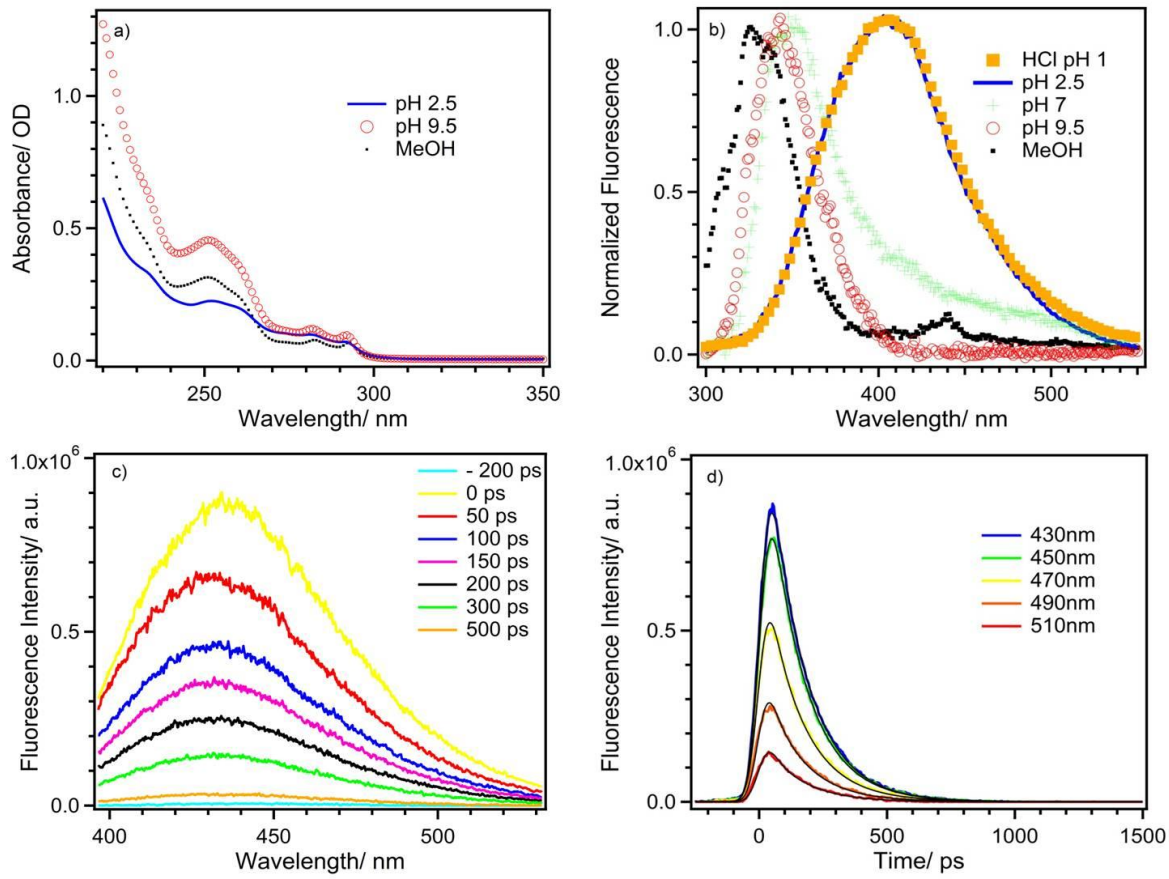

Figure 109*. (a) Ground state absorption and (b) steady-state fluorescence (upon 266 nm excitation) spectra of MB in MeOH and at pH 1, 2.5, 7 and 9.5. (c) Time resolved fluorescence spectra of MB at pH 2.5. (d) Streak camera fluorescence kinetics of MB at pH 2.5 at several different wavelengths together with their fits, yielding a single exponential lifetime of 140 ± 1 ps.*

The red-shifted MBH^+ fluorescence is similar to that of the hydroxyphenylbenzothiazole protonated form at 440 nm.[117,118] Time resolved fluorescence spectra of MB in pH 2.5 buffer (**Figure 109c**) exhibit a broad band centered at ~430 nm (in agreement with steady-state fluorescence), characterized by single exponential kinetics (**Figure 109d**), and therefore a single decay associated spectrum (DAS, Figure 110), having a decay time of 140 ps.

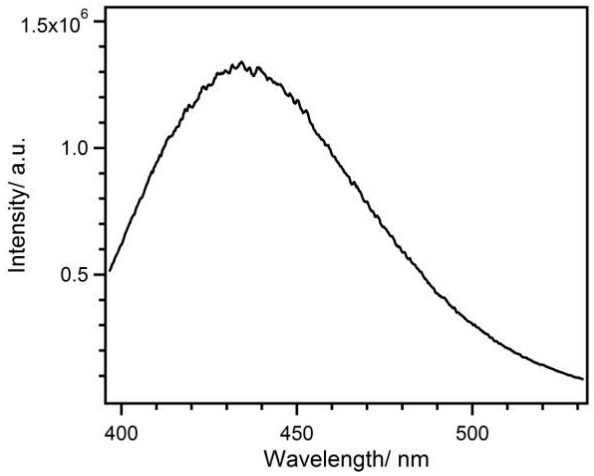

***Figure 110**. Decay associated spectrum of MB at pH 2.5.*

This shows that MBH^+ is formed within the time resolution of the experiment (<10 ps). This and no detectable fluorescence at ~340 nm of the excited major ground state species (neutral MB) suggest that MBH^+ is formed along a N-H hydrogen bond already present in the ground state, and therefore very fast. At intermediate pH 7 the fluorescence spectrum is dominated by the 340-nm band observed at pH 9.5, but has also a low amplitude of the pH 2.5 band at ~430 nm (**Figure 109b**), supporting the picture of ESPT from the aqueous solvent to the ring nitrogen, since at this pH the ground state population of MBH^+ is negligible; the low amplitude is of course a result of the low proton concentration at this pH.

3.7.4 Steady state and time resolved fluorescence investigation of BT

The absorption spectra of BT in sodium phosphate buffer at different pHs as well as in MeOH are shown in **Figure 110a**. The spectra in buffer at pH 2.5 and in MeOH are very similar. The absorption spectrum measured at pH 9.5 shows a shift of ~ 4 nm for all its spectral features compared to that at pH 2.5 and exhibits an extra band centered at ~335 nm. Based on the pK_a values listed in **Table 7,** at this pH the majority of the BT molecules have deprotonated (O^-) form. The additional absorption band can therefore be assigned to this species.

A similar red-shifted absorption band of hydroxyphenylbenzothiazole in aqueous ethanol solution, increasing in intensity with increasing pH, was attributed to the deprotonated (O^-) form, although in that structure a more extended delocalization of the anion compared to BT is expected.[125]

Steady state emission spectra of BT in MeOH and aqueous buffer solutions in the pH range 2.5-12, measured upon 266 nm excitation, are shown in **Figure 110b**. A small Stokes shift is observed in MeOH (λ_{max} ~390 nm) similarly to MB, suggesting no significant photochemistry and that emission originates from BT in the OH form

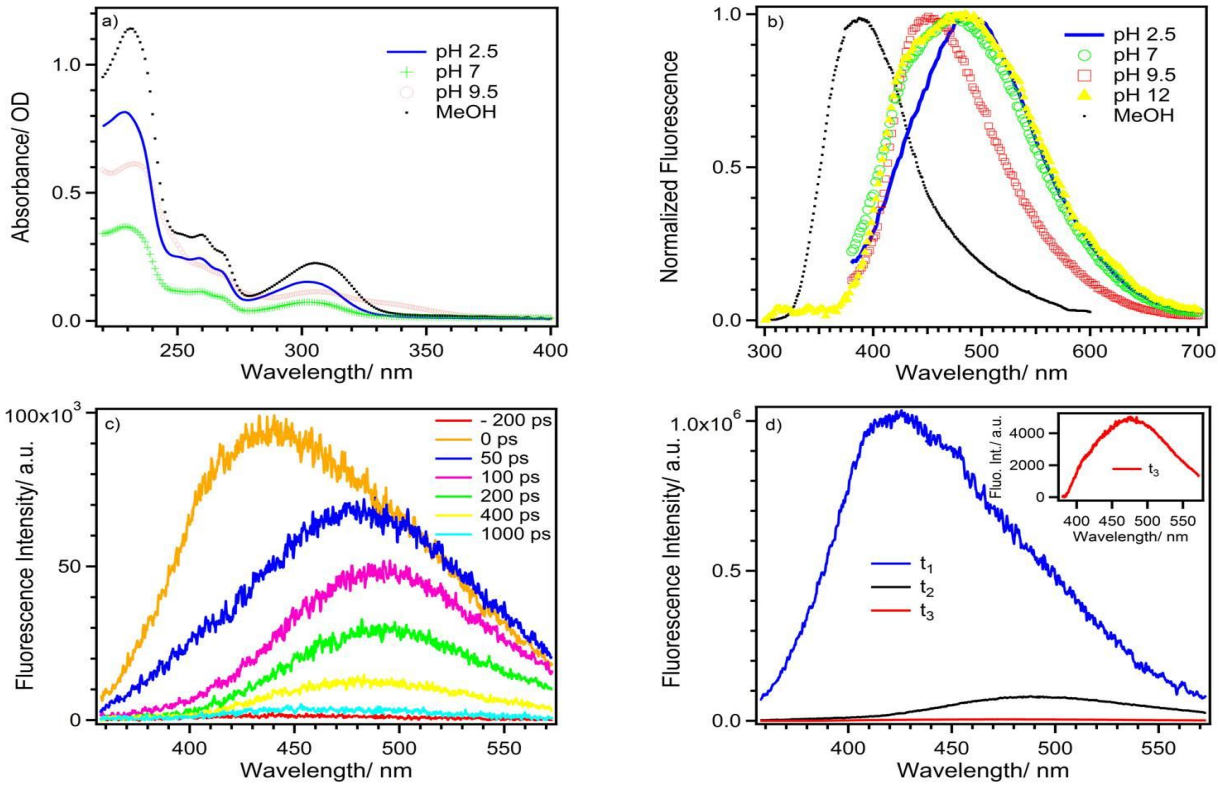

Figure 110. *(a) Ground state absorption and (b) steady-state fluorescence (upon 266 nm excitation) spectra of BT in MeOH and at various pHs. (c) Time resolved fluorescence spectra of BT in aqueous buffer at pH 2.5. (d) DAS of the three components of BT in pH 2.5 buffer with lifetimes* $t_1 < 10$ *ps,* $t_2 = 230 \pm 3$ *ps,* $t_3 = 1 \pm 0.2$ *ns.*

Accordingly, the time-resolved fluorescence spectra and kinetics at selected wavelengths show a time independent spectrum and wavelength independent kinetics with a decay time of 255 ps (**Figure 111**). The static fluorescence spectra in phosphate buffer solution at different pHs all exhibit large Stokes shifts (**Figure 110b**) and appear to be composed of at least two different emitting species with pH-dependent concentrations. At pH 12 dianionic BT^{2-} is the dominating ground state species with only a small (0.12 %) contribution of mono-anionic BT^{-} (**Table 7**). This sample composition gives rise to the fluorescence spectrum (**Figure 110b**) peaking at ~480 nm with a shoulder at ~430 nm (**Figure 112**), which we consequently assign to BT^{2-} (~480 nm) and BT^{-} (~430 nm) (more below). At pH 9.5, BT^{-} and BT^{2-} are at about the same concentrations and the static fluorescence spectrum composed of the ~430-nm BT^{-} and ~480-nm BT^{2-} emission bands.

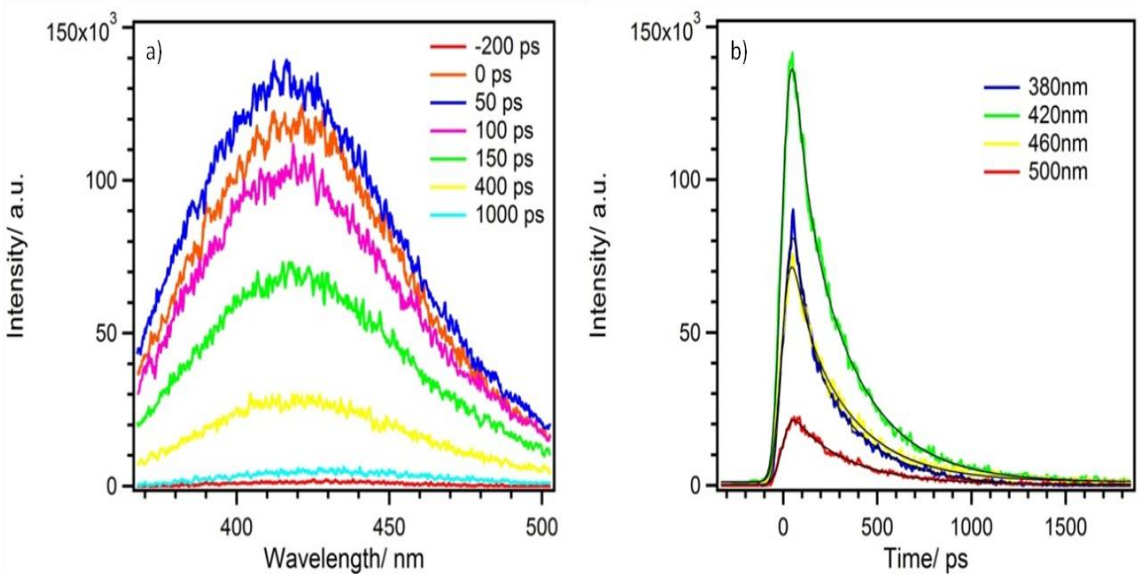

Figure 111: *(a) Time resolved fluorescence spectra and (b) fitted kinetics of BT in MeOH, yielding a single exponential lifetime of 255 ± 2 ps.*

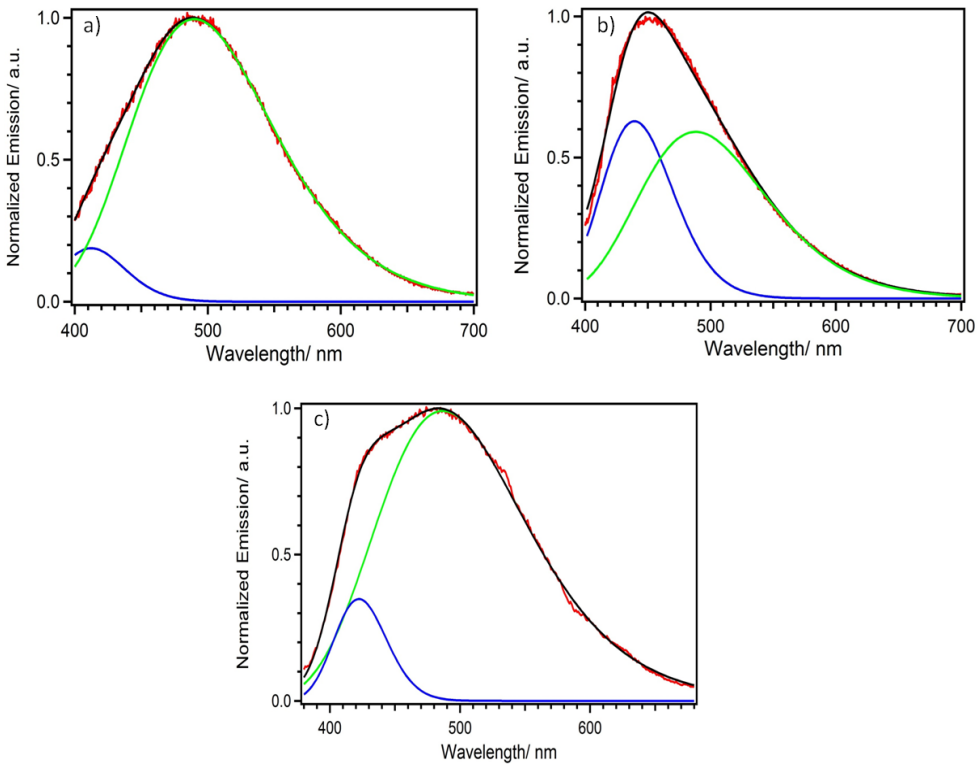

***Figure 112**: Experimental Steady state emission spectra of BT (red curve) together with their fit (black curve) and the constituting components in aqueous buffer at (a) pH 2.5, (b) pH 9.5 and at (c) pH 12, plotted in wavelength scale.*

At pH 2.5 the ground state population is 82 % of BT and 18 % of the species protonated also at the heterocyclic nitrogen (BTH_2^{2+}) based on pK_a in **Table 7**. Nevertheless, the steady state emission spectrum is not that of the neutral form (BT), but red-shifted by ~200 nm from the peak of the absorption band to λ_{max} ~ 490 nm (**Figure 112b**). In analogy with what was observed for MB and as will be clear from the time resolved fluorescence results (below), this emission originates mainly from BTH_2^{2+} formed through excited state proton transfer to the heterocyclic N. At pH 7, ground state BT is in its neutral form and the static fluorescence spectrum exhibits a double peak structure with maxima at ~430 and ~490 nm, i.e. those of BT^- and BTH_2^{2+}. The ground state concentrations of BT^- and BTH_2^{2+} are negligible at pH 7, suggesting that these fluorescence bands must be a result of de-protonation of the 4-OH group

due to ESPT/ESIPT, and ESPT from the solvent or ESIPT from the 4-OH to the heterocyclic nitrogen, respectively.

The picture of excited state proton transfer in BT hinted by the static fluorescence spectra may be substantiated with the help of time resolved fluorescence results. In the pH range 2.5-9.5 the time resolved fluorescence spectrum exhibits a fast 10-ps time scale red-shift from ~420 nm to ~500 nm. On a slower, several hundred ps time scale, the spectrum shifts back to ~450 nm and then decays without further change on the ns scale (**Figure 110c**). This time evolution (**Figure 113**) can be described by three pH-dependent DAS components having wavelength maxima approx. consistent with the static fluorescence bands in **Figure 110b** and characterized by exponential lifetimes: <420 nm (~10 ps); ~450±20 nm (1 ns; the very low amplitude of this component makes the determination of its wavelength maximum uncertain); ~490 nm (230 ps) (**Figure 110d**). At pH 12, where BT^{2-} is the dominating ground state species (~100 %) the time resolved fluorescence spectrum is dominated by an ~480-nm DAS component with an ~140 ps lifetime, and only a very low amplitude of the ~450-nm DAS (1 ns). The time resolved DASs can thus now be correlated to the various BT protonation states in the following manner: ~10 ps (< 420 nm) DAS $–BT^{+}$; 140 ps (~480 nm) DAS – di-anionic BT^{2-}; 230 ps (~500 nm) DAS $–BTH_2^{2+}/BT^{-+}$; 1 ns (~450 nm) DAS – mono-anionic BT^{-}.

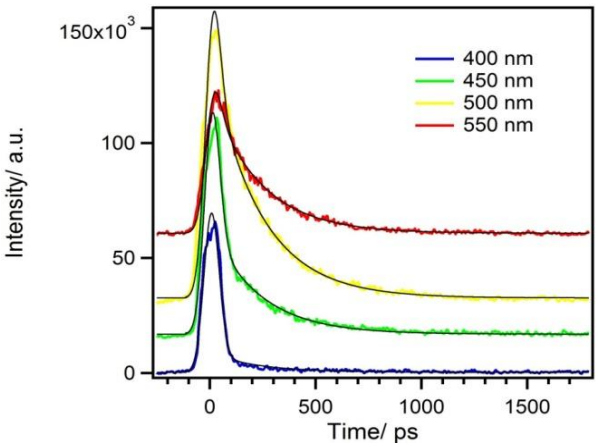

Figure 113. *Fitted fluorescence kinetics of BT in aqueous buffer at pH 2.5, yielding the lifetimes <10 ps, 230 ps, 1 ns.*

These correlations between BT protonation states, their fluorescence spectra and associated lifetimes now allows us to suggest the following excited state reaction scheme. (**Scheme 8**)

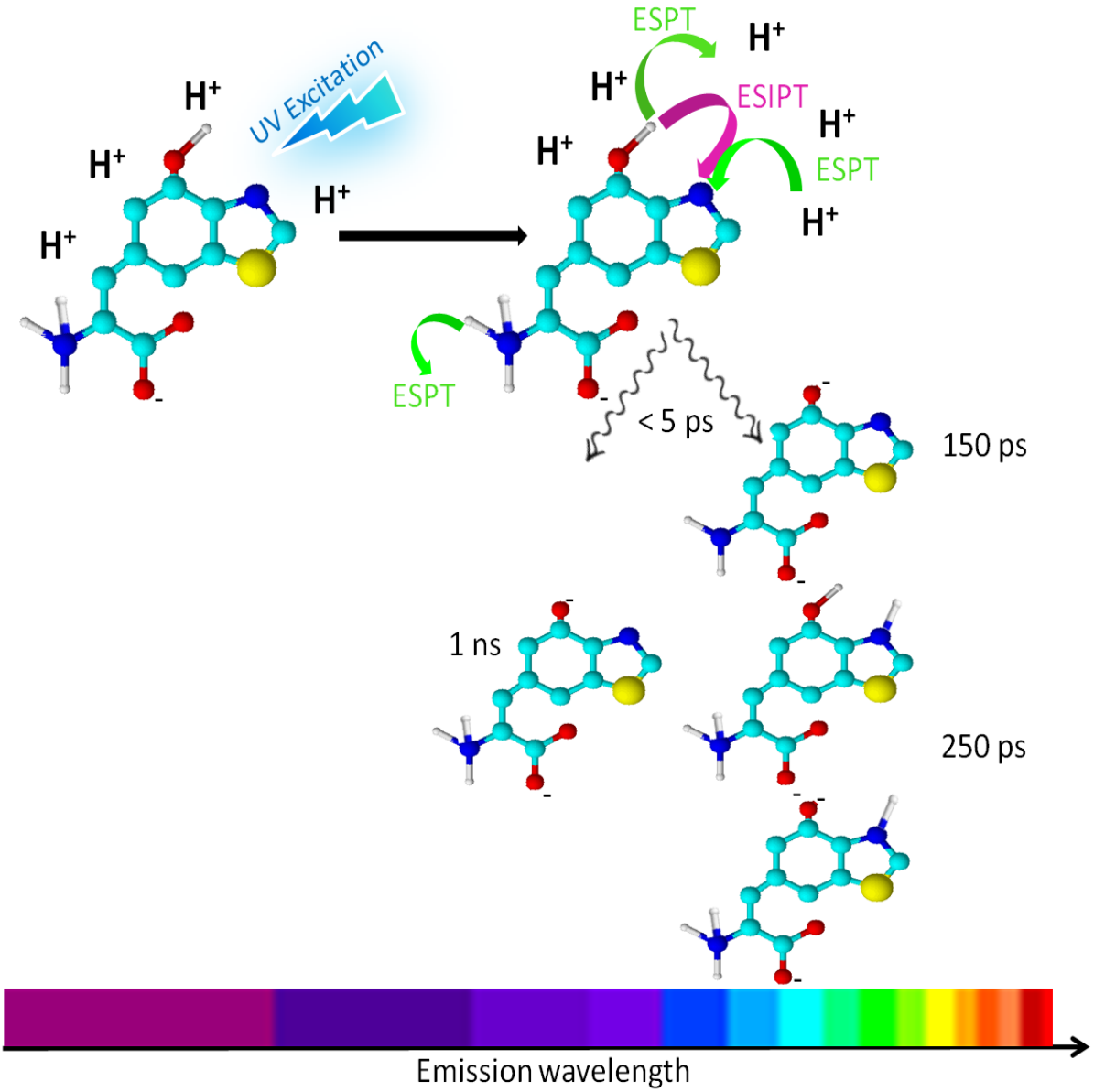

Scheme 8. *Summarizing the reaction model*

Upon photoexcitation of the neutral form of BT, the excited state decays in ~10 ps (~400 nm fluorescence) to form the excited state BTH_2^{2+}/BT^{-+} and BT^-, which then decay with lifetimes of ~230 ps (490-nm fluorescence) and 1 ns (~450-nm fluorescence). The processes responsible for this are ESPT from the 4-OH group to the solvent for formation of the anion, and 4-OH to heterocyclic-N ESIPT to form BT^{-+}, or solvent to heterocyclic-N ESPT for BTH_2^{2+} formation. Similarly to MB the latter process could significantly contribute at pH 2.5. These processes control the fluorescence dynamics of BT at pHs where the 4-OH group is protonated (< 9). At higher pH with this group de-protonated (4-O^-) no ESIPT and thus no significant protonation of the heterocyclic-N occurs, as is demonstrated by the much lower amplitude of 490-nm (230-ps) fluorescence at pH 9.5 (as a matter of fact part of the ~200-ps amplitude here must be due to BT^{2-} (see above)). At this pH the proton concentration in solution is also low making ESPT from the solvent negligible. At even higher pH 12, another red-shifted (~480 nm) fluorescence band appears, with almost the same maximum as that of BTH_2^{2+}/BT^{-+}, due to the ground state concentration of BT^{2-} present at this pH. The fluorescence lifetime of this species is ~140 ps.

Förster calculations using the fluorescence spectra of the correlated acid and base forms of a proton containing molecule indicate the feasibility of an ESPT process. Similarly to MB, such a calculation for the BT^+ (λ_{max} ~390 nm) and BTH_2^{2+} (λ_{max} ~490 nm) forms suggests that proton transfer from the solvent to the heterocyclic nitrogen is thermodynamically strongly favored. A Förster calculation using the fluorescence spectra in **Figure 110b** of the BT^+ and anionic BT^- forms, with maxima at ~400 and ~450 nm, respectively, the pK_a change in the excited state, ΔpK_a^*, can be estimated to -6.3 pH units. Since pK_a of the 4-OH group is ~8.8, this suggests that ESPT occurs if the solution pH is >2.5. This is consistent with the lower spectral amplitude of BT^- fluorescence at pH 2.5 in both static and time resolved spectra, as compared to pH 7 and 9.5 (**Figure 110b and d**). The excited state proton transfers discussed above are schematically summarized in **Scheme 8**

3.7.5 Steady state and time resolved fluorescence investigation of M- BT

The role of the amino acid side chain in the excited state properties of BT was examined with help of M-BT, lacking the alanyl side chain. The time resolved fluorescence spectra and kinetics at both pH 2.5 (**Figure 114**) and 9.5 (not shown) exhibit the same main pattern as that of BT – two spectral components characterized by maxima at 420-440 nm (10-20 ps) and 500-520 nm (100-150 ps). A component corresponding to the very low amplitude ~1 ns component of BT could not be identified with certainty due to the higher noise in these measurements. These results support the picture obtained above that the 4-OH and heterocyclic-N groups are the photochemical center of benzothiazole, but that the protonation state of the $NH_2/NH3^+$ group determines the excited state lifetime of the BT anion (BT^- vs. BT^{2-}).

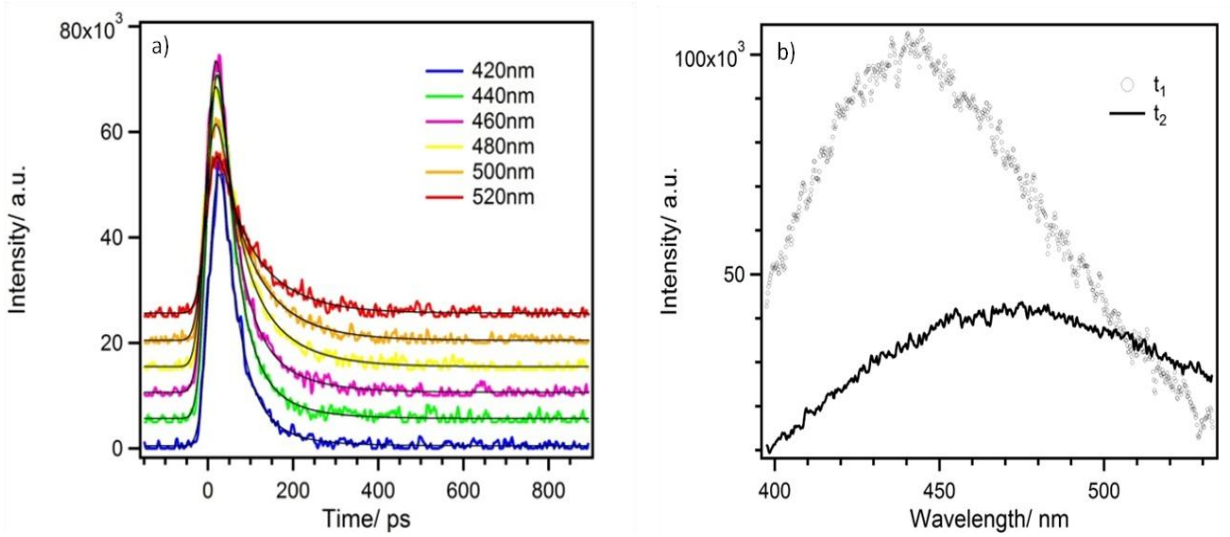

Figure 114.*(a) Fluorescence kinetics with exponential fits and (b) DAS for M-BT at pH 2.5; t_1 < 10 ps,t_2 = 98 ± 5 ps.*

3.7.6 Steady state and time resolved fluorescence investigation of BTCA

The absorption spectra of BTCA in buffer solution at various pHs are shown in **Figure 115a**. At wavelengths <300 nm the band structure is similar to that of BT, but with somewhat shifted peak maxima, and peak intensities varying with pH. In addition there is absorbance extending

further to the red, up to ~400 nm, indicating the presence of additional low-lying transitions. The fluorescence spectrum of BTCA in MeOH is a single broad band with λ_{max} ~440 nm (**Figure 115b**) and is characterized by a relatively small Stokes shift, similarly to BT. On the other hand in buffer solution at all pHs in the range 2.5 to 9.5 the fluorescence spectrum is broad and characterized by at least two bands at ~450 and 600 nm, with a greatly increasing amplitude of the red band at pH 9.5 (**Figure 115b**).

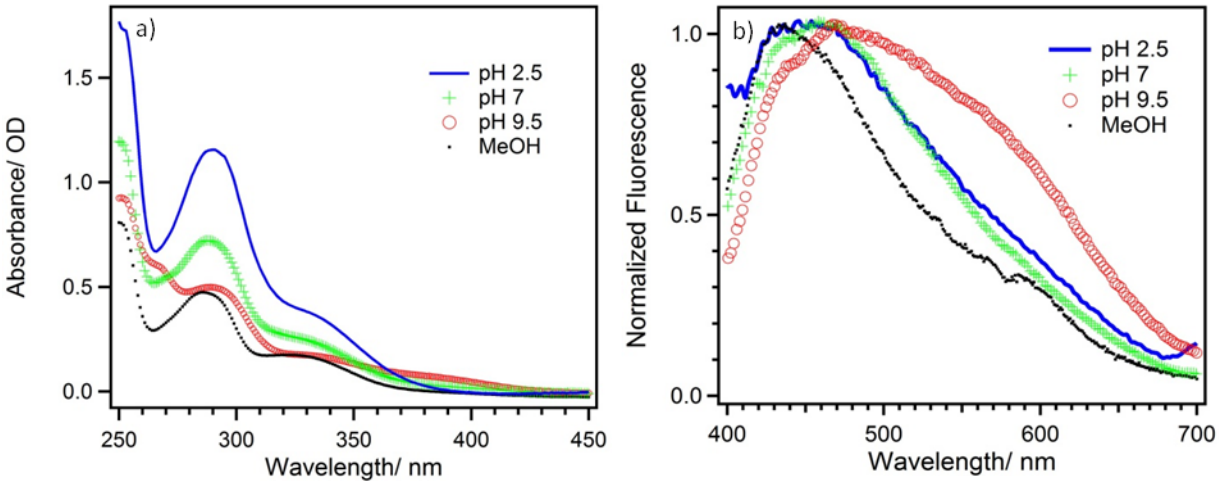

Figure 115. *(a) Absorption and (b) steady state fluorescence (upon 266 nm excitation) spectra of BTCA.*

At this pH the two COOH groups are fully deprotonated, the 4-OH is mostly deprotonated (82 %) and the NH_2/NH_3^+ amino acid group at a ~70/30 ratio determined by its pK_a = 9.11. The red ~600 nm shoulder of the fluorescence spectrum can consequently be associated with tri-anionic $BTCA^{3-}$ (COO^-, COO^-, O^-, NH_2). The corresponding fluorescence band was also observed for BT at ~480 nm (above); the fact that it is more red-shifted for BTCA makes it more easily distinguishable from the emission bands of the other species. As will be evident from the time resolved measurements, the 450-nm band is a superposition of BTCA and $BTCA^{2-}$.

In order to fully disentangle the various contributions to the fluorescence spectrum we turn to the time resolved measurements. The time resolved fluorescence of BTCA in the pH range 2.5-9.5 recovers DAS (**Figure 116**) components and lifetimes that appear to be

analogous to those identified for BT. A red-shifted component with a maximum at ~580 nm and decay time of ~100 ps, spectrally coincides with the red shoulder in the static fluorescence spectrum appearing at pH 9.5.

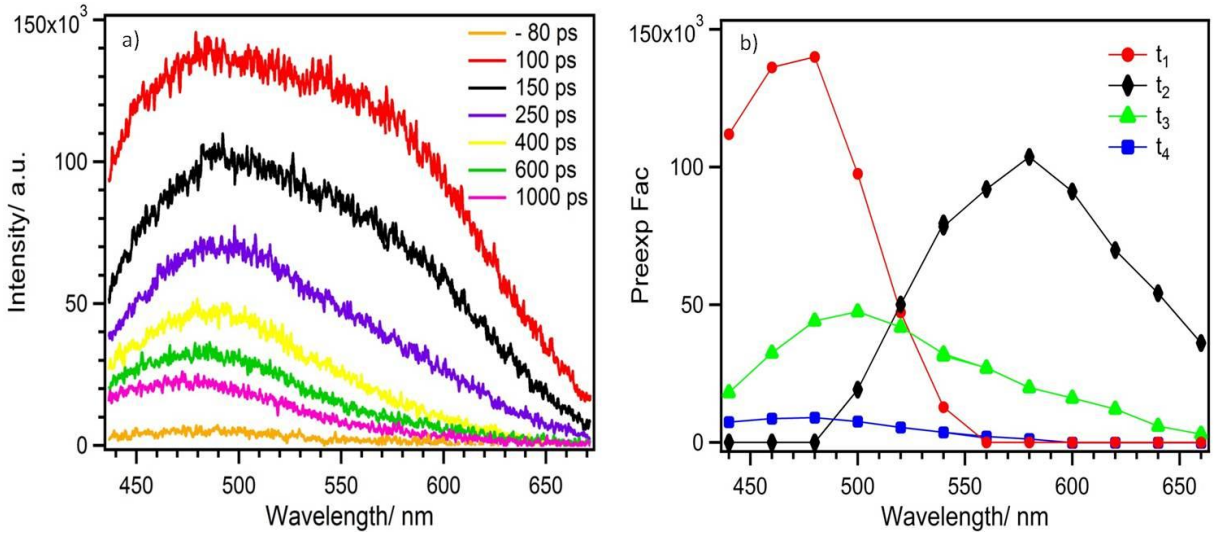

***Figure 116**. (a) Time resolved fluorescence spectra of BTCA at pH 7. (b) Preexponentiel factors representing DAS of BTCA at pH 7. t_1< 10 ps, t_2 = 86 ± 2 ps, t_3 = 282 ± 8 ps, t_4 = 2.9 ± 0.4 ns.*

Therefore it is straightforward to assign this DAS to the triple-anion $BTCA^{3-}$ with all functional groups deprotonated. The consequence of this is that the anionic species (of both BTCA and BT) with fluorescence maximum at ~450 nm and ns-lifetime belongs to the anionic O^- species with the amino acid group in its zwitterionic (NH_3^+, COO^-) state. The ~400-440-nm (~10 ps) and ~500-nm (282 ps) DAS components are assigned, analogously to BT, to the 4-OH and cationic (heterocyclic-N protonated) $BTCAH_2^{2+}$ forms. All these spectral assignments are similar to those of BT in **Scheme 8**, and therefore not repeated.

The excited state proton transfer processes underlying the complex fluorescence behavior of both BT and BTCA can now be summarized in a few points

. i) The neutral enol form of BT and BTCA in methanol has a fluorescence lifetime of ~250-300 ps, representing the sum of radiative and non-photochemical radiationless processes of the benzothiazole core.

ii) In aqueous buffer solution the OH at 4-position and the benzothiazole nitrogen atom control the photochemistry of both BT and BTCA via ESPT and ESIPT processes.

iii) The aminoacidic groups of the alanyl chain have a minor influence on the photochemistry (but protonation state of the amino group determines the excited state lifetime of anionic species).

iv) The ESPT and ESIPT produce several different excited state ionic species with lifetimes ranging from ~100 ps to ~3 ns.

The findings here for BT and BTCA pheomelanin building blocks can now be compared to those of 5,6-dihydroxyindole (DHI) and 2-carboxy-5,6-dihydroxyindole (DHICA), the building blocks of eumelanin. On the monomer level there does not seem to be a dramatic difference between the various building blocks – in buffer solution they all exhibit ESPT or ESIPT processes (to a varying extent) and the resulting excited states decay on the hundreds of ps to ns time scale. In alcohol solution (methanol) these processes are much slower, or completely stops1[26] Dimers and larger units of DHICA have remarkably different excited states dynamics compared to larger units of DHI – sub-ps decay of the excited states through excited state proton transfers[126]. This unique feature was correlated to the photoprotective functions of eumelanin. How incorporation of benzothiazole in pheomelanin backbone or its formation by benzothiazine ring contraction may change the excited state dynamics is a question that future work is addressing.

The different fluorescence characteristics of eumelanin and pheomelanin is an issue of interest as a possible diagnostic tool for the detection of malignant transformation in melanocytes which is associated with a switching from eumelanin to pheomelanin production.[127]The steady state fluorescence of model synthetic pheomelanins has been investigated in detail[128] but up to now no interpretation of the species responsible for the phenomena has been provided because of the lack of information on the behavior of the putative building blocks inside the pigment. In this regard the present investigation provide the

first description of the steady state and excited state dynamics of the two main benzothiazole units of pheomelanin under conditions of relevance to the physiological process and provide a new groundwork for the interpretation of the photoreactivity of pheomelanin and the associated damages of the epidermal tissues.

3.8 Photochemistry of pheomelanins: Spectroscopic investigation of natural and synthetic pigments and related 1,4-benzothiazines

3.8.1.Background

Pheomelanins contain both 1,4-benzothiazines and 1,3-benzothiazole as main structural components. In the previous chapter, a systematic investigation of the photochemistry of 1,3-benzothiazoles occurring in the natural pigments has been presented. The study was then extended to other putative structural elements of pheomelanins featuring the 1,4-benzothiazine system or both benzothiazine and benzothiazole units. In addition natural pheomelanins from red hair and model synthetic pigments were also analyzed in comparison with natural eumelanins isolated from black hair.

The main aim of this study is to characterize the evolution pathways of these species on photoexcitation, an issue that may help interpretation of the role of pheomelanins in the photosensitivity and proness to skin cancer of red haired people. For all these compounds, steady state fluorescence emission and time-resolved fluorescence measurement were performed

3.8.2 Sample preparation

As a first step in this work, the synthesis of benzothiazine–containing oligomers and synthetic pigments were carried out following previously reported procedures. These oligomers are the bibenzothiazine dimers (BTZ) and isoquinoline-benzothiazole dimers (BT-TIQ), that are the ultimate pheomelanin precursors that can prepared synthetically. (**Figure 117**) . As to the isoquinoline dimers, structural markers directly related to these compounds have recently been

obtained from natural pheomelanin and a solid state NMR study showed convincing 2D spectra providing evidence for the presence of these structural units in the natural pigments.

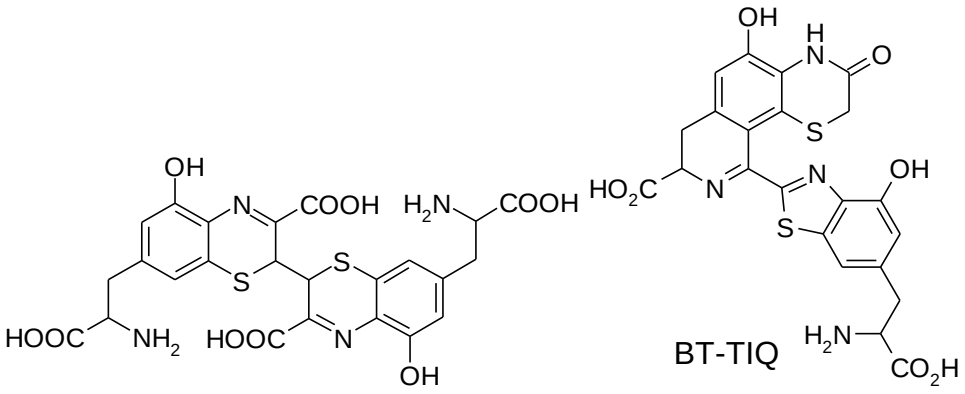

Figure 117. *Structure of the pheomelanin precursor containing benzothiazine units*

Regarding the pigments, three different synthetic pheomelanins were synthesized and investigated:

1)dopacys: synthetic pigment prepared from Dopa in the presence of cysteine by tyrosinase oxidation

2-3) cysdopa with and w/o Zn^{2+}: pigments prepared from the major pheomelanin prescursor cysteinyldopa in the absence or in presence of Zinc ions .

Finally, the natural red hair pheomelanin and black hair eumelanin pigments were obtained as previously described in the chapter 3.6.

3.8.3 Steady State Emission Spectra and Time-Resolved measurement

For all benzothiazine compounds, synthetic and natural pigments SSE (Steady State Emission) and TRE (Time-Resoled Emission) measurements were performed in aqueous buffer solutions at selected pHs, namely pH 2.5 and 7 (in some cases the measurements were carried out also under more acidic conditions, that is 1M HCl) .

BTZ-dimers

At pH 2.5, BTZ-dimer shows, both at SSE and TRE measurement, an extremely intense emission of fluorescence peaked at around 350 nm. However, the image obtained at the streak camera for the time-resolved experiments, shows also that this species is extremely long lived (>2 ns) and is beyond the temporal measurement range of the instrument (from 10 ps to 2 ns). This can be clearly seen comparing the images shown in **Figure 118** and **Figure 119** (right panels). At pH 2.5 the emission at 350 nm is clear, but the image shows a continuous band that goes all across the vertical section of the image.

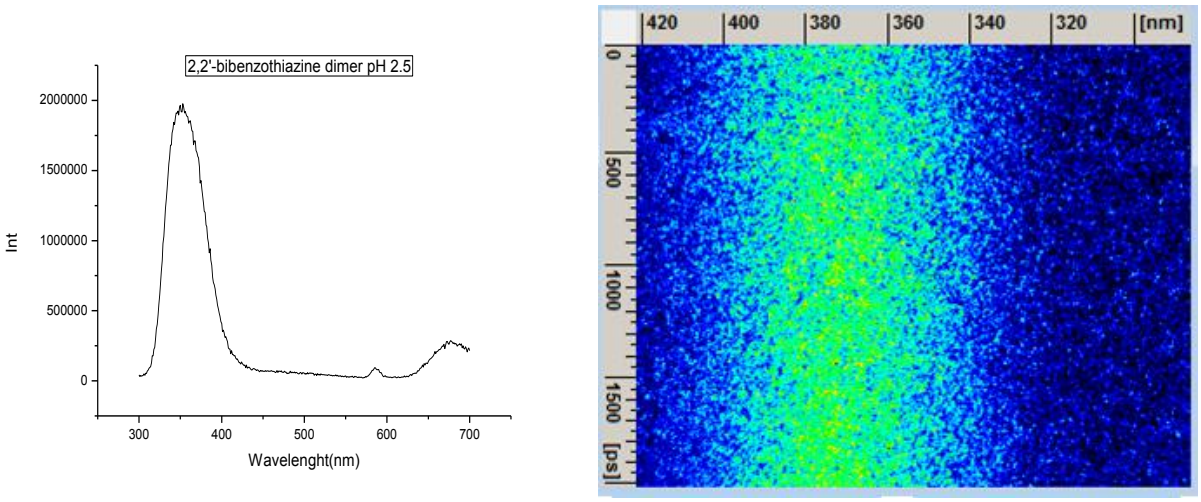

Figure 118. *SSE and Time-Resolved spectra of BTZ at pH 2.5*

At pH 7, the TRE is quite different showing a well defined zero time (an arbitrary time, set by the operator, that sets the starting point's time of the measure). At this pH , the steady state spectrum presents again the emission at 350 nm and a weak new band at around 480 nm appears. The time-resolved measurement shows that this more red-shifted band presents a clear signal with a lifetime in the temporal range of the instrument. A preliminary estimate the lifetime of this species should be around 480 ps . In Time-Resolved experiments, no clear signal was evident for the 350 nm band.

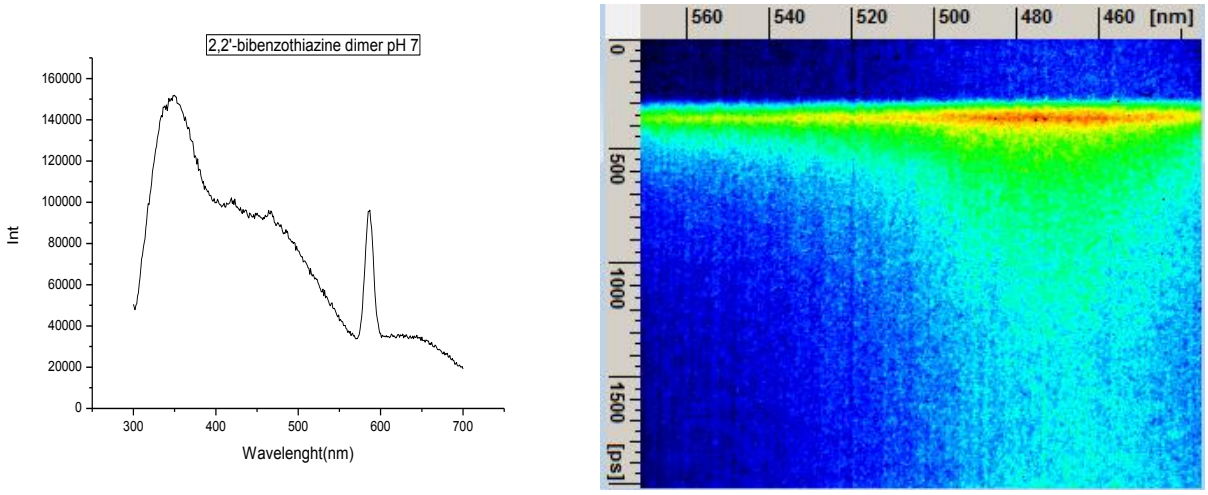

Figure 119. *SSE and Time-Resolved spectra of BTZ at pH 7*

BT-TIQ

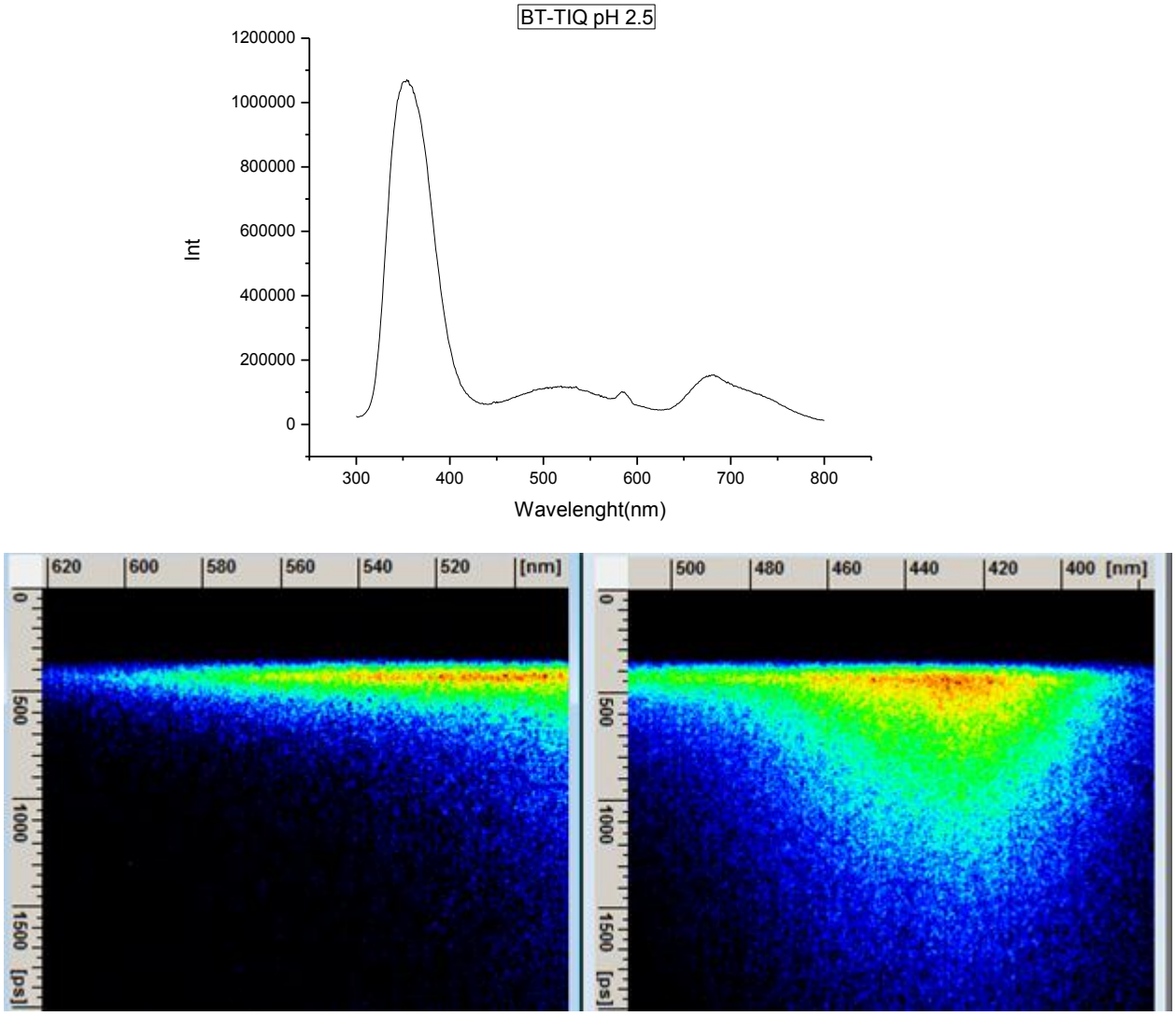

Figure 120. *SSE and Time-Resolved spectra of BT-TIQ at pH 2.5*

The isoquinoline-benzothiazole dimers was investigated under the same conditions as BTZ. At pH 2.5 (**Figure 120)** the steady state emission spectrum is quite similar to that of BTZ, that is a strong emission at 350 nm. In this case another weak band can be seen at 500 nm with a estimated lifetime of almost 1 ns. Surprisingly, in the time- resolved image only the 500 nm band can be seen and the 350 nm band is absent.

At pH 7(**Figure 121**), the 500 nm band is clearly the dominant band and the time-resolved experiment shows that its lifetime is really short-lived, 280 ps .

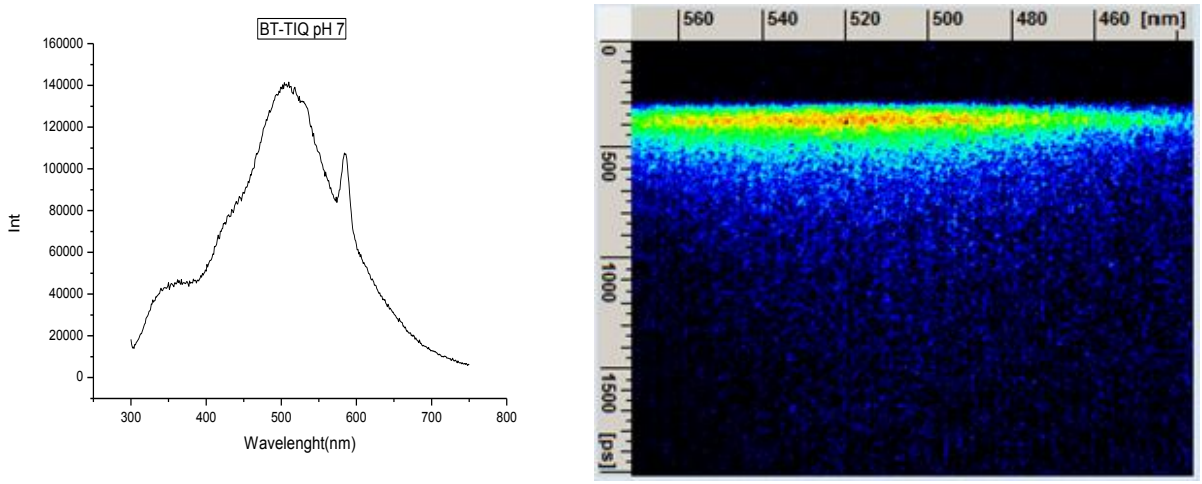

Figure 121. *SSE and Time-Resolved spectra of BT-TIQ at pH 7*

Synthetic pheomelanins : a) Cysdopa

As for the synthetic pigment cysdopa, obtained from peroxidase oxidation of the main pheomelanin precursor 5-S-cisteinyldopa, at pH 2.5 the same emission spectra exhibited by BTZ and BT-TIQ is observed (**Figure 122**), with the major peak at 350 nm. In this case, the time resolved experiment showed that this species has a lifetime >2 ns (image not shown).

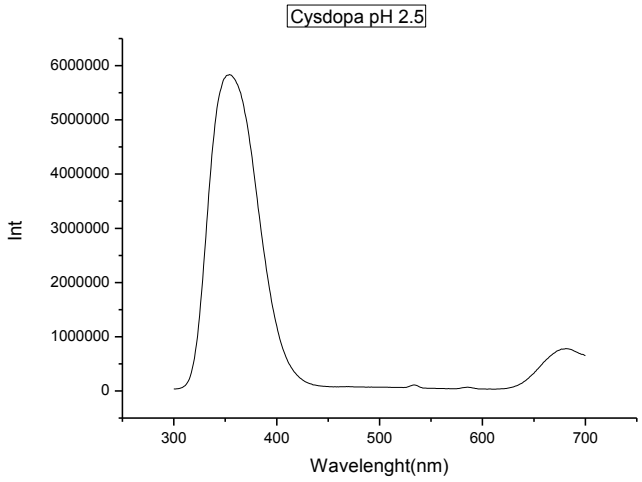

Figure 122. *SSE spectrum of Cysdopa at pH 2.5*

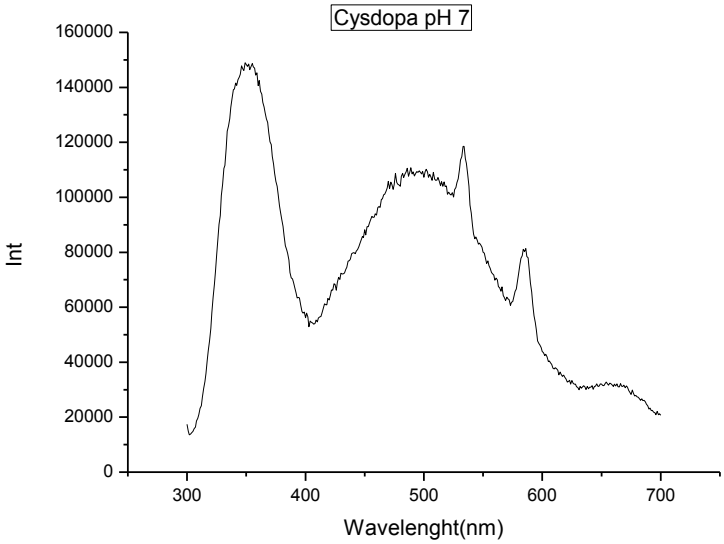

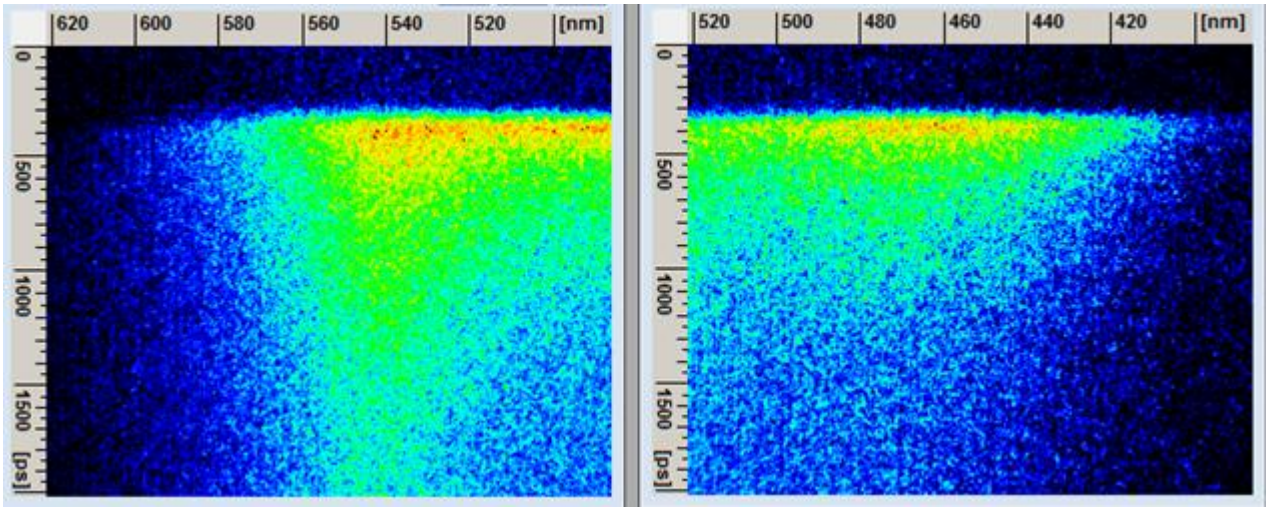

Figure 123. *SSE and Time-Resolved spectra of Cysdopa at pH 7*

At neutral pH (**Figure 123**), the SSE spectrum shows the usual two bands seen so far at this conditions, but this time with an almost 1:1 ratio. In the time-resolved measurement, a similar behavior as in BTZ at pH 7 is observed, showing only the signal at around 500 nm. Furthermore, in the case of Cysdopa, the time resolved image shows at least two bands with different lifetimes (680 ps for the blue band and 1.3 ns for the red band), that may be overlapped in the steady state spectrum.

Synthetic pheomelanin pigment: b) Cysdopa Zn

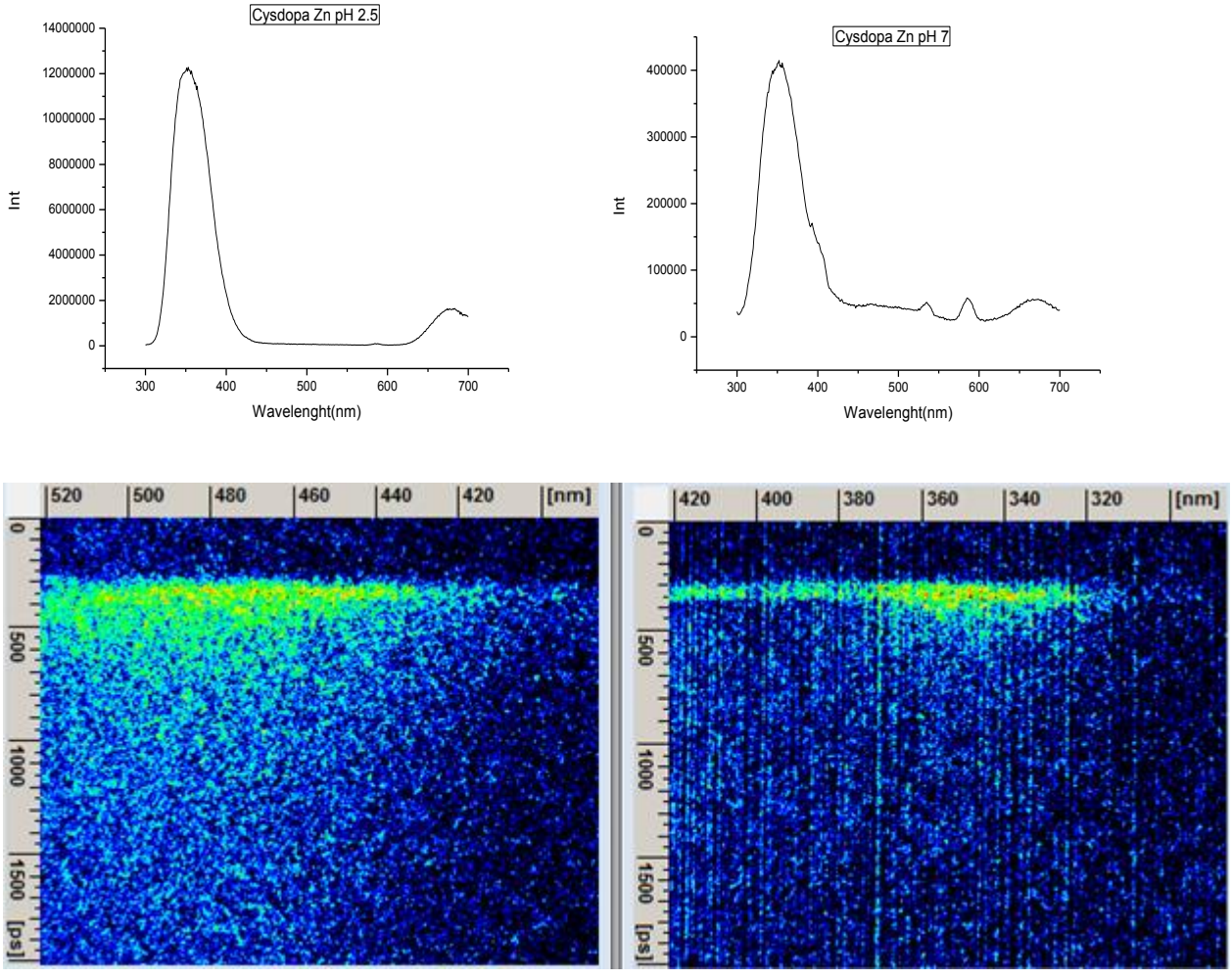

Figure 124 *SSE spectrum of Cysdopa Zn at pH 2.5 (top left), SSE and Time-Resolved spectra of Cysdopa Zn pH 7(top right and bottom)*

The SSE spectra (**Figure 124**, top left) at pH 2.5 obtained from the other synthetic pigment cysdopa, prepared from peroxidase oxidation of the main pheomelanin precursor 5-S-cisteinyldopa but this time in the presence of Zinc ions, has again the same emission at 350 nm. At pH 7 (**Figure 124**, top right) the 500 nm band is almost not present at all and only the 350 nm emission is observed. The time-resolved images of the pigment at this pH is somewhat different compared to the ones seen so far (**Figure 124**, bottom). They appear barely emissive and the lifetimes associated are extremely short. This may be caused by the presence of the Zinc ions that may in some manner cause this behavior.

Dopacys

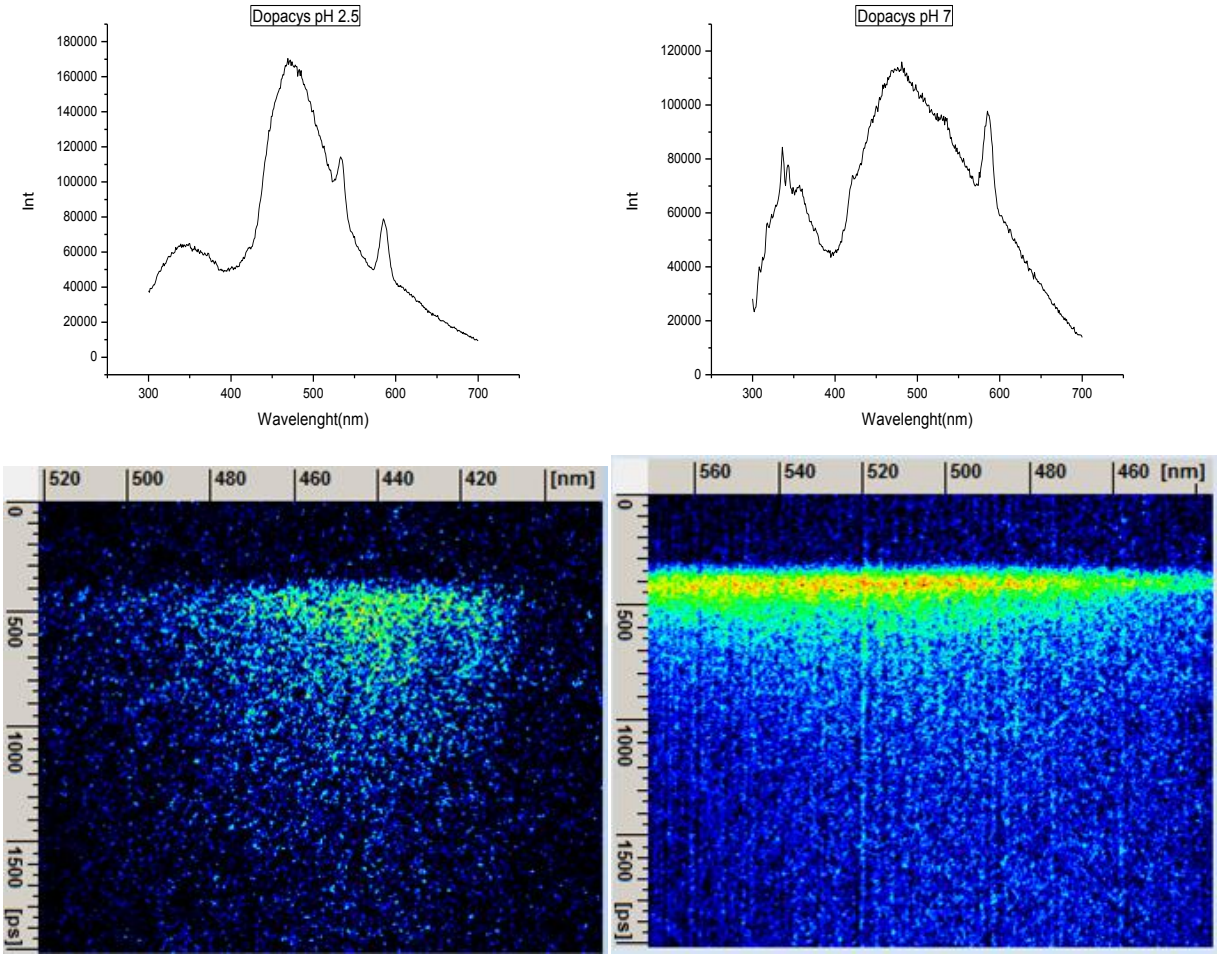

Figure 125. *SSE and Time-Resolved spectra of Dopacys at pH 2.5 (left), and pH 7(right)*

The final synthetic pheomelanin pigment (**Figure 125**) that was analyzed is dopacys, prepared from L-dopa and cysteine in the presence of tyrosinase under oxygen. SSE and time-resolved spectra show that in both pH 2.5 and pH 7 , only the band at 500 nm is observed. The lifetimes of these species , moreover, are extremely short-lived and in the case of Dopacys at pH 2.5, it appears that the emission is extremely faint.

Natural pigments:pheomelanin

Finally, the natural pheomelanin pigment from red human hair was examined. At pH 2.5(**Figure 126**) the steady state emission spectrum is quite different compared to the emissions seen so far, as a completely new band , at 310 nm is observed, with a smaller emission at 460 nm. The time resolved image, however, did not show any sign of this extremely blue shifted band, while the band at higher wavelengths was detected and associated to a short lived species (250 ps).

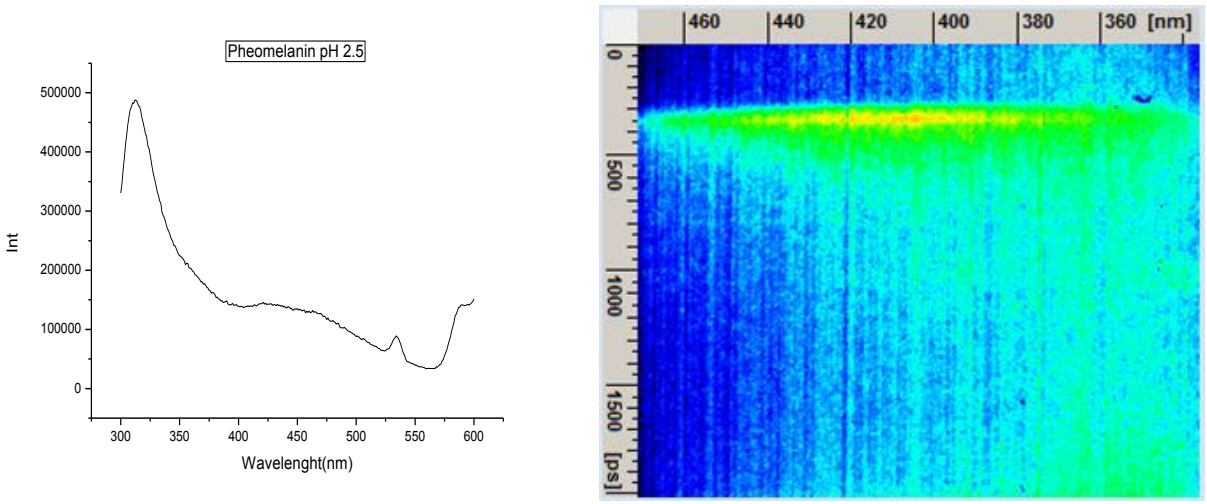

Figure 126 *SSE and Time-Resolved spectra of natural pheomelanin at pH 2.5.*

Surprised by this behavior, the experimental conditions were slightly changed in order to register the spectrum in a more acidic environment. **Figure 127** shows the steady state emission and the time resolved fluorescence measurements in HCl 1M. The SSE spectrum has the same components as in pH 2.5 (two peaks at 310 and 450 nm) , but this time, the 350 nm is

clearly present and is predominant together with the more blue shifted band. The time-resolved images confirms the presence of the 350 nm band and its lifetime could not be defined as it turned out to be too long-lived for the streak camera temporal range. From the same image, a similar 450 nm band found at pH 2.5 is observed.

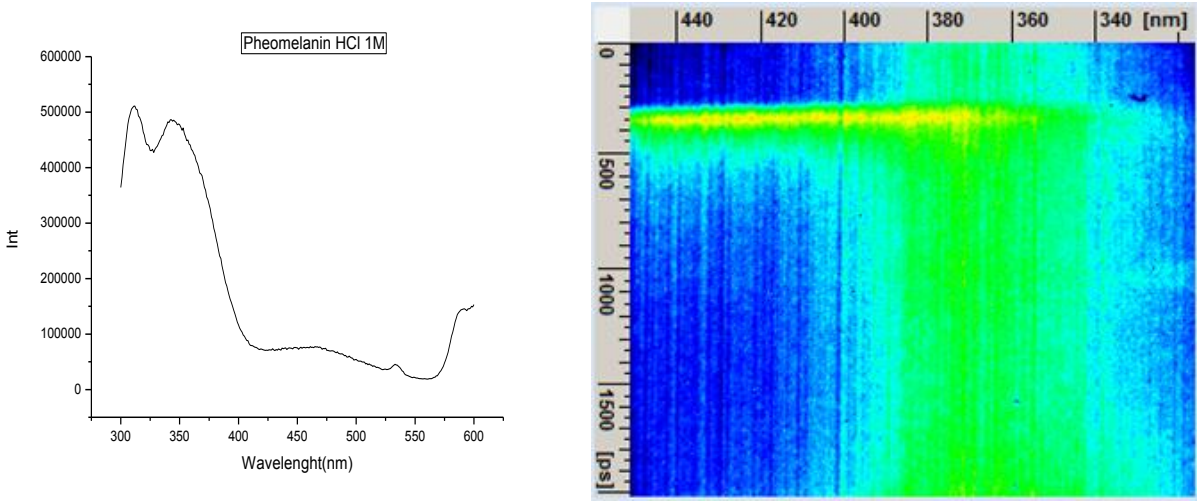

Figure 127 *SSE and Time-Resolved spectra of natural pheomelanin in HCl 1M.*

At neutral pH (**Figure 128**) , the 350 nm emission reappears in SSE , together with barely pronounced bands at 310 nm and 460 nm. At the streak camera, only the more red band is observed with a eximated lifetime of 600 ps.

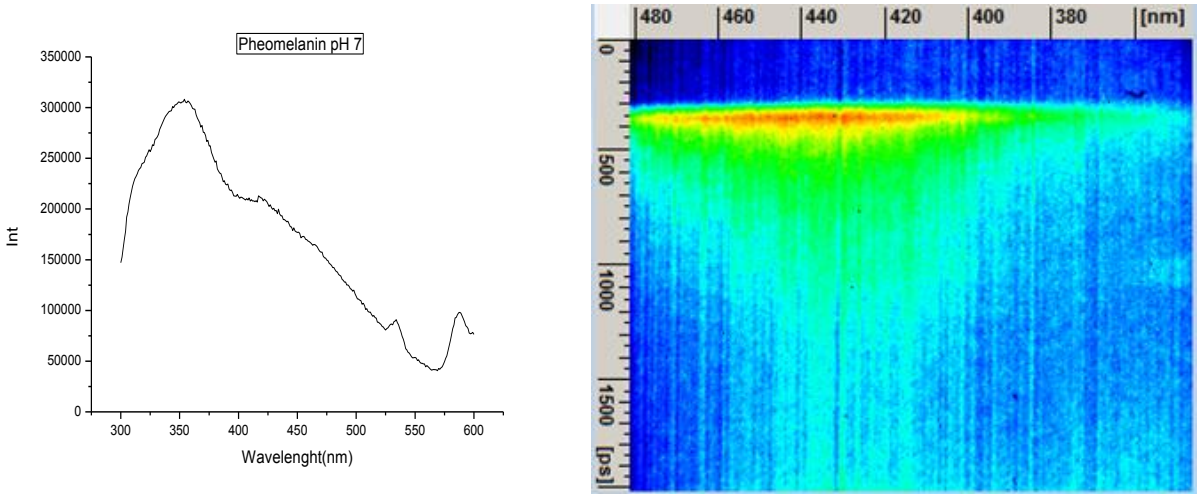

Figure 128 *SSE and Time-Resolved spectra of natural pheomelanin at pH 7.*

Natural pigment:eumelanin

The emission properties of the natural black human hair pigment, eumelanin, were also briefly investigated. For comparison the measurement were made at pH 2.5, pH 7 and also in HCl 1M. In acidic conditions, the steady state spectrum (**Figure 129**) at he most predominant bands are at 3650 nm and 450 nm. It should be noted that the fluorescence exhibited by the eumelanin pigment is much more intense compared to pheomelanins. This can be also seen in the time-resolved spectrum, where both the bands are visible, really intense and long lived

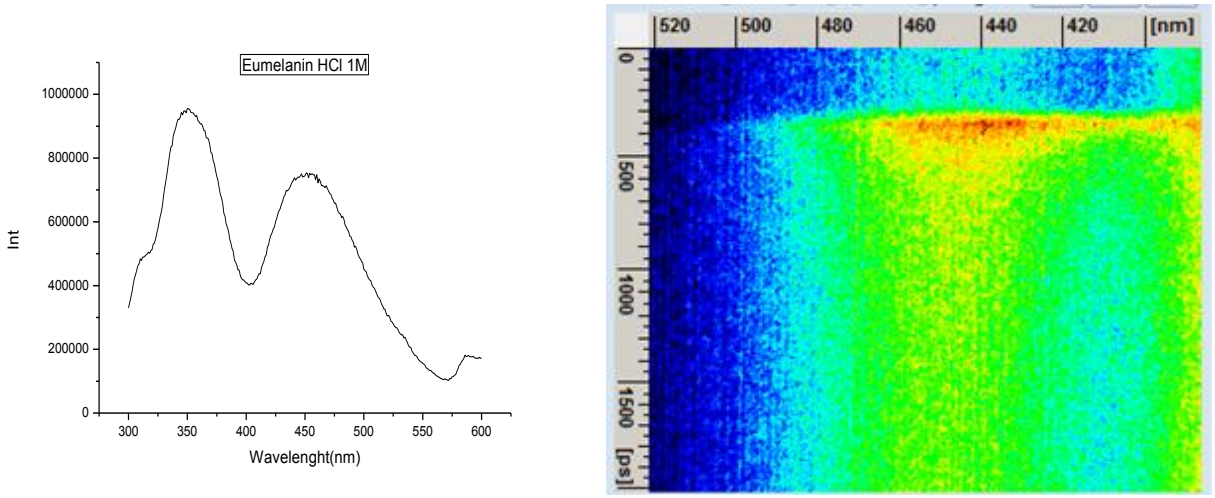

***Figure 129**. SSE and Time-Resolved spectra of natural eumelanin in HCl 1M*

At pH 2.5 in SSE (**Figure 130**), the band at 350 nm is no more apparent and that at 450nm is the predominant. The time-resolved experiment shows the same behavior found in the steady state, that is one band at around 450nm, which is really long-lived

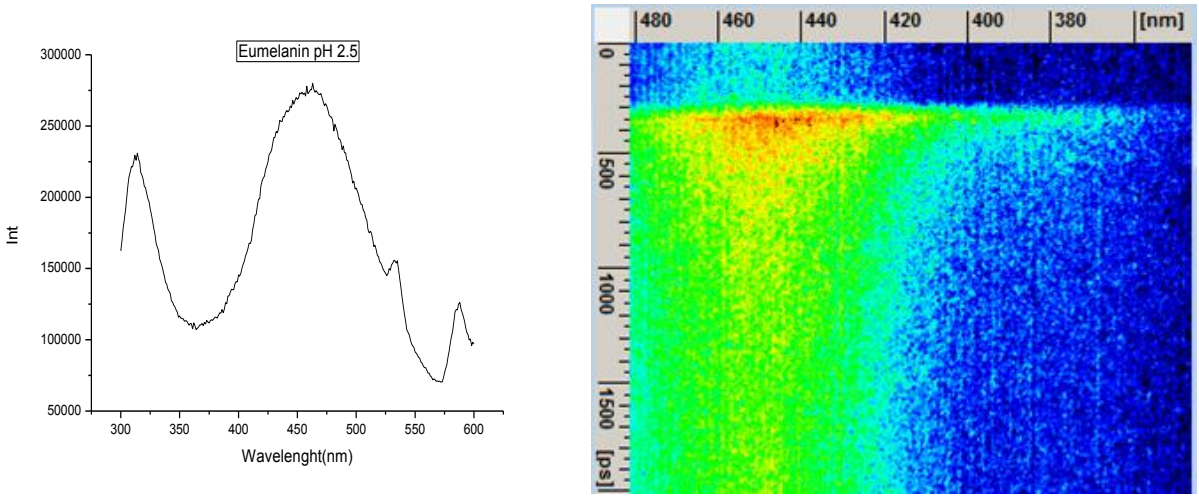

***Figure 130**. SSE and Time-Resolved spectra of natural eumelanin at pH 2.5.*

In neutral buffer solution (**Figure 131**), the SSE spectrum shows the same two peaks at a 1:1 ration, while in the time-resolved experiment, only the more red band is observed with a lifetime of 500 ps.

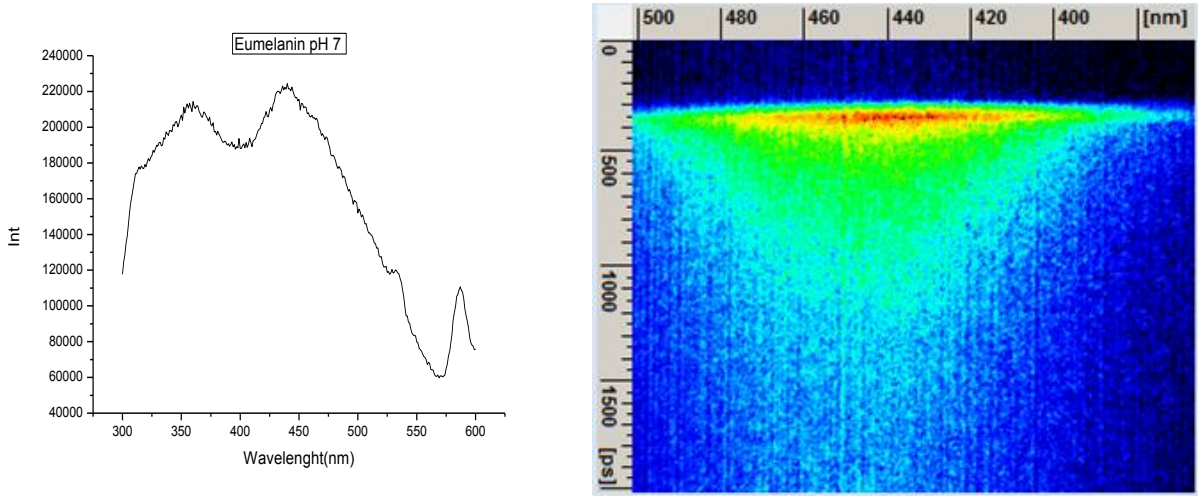

***Figure 131**. SSE and Time-Resolved spectra of natural eumelanin at pH 7.*

Table 8 summarizes the results obtained so far:

Sample	HCl 1M	pH 2.5	pH 7
Pheomelanin	350 nm- Long Lived	400 nm /250 ps	440 nm / 600 ps
Cysdopa		350 nm / Long Lived	460 nm /700 ps 540 nm / >1ns
Cysdopa/Zn		350 nm / Long Lived	350 nm / 180 ps 470 nm / 380 ps
Dopacys		450 nm (weak) / 400 ps	500 nm / 320 ps
BT-TIQ		430 nm / ~ 1 ns; 520 nm/260 ps	500 nm / 280 ps
BTZ dimers		370nm /Long Lived	470 nm/350 ps
Eumelanin	450 nm / Long Lived	450 nm / Long Lived	440 nm – 500 ps

***Table 8.** Lifetimes determined for the benzthiazine compounds, synthetic and natural pigments*

Interpretation of these results are still underway, and it may require some time, since the kinetics seems not to follow a multi exponential decay. However a first analysis suggests a major role played by benzothiazine-compounds compared to the benzothiazole ones, in determining the behavior of both the synthetic and the natural pigments

4.Conclusions

In this PhD project attention has been focused on 1,4-benzothiazines, the core structural unit of pheomelanin pigments, responsible for the red hair phenotype. The chromophore exhibited by these pigments has been associated to the presence of the $\Delta^{2,2'}$-bi-(2*H*-1,4-benzothiazine), occurring in a group of low molecular weight pheomelanins termed trichochromes that are closely related to indigos, a class of chromophores of potential practical interest but so far little explored in materials science.

As a first approach to develop new benzothiazine based functional dyes, a detailed structural re-examination of the stable yellow isomer of $\Delta^{2,2'}$-bibenzothiazine by an integrated 2D NMR and theoretical approach was carried out and it was shown that the stable yellow species is in fact the *cis* isomer rather than the trans isomer as previously suggested. More compelling evidence supporting structural revision came from a gradient-selected X-half filtered NOESY-HSQC experiment. In the same study it was also found that under strongly acidic conditions the initially-formed violet species (λ_{max} 556 nm), corresponding to the protonated derivative, undergoes further protonation to give a blue species (λ_{max} 590 nm), identified as the dication. Based on these data, a novel picture of $\Delta^{2,2'}$-bibenzothiazine as a four-state system with photochromic and pH-dependent behavior could be proposed.

To extend the scope offered by the push-pull chromophoric system exhibited by $\Delta^{2,2'}$-bibenzothiazines, 3-substituted-1,4-benzothiazines were prepared as stable and easily handled starting materials for access to new benzothiazine based functional dyes. The monomeric benzothiazines, namely the 3-phenyl- and the 3-methyl-2*H*-1,4-benzothiazine were obtained in 50-60% average yields by improvement of previously reported procedures involving reaction of the *o*-aminothiophenol with an alpha-haloketone.

The oxidative coupling of these monomers was investigated and the most interesting results were obtained starting from 3-phenyl-1,4-benzothiazine. Indeed, in the presence of micromolar peroxides or biometals (Fe(III), Cu(II), V(V) salts), and following a strong acid input, this benzothiazine monomer is efficiently converted to a green-blue $\Delta^{2,2'}$-bi-(3-phenyl-2H-1,4-benzothiazine) via colorless intermediates identified as single-bonded dimers. In the mechanistic scheme proposed peroxides or metal ions induce conversion of protonated 3-phenyl-1,4-benzothiazine to a resonance-stabilized benzothiazinyl radical intermediate that was evidenced and characterized by epr spectroscopy. Interestingly, 3-phenyl-2H-1,4-benzothiazine proved to be useful for the visual detection of peroxides in aged etheral solvents such as THF, ethyl ether, dioxane. Moreover, it was noticed that addition of rusty iron objects promoted oxidation of 3-phenyl-1,4-benzothiazine to its double bond dimers in a very fast and efficient manner. Under these conditions, 3-phenyl-2H-1,4-benzothiazine was found to serve as an efficient inhibitor against corrosion of the rusty iron objects induced by concentrated HCl.

New benzothiazine based functional dyes were prepared based on the cyanine chromophore.

The synthesis of the benzothiazine cyanines was pursued by two different approaches, one involving reaction with dialdehydes that may allow for the build- up of a conjugated bridge between the two benzothiazine units and the other based on the condensation of the benzothiazine with aromatic para N-alkyl substituted aldehydes exploiting the nucleophilicity of the enamine tautomer form of the benzothiazine. A new cyanine was obtained from 3-phenylbenzothiazine and excess formaldehyde or in even better yields up to 50% with glyoxal featuring an ethanediiyldene bridge between the benzothiazine units. This product showed a larger bathochromic shift compared to the parent $\Delta^{2,2'}$-bi-(2H-1,4-benzothiazine), that is an intense absorption at 484 nm shifted to 617 nm for the monocation and 654 nm for dication generated in acids.

The condensation products of the 3-substituted-1,4-benzothiazines with *p*-dimethylaminobenzaldehyde, vanillin, *p*-dimethylaminocinnamaldehyde and ferulaldehyde

were obtained in average to good yields in acidic methanol, purified and subjected to complete mono and 2D NMR characterization. All these products showed a strong pH dependence of the chromophores. In the case of the *N*-alkyl substituted products a marked batochromic shift upon acidification was observed (around 200 nm) that was partially reverted on further acidification as the result of protonation of the *N*-dialkyl substituent abating the donor potential of the cyanine push pull chromophore. High molar extinction coefficients (up to 18,000) were associated to the phenyl-substituted benzothiazine cyanines. Likewise the strongest emission of fluorescence was observed for the condensation products starting from 3-methyl-1,4-benzothiazine, with complete quenching of the fluorophore with acidification. Overall the newly synthesized cyanines offer a significant palette of colors and applications exploiting single components or mixtures of them may be easily envisaged.

The second major issue addressed in this PhD project concerns the role of the benzothiazine structural units in the biological function of pheomelanin pigment. Though commonly regarded as photosensitizer agent capable of amplifying generation of reactive oxygen species following UV radiation, recently, pheomelanin has also been implicated in UV-independent pathways of oxidative stress. To get an insight into these processes at molecular level the reactivity of natural and synthetic pheomelanins toward cellular antioxidants that are critical for maintaining the redox balance was investigated and the results obtained showed a marked ability of pheomelanin from red human hair, but not of eumelanin from black human hair, to reduce the levels of two representative cellular targets, namely glutathione and NADH, in vitro. In the absence of oxygen GSH and NADH depletion was not observed while the presence of enzymes as superoxide dismutase and catalase did not modify the effect of pheomelanin suggesting a ROS independent mechanism. Similar effects were obtained with a synthetic pigment confirming that the prooxidant effects are due to the pheomelanic component. The mechanism of GSH oxidation by pheomelanin was investigated by EPR spectroscopy, showing a decrease only of the pheomelanin component of the natural pigment, after 24 hours incubation with

GSH. The results may be interpreted invoking a role of the benzothiazine units inside the pigment backbone. These would be able to sustain a redox cycling in which the pigment acts as oxidant toward GSH and NADH and is then reconverted into the oxidized form by molecular oxygen which in turn is reduced to ROS. This mechanistic view includes ROS generation but the antioxidant consumption is the result of a direct interaction with the pigment and not with ROS as previously suggested.

A systematic investigation of the role of putative structural subunits of pheomelanin in the photoreactivity and photodegradation behavior of the pigment was also addressed. To this aim key intermediates of pheomelanogenesis, including benzothiazoles, benzothiazine dimers and dihydroisoquinoline were synthesized and the photochemistry was investigated in collaboration with the research unit headed by professor Sundstrom at the Department of Chemical Physics of Lund University (Sweden). Steady state absorption and emission spectra at different pHs showed marked differences that can be accounted for in terms of the ionization state of the functional groups. Regarding the benzothiazole compounds model of the structural units occurring in pheomelanin pigment, the results obtained showed that the OH at 4-position and the benzothiazole nitrogen atom control the photochemistry of both 6-(2-amino-2-carboxyethyl)-4-hydroxy-1,3-benzothiazole and 6-(2-amino-2-carboxyethyl)-4-hydroxy-1,3-benzothiazole-2-carboxylic acid via intramolecular and solvent proton transfer processes. Moreover, the aminoacidic groups of the alanyl side chain have a minor influence on the photochemistry. The study was then extended to other putative structural elements of pheomelanins featuring the 1,4-benzothiazine system or both benzothiazine and benzothiazole units and on natural and synthetic pheomelanins. Analysis of data showed the major role of benzothiazine, compared to benzothiazoles in determining the behavior of the natural pigment.

.

5.Materials

5.1 General Methods

Anhydrous ethyl ether, anhydrous DMSO, phenacyl bromide, chloracetone , formaldehyde , glyoxal, p-dimethylaminobenzaldehyde , vanillin, ferulaldehyde , Rhodamine B, *o*-aminothiophenol, $FeCl_3$ anhydrous, $CuSO_4$ 5 H_2O and V_2O_5, dioxane , picric acid , methanol, ethanol, sodium bisulfate, chloroform, p-dimethylaminocinnamaldehyde , o-aminothiophenol, L-Dopa, L-glutathione (GSH), L-glutathione oxidized (GSSG), β-nicotinamide adenine dinucleotide reduced (NADH) disodium salt hydrate, β-nicotinamide adenine dinucleotide (NAD+), β-nicotinamide adenine dinucleotide phosphate reduced (NADPH), β-nicotinamide adenine dinucleotide phosphate (NADP+), Ellman's reagent, hydrogen peroxide (30% v/v), horse radish peroxidase (EC 1.11.1.7), bovine erythrocytes superoxide dismutase (SOD) (EC 1.15.1.1), bovine liver catalase (EC 1.11.1.6),methylbenzothiazole (MB) were commercially available and were used as obtained

UV-vis spectra were UV spectra were recorded with a Jasco V-560 UV/VIS Spectrophotometer. ^1H NMR spectra were recorded at 200, 400 or 500 MHz, ^{13}C NMR spectra at 50 or 100 MHz. ^1H, ^1H COSY, ^1H, ^{13}C (DEPT) HSQC, and ^1H, ^{13}C HMBC experiments were run at 400 or 500 MHz, on instruments equipped with a 5 mm 1H/broadband gradient probe with inverse geometry using standard pulse programs. The HMBC experiments used a 100 ms long-range coupling delay. Chemical shifts are reported in δ values (ppm) downfield from TMS.

Analytical and preparative TLC were carried out on silica gel plates (0.25 and 0.50 mm, respectively) from Merck. Hexane-ethyl ether 7:3 v/v (eluant A) ; petroleum ether-ethyl acetate 7:3 v/v (eluant B) ; hexane-ethyl ether 8:2 v/v (eluant C) ; hexane-ethyl acetate 8:2 v/v (eluant

D) ; cyclohexane-ethyl acetate 9:1 v/v (eluant E) ; dichloromethane-hexane 8:2 v/v (eluant F) ; hexane-ethyl acetate 9:1 v/v (eluant G) ; hexane-ethyl ether 98/2 v/v (eluent H).

HPLC. HPLC analyses were performed on a Shimadzu SCL-10AV VP instrument equipped with a LC-10AD VP pump and a SPD-10AV VP UV-visible detector.

For $\Delta^{2,2'}$-bi-(3-phenyl-2H-1,4- benzothiazine) analyses, an octyl column (15 cm x 4.6 mm, 3 micron particle size) was used. An acetonitrile/water gradient was used as follows: 0-50 min: 50%-70% acetonitrile; 50-60 min: 70% acetonitrile. Flow rate was set at of 0.7 ml/min.

For TTCA and PTCA analyses a Synergi Hydro-RP 80A column (250 x 4.60 mm, 4 μm) was used, with 1% formic acid (pH altered to 2.8 with sodium hydroxide)/methanol 97:3 (v/v) as eluent, at a flow rate of 0.7 mL/min. Detection wavelength was set at 254 and 280 nm. 34

For GSH and GSSG analysis an EC detector set at + 500 mV vs. an Hg/Hg_2Cl_2 reference electrode was used as additional detector. A Sphereclone ODS (5 micron, 4.6x250 mm) column was used, with 0.01 M phosphate buffer (pH 3.0) containing/methanol 98:2 (v/v) as the eluent, at a flow rate of 0.7 mL/min.

For experiment of NADH/NADPH oxidation , detection wavelength was set at 260, or 340 nm using a Sphereclone ODS (250x4.6 mm, 5 μm) column

Preparative HPLC was carried out on an instrument coupled with a UV detector set at 254 or 280 nm using an Econosil C18 (250x22 mm,10 μm).

Semipreparative HPLC was carried out on an instrument coupled with a UV detector set at 340 nm using an Econosil C18 (250x10 mm,10 μm) column.

LC-MS analysis.

LC-MS were performed with a LC/MSD VL system (Agilent) equipped with a UV-vis detector and a quadrupole mass spectrometer with electrospray ionization source (ESI) operating in positive ionization mode in the following conditions: nebulizer pressure 50 psi; drying gas (nitrogen) 12 L/min, 350 °C; capillary voltage 4000 V; fragmentor voltage 50 V. A Sphereclone

ODS (250x4.6 mm, 5 μm) column was used.

Gradient A: 1 %formic acid (eluent a)/acetonitrile (eluent b): from 5 al 90 % b, 0-45 min.

Gradient B: (0.5% trifluoroacetic acid (eluent a)/MeOH(eluent b): from 10 to 15% b, 0-15 min; from 15 to 60% b, 15-55min; 60% b, 55-65 min; from 60 to 80% b, 65-80 min; 80% b, 80-90 min).

EPR spectroscopy.

EPR spectra were recorded using a Bruker spectrometer. The instrumental settings were as follows: sweep width, 160.0 G; resolution, 1024 points; modulation frequency, 100.00 kHz; modulation amplitude, 5.0 G. The amplitude of the field modulation was preventively checked to be low enough to avoid detectable signal overmodulation. EPR spectrum was measured with a microwave power of 6.394 mW to avoid microwave saturation of resonance absorption curve. Several scans, typically 128, were accumulated to improve the signal-to-noise ratio.

Computational Analysis:

All calculations were performed with the Gaussian package of programs. Geometry optimizations were carried out at the DFT level, with a hybrid functional (PBE0) and a reasonably large basis set [6-31+G(d,p)]. For each species, different tautomers/conformers were explored. Computations were performed either in vacuo, or by adoption of a polarizable continuum medium (PCM) to account for the influence of the solution environment. In view of the faster convergence, a scaled van der Waals cavity based on universal force field (UFF) radii was used, and polarization charges were modeled by spherical Gaussian functions. Vibrational-rotational contributions to the free energy were also computed. Additional energy computations were performed for the neutral form in vacuo at the MP2 level with

different basis sets, and at the CBS-QB3 level. UV/Vis spectra of the main species were computed in vacuo or in solution using the time-dependent density functional theory (TD-DFT)

approach,

with the PBE0 functional and the 6-311++G(2d,2p) basis set. To produce graphs, transitions below 5.6 eV were selected, and an arbitrary Gaussian line width of 0.15 eV was imposed; the spectra

were finally converted to a wavelength scale. NMR shielding tensors were computed within the Gauge-Including Atomic Orbitals (GIAO) ansatz at the PBE0/6-311+G(d,p) level. Computed isotropic shieldings were converted into chemical shifts using as reference the values obtained at the same level for benzene.

For computation of EPR parameters, geometry optimizations were carried out at the unrestricted DFT level, with the B3LYP functional [Becke, A.D. *J. Chem. Phys.* **1993**, *98*, 5648; Stephens, P.J.; Devlin, F.J.; Chabalowski, C.F.; Frisch, M.J. *J. Phys. Chem.* **1994**, *98*, 11623] and the N07D basis set, as optimized for B3LYP [Barone, V.; Cimino, P.; Stendardo, E. *J. Chem. Theory Comput.* **2008**, *4*, 751], either in vacuo or by adoption of a polarizable continuum medium. Single-point calculations were then carried out with the B3LYP functional and specifically tailored basis sets, namely EPR-II or EPR-III [Barone, V. In *Recent Advances in Density Functional Methods*, Part I, (Ed D.P. Chong), World Scientific, Singapore 1996]; the sets were completed for the sulfur center with a 6-31+G(d) or 6-311++G(2d) basis, respectively.

5.2 Photochromism and acidichromism of $\Delta^{2,2}$-Bi-(2H-1,4-benzothiazine)

Synthesis of BBTZs:

The *Z*-BBTZ was prepared following the reported procedure with modifications. The deep-violet reaction mixture as obtained was treated with 1 m Na_2CO_3 and the yellow precipitate was collected by centrifugation and purified by column chromatography (diethyl ether/hexane, 9:1) in the dark. The eluates taken to dryness under vacuum in an ice bath gave the product in 40% yield. UV and MS data are in agreement with those reported. Solutions of the yellow BBTZ in benzene or dichloromethane (3–5 mm) were exposed to sunlight in quartz vials and the conversion of the yellow to red form was followed by TLC analysis [*R*f (yellow species) = 0.44, *R*f (red species) = 0.66; diethyl ether/hexane, 9:1]. At maximum degree of conversion the solution was taken to dryness and rapidly purified by column chromatography (diethyl ether/hexane, 9:1). Back reaction of the red form was complete at room temperature after at least 18 h, and accelerated (2 h) by heating to 40 °C, in agreement with previous report

Yellow BBTZ (cis isomer)

^{1}H NMR ($CDCl_3$) δ (ppm):7.22 (m, 2H), 7.25 (m, 2H), 7.28 (m, 2H), 7.55 (m, 2H), 8.83 (s, 2H)

^{13}C NMR ($CDCl_3$) δ (ppm): 120.7 (C), 122.3 (C), 125.7 (CH x 2), 128.0 (CH x 2), 128.9 (CH x 2), 130.8 (CH x 2), 139.0 (C), 143.7 (CH x 2)

Red BBTZ (trans isomer)

^{1}H NMR ($CDCl_3$) δ (ppm):7.18 (m, 4H), 7.30 (m, 2H), 7.49 (m, 2H), 8.30 (s, 2H)

^{13}C NMR ($CDCl_3$) δ (ppm): 125.1 (CH x 2), 127.4 (CH x 2), 128.5 (CH x 2), 130.4 (CH x 2), 148.2 (CH x 2)

NMR Experiments:

The gradient-selected X-half filtered NOESY-HSQC sequence described by Gschwind et al. was implemented with a Bruker 600 DRX instrument equipped with a cryo probe and *z* axis gradients; X-half filter delays were optimized for a $^{13}C–^{1}H$ scalar coupling constant of 185 Hz, which is appropriate for the $^{13}C3–^{1}H3$ pair. The sample contained about 5 mg of the yellow form of the parent bibenzothiazine in 0.5 mL of $CDCl_3$. Spectra were recorded at 298.0 K using data sets of 4096_256 points with a mixing time of 2.0 s, 32 scans for each increment, and a relaxation delay of 4 s, and were calibrated on the residual solvent peak. The data matrix was zero-filled in both dimensions to give a matrix of 4K_1K points; apodization with a squared cosine-bell in F1 and exponential multiplication in F2 was applied.

5.3 Synthesis of 1,4-benzothiazines and investigation of their oxidation reactivity

Synthesis of 3-phenyl-2H-1,4-benzothiazine

A solution of *o*-aminothiophenol (1.068 mL) in anhydrous ethyl ether (5 mL) was treated at room temperaturebwith phenacyl bromide (2.32 g) in anhydrous ethyl ether (25 mL) under magnetic stirring. After 2 h the reaction mixture was filtered and the yellow solid washed with ethyl ether and dried. On TLC analysis (eluant A) the solid proved to be pure (2.51g, 82% yield**)**.

ESI+MS: m/z 226 ([M+H]+); UV: λmax (CH_3OH) 323 nm; ^1H NMR ($CDCl_3$) δ (ppm): 4.16 (s, 2H), 7.40-7.45 (m, 3H) , 7.48 (m, 1H) , 7.68 (t, J = 8 Hz, 2H), 7.80 (t, J = 8 Hz, 1H), 8.47 (d, J = 8Hz, 2H). 13C NMR (CDCl3) δ (ppm): 27.86 (CH2), 125.55 (CH), 125.60 (C), 127.37 (CH), 128.28 (CH), 129.81 (CH × 2), 131.01 (CH), 131.78 (CH× 2), 134.46 (C), 137.31 (CH), 139.39 (C), 164.10 (C).

Synthesis of 3-methyl-2H-1,4-benzothiazine

A solution of o-aminothiophenol (0,171mL) in anhydrous ethyl ether (0,83mL) was treated at room temperature with chloracetone (0,128mL) in anhydrous ethyl ether (4,17mL) under vigorous stirring. After 24 h the reaction mixture was centrifuged, the solid washed with chloroform and discarded . The supernatant was taken to dryness and on tlc analysis (eluant B) was shown to contain pure **2**. (57 mg, 48% yield).

ESI+MS: *m/z* 164 ($[M+H]^+$);

UV: λ_{max} (CH_3OH) 375 nm;

^{1}H NMR ($CDCl_3$) δ (ppm): 3.0 (s, 3H) , 3.71 (s, 2H) , 7.36 (m, 3H) 8.14 (d, *J*= 7,2 Hz, 1H)

^{13}C NMR ($CDCl_3$) δ (ppm): 24.19 (CH_3) , 28.95 (CH_2) , 124.28 (CH), 124.4 (C) , 127.58 (CH) , 128.11 (CH) , 131.06 (CH), 132.95 (C), 172.2 (C).

Oxidation of 3-methyl-(2H-1,4-benzothiazine):

3-Methyl-2*H*-1,4-benzothiazine (50 mg) was dissolved in methanol (4mL) and of HCl 12M (1mL). The mixture was taken under stirring at room temperature for 24h. The solution was extracted with water, sodium bisulfite and chloroform. The mixture obtained was separated by chromatographic column (eluant B). The main components was obtained at rf 0.35 (20 mg)

ESI+MS: *m/z* 323 ($[M+H]^+$);

UV: λ_{max} (CH_3OH) 414 nm

^{1}H NMR ($CDCl_3$) δ (ppm): 1.42 (s , 1H) , 2.9 (d.d , 2H), 6.65 (d , *J = 8Hz* , 1H) , 6.81 (t , *J = 8Hz* , 1H) , 7.03-7.15 (m , 5H) , 7.26 (d, *J = 8Hz* , 1H).

^{13}C NMR ($CDCl_3$) δ (ppm): 26.72 (CH_3) , 48.85 (CH_2) , 56.11 (C) , 115.22 (C) , 117.90 (CH) , 118.0(C), 119.40 (C) , 120.05 (CH) , 126.10 (CH) , 126.80 (CH) , 127.10 (CH) , 127.29 (CH) , 129.91 (CH) , 139.86 (C) , 140.25 (C) , 164.61(C) .

5.4 Oxidative coupling of 3-phenyl-(2H-1,4-benzothiazine) promoted by peroxides or biometals

Synthesis of 3-phenyl-2H-1,4-benzothiazine

Synthesis already reported in chapter 4.2

2,2'-Bi-(3-phenyl-2H-1,4-benzothiazine) (*2a/b*)

A solution of 3-phenyl-2H-1,4-benzothiazine (200 mg, 0.65 mmol) and picric acid (150 mg, 0.65 mmol) in ethanol (5 mL) was refluxed for 0.5 hours in an oil bath at 70°C. After cooling, the precipitate was collected by filtration and washed with ethanol (130 mg, 90% yield). HPLC analysis of the solid showed a pure component eluting at 47.6 min, while the filtrate consisted of both the RT 45.2 and 47.6 min components.

RT 47.6 min: ESI(+)MS: *m/z* 449 ([M+H]+); UV: λmax (CH_3OH) 259, 289, 334 (ε 13,000) nm; ^{1}H NMR ($CDCl_3$) δ (ppm): 4.20 (s , 1H) , 6.92 (d , *J= 7.6* Hz , 1H) , 7.16 (t , *J= 7.6 Hz* , 1H) , 7.33 (t , *J= 8 Hz* , 2H) , 7.40 (m , 1H) , 7.45 (m , 1H) , 7.66 (d, *J= 8Hz* , 2H) , 7.77 (d , *J=8Hz* , 1H). ^{13}C NMR ($CDCl_3$) δ (ppm): 31.34 (CH) , 120.2 (C),127.19 (CH), 127.31 (CH × 2) , 127.52 (CH) , 128.21 (CH x 2) , 128.49 (CH × 2) , 131.17 (CH) , 137.03 (CH) , 139.3 (C) , 142.01 (C) , 156.4 (C)

Δ–2,2'-Bi-(3-phenyl-2H-1,4-benzothiazine) (*3a/b*)

A solution of 3-phenyl-2H-1,4-benzothiazine (50 mg) in methanol (20 mL) and 12 M HCl (5 ml) was treated with H_2O_2 (16 mL). The solution was left under magnetic stirring for 0.5 hours at room temperature. The solution was extracted with water and chloroform. On addition of methanol a solid separated that was recovered after filtration (30 mg). TLC analysis

(cyclohexane/ethyl acetate 90:10) showed a mixture of two components (R*f* 0.68 and R*f* 0.60) that were separated by preparative TLC to give the R*f* 0.68 compound in pure form while the R*f* 0.60 band consisted of a major component and small but significant amounts of the R*f* 0.68 compound. Purity of the R*f* 0.68 compound was also confirmed by HPLC analysis under the conditions previously described (RT 55.0 min)

R*f* 0.68: ESI(+)MS: *m/z* 447 ([M+H]+); UV: λmax (CH_3OH) 342, 470 nm;

^1H and ^{13}C NMR ($CDCl_3$)

^1H NMR ($CDCl_3$) δ (ppm): 7.10 (t , *J= 8 Hz* , 2H), 7.15 (d, *J= 8Hz* , 2H) , 7.22 (t , *J= 7.6 Hz* , 1H) , 7.28 (m, CH), 7.30 (m, CH), 7.45 (d , *J= 7.6* Hz , 1H) ,7.55 (d , *J=8Hz* , 1H). ^{13}C NMR ($CDCl_3$) δ (ppm): 124.26 (C), 126.13 (CH), 126.91 (CH), 127.05 (CH), 127.82 (CH x 2), 128.05 (CH x 2), 128.76 (CH), 129.19 (C), 130.03 (CH), 138.55 (C), 141.58 (C), 156.68 (C)

EPR Spectroscopy

X-band EPR spectra were collected at 298 K in a CW spetrometer equipped with a variable temperature unit, after mixing a solution (12-25 mM) of 3-phenylbenzothiazine in methanol containing 3M HCl, with H_2O_2 (0.1 – 0.4 equivalents) in open (presence of atmospheric oxygen) suprasil quartz bulbe with 1 mm i.d. To increase S/N ratio up to 8 spectra were accumulated and digitally averaged. Blank experiments in the absence of H_2O_2 did not produce any detectable EPR signal even under continuous photolysis of the mixture in the cavity of the spectrometer with a 500 W Hg-lamp. Measured *g*-factor was corrected with respect of that of 2,4,6-tri-*tert*-butylphenoxyl radical (*g* = 2.0046) [Lucarini, M.; Pedrielli, P.; Pedulli, G.F.; Cabiddu, S.; Fattuoni, C. *J. Org. Chem.* **1996**, *61*, 9259].

Optimized hyperfine constants were obtained by interactive fitting of the experimental spectrum with simulated ones, using the Monte Carlo method, [Amorati, R.; Pedulli, G.F.; Valgimigli, L.; Johansson, H.; Engman, L. *Org. Lett.* **2010**, *12*, 2326]. Simulations were performed with WINESR software developed by Prof Marco Lucarini (University of Bologna).

5.5 Benzothiazine based cyanine dyes: a) synthesis and characterization of dimeric cyanines

Synthesis of 1-(o-aminophenylthio)-2,2-diethoxyethane:

1-(*o*-aminophenylthio)-2,2-diethoxyethane was prepared following a reported procedure. To a 1.25g solution of o-aminithiophenol in 5 mL anydrous DMSO, 0.23g sodium and 1.52 g bromoacetoaldehyde diethylacetal. After 1 h at 100 °C, the mixture was washed with water and axtracter with diethyl ether. The organic residue is washed 2-3-times with water and then dried over anhydrous sodium sulphate and taken to dryness. After chromatographic purification on silica gel (n-exane/ ethyl acetate 8/2) a pure compound was obtained in 70 % yield.

^{1}H NMR ($CDCl_3$) δ (ppm): ^{1}H NMR: ($CDCl_3$): 1.18 (t, 6H); 2.85 (d, 2H); 3.50(dd,4H), 3.53 (dd, 4H); 4.3 (s, 2H); 4.5 (t, 1H); 6.95 (m, 4 H)

Synthesis of 2,2'-(1,2-ethandiyliden)bis(2H-1,4-benzothiazine).

50 mg of 1-(*o*-aminophenylthio)-2,2-diethoxyethane was dissolved in 3mL of TFA. The mixture was taken under stirring for 48h at room temperature. The solution was extracted with water, sodium bisulfite and chloroform, and the organic layers were dried over anhydrous sodium sulphate and taken to dryness (45 mg). The residue thus obtained was separated by column chromatography (eluant C) to give the product 12 mg, 25% yield .

Uv (MeOH) : λ_{max} 503 nm; (MeOH)/HCl 1M λ_{max} 609 nm; (MeOH)/HCl 3M λ_{max} 650 nm

^{1}H NMR ($CDCl_3$) δ (ppm): 6.35 (s, 2H), 7.05 (d, 2H), 7.19 (m, 2 H), 7.22 (m, 2H), 7.43 (d, 2H), 7.93 (s, 2H) ^{13}CNMR: ($CDCl_3$) δ: 121.6 (C); 122.1 (CH), 125.5 (CH); 127.4 (CH); 128.4 (C); 128.7 (CH); 131.1 (CH); 139.8 (C); 153.4 (C);

Synthesis of 2Z,2'Z-(1,2-etandiilidene)bis(3-phenyl-2H-1,4-benzothiazine).

Method A:

50 mg of 3-phenyl-2H-1,4-benzothiazine was dissolved in 3mL of TFA and then was add 100µL of formaldehyde. The mixture was taken under stirring for 48h at room temperature. The solution was extracted with water, sodium bisulfite and chloroform, and the organic layers were dried over anhydrous sodium sulphate and taken to dryness (45 mg). The residue thus obtained was separated by column chromatography (eluant C) to give the product 13 mg, 25% yield .

Method B:

50 mg of 3-phenyl-2H-1,4-benzothiazine was dissolved in 4mL of methanol, than was add 100µL of formaldehyde and 1mL of HCl 12M. The mixture was taken under stirring at room temperature. The solution was extracted with water and chloroform. The organic layers were dried over anhydrous sodium sulphate and taken to dryness (43 mg). The residue thus obtained was separated by column chromatography (eluant D). to give the product 21.4 mg, 41 % yield.

Method C:

50 mg of 3-phenyl -2H-1,4-benzothiazine was dissolved in 4mL of methanol, than was add 102µL of glyoxal and 1mL of HCl 12M. The mixture was taken under stirring at room temperature. The solution was extracted with water and chloroform. The organic layers were dried over anhydrous sodium sulphate and taken to dryness (42 mg). The residue thus obtained was separated by column chromatography (eluant A) to give 25.5 mg of pure product, 49% yield.

Method D

50 mg of 3-phenyl -2H-1,4-benzothiazine was dissolved in 4mL of acetonitrile, than was add 102µL of glyoxal and 1mL of HCl 12M. The mixture was taken under stirring and under reflux at 60 °C. The solution was extracted with water and chloroform. The organic layers were dried over anhydrous sodium sulphate and taken to dryness to give 64 mg of pure product, 60% yield.

2Z,2'Z-(1,2-etandiilidene)bis(3-phenyl-2H-1,4-benzothiazine):

ESI+MS: *m/z* 485 ($[M+H]^+$);

UV: λ_{max} (CH_3OH) 486 nm;

^{1}H NMR ($CDCl_3$) δ (ppm): 6.85 (s , 1H) , 7.10 (m , 1H) , 7.12 (m 1H) , 7.19 (m , 1H) , 7.45 (m , 1H) , 7.48 (m , 1H) , 7.52 (m , 2H) , 7.77 (m , 2H);

^{13}C NMR ($CDCl_3$) δ (ppm): 123.4 (C), 124.9 (CH) , 125.9 (CH) , 126.9 (CH) , 127.8 (CH) , 128.5 (CH × 2) , 129.1 (CH), 129.2 (CH × 2) , 130.1 (CH) , 132.4 (C) , 138.7 (C) , 140.8 (C) , 160.2 (C).

5.6 Benzothiazine-based cyanine dyes: b)Cyanines by condensation of benzothiazines with aldehydes

Starting from 3-phenyl-1,4-benzothiazine

p-dimethylaminobenzaldehyde

50 mg (0,22 mmol) of 3-phenyl-2H-1,4-benzothiazine was dissolved in 4mL of methanol, than was add 33,1mg of p-dimethylaminobenzaldehyde and 1mL of HCl 12M. The mixture was taken under stirring at room temperature. The solution was extracted with water and chloroform. The mixture obtained was separated by chromatographic column (eluant E) to give pure cyanine **1** (28.5 mg, 44% yield).

Compound 1:

ESI+MS: *m/z* 357 ($[M+H]^+$);

UV: λ_{max} (CH_3OH) 440 nm;

^{1}H NMR ($CDCl_3$) δ (ppm): 2.97 (s, 6H), 6.73 (d, *j*= 8.8 Hz , 2H) , 6.90 (s, 1H) , 7.10 (d , *j*= 7.2 Hz , 1H) , 7.14 (m , 1H) , 7.17 (m , 1H) , 7.45 (m, 6H) , 7.85 (d , *j*= 7.6 Hz , 2H);

^{13}C NMR ($CDCl_3$) δ (ppm): 40.13 ($2\times CH_3$) , 111.39 (2×CH) , 117.19 (C) , 122.8 (C) ; 123.37 (C) , 125.06 (CH) , 126.49 (CH) , 127.15 (CH) , 128.37 (CH) , 129.22 (CH) , 129.51 (CH × 2) , 129.74 (CH) , 131.4 (CH × 2) , 134.89 (CH) , 140.2 (C) , 140.92 (C) , 150.19 (C) , 162.48 (C).

vanillin

50 mg (0,22 mmol) of 3-phenyl-2H-1,4-benzothiazine was dissolved in 4mL of methanol, than was add 33,8 mg of vanillin and 1mL of HCl 12M. The mixture was taken under stirring at room temperature. The solution was extracted with water and chloroform. The mixture

obtained was separated by column chromatography (eluant F) to give pure cyanine **2** (26.3 mg, 40% yield).

Compound 2:

ESI+MS: *m/z* 360 ($[M+H]^+$);

UV: λ_{max} (CH_3OH) 413 nm;

^1H NMR ($CDCl_3$) δ (ppm): 3.86 (s ,3H) , 6.86 (s , 1H) , 6.90 (d , *J* = 8 Hz , 1H) , 6.99 (s , 1H) , 7.01 (m , 1H) , 7.10 – 7.13 (m , 3H) , 7.41 (m , 3H) , 7.45 (d , *J* = 8 Hz , 1H) , 7.78 (m , 2H).

^{13}C NMR ($CDCl_3$) δ (ppm): 55.98 (CH_3) , 112.04 (CH) , 114.2 (CH) ,122.69 (C) , 123.00 (C) , 124.08 (CH) , 125.07 (CH) , 126.72 (CH) , 127.50 (CH), 128.46 (CH × 2) , 129.36 (CH) , 129.49 (CH × 2) ,129.73 (C) , 130.00 (CH) , 134.55 (C) , 138.6 (C) , 145.9 (C) , 146.18 (C) , 163.30 (C).

p-dimethylaminocinnamaldehyde

50 mg (0,22 mmol) of 3-phenyl-2H-1,4-benzothiazine was dissolved in 4mL of methanol, than was add 39 mg of p-dimethylaminocinnamaldehyde and 1mL of HCl 12M. The mixture was taken under stirring at room temperature. The solution was extracted with water and chloroform. The mixture obtained was separated by column chromatography (eluant D) to give pure cyanine **3** (23.4 mg, 33% yield).

Compound 3:

ESI+MS: *m/z* 383 ($[M+H]^+$);

UV: λ_{max} (CH_3OH) 464 nm;

^1H NMR ($CDCl_3$) δ (ppm): 3.00 (s , 6H) , 6.59 (d , *J* = 16 Hz , 1H) , 6.62 (d , *J*= 12 Hz , 1H) , 6.68 (d, *j* = 8 Hz , 2H) , 7.02 (d.d. , *J*= 12/16 Hz , 1H) , 7.13 (d , *J*= 8 Hz , 1H) , 7.18 (m , 2H)

, 7.36 (d , *J*= 8 Hz , 2H) , 7.46 (m , 4H) , 7.77 (m , 2H).

^{13}C NMR ($CDCl_3$) δ (ppm): 40.24 (CH_3 × 2) , 112.1 (CH × 2) , 119.1 (CH) , 119.59 (C) , 124.31 (C) , 124.97 (C) , 125.12 (CH) , 126.77 (CH) , 127.56 (CH) , 128.46 (CH × 2) , 128.49 (CH × 2) , 129.28 (CH × 2) , 129.6 (CH) , 129.76 (CH) , 134.1 (CH) , 138.87 (CH) , 139.31 (C) , 141.57 (C) , 150.77 (C) , 161.84 (C).

Ferulaldehyde

50 mg (0,22 mmol) of 3-phenyl-2H-1,4-benzothiazine was dissolved in 4mL of methanol, than was add 35 mg of ferulaldehyde and 1mL of HCl 12M. The mixture was taken under stirring at room temperature. The solution was extracted with water and chloroform. The mixture obtained was separated by column chromatography (eluant D) to give pure cyanine **4** (38 mg, 60% yield).

ESI+MS: *m/z* 386 ($[M+H]^+$);

UV: λ_{max} (CH_3OH) 436 nm;

^{1}H NMR ($CDCl_3$) δ (ppm): 3.95 (s , 3H) , 6.59 (d , *J* = 16 Hz , 1H) , 6.63 (d , *J*= 12 Hz , 1H) , 7.06 (d.d. , *J*= 12/16 Hz , 1H) , 7.15-7.18 (3H) , 6.97 (1H); 6.89 (d , *J*= 8 Hz , 2H), 7.46 (m , 4H), 7.77 (m , 2H).

^{13}C NMR ($CDCl_3$) δ (ppm): 55.98 (CH_3 × 2) ,108.43(CH),114.70(CH), 121.42 (CH) , 124.05 (C) , 124.23 (C), 125.14 (CH), 126.73 (CH), 127.53 (CH), 128.52 (CH × 2), 129.27 (CH x 2),129.49 (C , 129.91 (CH) ,133.21 (CH), 138.23 (CH), 139.14 (C), 139.31 (C), 146.52 (C),146.72(C), 161.36 (C).

<u>Starting from 3-methyl-1,4-benzothiazine</u>

p-dimethylaminobenzaldehyde

50 mg of (0,31 mmol) 3-methyl-2H-1,4-benzothiazine was dissolved in 4mL of methanol, than was add 85µL of p-dimethylaminobenzaldehyde and 1mL of HCl 12M. The mixture was taken under stirring at room temperature. The solution was extracted with water, calcium carbonate and chloroform. The mixture obtained was separated by column chromatography (eluant G) to give pure cyanine **5** (54.1 mg, 60% yield)

Compound 5:

ESI+MS: *m/z* 295 ($[M+H]^+$);

UV: λ_{max} (CH_3OH) 429 nm;

^1H NMR ($CDCl_3$) δ (ppm): 2.54 (s , 3H) , 3.00 (s , 6H), 6.75 (d , *J= 8* Hz, 2H) , 6.97 (s , 1H) , 7.09 (m, 1H) , 7.10 (m , 1H) , 7.15 (m , 1H) , 7.32 (d , *J= 8* Hz , 1H) , 7.54 (d , *J= 8* Hz, 2H) .

^{13}C NMR ($CDCl_3$) δ (ppm): 25.71 (CH_3) , 39.36 (CH_3 × 2) , 111.31 (CH×2) , 118.82 (C) , 122.35 (C) , 123.42 (C) , 124.90 (CH) , 125.79 (CH) , 127.23 (CH) , 129.20 (CH) , 131.18 (CH × 2) , 134.57 (CH) , 139.04 (C) , 159.52 (C).

vanillin

50 mg (0,31 mmol) of 3-methyl-2H-1,4-benzothiazine was dissolved in 4mL of methanol, than was add 45mg of vanillin and 1mL of HCl 12M. The mixture was taken under stirring at room temperature. The solution was extracted with water, calcium carbonate and chloroform. The mixture obtained was separated by column chromatography (eluant G) to give pure cyanine **6** (20 mg, 44% yield)

Compound 6:

ESI+MS: *m/z* 298 ($[M+H]^+$);

UV: λ_{max} (CH_3OH) 401 nm;

^{1}H NMR ($CDCl_3$) δ (ppm): 2.55 (s , 3H) , 3.95 (s , 3H) , 6.98 (s ,1H) , 6.99 (m , 1H) , 7.09 (m , 1H) , 7.11-7.14 (m , 4H) , 7.37 (m , *J= 8Hz* ,1H).

^{13}C NMR (CD_3OD) δ (ppm): 25.87 (CH_3) , 55.95 (CH_3) , 111.70 (CH) , 114.41 (CH) , 121.4 (C) , 121.8 (C) , 123.55 (CH) , 124.80 (CH) , 126.58 (CH) , 127.42 (CH × 2) , 127.70 (CH) , 129.18 (CH) , 138.84 (C) , 145.84 (C) , 146.25 (C) , 158.90 (C) .

***p-dimethylaminocinnamaldehyde*:**

50 mg (0,31 mmol) of 3-methyl-2H-1,4-benzothiazine was dissolved in 4mL of methanol, than was add 54 mg of p-dimethylaminocinnamaldehyde and 1mL of HCl 12M. The mixture was taken under stirring at room temperature. The solution was extracted with water, calcium carbonate and chloroform. The mixture obtained was separated column chromatography (eluant D) to give pure cyanine **7** (22 mg, 32% yield).

Compound 7:

ESI+MS: *m/z* 321 ($[M+H]^+$);

UV: λ_{max} (CH_3OH) 458 nm;

^{1}H NMR ($CDCl_3$) δ (ppm): 2.43 (s, 3H) ; 3.00 (s , 6H) ; 6.70 (d , *J*= 8Hz , 2H) , 6.73 (d , *J* = 12 Hz , 1H) , 6.75 (d , *J* = 16 Hz , 1H) , 6.91 (d.d. , *J* = 12/16 Hz , 1H) , 7.10 (m , 2H) , 7.15 (m , 1H) , 7.33 (d , *J*= 8 Hz , 1H) , 7.39 (d , *J*= 8 Hz , 2H).

^{13}C NMR ($CDCl_3$) δ (ppm): 24.92 (CH_3); 40.55 (2×CH_3); 112.19 (2×CH) ; 119.38 (CH) ; 120.60 (C); 123.26 (C); 124.81 (CH) ; 125.16 (C) ; 126.4 (CH); 127.2 (CH) ; 127.62 (CH) ; 128.28 (2× CH) ; 129.41 (CH) ; 137.85 (CH) ; 140.01 (C) ; 150.59 (C) ; 158.88 (C).

Ferulaldehyde

50 mg (0,31 mmol) of 3-methyl-2H-1,4-benzothiazine was dissolved in 4mL of methanol, than was add 54 mg of ferulaldehyde and 1mL of HCl 12M. The mixture was taken under stirring at room temperature. The solution was extracted with water, calcium carbonate and chloroform. The mixture obtained was separated on column chromatography (eluant D) to give pure cyanine **8** (22 mg, 32% yield).

Compound 8

ESI+MS: *m/z* 323 ($[M+H]^+$);

UV: λ_{max} (CH_3OH) 434 nm;

^{1}H NMR ($CDCl_3$) δ (ppm): 2.52 (s , 3H), 3.95 (s , 3H) , 6.80 (d , *J* = 16 Hz , 1H) , 6.83 (d , *J*= 12 Hz , 1H) , 7.01 (d.d. , *J*= 12/16 Hz , 1H) , 7.10-7.25 (3H), 7.38 (d, 1H), 6.85 (d, 2H), 6.99 (d, 2H), 7.07 (s, 1H)

^{13}C NMR ($CDCl_3$) δ (ppm):25.02 (CH_3), 55.98 (OCH_3) , 110.33 (CH), 114.52 (CH), 120.72 (CH), 121.05 (C), 122.42 (CH), 124.59 (CH), 125.13 (C),126.12 (CH), 127.44 (CH), 128.29 (C), 129.61 (CH), 130.11 (CH), 138.09 (CH), 140.14 (C), 145.92 (C), 146.56 (C), 156.36 (C)

5.7 Role of benzothiazine structural units in pheomelanin properties: UV-independent prooxidant effects of natural and model pigments

Isolation of hair melanin

Red hair pheomelanin (RHP) and black hair eumelanin (BHE) were isolated as previously reported with modifications (Greco et al., 2009; Thureau et al., 2012). Briefly, hairs (5 g) were washed with acetone/ dichloromethane/diethyl ether (2:1:1 v/v/v, 250 ml) and allowed to airdry overnight. The washed hairs were finely minced with scissors and suspended by use of a glass/glass potter in 0.1 M phosphate buffer pH 7.4 (200 ml). The resulting mixture was incubated with proteinase K (40 mg, 13 U/mg) and dithiothreitol (600 mg) in an argon atmosphere under vigorous stirring at 37°C. After 18 h, the mixture was centrifuged at 1258 g for 20 min at 4°C; the resulting precipitate was washed with 1% acetic acid (3 9 5 ml), while the supernatant was acidified to pH 3 with 2 M HCl, stored at 4°C for 1 h, and centrifuged at 1258 g for 20 min at 4°C, to give a precipitate that was washed with 1% acetic acid (3 9 5 ml). The combined precipitates were suspended in 0.1 M phosphate buffer (pH 7.4) (25 ml) and treated again with proteinase K (24 mg) and dithiothreitol (360 mg) as bove. After 18 h, the mixture was treated as above, and the combined precipitates were subjected to two further digestion treatments with proteinase K (20 mg for the first treatment and 3 mg for the second) and dithiothreitol (8 mg for the first treatment and 13 mg for the second) as above. The final precipitate was washed with water and lyophilized. The pellet obtained was resuspended in 0.1 M phosphate buffer (pH 7.4) at a concentration of 50 mg/ml containing Triton X-100 (200 ll for 100 mg of pellet) and taken under stirring at 37°C. After 4 h, the mixture was centrifuged at 20 124 g for 20 min at 4°C; the resulting precipitate was washed with 1% acetic acid (3 9 5 ml), while the supernatant was acidified to pH 3 with 2 M HCl, stored at 4°C for 1 h, and centrifuged at 20 124 g for 20 min at 4°C, to give a precipitate that was washed with ultrapure

water (3 9 5 ml). The combined precipitates were subjected to a further digestion treatment with proteinase K (3 mg) and dithiothreitol (13 mg) as described above. The final precipitate was washed with water and lyophilized to obtain 132 mg of red hair pheomelanin (RHP) and 157 mg of black hair eumelanin (BHE). 5 mg of RHP, BHE or hair samples was treated with alkaline H_2O_2 and analyzed by HPLC as previously described for TTCA (in the case of pheomelanin) and PTCA (in the case of eumelanin) (Greco et al., 2009; Panzella et al., 2007). The yields of TTCA obtained by degradation of red human hair and purified RHP were 150 ng/mg and 1630 ng/mg, respectively; PTCA yields obtained by degradation of black hair and purified BHE were 200 ng/mg and 4000 ng/mg, respectively.

Preparation of synthetic melanins.

CD-mel by peroxidase/H_2O_2 oxidation was prepared by treatment of 5SCD (150 mg, 0.32 mol) in 0.1 M phosphate buffer, pH 6.8 (37.5 mL) with peroxidase (3.4 mg, 16.7 U/mL final concentration) and 30% v/v H_2O_2 (38 μL). The oxidation mixture was allowed to stand at room temperature under vigorous stirring for 2 h and then acidified to pH 3 with 3 M HCl. The melanin precipitate was collected by centrifugation (7000 rpm, 20 min, 4 °C) and was washed three times with 1% acetic acid and once with H2O (118 mg, 79% yield).

When required, the reaction was run in the presence of $ZnSO_4 \times 7H_2O$ (111 mg, 1.2 molar eq) yielding 137 mg of product (52% yield).

3-S-cysteinyl-5-methylcathecol melanin was prepared by treatment of 3-S-cysteinyl-5-methylcathecol (100 mg) in 0.1 M phosphate buffer, pH 6.8 (25 mL) with peroxidase (2.3 mg, 17.3U/ml) and 30% v/v H_2O_2 (25 μl). The oxidation mixture was treated as above to give 28 mg of melanin (28% yield).

Chemical degradation of natural and synthetic melanins.

Finely minced hair (10 mg) or purified hair melanins (5 mg) were suspended in 1 M NaOH

(1mL) and treated with H_2O_2 (50 μL, final concentration 1.5%) at room temperature and under vigorous stirring for 24 h. The mixture was treated with 5% Na2S2O5 (200 μL), taken to pH 4 with HCl 4 M, filtered through nylon membranes (13 mm, 0. 45 μm) and analyzed by HPLC.

GSH depletion

A solution of GSH (3.0 mg, 9.8 μmol) in 0.1 M phosphate buffer (pH 7.4) (65 ml) in the presence of RHP (3.0 mg) was allowed to stand under vigorous stirring at room temperature, in the dark. The mixture was periodically analyzed by HPLC with UV (220 nm) and electrochemical detection using 10 mM NaH_2PO_4 (pH 3.0 with phosphoric acid) at a flow rate of 0.7 ml/min as the eluant. In control experiments, the reaction was run (i) in the absence of melanin; (ii) in the presence of CD-mel, BHE, 30 μM $FeCl_3$ or 6 μM $CuSO_4$ x $5H_2O$ instead of RHP; (iii) in the presence of SOD (4 U/ ml), catalase (25 U/ml) or both of them; iv) under an Ar atmosphere

In other experiments, GSH depletion by RHP was followed using Ellman's reagent (Ellman, 1959). Briefly, a solution of GSH (3.0 mg, 9.8 μmol) in 0.1 M phosphate buffer pH 7.4 (4.9 ml) was allowed to stand under vigorous stirring at room temperature, in the dark, in the presence of variable amounts of RHP (0.6–6.0 mg). 100 μl of the mixture was periodically withdrawn and added to 2.7 ml of 0.1 M phosphate buffer (pH 7.4) followed by 50 μl of Ellman's solution [16 mg of Ellman's reagent in 4 ml of 0.1 M phosphate buffer (pH 7.4)], and after 15 min, the absorbance at 412 nm was recorded by use of a UV/vis spectrophotometer. In control experiments, the reaction was run in the absence of melanin, in the presence of CDmel or in the presence of BHE. A blank experiment without GSH was also performed in order to evaluate the contribution of the absorption of melanin samples at the analytical wavelength.

NADH/NADPH depletion .

A solution of NADH/NADPH (3.0 mg, 4.2 μmol) in 0.1 M phosphate buffer pH 7.4 (28 ml) in

the presence of RHP (3.0 mg) was allowed to stand under vigorous stirring at room temperature, in the dark. The mixture was periodically analyzed by HPLC with UV detection (260 and 340 nm) using 0.2 M phosphate buffer (pH 6.0)/methanol 86/14 v/v at a flow rate of 0.7 ml/min as the eluant. In control experiments, the reaction was run (i) in the absence of melanin; (ii) in the presence of BHE; (iii) under an Ar atmosphere.

Dopa and 5SCD depletion

A solution of dopa (3.0 mg, 15 lmol) or 5SCD (4.7 mg, 15 lmol) in 0.1 M phosphate buffer pH 7.4 (15 ml) in the presence of RHP (1:2 w/w) was allowed to stand under vigorous stirring at room temperature in the dark. The mixture was periodically analyzed by HPLC with UV detection (254 nm) using 0.5% trifluoroacetic acid/methanol 9:1 v/v at flow rate of 0.8 ml/min as eluant. In control experiments, the reaction was run (i) in the absence of melanin; (ii) in the presence of BHE instead of RHP; (iii) in the presence of SOD (4 U/ml), catalase (25 U/ml) or both of them; (iv) under an Ar atmosphere.

EPR experiments

A solution of GSH (5 mg, 16 lmol) in 0.1 M phosphate buffer (pH 7.4) (2 ml) in the presence of RHP (1 mg) was allowed to stand under vigorous stirring at room temperature, in the dark. The mixture was periodically analyzed by HPLC with UV and electrochemical detection and by EPR. For the latter measurements, pheomelanin samples were transferred to flame-sealed glass capillaries which, in turn, were coaxially inserted in a standard 4-mm quartz sample tube containing light silicone oil for thermal stability. In other experiments, the reaction was run (i) in the absence of GSH; (ii) in the presence of CD-mel (with or without GSH) instead of RHP.

Statistical analysis

Data sets were initially assessed for normality. Means were statistically compared using independent samples two-tailed t tests.

5.8 Photochemistry of pheomelanins: spectroscopic investigation of benzothiazole building blocks

Sample preparation.

BT and BTCA were prepared from 5-S-cysteinyldopa according to Greco et al. MB was commercially available. M-BT was prepared by a modification of the procedure followed for BT preparation. In brief a solution of 4-methylcathecol (1.26 g, 0.01 mol) in ice-cold water (100 mL) was treated with sodium periodate (2.35 g, 1.1 eq) in water (100 mL) in an ice bath. The bright red reaction mixture is extracted with cold dichloromethane and the organic phase was dried over anhydrous sodium sulfate and evaporated to dryness. The product formed was identified as 4-methyl-1,2-benzoquinone (700 mg, purity 64% as determined by UV taking the molar extinction coefficient at 389 nm as 1585 $M^{-1}cm^{-1}$) [2]. To a stirred solution of L-cysteine (439 mg) in 0.1 HCl (20 mL) a solution of the 4-methyl-1,2-benzoquinone (439 mg) dissolved in ethanol (40 mL) was added dropwise over about 3 hours. The reaction mixture was extracted with diethyl ether (180 mL) and ethyl acetate (80 mL). The aqueous phase was recovered, dried under vacuum and washed with water in order to remove excess acid. The identity of the product was secured by UV and LC-MS (Gradient A, detection at 254 nm, R_t 4.0 min, *m*/*z* 244 $(M+H)^+$). UV (0.1M HCl) λ_{max} 289 nm; 253 nm (taking the molar extinction coefficient as ε = 2951 $M^{-1}cm^{-1}$ and ε = 3715 $M^{-1}cm^{-1}$).The resulting mixture was fractionated by preparative HPLC/UV (eluent: 1% formic acid/methanol 85:15 (v/v); flow rate: 20 mL/min; UV: 254 nm). After concentration in a rotary evaporator the residue was lyophilized yielding the product as pale yellow powder (362 mg, 41% yield)

Fluorescence experiments

The experimental conditions of the optical measurements were described previously[127,129]. Absorption spectra were recorded with an Agilent spectrophotometer, and a SPEX Fluorolog was used to record steady state fluorescence spectra with an excitation wavelength of 266 nm. Time resolved fluorescence data were collected using a Hamamatsu streak camera C6860 device coupled to a Chromex spectrograph. The temporal resolution varied between ~10 to 60 ps depending on the investigated time range. The 266 nm laser beam used to excite the sample was generated by frequency tripling 150 fs, 800 nm, Ti:Sa pulses at a repetition rate of 82 MHz (Spectra-Physics, Tsunami). The laser beam was focused on the sample in a 2 mm rotating quartz cuvette. Fluorescence was collected at magic angle using two 1-inch diameter 50 mm focal length quartz lenses and focused on the spectrograph. All time-resolved fluorescence measurements were performed at room temperature (20 ± 1°C), under aerated conditions.

Data analysis

Time resolved fluorescence (TRF) data were analyzed using singular value decomposition (SVD) and global fit (GF) procedures, as described elsewhere[130-132]. Briefly, SVD is a tool that allows us to minimize significantly the number of relevant kinetic and spectral components required to describe the entire evolution of the system. It also suppresses the noise from the data without losing any relevant information. It consists in decomposing the M x N data matrix (E) into a product of three components according to:

$$E = USV^T, \qquad (1)$$

where U and V^T stand for orthogonal matrices of M x M basis spectra and N x N basis kinetics traces, respectively. The diagonal elements of the S matrix yield the singular values Si. A nonlinear least square global fit (GF) to the V^T traces is performed using a multiexponential function convoluted with a Gaussian instrumental response function (IRF) as described in equation 2,

$$V_i^T = \sum_{k=1}^{K} a_{i,k} e^{-t/\tau_k} \otimes e^{\left[-\left(\frac{t-t_0}{0.6*\Delta_{IRF}}\right)^2\right]}, \quad (2)$$

where $a_{i,k}$ is the amplitude of the k^{th} decay. The Gaussian term describes the convolution with the IRF, where Δ_{IRF} and t_0 are the full width half maximum (FWHM) and time zero, respectively. The coefficients $a_{i,k}$ are used to calculate the corresponding decay-associated spectra (DAS) of the involved kinetics by using the set of properly weighted U_i spectral SVD components via:

$$DAS_{k=1,2,3} = \sum_{i=1}^{N} a_{i,k} \cdot s_i \cdot U_i \quad (3)$$

The individual DAS show the contribution of corresponding lifetimes τ_i in the spectral evolution of the system. Given lifetimes and DAS maxima are characterized by approx. 10 % and ±5 nm error, respectively.

The GF procedure consists of fitting simultaneously all the kinetic traces contained in a data matrix by setting the time constants as common parameters. Both SVD and GF procedures give the same result.

5.9 Photochemistry of pheomelanins: Spectroscopic investigation of natural and synthetic pigments and related 1,4-benzothiazines

Isolation of hair melanin

This procedure was already described in 4.6

Preparation of synthetic melanins.

The synthesis of these synthetic pigments was already described in 4.6

Synthesis of 10-[6-(2-amino-2-carboxyethyl)-4-hydroxybenzothiazol-2-yl]-8- carboxy-5-hydroxy-3-oxo-3,4,7,8-tetrahydro-2H-[1,4]thiazino[5,6-h]isoquinoline

To a solution of 5SCD (30 mg, 12 mM) in 0.1 M phosphate buffer (pH 6.8)(6 mL) zinc sulfate (1.2 molar eq.) was added. After 30 min peroxidase (50 U/mL final concentration), and 30% v/v H2O2 up to a 38 mM final concentration were sequentially added. The mixture was allowed to sit at room temperature under vigorous stirring for 5 h.

For preparative purposes the reaction was carried out on three aliquots of 5SCD (30 mg each), and after 5 h the mixtures were acidified to pH 2, the solid was collected by centrifugation (7000 rpm, 4 C°, 30 min), and purified by semipreparative HPLC (gradient B, detection at 340 nm) to afford the product eluting at tR 39.8 min (3 mg, 3% yield).

Synthesis of 2,2'-Bi[7-(2-amino-2-carboxyethyl)-3-carboxy-5-hydroxy-2H-1,4-benzothiazine]

A 2 mM solution of CD (50 mg) in 0.05 M phosphate buffer (pH 7.4, 80 mL) was allowed to stand at room temperature under vigorous stirring in the presence of ZnSO4 (27 mg) for 10 minutes. Na2S2O8 was added (90 mg) and after 30 minutes the reaction mixture was acidified to pH 3 with 6 M HCl. After 30 minutes the mixture was taken to pH 6 and allowed to precipitate at 4 °C. The precipitate was collected by centrifugation (6000 g, 15 min, 4 °C),

washed once with H2O and lyophilized. The product was purified by preparative HPLC (eluent: 0.5% TFA/methanol 50:50 (v/v); flow rate: 15 mL/min; UV: 254 nm).The identity of the product was secured by LC-MS (gradient B, detection at 254, flow rate: 0.7 mL/min, Rt 42.9 min, m/z 591 [M+H]+).

Fluorescence experiments

The experimental conditions of the optical measurements were described in 4.7

6.References

1) L. Le Bozec, C.J. Moody, *Aust. J. Chem*. **2009**, *62*, 639–647

2) T. Fojo, M. Menefee, *Ann. Oncol*., **2007**, *18*, 3-8

3) G. Pettit, K. Yoshiaki, C.L. Herald, C. Dufresne, R.L Cerny, D.L Herald, J.M. Schimdt, H. Kizu, *J. Am. Chem. Soc.,* **1989**, *111*, 5015-5017

4) C.M. Ireland, A.R Durso Jr., R.A. Newman, M.P. Hacker, *J. Org. Chem*, **1982**, *47*, 1807-1811

5) C. Garcia-Ruiz, F. Sarabia, *Mar. Drugs*, **2014**, *12*, 1580-1622

6) R.J. Mulder, C.M. Shafer, T.F. Molinski, *Bioorg. Med. Chem. Lett.,* **2009**, *19*, 2928-2930

7) S. Kapur, D. Mamo, *Prog Neuropsychopharmacol Biol Psychiatry*, **2003**, *27*, 1081-1090

8) M.J. Hughes, I.A. Coret, *Am. J. Physiol*, **1972**, *23*, 1257-1262

9) P.J. Donovick, *Biotechnic and Histochemistry*, **1974**, *49*, 49-51

10) J.L. Vennerstrom, M.T. Makler, C.K. Angerhofer, J.A. Williams, *Antimicrob.Agents Chemoter.,* **1995,** *39*, 2671-2677

11) R. H. Thomson, *Angew. Chem. Intl. Ed. Engl.* **1974**, *13*, 305-312.

12) S. Ito, K. Wakamatsu, *Pigm. Cell Melanoma Res*. **2011**, *24*, 63–74.

13) F. Rouzaud, A. Kadekaro, Z.A. Abdel-Malek, V.J. Hearing, *Mutat. Res.* **2005**, *571*, 133–152.

14) R.M. El-Shishtawy , *Int. J. Photoenergy*, **2009** , 1-21.

15) K. R. J. Thomas, Y.-C. Hsu , J. T. Lin et al., *Chem. Mater*, **2008** , *5* , 1830-1840,.

16) Y. Di Iorio, M.A. Brusa, A. Feldhoff, M.A. Grela, *ChemPhysChem* , **2009**,*10*,1077-1083.

17) C. Dejoie et al , *Appl Mat & Intergaces* , **2010** , *2* , 2308-2316.

18) J. L. Meinershagen , T. Bein , *J. Am. Chem. Soc.* , **1999** , *121*, 448-449.

19) S. Jockusch, N.J. Turro, and F.R. Blackburn, *J. Phys. Chem*, **2002,** *40*, 9236-9241.

20) S. Wang, M.-S. Choi, and S.-H. Kim , *J. Photoc. Photobio. A*, **2008** , *2-3*, 150-155.

21) F. Pina, TA Hatton, *Langmuir*, **2008**, *24*, 2356-2364.

22) F. Han,L. Chi, W. Wu, X. Liang, M. Fu, J. Zhao, *Photochem. Photobiol*., **2008**, *196*, 10-23

23) B. L. Kaul , *Helv. Chim.Acta* , **1974** , *37*, 2664-2678.

24) G. Prota , E. Ponsiglione and R. Ruggiero , *Tetrahedron* , **1974** , *30*, 2781-2784.

25) J. D. Simon , M.R. Goldsmith , L. Hong , V.R. Kempf , L.E.L. McGuckin , T. Ye, G. Zuber, *Photochem. Photobiol*, **2006**, *82*, 318-323.

26) F. Chioccara, G. Prota , R.H. Thomson , *Tetrahedron Lett.* **1976** ,1407-1409.

27) L. M. Zimmermann-Dimer, D. C. Reis, C. Machado, V. G. Machado, *Tetrahedron*, **2009** , *65*, 4239–4248.

28) A. Ehret, L. Stuhl, M.T. Spitler, *J. Phys. Chem. B*, **2001**, *105*, 9960-9965

29) G. Prota, R.A. Nicolaus, W. Montagna F. Hu, *Advances in Biology of Skin, vol 8. New York: Pergamon Press;* **1967**. 323–328

30) P. Valverde, E. Healy, I. Jackson, J.L Rees, A.J. Thody, *Nature Genetics*, **1995**, *11*, 328-330

31) J.L. Rees, *Annu. Rev. Genet.* **2003**, *37*, 67-90.

32) N.F. Box, J.R. Wyeth, L.E. O'Gorman, N.G. Martin, R.A. Sturm, R. A. *Hum. Mol. Genet.* **1997**, *6*, 1891-1897.

33) E. Healy, S.A. Jordan, P.S. Budd, R. Suffolk, J.L. Rees, I.J. Jackson, *Hum. Mo.l Genet.* **2001**, *10*, 2397-2402.

34) Simon, J. D.; Peles, D. N.. *Acc. Chem. Res*. **2010**, *43*, 1452–1460.

35) S. Ito, K.Wakamatsu, *Pigm. Cell Melanoma Res*., **2011**, *24*, 63–74.

36) S. Ito, G. Prota, *Experientia*, **1977**, *33*, 1118–1119.

37) L. Panzella, M. De Lucia, A. Napolitano, M. d'Ischia, *Tetrahedron Lett*., **2007**, *48*, 7650–7652.

38) A. Napolitano, M. De Lucia, L. Panzella, M. d'Ischia, *Photochem. Photobiol.* **2008**, *84*, 593-599

39) S. Crescenzi, G. Misuraca, E. Novellino, G. Prota, *Chim. Ind*. **1975**, 57, 392–393.

40) G. Greco, L. Panzella, L. Verotta, M. d'Ischia, A. Napolitano, *J. Nat. Prod*., **2011**, 74, 675–682.

41) A. Napolitano, S. Memoli, O. Crescenzi, G. Prota, *J. Org. Chem*. **1996**, *61*, 598–604.

42) C. Costantini, O. Crescenzi, G. Prota, A. Palumbo, *Tetrahedron*, **1990,** *46*, 6831–6838.

43) A. Napolitano, P. Di Donato, G.Prota, *J. Org. Chem*. **2001**, *66*, 6958–6966.

44) L.N. Pho, S.A. Leachman, G. *Ital. Dermatol. Venereol*., **2010**, *145*, 37–45.

45) D. Mitra, X. Luo, A. Morgan, J. Wang, M.P. Hoang, J. Lo, C.R. Guerrero, J. Lennerz, M.C. Mihm, J.A. Wargo, K.C. Robinson, S.P. Devi, J.C. Vanover, J.A: D'Orazio, M. McMahon, M.W. Bosenberg, K.M. Haigis, D.A: Haber, Y. Wang, D.E. Fisher, *Nature*, **2012**, *491*, 449–453.

46) M.R. Chedekel, S.K. Smith, P.W: Post, A. Pokora, D.L. Vessell, *Proc. Natl. Acad. Sci. U.S.A.* **1978**, *75*, 5395-5399.

47) M. Brenner, V.J. Hearing, . *Photochem. Photobiol.* **2008**, *84*, 539-549.

48) J. Riesz, T. Sarna, P. Meredith, *J. Phys. Chem. B.* **2006**, *110*, 13985-13990.

49) S. Schmitz, P.D. Thomas, T.M. Allen, M.J. Poznansky, K. Jimbow, *Photochem. Photobiol.* **1995**, *61*, 650-655.

50) S. Takeuchi, W. Zhang, K. Wakamatsu, S. Ito, V.J. Hearing, K.H. Kraemer, D.E. Brash, D. E. *Proc. Natl. Acad. Sci. U.S.A.* **2004**, *101*, 15076-15081.

51) D. N Peles, L. Hong, D. N. Hu, S. Ito, R.J. Nemanich, J.D. Simon, J. D. *J. Phys. Chem. B.* **2009**, *113*, 11346–11351.

52) S. Ito, *Pigment Cell Res*. **2003**, *16*, 230–236.

53) S. Ito, K. Wakamatsu, *Photochem. Photobiol.* **2008**, *84*, 582–592.

54) T. Ye, L. Hong, J. Garguilo, A. Pawlak, G.S. Edwards, R.J. Nemanich, T. Sarna, J.D. Simon, *Photochem. Photobiol.* **2006**, *82*, 733-737.

55) T. Ye, J. D. Simon, *Photochem. Photobiol.*, **2003**, *77*, 41–45.

56) P. Di Donato, A. Napolitano, *Pigment Cell Res*, **2003**, *16*, 532–539.

57) T. Ye, L. E. Lamb, K. Wakamatsu, S. Ito and J. D. Simon, *Photochem. Photobiol,* **2003**, *2*, 821–823.

58) A. Napolitano, P. Di Donato ,G. Prota, *J. Org. Chem*, **2001**, *66*, 6958–6966.

59) Z.A. Abdel-Malek, S. Ito, *Pigment Cell Melanoma Res.* **2013**, *26*, 164-166.

60) C. Printz, *Cancer* **2013**, *119*, 1118.

61) C. Rodwell, *Nat. Rev. Cancer* **2012,** *12*, *79.*

62) A.M. Morgan, J. Lo, D.E. Fisher, *Bioessays* , **2013,** *3*, 672–676.

63) G. Greco, L. Panzella, G. Gentile , M.E. Errico, C. Carfagna, A. Napolitano, M.d'Ischia, *Chem. Commun*., **2011**, *47*, 10308–10310.

64) M. J. Frisch, G. W. Trucks, H. B. Schlegel, G. E. Scuseria, M. A. Robb, J. R. Cheeseman, G. Scalmani, V. Barone, B. Mennucci, G. A. Petersson, H. Nakatsuji, M. Caricato, X. Li, H. P. Hratchian, A. F. Izmaylov, J. Bloino, G. Zheng, J. L. Sonnenberg, M. Hada, M. Ehara, K. Toyota, R. Fukuda, J. Hasegawa, M. Ishida, T. Nakajima, Y. Honda, O. Kitao, H. Nakai, T. Vreven, J. A. Montgomery Jr., J. E. Peralta, F. Ogliaro, M. Bearpark, J. J. Heyd, E. Brothers, K. N. Kudin, V. N. Staroverov, R. Kobayashi, J. Normand, K. Raghavachari, A. Rendell, J. C. Burant, S. S. Iyengar, J. Tomasi, M. Cossi, N. Rega, J. M. Millam, M. Klene, J. E. Knox, J. B. Cross, V. Bakken, C. Adamo, J. Jaramillo, R. Gomperts, R. E. Stratmann, O. Yazyev, A. J. Austin, R. Cammi, C. Pomelli, J. W. Ochterski, R. L. Martin, K. Morokuma, V. G. Zakrzewski, G. A. Voth, P. Salvador, J. J. Dannenberg, S. Dapprich, A. D. Daniels, Ö. Farkas, J. B. Foresman, J. V. Ortiz, J. Cioslowski, D. J. Fox, *Gaussian 09*, Revision A.01, Gaussian, Inc., Wallingford, CT, **2009**.

65) C. Adamo, V. Barone, *J. Chem. Phys.* **1999**, *110*, 6158–6169.

66) a) M. Cossi, G. Scalmani, N. Rega, V. Barone, *J. Chem. Phys.* **2002**, *117*, 43–54; b) G. Scalmani, V. Barone, K. N. Kudin, C. S. Pomelli, G. E. Scuseria, M. J. Frisch, *Theor. Chem. Acc.* **2004**, *111*, 90–100.

67) A. K. Rappé, C. J. Casewit, K. S. Colwell, W. A. Goddard III, W. M. Skiff, *J. Am. Chem. Soc.* **1992**, *114*, 10024–10035.

68) a) M. Caricato, G. Scalmani, M. J. Frisch in *Continuum Solvation Models in Chemical Physics* (Eds.: B. Mennucci, R. Cammi), John Wiley & Sons, Chichester, **2007**, 64–81.

69) a) R. Bauernschmitt, R. Ahlrichs, *Chem. Phys. Lett.* **1996**, *256*, 454–464; b) C. Adamo, G. E. Scuseria, V. Barone, *J. Chem. Phys.* **1999**, *111*, 2889–2899; c) G. Scalmani, M. J. Frisch, B. Mennucci, J. Tomasi, R. Cammi, V. Barone, *J. Chem. Phys.* **2006**, *124*, 094107-1-15.

70) a) R. Ditchfield, *Mol. Phys.* **1974**, *27*, 789–807; b) K. Wolinski, J. F. Hilton, P. Pulay, *J. Am. Chem. Soc.* **1990**, *112*, 8251–8260.

71) L. Minale, E. Fattorusso, G. Cimino, S. De Stefano, R. A. Nicolaus, *Gazz. Chim. Ital.* **1969**, *99*, 431–449

72) G. Prota, F. Giordano, L. Mazzarella, C. Santacroce, D. Sica, *J. Chem. Soc. C* **1971**, *15*, 2610–2616.

73) R. S. Becker, L. V. Natarajan, *Chem. Phys. Lett.* **1986**, *132*, 141–143.

74) J. A. Montgomery Jr., M. J. Frisch, J. W. Ochterski, G. A.Petersson, *J. Chem. Phys.* **1999**, *110*, 2822–2827

75) R. M. Gschwind, X. Xie, P. R. Rajamohanan, *Magn. Reson. Chem.* **2004**, *42*, 308–312.

76) C. Santacroce, D. Sica, R. A. Nicolaus, *Gazz. Chim. Ital.* **1968**, *98*, 85–96.

77) D. Sica , C. Santacroce and G. Prota , *J. Heterocyclic Chem*, **1970** , *7*, 1143-1147.

78) K. Fujii, *Yakugaku Zasshi,* **1957**, *77*, 347.

79) P. Bottex, B. Sillion, G. De Gaudemaris, J.J. Basselier, *Compt. Rend.* **1968**, *267*, 186.

80) D. Sica , C. Santacroce, G. Prota , *J. Heterocyclic Chem*, **1970** , *7*, 1143-1147.

81) R.C. Sealy, J.S. Hyde, C.C. Felix, I.A. Menon, G. Prota, H.M. Swartz, S. Persad, H.F. Haberman, *Proc. Natl. Acad. Sci. U.S.* **1982**, *79*, 2885.

82) A.D. Becke, *J. Chem. Phys.* **1993**, *98*, 5648.

83) V. Barone, *In Recent Advances in Density Functional Methods, Part I;* Chong, D. P., Ed.; World Scientific: Singapore, **1996**.

84) V. Barone, P. Cimino, E. Stendardo, *J. Chem. Theory Comput*. **2008**, *4*, 751.

85) R. Amorati, G.F. Pedulli, L. Valgimigli, H. Johansson, L. Engman, L. *Org. Lett*. **2010**, *12*, 2326.

86) C. Adamo, V. Barone, *J. Chem. Phys*. **1999**, *110*, 6158.

87) S. Miertus, E. Scrocco, J.Tomasi, *J. Chem. Phys*. **1981**, *55*, 117.

88) J. Nagahama, H. Yumoto, *Surf. Coat. Technol***. 2003**, *169_170*, 658–661.

89) F. Chioccara , G. Prota, R.H. Thomson , *Tetrahedron Lett.* **1975**,811-814

90) F. López Arbeloa, P. Ruiz Ojeda and I. López Arbeloa, *J. Luminesc.*, **1989**, *44*, 105-112

91) L. Panzella, G. Szewczyk, M. d'Ischia, A. Napolitano, T. Sarna, *Photochem. Photobiol* **2010**, *86*, 757–764.

92) M. d'Ischia, K. Wakamatsu, A. Napolitano,et al., *Pigment Cell Melanoma Res*, **2013**, *26*, 616–633.

93) Y. Liu,J.D. Simon, *Pigment Cell Res.* **2003**, *16*: 72–80

94) S. Ito, *Biochim. Biophys. Acta*, **1986,** *883*, 155–161.

95) G. Prota, *Melanins and melanogenesis*, **1992**

96) L. Novellino, A. Napolitano, G. Prota, *Biochim. Biophys. Acta*, **2000**, *1475*, 295-306.

97) G. Greco, K. Wakamatsu; L. Panzella, S. Ito, A. Napolitano, M. d'Ischia,. *Pigment Cell Melanoma Res.* **2009**, *22*, 319-327.

98) K. Wakamatsu, Y. Nakanishi, N. Miyazaki,L. Kolbe, S. Ito, *Pigm. Cell Melanoma Res*. **2012**, *25*, 434–445.

99) A. Mayevsky, G.G. Rogatsky, *Am. J. Physiol. Cell Physiol.*, **2007**, *292*, C615–C640.

100) G.L. Ellman, *Tissue sulfhydryl groups. Arch. Biochem* **1959**

101) Y. Liu, L. Hong, K. Wakamatsu, S. Ito, B. Adhyaru, C.Y. Cheng, C.R. Bowers, J.D. Simon *Photochem. Photobiol.*, **2005,** *81*, 135–144.

102) E. Cesareo, L. Korkina, G. D'Errico, G. Vitiello, M. S. Aguzzi, F. Passatelli, J.Z. Pedersen, A. Facchiano , *PLoS ONE 7*, **2012** , e48849.

103) E.B. Vsevolodov, S. Ito, K. Wakamatsu, I.I. Kuchina, I.F. Latypov, *Pigment Cell Res.,* **1991**, *4*, 30–34.

*104)*A. Samokhvalov, L. Hong,Y. Liu, J. Garguilo, R.J. Nemanich, G.S. Edwards, J.D. Simon, *Photochem. Photobiol*., **2005**, *81*, 145–148.

105) A.A.Suzukawa, A. Vieira, S.M. Winnischofer, A.C. Scalfo, P. Di Mascio, A.M. Ferriera, J.L. Ravanat, L. Martins Dde, M.E. Rocha, G.R. Martinez, *Free Radic. Biol. Med*., **2012**, *52*, 1945–1953.

106) E. Chikvaidze, I. Khachatryan, *Int. J. Cosmet. Sci.,* **2011,** *33*, 322–327.

107) S. Chio, J.S. Hyde, R.C. Sealy, *Arch. Biochem. Biophys.*, **1982**, *215*, 100–106.

108) K. Jimbow, O. Ispida, S. Ito, Y. Hori, C.J.Witkop Jr, R.A. King, *J. Invest. Dermatol.***1983,** *81*, 506–511.

*109)*S. Ito, *Proc. Natl Acad. Sci. USA,* **2006**, *103*, 14647–14648.

110) C. Hansson, H. Rorsman, E. Rosengren, *Acta Derm. Venereol.*, **1980**, *60*, 399–402.

111) A. Napolitano, S. Memoli, A.J. Nappi, M. d'Ischia, G. Prota, *Biochim. Biophys. Acta.,* **1996**, 1291. 75–82.

112) K. Murakami, K. Wakamatsu, Y. Nakanishi, H.Takahashi, S.Sugiyama, S.Ito, *Blood Purif.,* **2007**, *25*, 483–489.

113) L. Panzella, K. Wakamatsu, G. Monfrecola, S. Ito, F. Ayala, A. Napolitano, *Exp Dermatol*, **2011**, *20*, 288–290.

114) K. Wakamatsu, T. Kageshita, M. Furue, et al., *Melanoma Res,* **2002**, *12*, 245–253.

115) I.M. Hadshiew, M.S. Eller, B.A. Gilchrest, B.A., *Am. J. Contact Dermatol*., **2000**, *11*, 19–25.

116) V.A. Terra, F.P.Souza-Neto, R.C. Pereira, T.N.Silva, A.C.Costa, R.C.Luiz, R. Cecchini, A.L. Cecchini, . *J. Photochem. Photobiol B,* **2012**, *109*, 34–41.

117) R.S. Becker, C. Lenoble, A. Zein, *J. Phys. Chem.* **1987**, *91*, 3509-3511**.**

118) C.A.S. Potter, R.G. Brown, F. Vollmer, W. Rettig**,** *J. Chem. Soc. Faraday Trans.*, **1994**, *90*, 59-67**.**

119)S. Luber, K. Adamczyk, E.T.J. Nibbering, V.S. Batista, *J. Phys. Chem. A,* **2013**, *117*, 5269-5279**.**

120) G. Greco, L. Panzella, A. Napolitano,M. d'Ischia, *Tetrahedron Lett.* **2009**, *50*, 3095-3097**.**

121) W.J. Catallo, T. Junk, *J. Environ. Qual.*, **2005**, *34*, 1746-**1754.**

122) P.E**.** Todesco, P. Vivarelli**,** *Gazz. Chim Ital*. **1964**, *94*, 372-381.

123) J.M. Berg, J.L. Tymoczko, L. Stryer, *Biochemistry*; W. H. Freeman and company: New York, 2002.

124) P.K. Feng, Q. Fernando, *J. Org. Chem.,* **1960**, *82*, 2115-2118

125) A. Brenlla, M. Veiga, J.L. Perez Lustres, M.C. Rios Rodriguez, F. Rodriguez-Prieto, M. Mosquera, *J. Phys. Chem. B,* **2013**, *117*, 884-896.

126) A. Corani, A. Huijser, A. Iadonisi, A. Pezzella, V. Sundström, M. d'Ischia, *J. Phys. Chem. B,* **2012**, *116*, 13151-13158.

127) A. Corani,A. Pezzella, T. Pascher, T. Gustavsson, D. Markovitsi, A. Huijser, M. d'Ischia, V. Sundström, V., *J. Phys. Chem. Lett.,* **2013**, *4*, 1383-1388.

128) D. Leupold, M. Scholz, G. Stankovic, J. Reda, S. Buder, R. Eichhorn, G. Wessler, M. Stucker, K. Hoffmann, J. Bauer, et al., *Pigment Cell Melanoma Res.,* **2011**, *24*, 438-445.

129) A. Huijser, A. Pezzella, J. Hannestad, L. Panzella, A. Napolitano, M. d'Ischia, V. Sundstrom, *Chemphyschem*, **2010**, *11*, 2424-2431.

130) A. Cannizzo, A. Blanco-Rodriguez, A. El Nahhas, J. Sebera, S. Zalis, A. Vlcek, M. Chergui, *Journal of the American Chemical Society*, **2008**, *130*, 8967-8974.

131) A. El Nahhas, A. Cannizzo, F. van Mourik, A. Blanco-Rodriguez, S. Zalis, A. Vlcek, M. Chergui, *Journal of Physical Chemistry a,* **2010**, *114*, 6361-6369.

132) A. El Nahhas, C. Consani, A. Blanco-Rodriguez, K. Lancaster, O. Braem, A. Cannizzo, M. Towrie, I. Clark, S. Zalis, M. Chergui, A. Vlcek, *Inorganic Chemistry,* **2011**, *50*, 2932-2943.

Publication list

1) Matteo Adinolfi, Domenica Capasso, Sonia Di Gaetano, Alfonso Iadonisi, Loredana Leone, Antonello Pastore "A straightforward synthetic access to symmetrical glycosyl disulfides and biological evaluation thereof."
Org. Biomol. Chem., **2011**, *9*, 6278-6283

2) Matteo Adinolfi, Marco d'Ischia, Alfonso Iadonisi, Loredana Leone, Alessandro Pezzella, Silvia Valerio "Glycosylated Eumelanin Building Blocks by Thioglycosylation of 5,6-Diacetoxyindole with an Expedient Selenium-Based Dynamic-Mixture Methodology"
Eur. J.Org. Chem **2012,** *23***,** 4333-4338

3) Loredana Leone, Orlando Crescenzi, Alessandra Napolitano, Vincenzo Barone and Marco d'Ischia "The $\Delta^{2,2'}$-Bi(2*H*-1,4-benzothiazine) Structural Motif of Red Hair Pigments Revisited: Photochromism and Acidichromism in a Unique Four-State System "
Eur. J. Org. Chem., **2012**, *27*, 5136-5140

4) Alessandra Napolitano, Lucia Panzella, Loredana Leone, and Marco d'Ischia "Red Hair Benzothiazines and Benzothiazoles: Mutation-Inspired Chemistry in the Quest for Functionality"
Acc Chem Res. **2012**, *46*, 519–528

5) Loredana Leone, Orlando Crescenzi, Riccardo Amorati, Luca Valgimigli, Alessandra Napolitano, Vincenzo Barone, and Marco d'Ischia"Red-Hair-Inspired Chromogenic System Based on a Proton-Switched Dehydrogenative Free-Radical Coupling"
*Org. Lett.***, 2013,** *15*, 4494-4497

6) Lucia Panzella, Loredana Leone, Giorgia Geeco, Giuseppe Vitiello, Gerardino D'Errico, Alessandra Napolitano, Marco d'Ischia "Red human hair pheomelanin is a potent pro-oxidant mediating UV-independent contributory mechanisms of melanomagenesis"
Pigment Cell Melanoma Res. **2013**, *27*, 244-252.

7) Amal El Nahhas, Torbjörn Pascher, Loredana Leone, Lucia Panzella, Alessandra Napolitano, Villy Sundström "Photochemistry of pheomelanin building blocks and model chromophores – excited state intra- and inter-molecular proton transfer."
Submitted at *J. Phys Chem. Lett.*

Communications at international meetings

Matteo Adinolfi, Marco d'Ischia, Alfonso Iadonisi, Loredana Leone, Lucia Panzella, Alessandro Pezzella, Silvia Valerio

Glycosylation as a tool for eumelanin polymers investigation.

NatPharma16th European Carbohydrate Symposium 3-7 July 2011, Sorrento

Poster communication

Matteo Adinolfi, Marco d'Ischia, Alfonso Iadonisi, Loredana Leone, Lucia Panzella, Alessandro Pezzella, Silvia Valerio

Synthesis of thioglycosylated indoles as precursors of solubile eumelanin polymers

Poster communication

Loredana Leone, Alessandra Napolitano and Marco d'Ischia

Synthesis and Characterization of New 1,4-Benzothiazine-Based Chromophore

SISOC-IX (9^{th} Spanish-Italian Symphosium on Organic Chemistry) Tenerife, 10-14 February 2012

Poster communication

A. Napolitano, L. Panzella, L. Leone, M. d'Ischia

The bright and dark side of red hair pigments

17^{th} Meeting of the European Society for Pigment Cell Reasarch Geneva, Switzerland, 11^{th}-13^{th} September 2012

Loredana Leone, Orlando Crescenzi, Alessandra Napolitano, Vincenzo Barone and Marco d'Ischia

The Δ–2,2'-Bi(2H-1,4-benzothiazine) Structural Motif of Red Hair Pigments Revisited: Photochromism and Acidichromism in a Unique Four-State System

XV Ischia Advanced School of Organic Chemistry (IASOC), Ischia, September 2012

Poster communication